

Einfluss elektronischer Faktoren auf die katalytische Aktivität von *chiral-at-metal* Ruthenium Komplexen

Dissertation

zur Erlangung des Grades eines

Doktor der Naturwissenschaften

(Dr. rer. nat.)

des Fachbereich Chemie

der Phillips-Universität Marburg

vorgelegt von

M. Sc.

Erik Winterling

aus

Hanau

Marburg/Lahn

Februar 2022

Die vorliegende Dissertation wurde am Fachbereich Chemie der Phillips-Universität Marburg unter der Leitung von Herrn Prof. Dr. Eric Meggers in der Zeit von Februar 2018 bis August 2021 angefertigt.

Vom Fachbereich Chemie der Philipps-Universität Marburg (Hochschulkennziffer 1180) als Dissertation am 19.04.2022 angenommen.

Erstgutachter: Prof. Dr. Eric Meggers

Zweitgutachter: Prof. Dr. Jörg Sundermeyer

Tag der Disputation: 26.04.2022

Danksagung

Mein besonderen Dank gilt Herrn Prof. Dr. Eric Meggers für die Möglichkeit meine Promotion in seinem Arbeitskreis durchzuführen zu können. Sowohl für die interessante und offene Aufgabenstellung, als auch die Möglichkeit eigene Ideen einbringen zu können und damit Erfahrungen zu sammeln. *Vielen Dank!*

Ich bedanke mich weiterhin bei Herrn Prof. Dr. Jörg Sundermeyer für die Übernahme des Zweitgutachtens der vorliegenden Arbeit. Bei Herrn Prof. Dr. Andreas Seubert bedanke ich mich herzlich für die Bereitschaft, Teil der Prüfungskommission zu sein.

Danke an die Mitarbeiter der Service-Abteilungen des Fachbereichs für schnelle und kompetente Hilfe von analytischen Messungen. Besonderen Dank gilt Dr. Xiulan Xie und Cornelia Mischke der NMR-Abteilung für die unkomplizierte Terminabsprache, Messung und Rückfragen. Den Mitgliedern der Kristallographieabteilung, Dr. Klaus Harms, Dr. Sergei Ivlev, Michael Marsch und Radostan Riedel danke ich für die Messung und Lösung der Einkristalle.

Ich danke allen aktuellen und bisherigen Mitgliedern des Arbeitskreises Meggers für die freundliche Arbeitsatmosphäre. Besonderen Dank für die organisatorischen Abläufe im Labor geht an Marcel Hemming, der guten Seele des Labors, als auch meinen Laborpartnern Yvonne Grell, Philipp Steinlandt, Nemrud Demirel und Dominik Baran. Die Arbeit im Labor wäre ohne euch definitiv nur halb so spaßig gewesen und so manch' Problem nicht gelöst worden. Dr. Frank Abendroth danke ich für seinen großen Erfahrungsschatz den er gerne teilt. Zijun Zhou danke ich für seine Mithilfe und Ideen, sowohl bei der Komplexsynthese als auch bei den Katalysen!

Lilu Zhang und Ina Pinnschmidt danke ich für die Organisation von Bestellungen und Fragen diesbezüglich. Ich danke auch meinem Vertiefungsstudenten Erik Wilhelmi, der bei den $2H$ -Azirinen geholfen hat. Ich hoffe, du konntest etwas mitnehmen auch wenn das Thema nicht so gelaufen ist wie geplant!

Weiterhin danke ich Dr. Johanna Schepp, Dr. Thomas Mietke, Philipp Steinlandt, Nemrud Demirel und Dominik Baran für das Korrekturlesen der Arbeit und das Ausmerzen von so einigen Fehlerleuten!

Meinem ehemaligen Mitbewohner Jakob Möbs danke ich für die gemeinsame Zeit und auch die Hilfestellung mit der ersten groben Kristallstruktur-Lösung die schlussendlich den Wendepunkt markiert hat.

Meiner Familie, die mich während des kompletten Studiums unterstützt hat und ohne die ich die Promotion nicht durchgestanden hätte. Einfach nur *Danke!*

Und last but not least möchte ich meiner Freundin Angelika Diehl dafür danken, mich in der ganzen Zeit unterstützt und vor Allem auch ertragen zu haben. Mir fehlen die Worte um das Auszudrücken was angemessen wäre. *Danke!*

Publications

Publication presented in this thesis:

E. Winterling, S. Ivlev, E. Meggers, *Organometallics* **2021**, *40*, 1148-1155.

Z. Zhou, S. Chen, Y. Hong, E. Winterling, Y. Tan, M. Hemming, K. Harms, K. N. Houk, E. Meggers, *J. Am. Chem. Soc.* **2019**, *141*, 19048-19057.

Kurzdarstellung

Übergangsmetallkomplexe mit metallzentrierter Chiralität, auch *chiral-at-metal* Komplexe genannt, bieten einen nützlichen und erweiterbaren Werkzeugkasten für die asymmetrische Katalyse. Die vorliegende Arbeit konzentriert sich auf die Synthese von chiralen Rutheniumkomplexen mit bisher nicht verwendeten Substituenten, um den elektronischen Einfluss auf die Reaktivität und Enantioselektivität zu untersuchen.

Im ersten Teil der Arbeit (Kapitel 3.1) wird die Synthese von Bis(pyridinyl-NHC)-Rutheniumkomplexen mit 5-Bromo und 4-Dimethylaminosubstitution am Pyridinrest vorgestellt. Bei der Untersuchung der Strukturisomere wurde die Bildung eines gemischten normalen/abnormalen NHC-Komplexes beobachtet und weiter untersucht. Durch Senkung der Temperatur und Verlängerung der Reaktionszeit wurde ein Verhältnis von 9,8:1 zugunsten des gemischten nNHC/aNHC-Komplexes erreicht. Die Bildung dieser gemischten Koordination wurde nur für 5-CF₃ (62%) und 5-Brom (53%) substituierten Komplexen beobachtet, während sowohl die Trimethylsilyl- als auch die 4-Dimethylamino-substitution eine selektive Bildung des nNHC-Komplexes ergab.

Die Trennung der diastereomeren Komplexe wurde durch den Einsatz von (Tolylsulfonyl)benzamidin als chirale Hilfsstoffe realisiert. Aufgrund der nicht C₂-Symmetrie der gemischten Komplexe können vier Diastereomere gebildet werden. Zwei der resultierenden Komplexe waren stabil auf Kieselgel und zeigten identische metallzentrierte Chiralität. Durch Brønsted-Säure induzierte Destabilisierung der Hilfsliganden wurden die entsprechenden Komplexe unter Retention der Konfiguration mit bis zu > 99% *ee* erhalten. Dieses Protokoll wurde erfolgreich auf Di-isopropylphenyl-substituierte Komplexe angewandt, was den Zugang zu sterisch anspruchsvolleren Komplexen ermöglichte.

Der zweite Teil dieser Arbeit (Kapitel 3.2) befasst sich mit der Anwendung der erhaltenen Komplexe in der asymmetrischen Katalyse. Im Einzelnen wurde die Ringkontraktion von Isoxazolen zu 2*H*-Azirinen untersucht. Dabei ermöglichte der 5-Brom-substituierte Komplex eine schnellere Umwandlung bei niedrigeren Temperaturen im Vergleich zu den zuvor berichteten Rhodiumkomplexen. Nach einem breiten Screening der Reaktionsbedingungen wurde ein Maximum von 67% *ee* erreicht. Während der Untersuchung wurden sowohl nichtlineare Effekte als auch eine Licht induzierte Racemisierung des Produkts beobachtet, die durch die verwendeten Rutheniumkomplexe katalysiert wurde. Für die asymmetrische C(sp³)-H-Aminierungsreaktion wurde festgestellt, dass der neu erhaltene gemischte nNHC/aNHC-Komplex eine 160-fach erhöhte *turnover frequency* im Vergleich zum analogen nNHC-Komplex bietet. Dies ermöglichte eine Verkürzung der Reaktionszeit auf bis zu 10 Minuten. Bei der Alkynylierung von Trifluoracetophenon waren die Unterschiede zwischen den nNHC- und den gemischten nNHC/aNHC-Komplexen vernachlässigbar. Die Di-isopropylphenyl-substituierten Komplexe zeigten bei einer propargylischen Substitution eine höhere Enantioselektivität (bis zu 55% *ee*), der gemisch-

te nNHC/aNHC-Komplex lieferte eine niedrige Enantioselektivität (11% *ee*), während der bis-nNHC-Komplex keine asymmetrische Induktion zeigte. Erste UV-Vis-Studien mit Acylimidazolen zeigten eine breite Absorption um 550 nm. Unter den getesteten Komplexen zeigte die 4-Dimethylaminosubstitution ein Maximum bei 640 nm, gefolgt von den gemischten nNHC/aNHC-Komplexen, während die bis-nNHC-Komplexe Maxima bei 520 nm zeigten. Dies könnte in weiteren Studien über die mögliche Anwendung von Rutheniumkomplexen in der asymmetrischen Photokatalyse genutzt werden.

Abstract

Transition metal complexes with metal centered chirality, also called chiral-at-metal complexes, provide a useful and expandable toolbox for asymmetric catalysis. This thesis focuses on the synthesis of chiral-at-metal ruthenium complexes with previously unused substituents to explore the electronic influence concerning reactivity and enantioselectivity.

Within the first part of the thesis (Chapter 3.1) the synthesis of bis(pyridinyl-NHC) ruthenium complexes with 5-bromo and 4-dimethyl amino substitution at the pyridine moiety is presented. During the investigation of structural isomers, the formation of a mixed normal/abnormal NHC complex was observed and further investigated. By lowering the temperature and extending the reaction time, a ratio of 9.8:1 in favor of the mixed nNHC/aNHC complex was achieved. Formation of this mixed coordination was only observed for 5-CF₃ (62%) and 5-bromo (53%) substituted complexes, while trimethylsilyl as well as 4-dimethyl amino substitution showed selective formation of the nNHC complex.

The separation of diastereomeric complexes was realized by application of (tolylsulfonyl)benzamides as chiral auxiliaries. Due to the non-C₂-symmetry of the mixed complexes, four diastereomers can be formed. Two of the resulting complexes were stable against silica gel and were found to consist of the same metal-centered chirality. Brønsted acid induced labilization of the auxiliary ligand under retention of configuration created the corresponding complexes with up to > 99% *ee*. The same protocol was applied to di-isopropylphenyl substituted complexes, providing access to sterically more demanding complexes.

The second part of this thesis (Chapter 3.2) focuses on the application of the obtained complexes in asymmetric catalysis. In detail, the ring contraction of isoxazoles to 2*H*-azirines was investigated. Here, the 5-bromo substituted complex allowed a faster conversion at lower temperatures compared to the previously reported rhodium complexes. After a broad screening of reaction conditions, a maximum of 67% *ee* was obtained. During the investigation, non-linear effects were observed as well as a light induced racemisation of the product catalyzed by the applied ruthenium complexes. For the asymmetric C(sp³)-H amination reaction, the newly obtained mixed nNHC/aNHC complex was found to provide an 160-fold increased turnover frequency compared to the analogous nNHC complex. This allowed a reduction of the reaction time down to 10 min. For the alkynylation of trifluoroacetophenone, the differences between the nNHC and mixed nNHC/aNHC complexes were negligible. For a propargylic substitution, the di-isopropylphenyl substituted complexes showed higher enantioselectivity (up to 55% *ee*), the mixed nNHC/aNHC complex provided low enantioselectivity (11% *ee*) while the bis-nNHC complex induced no enantioselectivity. Initial UV-Vis studies with acyl imidazoles indicated a broad absorption around 550 nm. Among the tested complexes, the 4-dimethyl amino substitution showed a maximum at 640 nm, followed by the mixed nNHC/aNHC complexes, while the bis-nNHC complexes showed max-

ima at 520 nm. This could be used in further studies concerning the potential application of ruthenium complexes in asymmetric photocatalysis.

Contents

1. Theoretical Background	1
1.1. <i>N</i> -Heterocyclic Carbenes	1
1.1.1. Normal NHCs	2
1.1.2. Abnormal NHCs	4
1.2. <i>2H</i> -Azirines	8
1.2.1. Enantioselective Synthesis of <i>2H</i> -Azirines	9
1.3. Chiral-at-Metal Ruthenium Complexes	14
1.3.1. Contribution of the Meggers group	15
2. Aims and Objective	23
3. Results and Discussion	25
3.1. Synthesis of Modified Chiral-at-Ruthenium Complexes	25
3.1.1. Synthesis of Ruthenium Complex 64i	25
3.1.2. Synthesis of Electronically Modified Ruthenium Complexes	29
3.1.3. Synthesis of aNHC Complexes 114a and 114b	40
3.2. Comparison of the Ruthenium Complexes	58
3.2.1. Ring Contraction of Isoxazolones to <i>2H</i> -Azirines	58
3.2.2. Asymmetric Ring-Closing C(sp ³)-H Amination	66
3.2.3. Alkynylation	67
3.2.4. Propargylic Substitution	69
3.3. UV-Vis Absorption	72
3.3.1. UV-Vis Absorption Measurements	72
4. Summary and Outlook	77
5. Experimental Part	81
5.1. General Materials and Methodes	81
5.2. General Procedures	83
5.3. Synthesis of Imidazolium Salts	85
5.4. Synthesis of Ruthenium Complexes	95
5.5. Synthesis of Auxiliaries	108
5.6. General Procedure for Asymmetric C,H Amination	110
5.7. Azirination	111
5.8. Propagyl Substrates	114
5.9. Propargylic Substitution	116
6. References	117
A. Appendix	125
A.1. List of Synthesized Compounds	125
A.2. NMR Yield Calculation	127
A.3. Late Stage Transition Metal Catalyzed Cross Coupling	129

A.4. 2 <i>H</i> -Azirine Extended Screening Table	129
A.5. HPLC Spectra	132
A.6. CD-Spectra	137
A.7. Representative NMR Spectra	138
B. Crystallographic Appendix	159
C. List of Abbreviations	174
D. Statement	176
E. Curriculum Vitae	177

1. Theoretical Background

Chiral molecules gain attention both by industrial and academic research as the demand for enantiopure chiral molecules in the chemical and pharmaceutical industry is significant.^[1] Such non-racemic molecules are either accessed from nature, as part of the *chiral pool* via resolution of racemates, or synthesized in an asymmetric fashion. The asymmetric synthesis mediated by a chiral catalyst is an economic approach as substoichiometric amounts are needed.^[2-4]

The catalytic approaches are classified in three fields, namely biocatalysis, transition metal catalysis and organocatalysis.^[5] Starting in the late 60s, and predominantly during the last decades, transition metal catalysts have been developed for a variety of asymmetric transformations.^[6] The importance of this field was emphasized by awarding the Nobel Prize to Knowles, Noyori and Sharpless for their pioneering work on asymmetric hydrogenation and oxidation in 2001.^[6-9]

In the following, the overall topics of *N*-heterocyclic carbenes as ligands for catalysis (Section 1.1), 2*H*-azirines as synthetic targets (Section 1.2) and chiral-at-metal complexes with a focus on ruthenium complexes (Section 1.3) will be discussed.

1.1. *N*-Heterocyclic Carbenes

Cyclic carbenes which contain at least one α -amino substituent are called *N*-heterocyclic carbenes (NHCs). The structural classes of NHC ligands can be distinguished into normal (**A**, nNHC) and abnormal (**B**, aNHC) NHCs. Due to the delocalised charges, aNHC are also called mesoionic carbenes (MIC) being consistent with the IUPAC definition of mesoionic compounds.^[10] The term remote (rNHC) is used for *N*-heterocyclic carbenes without a direct linked carbene to the heteroatom as in 4-pyrazolylidenes (**C**) or 4-pyridylidene (**D**). The classification into (non) and remote is independent to the classification of nNHC and aNHC, therefore four combinations are possible (Figure 1).^[11-13]

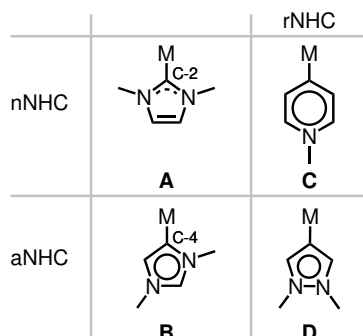


Figure 1: Examples for the structural classes of NHC ligands.

1.1.1. Normal NHCs

The first examples for NHCs were reported by Wanzlick^[14] with the mercury complex **1** and Öfele^[15] chromium complex **2** in the 1960s. The isolation of a free carbene **3** by the group of Arduengo^[16] was a breakthrough in this field as the divalent carbon atom with six valence electrons was considered to be unstable and to tend towards dimerisation (Figure 2).^[17–20]

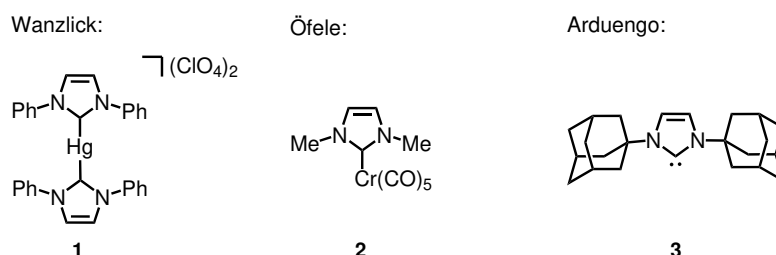


Figure 2: First examples for NHC.

Over the time, NHCs gained more and more attention, growing from a laboratory curiosity into prominent spectator ligands, side by side to cyclopentadienyl (C_5R_5 , short Cp) and phosphines.^[21] Cp ligands, bearing 5 electron ligands (or 6 in case of ionic model) are not as closely related to the NHCs as the monodentate 2 electron phosphine ligands. Among these three types of ligands, the NHCs show a unique feature as the substituents of N-1 and N-3 (in case of imidazolidinylidene as an example) point towards the coordinated metal, while substituents of a Cp are in plane, pointing away from the C_5 centroid (Figure 3). The substituents of a phosphine point away from the coordinated metal. With the substituents in close proximity to the active side of the catalyst, the steric effects are more prominent. As a result, a monodentate NHC ligand will tend to rotate to minimize any steric clashes with other ligands.^[21]

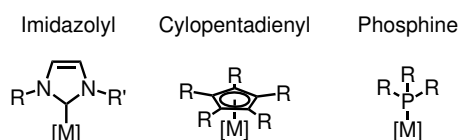


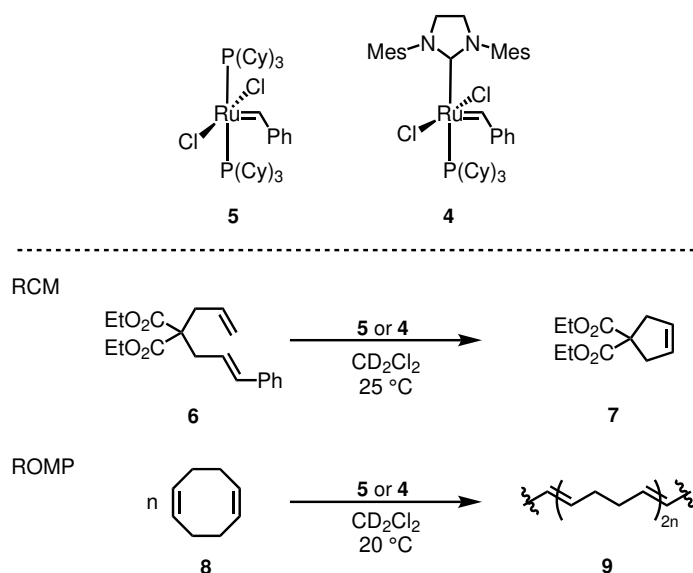
Figure 3: Overview of nNHC, Cp and phosphine ligands.

A side by side comparison using a Tolman type method¹ revealed that NHCs are stronger electron donors compared to phosphines. In detail, the σ -donor strength is much stronger than the donor capability of phosphines. The π -acceptor strength on the other hand is less clear as calculations for both cases, stronger and weaker are reported, so a dependency of substitution, metal and co-ligands can be considered.^[23–28]

NHCs are known to show higher field and higher *trans* effects compared to phosphines, resulting in changed binding characteristics. In case of the Grubbs catalysts (Scheme 1), the Gen. 2 catalyst **4** showed

¹Comparison of $\nu(\text{CO})$ values of metal carbonyl complexes.^[22]

higher binding affinity towards the substrates compared to the Gen. 1 catalyst **5** bearing a phosphine ligand. This improved the activity of ring-closing metathesis (RCM) of malonate **6** to cyclopentene **7** and ring-opening metathesis polymerisation (ROMP) of cyclooctadiene (COD, **8**) to polyene **9** by 100 to 1000 times.^[29–32]



Scheme 1: Grubbs catalyst Gen. 1 (**5**) and Gen. 2 (**4**) for the RCM and ROMP catalysis.

Compared to Cp or phosphine ligands, the chemistry of NHC ligands is more complex as there are no analogues of the so called abnormal NHC (aNHC), which will be discussed later (Chapter 1.1.2), in the field of Cp or phosphine ligands. The C-5 coordination was calculated to be thermodynamically less favored by 23.3 kcal/mol than C-2 coordination. Measurements with a Tolman type method as mentioned earlier suggested a stronger electron donor characteristic of the aNHC bond compared to the nNHC bond.^[27,33] The abnormal binding mode shows different effects considering the C–M bond. Although they are considered to be a stronger electron donor compared to nNHCs, the bond strength is decreased and they have a tendency to cleave from the metal more easily than their nNHC counterparts.^[34–36]

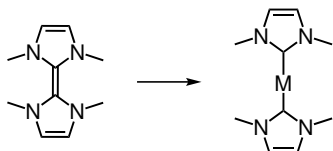
Synthesis Methods

With the growing interest in NHC complexes, several synthesis methods were developed and led the way to specialized catalysts with specific, tunable properties such as steric demand, solubility and electronic effects. For many applications, the NHC ligand is generated by an *in situ* deprotonation of a precursor, such as imidazolium salts, leaving the exact nature of the catalyst unclear. This opens up the possibility of aNHCs which will be discussed later (Chapter 1.1.2).^[31] Over the years, several synthesis methods such as *Lappert method*,^[37,38] *proton abstraction*,^[39] *oxidative addition*,^[40,41] *transmetalation*,^[42] *direct metalation*^[43,44] and *thermal elimination*^[45] were developed (Scheme 2).

1. Theoretical Background

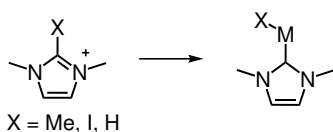
Lappert Method

Metal insertion into C,C double bond.^[37,38]



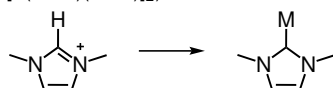
Oxidative Addition

Oxidative addition of a low valent or metal hydride precursor into the C-X bond (X = Me, I, H).^[40,41]



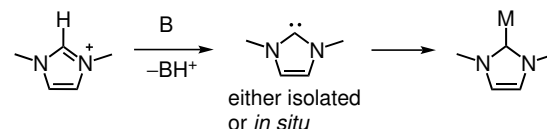
Direct Metalation

Direct metalation using a metal precursor with basic ligands as internal base (e.g. Pd(OAc)₂ or [Ir(COD)(OMe)]₂).^[43,44]



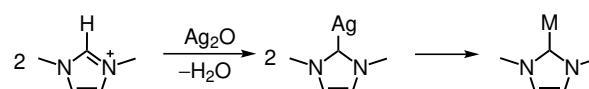
Proton Abstraction

Generation of a free carbene via a proton abstraction with a strong base (e.g. NaH, *n*-BuLi, KO^t-Bu and subsequent metalation).^[39]



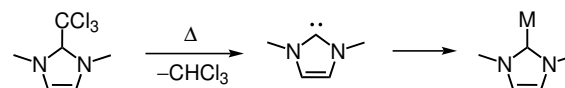
Transmetalation

Transmetalation from a previously prepared silver-NHC complex from the imidazolium precursor and Ag₂O.^[42]



Thermal Elimination

Elimination of H-X from the C-2 carbon atom from a protected form such as NHC-alcohol or -chloroform adduct of the imidazolium precursor.^[45]



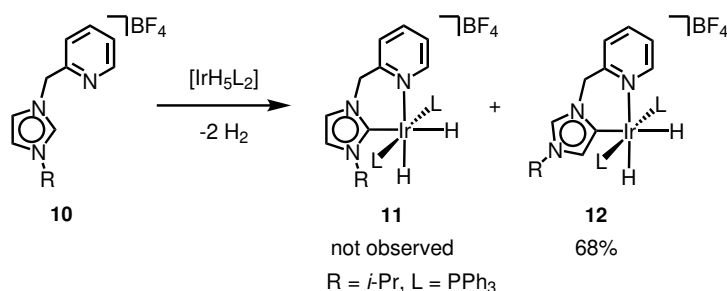
Scheme 2: Synthesis pathways for NHC complexes.

A common issue for bis-NHC ligands are low yielding processes (e.g. transmetalation), as in contrast to phosphines, the NHC ligands binds irreversible and therefore initial kinetic binding modes are maintained. Phosphines as reversible binding ligands can be corrected afterwards to get access to the thermodynamic chelate product.^[21] The formation of aNHC complexes was not reported for the Lappert method, proton abstraction or the thermal elimination pathway.^[31]

1.1.2. Abnormal NHCs

Until the discovery of the Crabtree group in 2001, the metal complexes bearing imidazolyl NHC ligands were expected to coordinate via the C-2 atom. By reacting IrH₅(PPh₃)₂ with the pyridin substituted imidazolium salt **10** in THF under reflux conditions, the expected nNHC complex **11** was not observed. Instead the aNHC complex **12** was characterized by X-ray structure as well as NMR spectroscopy (Scheme 3).^[46]

¹H-NMR spectroscopy showed a low field signal 8.72 ppm which was assigned to the imidazole C-2 proton while a similar signal at 5.17 ppm was assigned to the C-5 proton. The M-C bond length determined



Scheme 3: First reported aNHC complex **12** by the group of Crabtree in 2001.

via X-ray was reported with 2.110(6) Å, suggesting no or a weak M–C π backdonation. The thermal rearrangement into the nNHC complex **11** was tested by heating to 100 °C for 1 h, but no rearrangement was observed. Further heating to 160 °C showed gradual decomposition of the complex. As DFT calculations indicated an energetic difference of > 20 kcal/mol between the nNHC and the less stable aNHC binding mode, the aNHC complex **12** was suggested to be the kinetic product.^[46] Using strong acids like HBF₄, the conversion from aNHC **12** to nNHC **11** was reported in 2011.^[47]

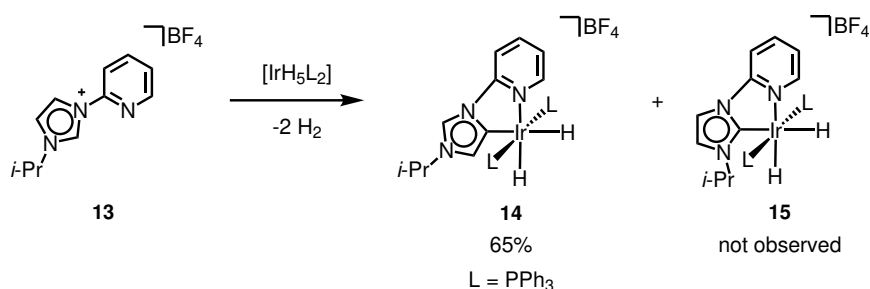
A year after the first report, the same group investigated the effect of anions from the imidazolium ligand precursor (Table 1).^[48] With a methyl group at the imidazole *N*, bromine gave a ratio of 91:9 of nNHC to aNHC complex (entry 1). The ratio shifted to 45:55 for BF₄ (entry 2) and 50:50 for PF₆ (entry 3). A further increase of aNHC complex **12** with a 11:89 ratio was observed with the SbF₆ anion (entry 4). A sterically more demanding group such as *i*-Pr with bromine anion gives a 84:16 ratio (entry 5). Changing to BF₄, the nNHC complex was not observed and exclusively the aNHC complex **12** was formed (entry 6).

Table 1: Ratio of nNHC **11** to aNHC **12** for different alkyl groups and anions.^[48]

entry	R	anion	nNHC 11	aNHC 12
1	Me	Br	91	9
2	Me	BF ₄	45	55
3	Me	PF ₆	50	50
4	Me	SbF ₆	11	89
5	<i>i</i> -Pr	Br	84	16
6	<i>i</i> -Pr	BF ₄	0	100

The authors proposed an ion pairing effect of the imidazolium salt with the anion as the nature of the anion affects the ratio of nNHC to aNHC by stabilization of the transition state leading to the aNHC complex **12**.^[48,49] Also for ligands with small bite-angle such as pyridin-2-yl imidazolium salts **13**, the formation of aNHC complex **14** was observed similar to the methylene bridged precursors **10**, while the nNHC complex **15** was not reported (Scheme 4).^[34]

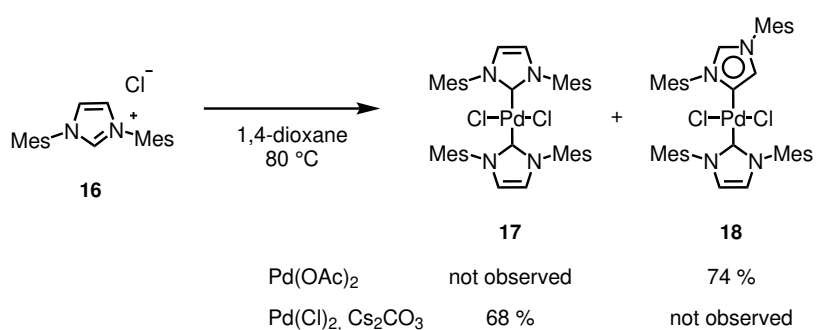
1. Theoretical Background



Scheme 4: Synthesis of the aNHC complex **14** with pyridin-2-yl imidazolium salt **13** which lacks the bridging methylene group compared to imidazolium salt **10**.

A selective formation of the aNHC complex was also promoted by the introduction of a blocking group such as Me, *i*-Pr or Ph at the C-2 carbon of the imidazolium.^[49] This was mainly used for the transmetalation pathway proceeding via a silver carbene intermediate, although some of these blocking groups are less stable (Me, PhCH₂, partially Et) as they can be cleaved via a redox pathway.^[31] This was also reported for Rh(I) and Pd(0).^[50,51]

Besides iridium, aNHC complex of copper^[52], iron^[53] or palladium^[36] have been reported shortly after. In 2004, the group of Nolan reported the first mixed, nNHC/aNHC complex with monodentate ligands. The reaction of Pd(OAc)₂ with *N,N'*-bis(mesityl)imidazolium chloride (**16**) was expected to form the bis-nNHC complex **17** but instead, the mixed nNHC/aNHC complex **18** was obtained in 74% yield. The bis-nNHC complex **17** was not observed. Under basic conditions with Cs₂CO₃ and Pd(Cl)₂, the mixed complex **18** was not obtained and the bis-nNHC complex **17** was isolated in 68% yield (Scheme 5). Treating the mixed complex **18** with different bases did not yield any interconversion into the bis-nNHC complex **17**.^[36]

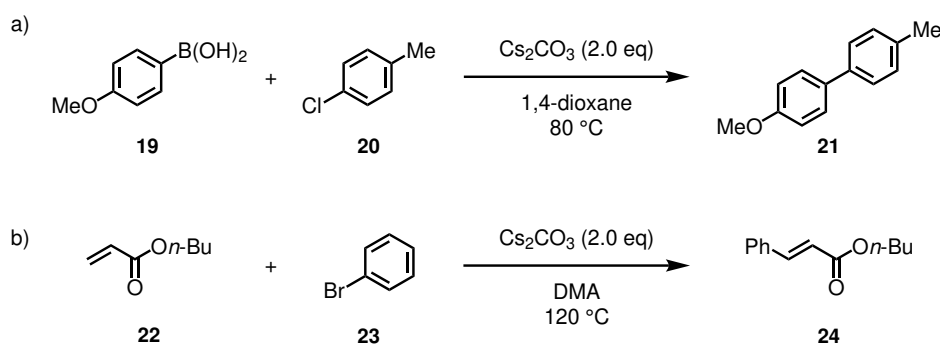


Scheme 5: Synthesis of the bis-nNHC complex **17** as well as the mixed nNHC/aNHC complexes **18**.

Both isolated complexes **17** and **18** were compared with *in situ* generated catalysts from the imidazolium salt **16** and Pd(OAc)₂ in terms of reactivities in a Suzuki Miyaura coupling and a Heck type reaction (Table 2). The bis-nNHC complex **17** showed no conversion for both reactions (entry 1), while the mixed

nNHC/aNHC complex **18** showed 44% yield for the Suzuki coupling and 77% yield for the Heck reaction (entry 2). The *in situ* generated catalyst from a 2:1 ratio of ligand **16** to Pd(OAc)₂ (entry 3) surpassed the mixed nNHC/aNHC complex **18** for the Suzuki-Miyaura with a yield of 76%, while the Heck reaction showed slight decreased yield of 66%. Using an 1:1 ratio (entry 4), the yield for the coupling decreased by 48% to 28% yield, while the Heck type reaction was less affected with a decrease of 10% to 56% yield.

Table 2: Comparison of bis-nNHC complex **17**, mixed nNHC/aNHC complex **18** and *in situ* generated catalysts for the a) Suzuki Miyaura coupling and b) Heck type reaction.^[36]



entry	catalyst (2 mol%)	yield /%	
		21	24
1	17	< 5	< 5
2	18	44	77
3	16 , Pd(OAc) ₂ (2:1)	76	66
4	16 , Pd(OAc) ₂ (1:1)	28	56

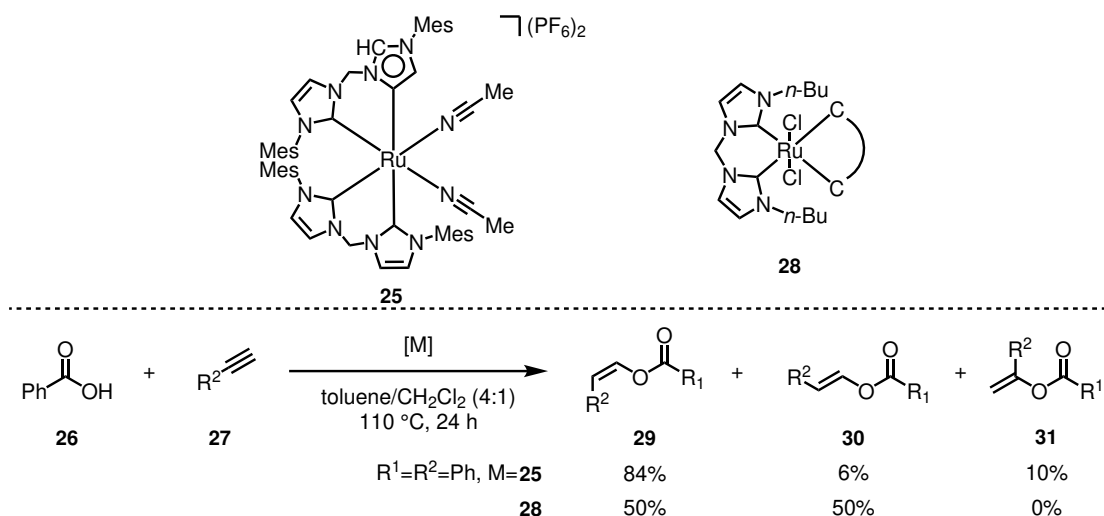
The results of the *in situ* generated catalysts show a closer resemblance to the mixed nNHC/aNHC complex **18** rather to the normal binding mode **17**, indicating previous *in situ* generated catalysts might not be bis-nNHC complexes in nature as it was expected for several years.^[36]

Although aNHC complexes of other metals such as rhodium, platinum, silver as well as yttrium and samarium were synthesized since 2001, the majority of reported aNHC complexes are based on iridium, tracing back to the work of Crabtree *et al.*^[31,54]

The first example of a ruthenium aNHC **25** complex with imidazol ligands was reported in 2012 by the group of Bera *et al.* They used these aNHC complexes as a catalyst for an addition of carboxylic acids **26** to terminal alkynes **27** (Scheme 6).^[55] The aNHC catalyst **25** was compared to a nNHC catalyst **28** in terms of selectivity and activity for the reaction. The aNHC complex **25** showed a selectivity of the *Z-anti*-Markovnikov product **29**, while the *E-anti*-Markovnikov product **30** and the Markovnikov product **31** were obtained in small amounts. Complex **28** showed no differentiation between *E* and *Z* product, while the Markovnikov product **31** was not detected. In terms of activity, the authors reported higher activity

1. Theoretical Background

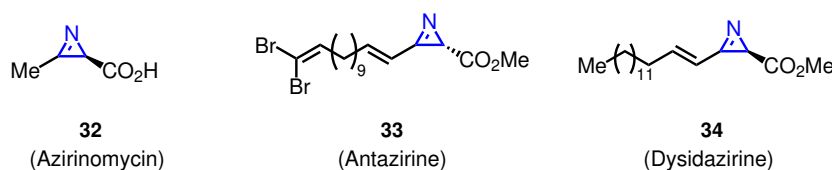
with the aNHC complex **25** for sterically less hindered substrates and generally a higher *Z*-selectivity compared to the nNHC complex **28**.



Scheme 6: Addition of Carboxylic acids to terminal alkynes catalyzed by the ruthenium aNHC complex **25** with a comparison to a ruthenium nNHC complex **28**.

1.2. 2*H*-Azirines

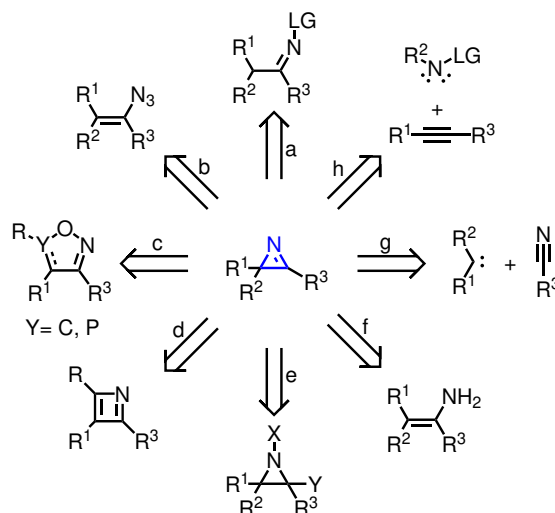
2*H*-Azirines count to the class of small heterocyclic compounds and are an important area of research as this structural motif is present in a variety of biologically active molecules.^[56–58] Among this class of compounds, 2*H*-azirines exhibit the smallest ring size which comes along with an increased ring strain of 45–48 kcal/mol. This results in a useful and reactive building block as the release of this ring strain is a driving force for many reactions.^[59–63] The synthesis of enantiomerically pure 2*H*-azirines is desirable as this structural motive is known in antibiotic natural products such as Azirinomycin (**32**),^[64] Antazirine (**33**),^[65] and Dysidazirine (**34**) (Scheme 7).^[66]



Scheme 7: Natural products Azirinomycin (**32**), Antazirine (**33**) and Dysidazirine (**34**) containing chiral 2*H*-azirines (highlighted in blue).

There are several intramolecular synthetic methods known to access 2*H*-azirines: The Neber-type reactions via base catalyzed eliminations of leaving groups containing imines such as oxime and hydrazone derivatives (Scheme 8, route a).^[67,68] Cyclisation of vinyl azides via thermal or photochemical denitrogenation reactions (route b).^[69–71] Ring contraction reactions of five- and four-membered heterocycles

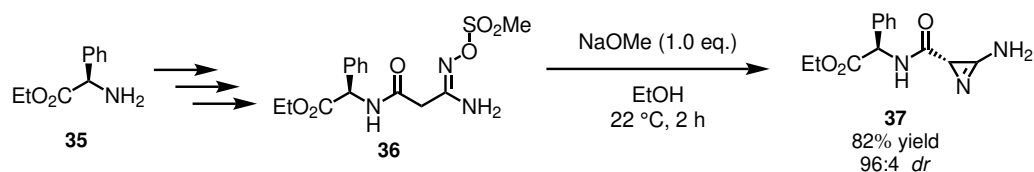
(route c and d).^[72–80] Base-mediated elimination reactions from aziridines (route e)^[81–85] or oxidation of enamines (route f).^[86–93] Intermolecular reactions like cycloadditions of carbenes and nitriles (route g)^[94] or addition of nitrenes to alkynes (route h)^[94–98] are known, although they are reported^[99] to have diminished yields compared to intramolecular versions. In the following, selected examples of asymmetric transformations will be discussed.



Scheme 8: Intra- and intermolecular synthesis paths to 2*H*-azirines: a) Neber-rearrangement, b) thermal or photochemical denitrogenation, c) ring contraction of five membered rings, d) ring contraction of four membered rings, e) base-mediated elimination from aziridines, f) oxidation of enamines, g) cycloaddition of carbenes and nitriles, h) addition of nitrenes to alkynes.

1.2.1. Enantioselective Synthesis of 2*H*-Azirines

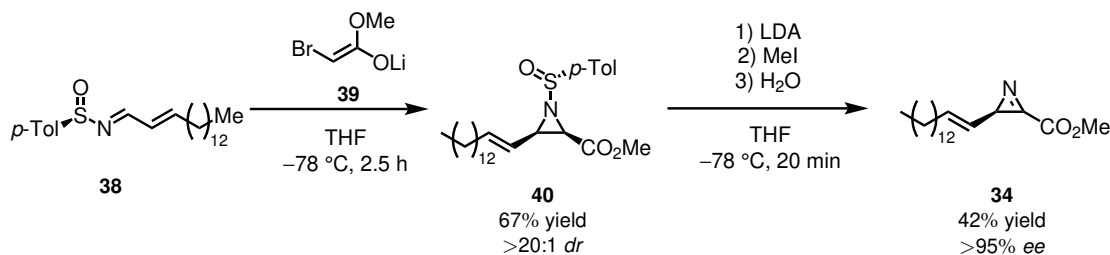
The first examples of asymmetric 2*H*-azirines are based on diastereoselective control using chiral auxiliaries in stoichiometric amounts. Among the synthetic methods depicted in Scheme 8, the first diastereoselective Neber-rearrangement was reported by the group of Vosekalna in 1993 (Scheme 9).^[67] The synthesis started from enantiopure (*R*)-phenylglycine (**35**), which was subsequently converted into (*R*)-amidoxime **36**. Treatment with NaOMe led to the formation of (*2R,3'R*)-2*H*-azirine **37** in 82% yield and 96:4 *dr*. During this step, the *O*-mesyl group (*O*-SO₂Me) acts as the leaving group and the stereochemistry is controlled by the chiral auxiliary. Starting from (*S*)-**35**, the product (*2S,3'S*)-**37** was obtained analogously.



Scheme 9: First asymmetric Neber-type reaction.^[67]

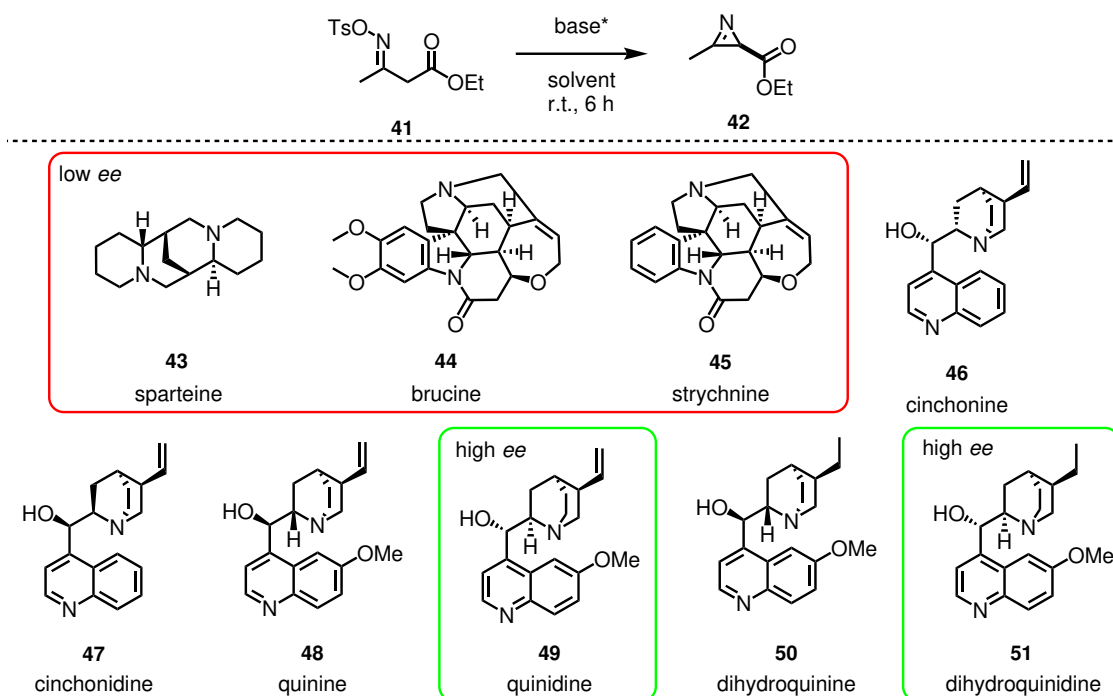
1. Theoretical Background

In 1995, the Davis group reported the first enantioselective synthesis of (*R*)-Dysidazirine (**34**) via a diastereoselective, base-mediated elimination reaction from aziridine **40** (Scheme 10).^[82] The chiral sulfinyl group induces stereoinduction during the reaction of sulfinimine **38** with the lithium enolate **39**. In contrast to the Neber-type reaction (Scheme 9), the chiral auxiliary is also the leaving group and is therefore not retained in the product thus eliminating the necessity of a subsequent auxiliary cleavage.



Scheme 10: First enantioselective synthesis of (*R*)-Dysidazirine **34**.^[82]

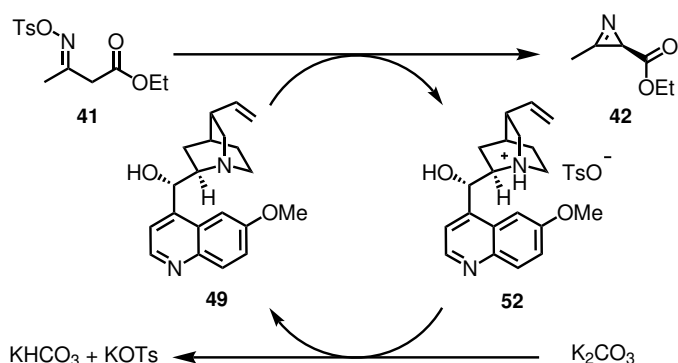
While the examples shown previously rely on stoichiometric amounts of the chiral source, the group of Zwanenburg reported an asymmetric Neber-type reaction using chiral bases as source of chirality. Deprotonation of the ketoxime tosylates **41** and a tightly bound intermediate with the chiral base led to the 2*H*-azirine **42** with varying *ee*. A screening of alkaloid bases showed asymmetric induction by selected alkaloids (Table 3). In detail, sparteine (**43**, Table 3, entry 1), brucine (**44**, entry 2), and strychnine (**45**, entry 3) did not provide high *ee* while three pairs of cinchona alkaloids (entry 4 to 9) showed higher *ee*. Dihydroquinidine (**51**, entry 9) exhibiting the highest enantioselectivity with 47% *ee*. The solvent was found to be critical as protic solvents like EtOH (entry 10) provide no asymmetric induction while CH_2Cl_2 (entry 9) and especially toluene (entry 11) showed higher enantioselectivity of 47% and 70% *ee*, respectively.^[100]

Table 3: Screening of chiral bases and solvents for the chiral base mediated Neber-type reaction.^[100]

entry	base	solvent	yield /%	ee /%
1	sparteine (43)	CH ₂ Cl ₂	53	0
2	brucine (44)		38	5 (<i>S</i>)
3	strychnine (45)		37	4 (<i>S</i>)
4	cinchonine (46)		52	32 (<i>R</i>)
5	cinchonidine (47)		43	24 (<i>S</i>)
6	quinine (48)		34	24 (<i>S</i>)
7	quinidine (49)		37	45 (<i>R</i>)
8	dihydroquinine (50)		41	22 (<i>S</i>)
9	dihydroquinidine (51)		47	47 (<i>R</i>)
10		EtOH	75	0
11		toluene	74	70 (<i>R</i>)

After optimization of the reaction parameters, the chiral base was regenerated *in situ* from the protonated species **52** with K₂CO₃, enabling the application of catalytic amounts of chiral base (10 mol%, Scheme 11).

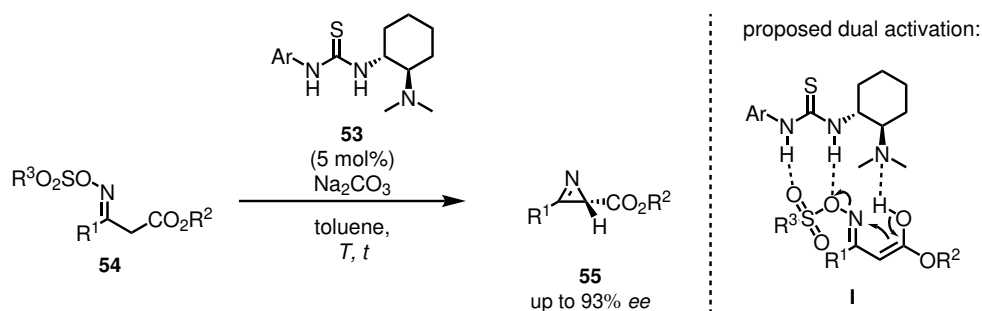
With this catalytic approach, the product **42** was obtained with 70% *ee*, while the stoichiometric methods provide under optimized conditions up to 82% *ee*. The authors proposed a tightly bound substrate/base



Scheme 11: Neber-type reaction using catalytic amounts of **49** as source of chirality. Reprinted with permission from Ref [100]. Copyright 1996 American Chemical Society.

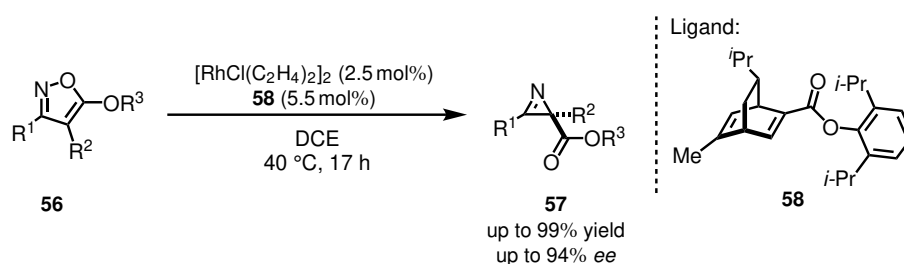
complex as the cinchona alkaloids with a hydroxy group (**46** to **51**) exhibit increased enantioselectivity compared to the bases without hydroxy group (**43** to **45**). This is further supported by the low *ee* in polar solvents such as EtOH, as they can interfere by solvation. This provided a new widely applicable synthetic method to obtain enantiomerically enriched 2*H*-azirine carboxylic esters under mild conditions via asymmetric catalysis conditions without the need of preliminary functionalisation using chiral auxiliaries.

Another catalytic approach by the group of Takemoto was based on chiral thiourea organocatalysts **53** (Scheme 12). These thioureas served as the source of chirality as well as activating the leaving group by H-bonding (**I**). After optimization, a maximum of 93% *ee* was achieved by lowering the temperature down to $-20\text{ }^\circ\text{C}$ and a reaction time of 48 h with a 3,5-(CF_3)₂ substituted sulfonyl group. Control experiments showed the crucial role of thiourea in combination with amide and sulfonamide as the absence led to a decrease of enantioselectivity.^[101]



Scheme 12: Chiral thiourea catalysed asymmetric Neber-type reaction.^[101]

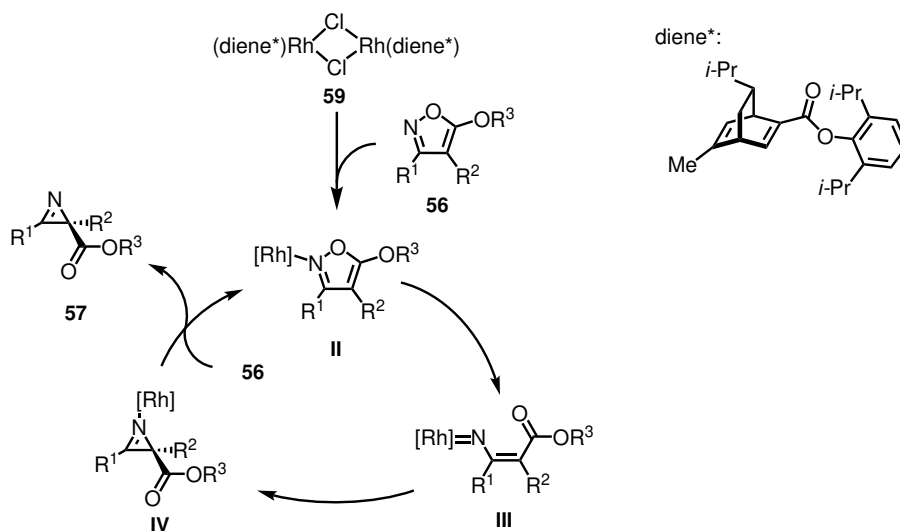
In terms of transition metal catalysis, two examples were shown in 2016: an approach by the Hu group using a kinetic resolution catalysed by a scandium complex with chiral a ligand,^[102] and a racemic ring contraction reaction of isoxazoles by the group of Ohe.^[73] Two years later, the Ohe group reported the enantioselective transformation of isoxazoles **56** to azirine **57**, catalyzed by $[\text{RhCl}(\text{C}_2\text{H}_4)_2]_2$ and a chiral dien ligand **58** (Scheme 13).^[77]



Scheme 13: Results by the Okamoto-group using a chiral diene/rhodium catalyst system for the ring contraction of isoxazoles **56** to chiral 2*H*-azirines **57**.^[77]

The reported substrate scope contains a variety of aromatic groups at R^1 and for R^2 aliphatic, aromatic or halogen moieties were tolerated. Modifications of R^3 were also reported in form of methyl, ethyl, and *i*-Pr substitution, which resulted in the corresponding ester functionality.^[77]

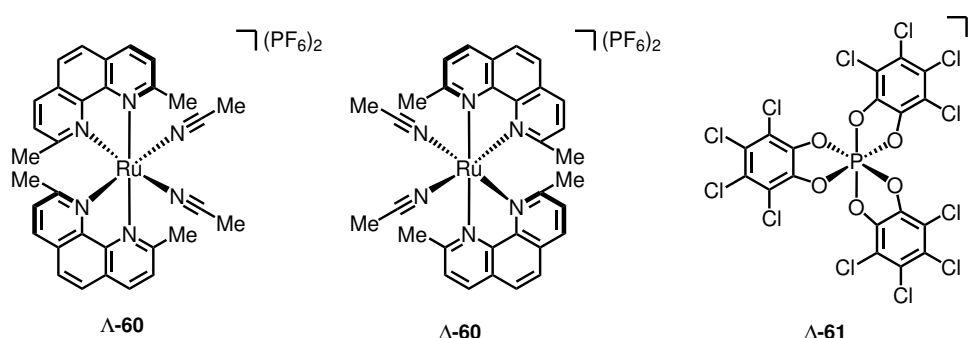
The proposed catalytic cycle (Scheme 14) starts with the coordination of the substrate **56** to the pre-formed chiral diene dirhodium species **59** which forms the isoxazole complex **II**. After *N,O*-bond cleavage, rhodium imido complex **III** is formed, which undergoes a ring reconstruction via nitrene insertion to the azirine complex **IV**. Subsequent release of the product **57** and coordination of substrate **56** leads to intermediate **II**, closing the catalytic cycle. This catalytic cycle is further supported by DFT calculations. The authors reported that no transition states with sufficient low activation barrier were found for a concerted [1,3]-sigmatropic rearrangement from **II** to **IV**.^[77]



Scheme 14: Catalytic cycle of the ring contraction reported by the Okamoto group.^[77]

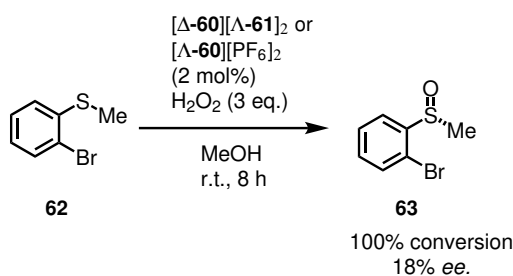
1.3. Chiral-at-Metal Ruthenium Complexes

The first report of octahedral ruthenium (II) complexes with achiral 2,9-dimethyl-1,10-phenanthroline ligands by the group of Fontecave was published in 2003 (Scheme 15). The isolation of each enantiomer was achieved by selective crystallization. Treating a 5 mM solution of *racemic* complex **60** with 1 eq Λ -tris[tetrachlorobenzene-1,2-bis(olato)]phosphate(V) (**61**, TRISPHAT) led to precipitation of complex $[\Delta\text{-60}][\Lambda\text{-61}]_2$ which was filtered off. The obtained yield ranged from 45% to 50% with the opposite enantiomer $[\Lambda\text{-60}][\text{PF}_6]_2$ in solution. The same method could be applied using the opposite enantiomer $\Delta\text{-61}$ leading to the precipitation of $[\Lambda\text{-60}][\Delta\text{-61}]_2$. The shown configurations Δ and Λ can be described as right-handed or left-handed propeller respectively.^[103]



Scheme 15: Initial work by the group of Fontecave in 2003 with the ruthenium complexes **60** in Λ and Δ configuration and the TRISPHAT anion **61** in Δ configuration.^[103]

The complex $[\Delta\text{-60}][\Lambda\text{-61}]_2$ was applied within the same work as catalyst for the asymmetric oxidation of sulfide **62** with H_2O_2 to sulfoxide **63** (Scheme 16) with up to 18% *ee*. The same result was obtained using $[\Lambda\text{-60}][\text{PF}_6]_2$ which resulted in the product **63** with the opposite configuration. This was the first example of chiral-at-metal complexes applied as asymmetric catalysts.^[103]

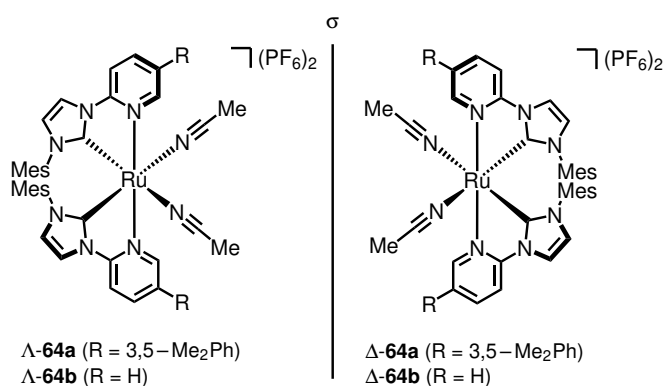


Scheme 16: Asymmetric oxidation of the sulfide **62** to the sulfoxide **63** using the chiral-at-metal complexes **60**.^[103]

1.3.1. Contribution of the Meggers group

Initial Ruthenium Catalyst

Based on the octahedral geometry, the Meggers group as well as others developed chiral-at-metal complexes for asymmetric catalysis.^[104–113] The Meggers group showed a novel chiral-at-ruthenium complex based on two pyridinyl-imidazole-NHC ligands, featuring a similar propeller shaped geometry (Scheme 17).

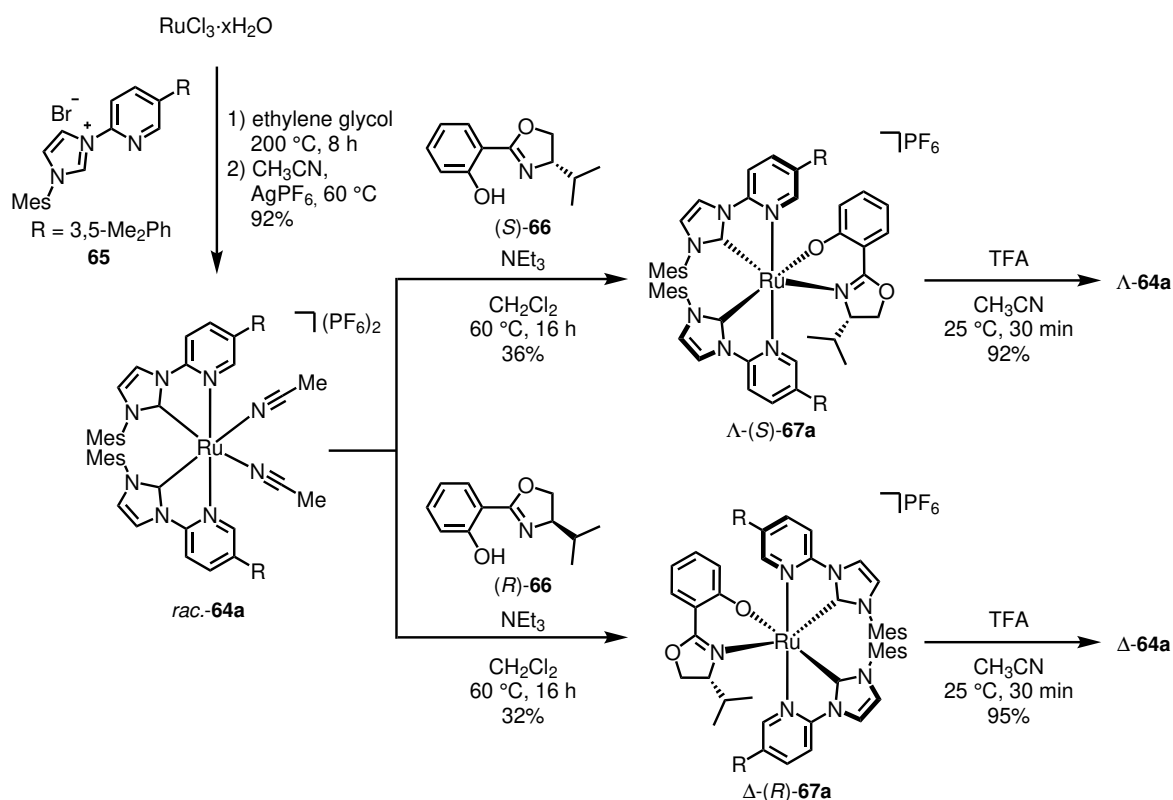


Scheme 17: Chiral-at-metal ruthenium catalysts **64a** and **64b**.^[114]

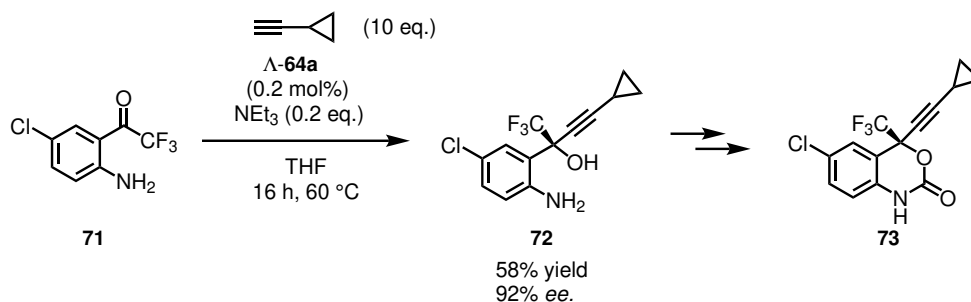
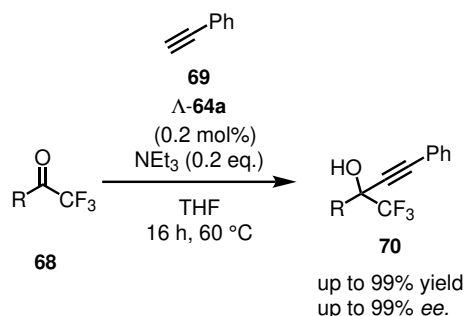
The complex **64a** was synthesized by reacting RuCl₃ hydrate with *N*-(pyridinyl)-imidazolium salt **65** which provided the racemic complex **64a** (Scheme 18). The key step for the chiral resolution is based on the reaction with enantiopure salicyl oxazoline (*S*)-**66** as chiral auxiliary. This reaction converts the racemic complex into two diastereomeric complexes, namely Λ -(*S*)-**67a** and Δ -(*S*)-**67a**. These were separated based on their different physicochemical properties for example during purification via column chromatography, although Δ -(*S*)-**67a** complex was not detected in this example. The unreacted complex was enriched in Δ -**64a** and was subsequently reacted with the chiral auxiliary (*R*)-**66**, providing the corresponding complex Δ -(*R*)-**67a** in 32% yield.

This novel chiral-at-ruthenium complex **64a** was suitable for the asymmetric alkylation of trifluoromethyl ketones **68** with phenylacetylene (**69**) providing access to trifluoromethyl propargyl alcohols **70** with high yields and enantioselectivities (Scheme 19).^[114] During the investigation, a variety of alkynes was converted, including substituted phenyl moieties, heteroaromatic as well as aliphatic substrates. A noteworthy substrate is ketone **71** which was reacted using this strategy, providing the propargylic alcohol **72** with 58% yield and 92% *ee*. This intermediate could be further converted into the HIV-1 reverse transcriptase inhibitor Efavirenz (**73**).

1. Theoretical Background



Scheme 18: Synthesis of enantio enriched chiral-at-metal ruthenium complexes Δ - and Λ -**64a**^[114]

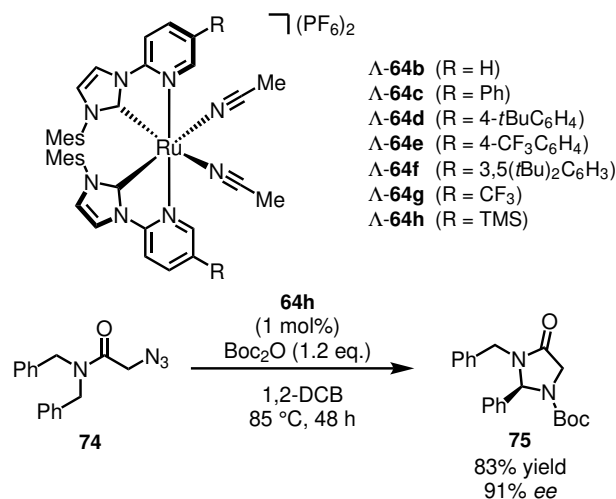


Scheme 19: Asymmetric alkyne synthesis of trifluoro methyl ketones **68** with phenylacetylene **69** with chiral-at-ruthenium catalysts **64a** and **64b** and an exemplary application for the synthesis of the Efavirenz precursor **72**.^[114]

Density functional theory (DFT) calculations suggested a transfer of the nucleophilic alkynyl via a ruthenium alkynyl intermediate to the electrophilic ketone **68**. The trifluoromethyl group was essential for this transformation, increasing the electrophilicity of the ketone. Later, the Meggers group expanded the scope by using perfluorinated acetophenone derivatives, while acetophenone remained still unreactive towards this transformation.^[115,116]

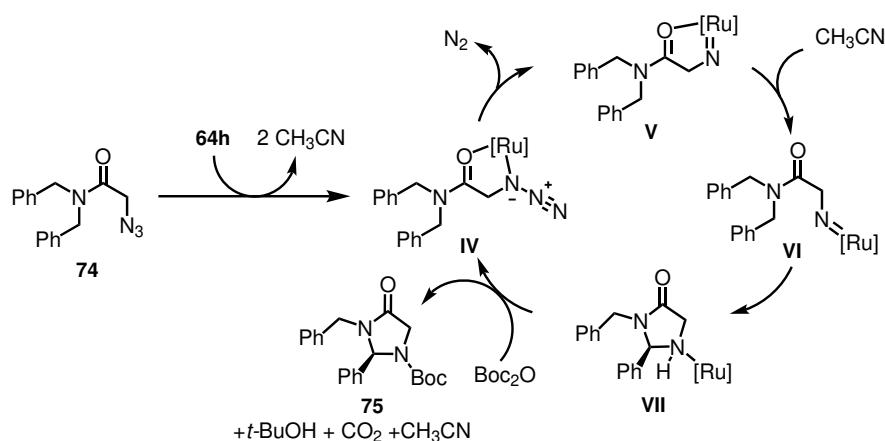
C(sp³)-H Amination of 2-Azido Acetamides

The established catalysis framework was expanded by the Meggers group in 2019 and applied to asymmetric intramolecular C(sp³)-H amination of 2-azido acetamides **74**, which provided imidazolidinones **75** (Scheme 20). The reaction was conducted in presence of di-*tert*-butyl dicarbonate (Boc₂O) in 1,2-dichlorobenzene (1,2-DCB) at 85 °C for 48 h. After various changes on the the catalyst, complex **64h** was found to provide the best result of 83% yield and 91% *ee*.^[117]



Scheme 20: Asymmetric intramolecular C(sp³)-H amination of 2-azido acetamides **74** with chiral-at-metal ruthenium complexes.^[117]

During the investigations, the reaction was found to be selective for benzylic positions as ethylphenyl substitution was not converted into the corresponding product. Experimental data and DFT calculations supported the proposed mechanism (Scheme 21), starting from the coordination of substrate **74** to the ruthenium complex **64h**, which forms the azido intermediate **IV**. Release of N₂ leads to the chelated ruthenium-imido intermediate **V**. Dissociation of the amide under the formation of the nitrene **VI** followed by the C-H insertion leads to the ruthenium coordinated imidazolidinone **VII**. The last step consists of the release of the product **75** in presence of Boc₂O under release of CO₂, *t*-BuOH, CH₃CN and re-coordination of **74**, forming **IV** and completing the catalytic cycle.^[117]

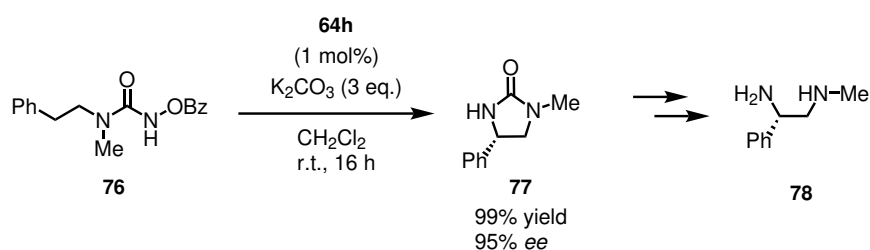


Scheme 21: Proposed mechanism of C(sp³)-H amination of 2-azido acetamides.^[117]

Determination of the kinetic isotope effects (KIEs) indicated a singlet nitrene insertion mechanism with a concerted N-C and N-H formation in contrast to a step-wise mechanism, which would indicate a triplet nitrene. The singlet nitrene was further investigated using an asymmetrical substrate bearing an electron rich and an electron deficient aromatic system. The ratio of the products was determined with 1.4:1 in favor of the electron rich system, hence the nitrene can be described as electrophilic.^[117]

Ring Closing Amination of *N*-Benzoyloxyureas

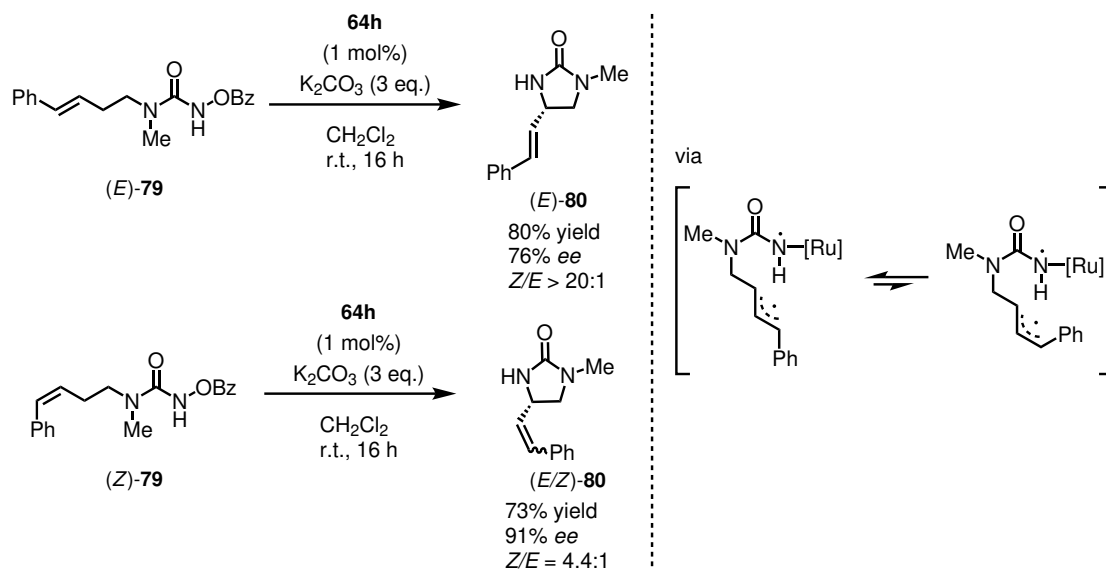
Based on the activity of the catalyst scaffold for metal-nitrene based conversions, the Meggers group was able to show the enantioselective intramolecular C(sp³)-H amination of *N*-benzoyloxyurea derivatives **76**. This provides an access to asymmetric cyclic urea derivatives **77** (Scheme 22) which can be converted into chiral 1,2-diamines **78**.^[118]



Scheme 22: C(sp³)-H amination of *N*-benzoyloxyureas.^[118]

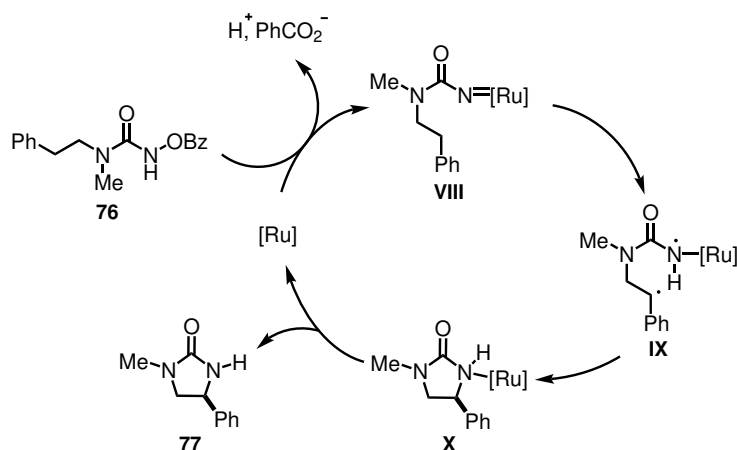
Optimization of the catalyst showed the most favorable catalyst for this reaction was the trimethylsilyl functionalized catalyst **64h**. The effect of the leaving group showed similar results for phenyl, *p*-methoxyphenyl as well as *p*-trifluoromethylphenyl (95% *ee* for phenyl, 94% *ee* for *p*-methoxyphenyl and *p*-trifluoromethylphenyl). A non-aromatic leaving group such as *t*-Bu resulted in a diminished yield of 27% and 91% *ee*.

Mechanistic investigations showed a KIE of 4.35, suggesting a triplet nitrene intermediate which stands in contrast to the previous mechanism (Scheme 21) with a KIE of 1.5. Olefin isomerisation (Scheme 23) further supports a stepwise pathway as isomer (*E*)-**79** reacted under complete retention of alkene configuration, while (*Z*)-**79** showed eroded *Z/E* *dr* of 4.4:1.



Scheme 23: Olefin isomerisation control experiment of benzoylurea derivatives.^[118]

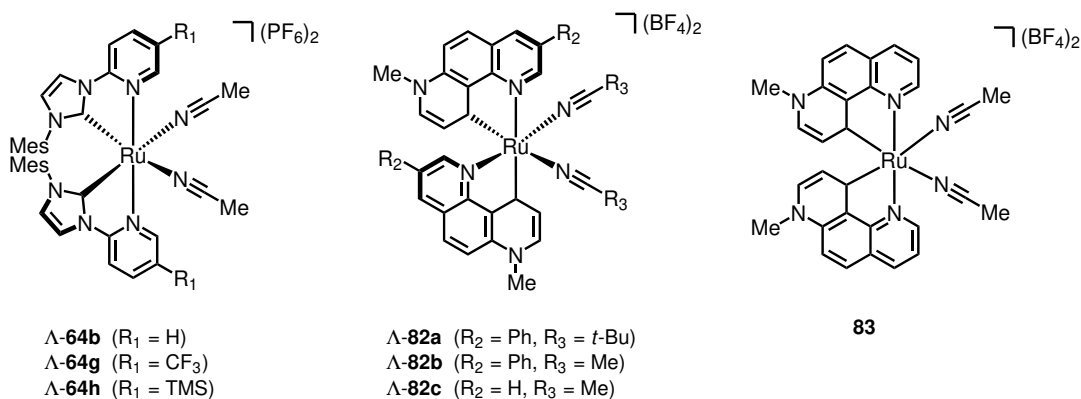
Based on these experiments, a catalytic cycle was proposed (Scheme 24). Coordination of the substrate **76** to the metal catalyst and insertion into the *N,O*-bond leads to release of benzoic acid and the formation of a ruthenium nitrenoid **VIII**. As indicated by the experiments, a stepwise pathway with a 1,5-hydrogen atom transfer (HAT) would provide the intermediate **IX**. Radical-radical recombination of this intermediate would lead to the ruthenium bound product **X**. Release of the product **77** completes the catalytic cycle, regenerating the ruthenium catalyst.



Scheme 24: Proposed catalytic cycle for the C(sp³)-H amination of benzoylurea through a triplet ruthenium nitrenoid.^[118]

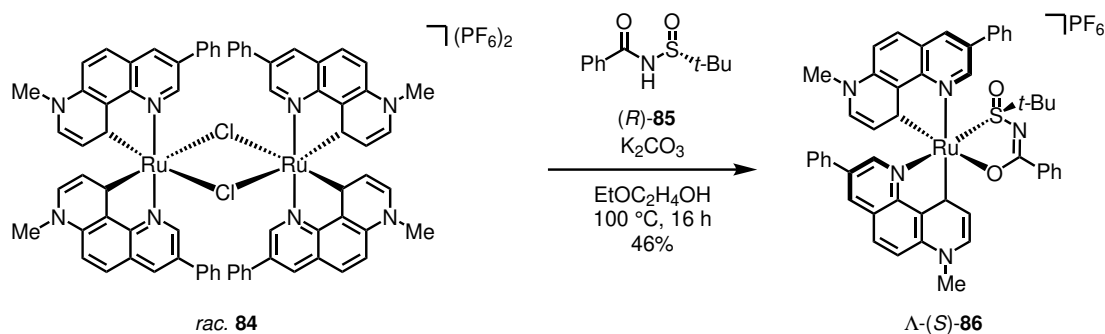
Non- C_2 -Symmetric Chiral-at-Ruthenium Catalyst

While the ruthenium catalysts presented previously by the Meggers group displayed C_2 -symmetry, the Meggers group reported in 2019 a novel type of chiral-at-metal ruthenium complex **82** (Scheme 25).^[119] Based on two 7-methyl-1,7-phenantroline ligands, which therefore belonging to the rNHC complexes, displays the same stereogenic metal centered chirality of Δ and Λ configuration as the previous complexes **64**.



Scheme 25: New non- C_2 -symmetric chiral-at-ruthenium catalysts **82** in comparison to the bis-pyridinimidazolylidene complexes **64** and the C_2 -symmetric complex **83**.

The synthesis proceeded via a racemic chloro-bridged dimer complex **84** and upon reaction with a chiral *N*-benzoyl-*tert*-butanesulfinamide **85**, the core structure isomerised and the auxiliary complex **86** was obtained (Scheme 26). After removal of the sulfinamide, the non- C_2 -symmetric core structure was maintained. Its C_2 -symmetric counterpart **83** was also synthesized from **84** with AgBF_4 in a *racemic* fashion for comparison.

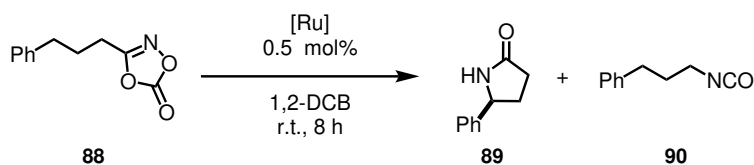


Scheme 26: Isomerisation from C_2 -symmetric complex **84** to non- C_2 -symmetric complex **86**.

This new coordination mode affected the catalytic properties of this complex compared to its C_2 -symmetric counterpart **83** and the established pyridinylimidazole based complexes **64** as shown for the intramolecular $\text{C}(\text{sp}^3)\text{-H}$ amidation reaction of dioxazolone **88** (Table 4). While the non- C_2 -symmetric

complexes **82a**, **82b** and **82c** show high selectivity for the amidation product **89** of 84% to 93% yield over the Curtius-type rearrangement product **90** (entry 1-3), the C_2 -symmetric complex **83** showed a diminished yield for **89** of 38% and an increased yield of 60% for the isocyanate **90** (entry 4). On the other hand, the pyridinyl nNHC complexes **64** showed no evidence for the amidation product **89** (entries 5 to 7), only the isocyanate **90** was detected.

Table 4: C(sp³)-H amidation reaction of dioxazolone **88** catalyzed by different chiral-at-metal ruthenium catalysts.



entry	catalyst	yield /%		
		89	90	<i>er</i>
1	Λ - 82a	93	6	95:5
2	Λ - 82b	92	7	94:6
3	Λ - 82c	84	15	92:8
4	<i>rac.</i> 83	38	60	
5	Λ - 64b	-	>99	
6	Λ - 64g	-	>99	
7	Λ - 64h	-	>99	

Hirshfeld charge analysis showed a corresponding trend as nitrene complexes derived from the non- C_2 -symmetric complex **82c** showed a total Hirshfeld charge of the nitrene of -0.12 , hence a more electron-rich nitrene, C_2 -symmetric complex **83** showed a total charge of -0.11 and **64b** showed a total charge of -0.06 . This corresponds to the reported favored C-H amidation by the Chang group as the electron rich nitrene decrease the C-H amidation barrier.^[120]

This example shows the lower symmetry of complexes change the chemoselectivity of a catalyst by altering the electron density of nitrene intermediates. While higher symmetry is preferred to minimize the amount of possible competing pathways, it was crucial for the selectivity towards the C-H amidation pathway. The overall non- C_2 -symmetric design as well as the abnormal carbene binding mode could therefore be used for further reaction designs.

2. Aims and Objective

In previous studies, the chiral-at-metal ruthenium complexes by the Meggers group, bearing two bidentate *N*-(2-pyridinyl) substituted NHC ligands as well as the non- C_2 -symmetric rNHC, were proven as efficient catalysts for asymmetric alkynylation of trifluoromethyl ketones,^[114] intramolecular C(sp³)-H amination with azides^[121], 1,4,2-dioxazol-5-ones^[119], 2-azidoacetamides^[117], and *N*-benzoyloxyurea^[118] compounds **76** (Figure 4).

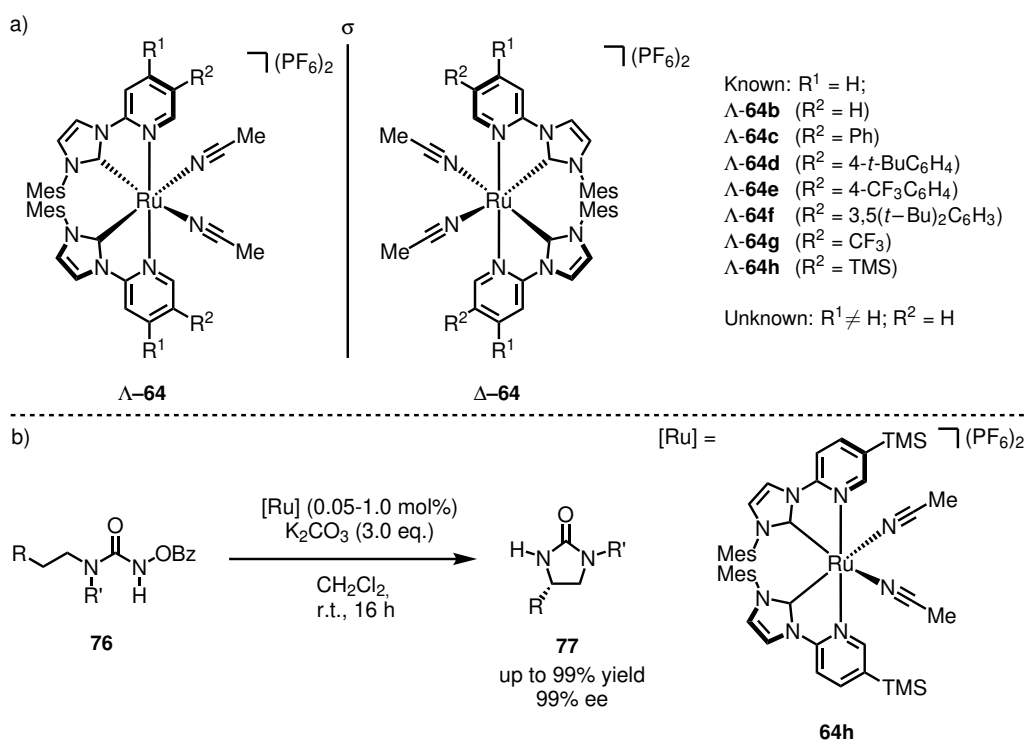


Figure 4: a) Overview of the chiral-at-metal ruthenium complexes with *N*-(2-pyridinyl) substituted NHC ligands. b) Enantioselective amination of *N*-benzoyloxyurea **76** with a chiral-at-metal ruthenium catalyst **64h** by Zhou.^[118]

The substitution at the C-5 position of the pyridine moiety, marked as R², with predominantly electron withdrawing groups (EWG) or steric demanding groups is a common pattern among these catalytically active complexes, while substitution of the C-4 or electron donating groups (EDG) and the resulting effects were not investigated so far (Figure 5).

As the catalytic properties depend on steric and electronic influences of the ligands, the first objective of this thesis was therefore to modify the chiral-at-metal ruthenium complexes at the pyridine moiety in order to obtain further insights into the effects towards catalytic activity and selectivity. Especially the absence of electron donating substituents as well as modifications of R₁, located at the C-4 position of the pyridin moiety, were chosen as points of interests.

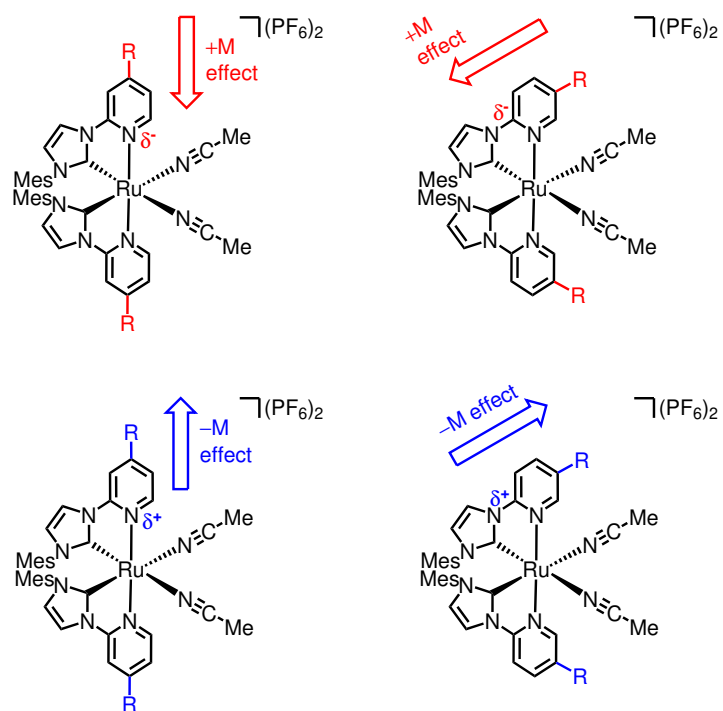


Figure 5: Proposed points of modification with EWG and EDG substituents.

As a secondary objective, by combination of the non- C_2 -symmetric rNHC^[19] with the structural stability of the *N*-(2-pyridinyl)-substituted NHC ligand-system, a modification of the scaffolds to expand the toolbox and provide further insights into the potential of the catalytic system was investigated.

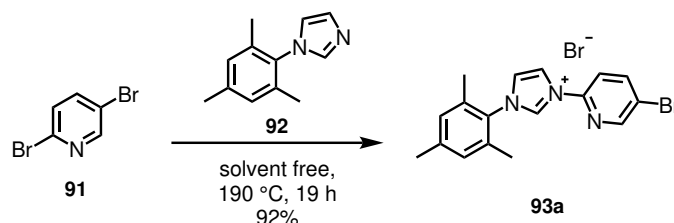
The newly synthesized complexes were to be investigated in regards of changes in the catalytic behavior in terms of activity and selectivity for amination reactions as well as their potential application for currently inaccessible reactions.

3. Results and Discussion

3.1. Synthesis of Modified Chiral-at-Ruthenium Complexes

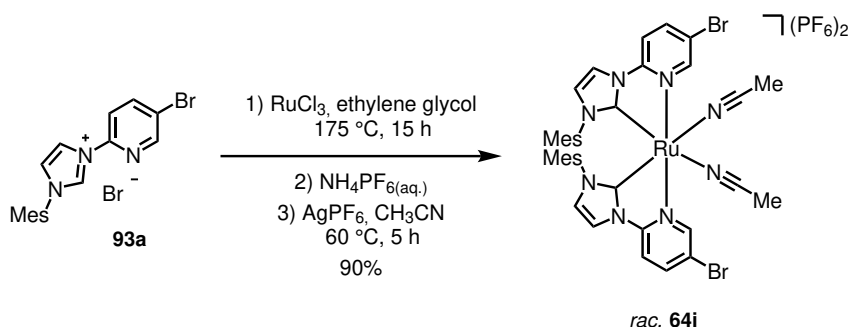
3.1.1. Synthesis of Ruthenium Complex **64i**

The experimental study was initialized with the modification of the chiral-at-metal ruthenium complex **64** by substitution of the pyridinyl moiety with a bromine, which is assumed to provide distinct steric and electronic properties. The synthesis of such compounds which has first been reported by Gründemann *et al.*^[122] and has been modified by the Meggers group over the past years.^[114,117,121] The imidazolium salt was synthesized by reacting 2,5-dibromopyridine (**91**) with 1-mesitylimidazole (**92**) at 190 °C for 19 h and the target imidazolium salt **93a** was obtained in 92% yield as an off-white solid (Scheme 27).



Scheme 27: Synthesis of imidazolium salt **93a** starting from 2,5-dibromopyridine (**91**) and 1-mesitylimidazole (**92**).

Following modified literature conditions, imidazolium salt **93a** and RuCl₃ were stirred in ethylene glycol at 175 °C for 15 h followed by treatment with a saturated aqueous NH₄PF₆ solution (Scheme 28).^[114,117] The yellow precipitation was collected by suction, firmly rinsed with water, redissolved in CH₃CN and stirred with AgPF₆ at 50 °C for 5 h which provided the *racemic* complex **64i** in 90% yield.



Scheme 28: Metalation of the ligand **93a** with RuCl₃ in ethylene glycol following the published procedure by the Meggers group.^[114,117]

The obtained yields were with 90% in the upper range compared to the previous ruthenium complexes of the Meggers group (51% to 92%).^[114,117] Crystals suitable for single X-ray diffraction were obtained by

3. Results and Discussion

slow diffusion of Et₂O into a solution of **64i** in CH₃CN, crystallizing in the monoclinic *C2/c* spacegroup (Figure 6). The structural motives of the mesitylene and the pyridine from each ligand are arranged in a parallel orientation with a distance of 3.511 Å which is consistent with the literature for a π - π interaction of such systems.^[123]

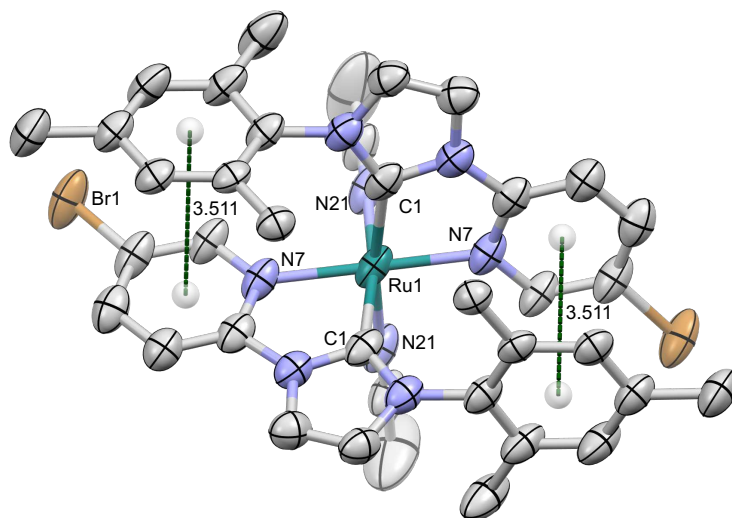
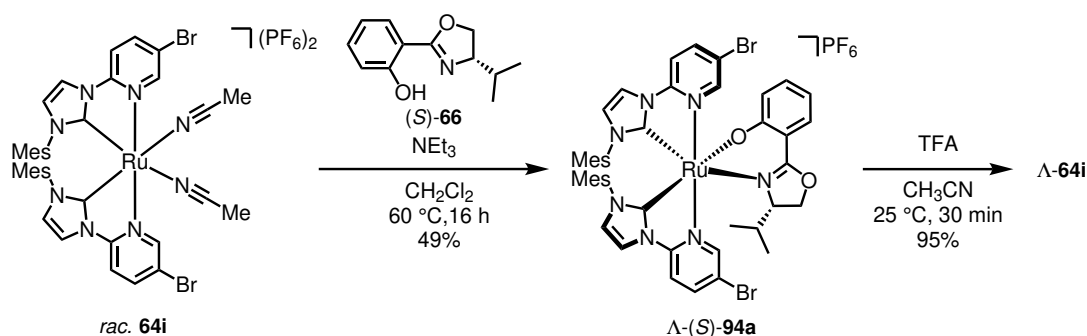


Figure 6: Crystal structure of complex **64i**. ORTEP drawing with 50% probability thermal ellipsoid. The PF₆⁻ counteranion and the solvent molecules are omitted for clarity. Selected bond lengths [Å] and angles [°]: Ru1-C1#1 2.028(5), Ru1-C1 2.028(5), Ru1-N21#1 2.035(5), Ru1-N21 2.035(5), Ru1-N7#1 2.087(5), Ru1-N7 2.087(5); C1#1-Ru1-C1 97.4(3), C1#1-Ru1-N21#1 170.6(2), C1#1-Ru1-N21#1 86.6(2), C1#1-Ru1-N21 86.6(2), C1#1-Ru1-N21 170.6(2), N21#1-Ru1-N21 90.8(3), C1#1-Ru1-N7#1 77.58(19), C1#1-Ru1-N7#1 98.24(19), N21#1-Ru1-N7#1 93.47(19), N21#1-Ru1-N7#1 90.90(18), C1#1-Ru1-N7 98.24(19), C1#1-Ru1-N7 77.58(19), N21#1-Ru1-N7 90.90(18), N21#1-Ru1-N7 93.47(19), N7#1-Ru1-N7 173.8(2). The distance of the centroids is indicated with a dotted green line and given in Å.^[124]

In order to obtain enantiomerically enriched chiral-at-metal complexes, the previously reported chiral auxiliary mediated procedure by the Meggers group^[114] was applied by reacting the complex **64i** with a slight excess of salicyloxazoline (*S*)-**66** under basic conditions in CH₂Cl₂ at 60 °C for 16 h in a pressure tube (Scheme 29). Due to the different physicochemical properties of the two diastereomers, they can be separated via column chromatography during which the diastereomer Δ -(*S*)-**94a** decomposes due to auxiliary cleavage. The complex Λ -(*S*)-**94a** was obtained in 49% yield as an orange to red solid.

With pure Λ -(*S*)-**94a** in hand, an acid induced protonation of the auxiliary in presence of CH₃CN was conducted as the second step by treating a solution of the complex Λ -(*S*)-**94a** in CH₃CN with TFA at 25 °C. The desired enantiomerically enriched complex Λ -**64i** was obtained in 95% yield as a yellow solid.



Scheme 29: Chiral-auxiliary-mediated synthesis of enantiomerically enriched Λ -**64i** using the chiral salicyl oxazoline (*S*)-**66**.

In order to determine the absolute configuration, HPLC-spectra and enantioselectivity for known catalytic reactions were compared to complexes with known configuration.

HPLC analysis (Figure 7) of the enantiomerically enriched complex Λ -**64i** was compared to reported complexes of known configuration. The reported order of elution is Λ as the first eluting complex followed by the corresponding Δ complex.^[114] The major signal with a retention time of 43.5 min corresponds to the first eluting enantiomer, which further suggests Λ -configuration. The minor signal which would be expected at a retention time of 46.0 min was not observed. However, accurate determination of *ee* is not possible due to strong tailing of the major signal. A baseline separation for the two signals was not achieved.

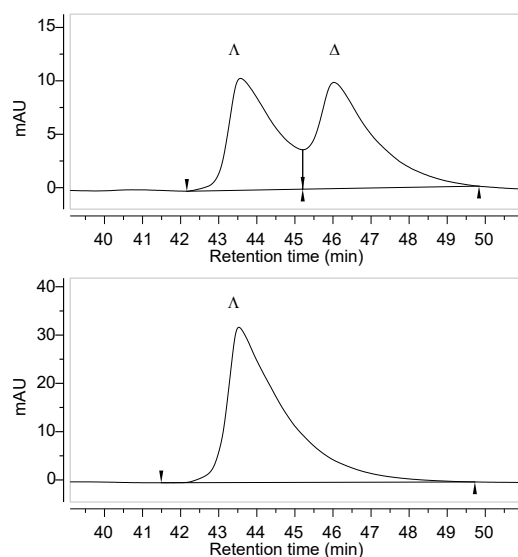


Figure 7: HPLC traces of the racemic (top) and non-racemic (bottom) complex **64i**. Conditions: Chiralpak IB (250 x 4.6 mm), 0.8 mL min⁻¹, H₂O + 0.05% TFA/CH₃CN 75:25, gradient to 70:30 in 50 min, 40 °C, 254 nm.

The complex Λ -**64i** was applied in the previously reported^[14] alkylation of trifluoromethyl ketones and selectivity as well as absolute configuration of the product were compared with the previously reported catalysts. The results, which suggested Λ -configuration, will be shown later in this work (Chapter 3.2.3). CD-spectra analysis (Figure 8) showed positive extrema at 252 nm, 293 nm and 352 nm with negative extrema at 228 nm, 278 nm, 321 nm.

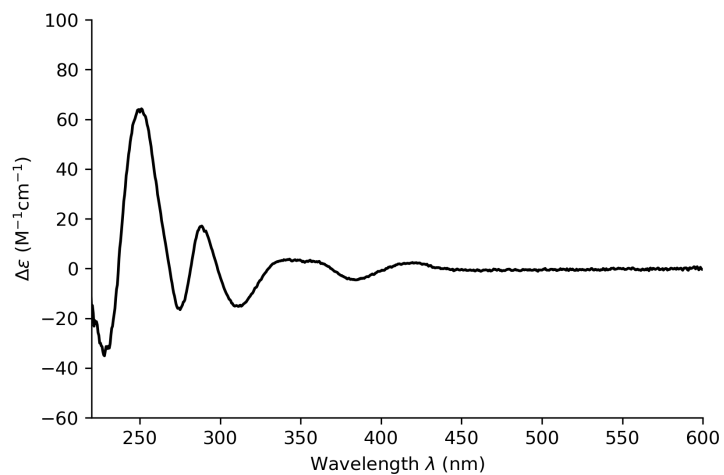
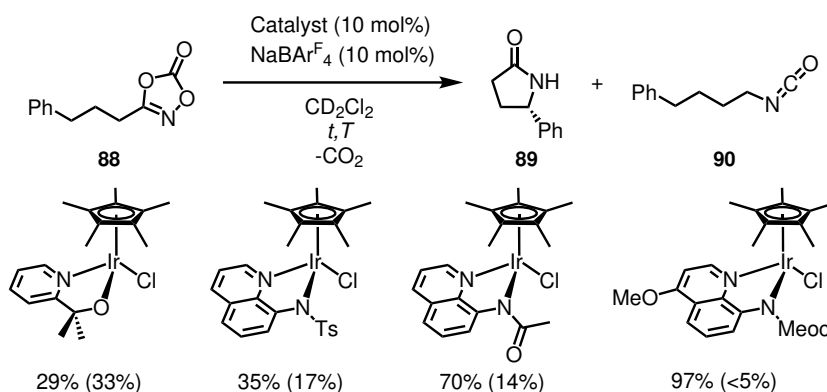


Figure 8: CD-spectrum of Λ -**64i** (MeOH, 0.2 mM).

3.1.2. Synthesis of Electronically Modified Ruthenium Complexes

Catalyst Design

Beside sterics, the electronic properties of the metal center alters the catalytic activity. The Chang group reported 2018 an iridium catalyzed C(sp³)-H amidation starting from 1,4,2-dioxazol-5-ones **88** for a selective formation of γ -lactams **89**.^[120] Here, they managed to change the selectivity by altering the electronic properties of the iridium center via the contact atom of their ligand. Electron donating groups as well as more electron donating contact atoms facilitate the C(sp³)-H insertion to the γ -lactam **89** while suppressing the formation of isocyanate **90** by Curtius rearrangement (Scheme 30). The catalyst system is based on a Cp*-Ir(III) center with a bidentate ligand which was subsequently modified during their research. Starting from an oxygen donor which gave a ~ 1:1 ratio of **89** to **90**, several modifications were made ending with a nitrogen donor ligand that was further modified by electron donating groups (here in form of an OMe and a methoxycarbonyl, short Meoc, group) changing the selectivity of **89** to **90** > 20:1. The change in selectivity is remarkable, especially since DFT calculations indicate a significant higher energy barrier for the C(sp³)-H insertion (12 kcal/mol) compared to the Curtius-type rearrangement (9.6 kcal/mol).^[120]



Scheme 30: C(sp³)-H Amidation reaction catalyzed by different iridium catalysts by the Chang group. The electronic nature of the ligand influences the ratio of insertion and the Curtius rearrangement pathway. The yields are given for **89** and for **90** in parenthesis.^[120]

Based on the previous design with two pyridinyl-NHC ligands and two acetonitrile ligands, it was proposed that modifications of the pyridine moiety should give insights about the electronic effects towards their catalytic properties (Figure 9). A substitution in the 4-position should modulate the N-M bond of the pyridine as the M-effect alters the σ -donor as well as the π -acceptor properties. On the other hand, the modulation of the 5-position should remotely modulate the NHC moiety of the ligand and therefore the C-M bond. This bond is located *trans* to the labile acetonitrile ligands, which are subsequently replaced during the catalytic cycle. Changes in this position would also affect the bond strength of the acetonitriles which could either increase or decrease the exchange rate. As reference systems, a substitution

with a NO₂-group was chosen as the electron withdrawing group as well as a NMe₂-group as the electron donating group.

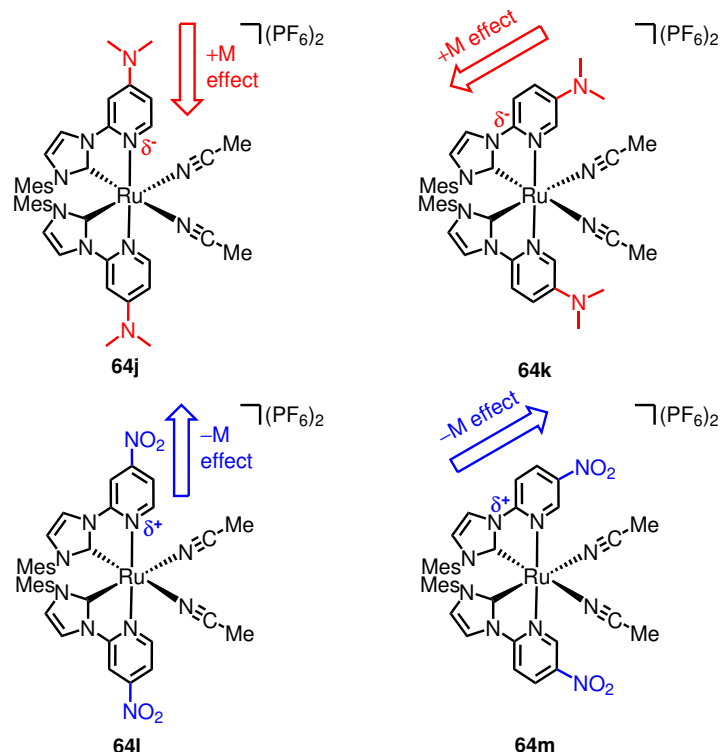


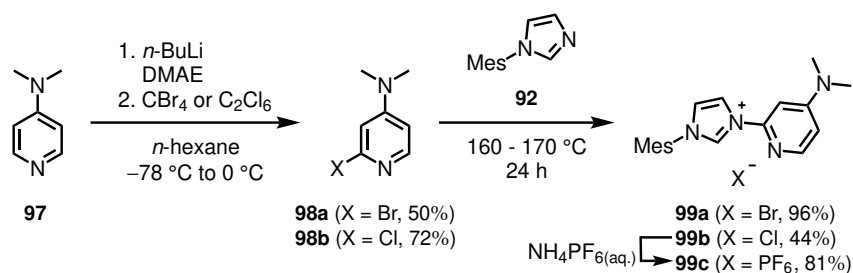
Figure 9: Design concept of chiral-at-metal ruthenium complexes **64j–m** with different modifications of the pyridine moiety at the 4-position (left side) and the 5-position (right side) with electron donating (red) and withdrawing (blue) substituents.

Synthesis of the *N,N*-Dimethylamino Substituted Derivative in C4 Position

The ligand synthesis was planned based on a reported synthesis procedure which includes the S_NAr type reaction of **92** with 2-substituted pyridines (Scheme 31). Starting with the 4-NMe₂ substitution, *N,N*-dimethylaminopyridine (**97**, DMAP) was used as a commercially available starting material. According to a published procedure by Cuperley *et al.*^[125], subsequent lithiation and addition of a halide source like CBr₄ or C₂Cl₆ gave the corresponding halogenated DMAP derivatives **98a** and **98b** in 50% respectively 72% yield as beige to brown solids.

For the next step, the S_NAr type reaction of the pyridines **98a** and **98b** with imidazole **92**, the temperature was decreased to 160 °C and 170 °C, respectively. Here, it was crucial to immerse the reaction vessel fully into the oil bath to avoid sublimation of the pyridines. The ligand precursor as bromide salt (**99a**) was obtained in 96% yield as a beige to brown solid, while the corresponding chloride salt **99b** was obtained in 44% yield as a brown solid. The PF₆-derivative **99c** was precipitated by treating an aqueous solution

of **99b** with a saturated aqueous solution of NH_4PF_6 , providing the target product **99c** with 81% yield as an off white solid.



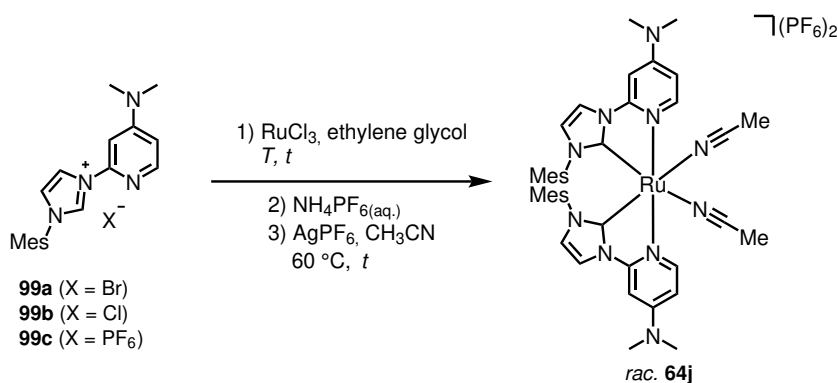
Scheme 31: Synthesis of the 4-*N,N*-dimethylamino substituted ligand precursors **99a–c**.

In theory, chlorine as the more electronegative element should show an increased reactivity as the C–Cl-bond is more polarised compared to the C–Br-bond, but the yield indicated the opposite trend. One explanation could be the mentioned sublimation of the pyridines and the lower molecular weight of pyridine **98b** might ease this process and could not be fully compensated with the decreased reaction temperature.

In order to synthesize the corresponding ruthenium complex, the ligand precursor was reacted with RuCl_3 under similar reaction conditions as shown before (Chapter 3.1.1). Precursor **99a** resulted in the target product **64j** in 43% yield (Table 5, entry 1). Precursor **99b** provided under similar conditions an isolated yield of 50% (entry 2), while imidazolium **99c** showed 56% yield of complex **64j** (entry 3). Furthermore, a second complex was observed under these conditions in a ratio of 73:27 as determined via $^1\text{H-NMR}$ of the crude mixture (Figure 10). Due to insufficient separation, only complex **64j** was isolated. A side by side comparison of the ligand precursor as bromide (**99a**) and chloride (**99b**) salt (entry 4 and 5) with a prolonged reaction time for the third step increased the yield of the target complex **64j** to 58% starting from precursor **99a**. However, the chloride salt **99b** provided the same unidentified complex as major product with impurities. As the reaction time in the third step as well as the nature of the precursor anion seems to affect the reaction, additional experiments were performed. Maintaining the precursor as bromide salt (**99a**), decreasing the temperature of the first step to $120\text{ }^\circ\text{C}$ and keeping the time of the third step short with 1 h, the selectivity towards **64j** is maintained (entry 6). $^1\text{H-NMR}$ -analysis of the crude product showed only traces of the unknown complex. As the unknown complex was already observed using precursor **99c** with PF_6^- -anion, an increase of the reaction time in the third step resulted in no formation of the target complex **64j**.

3. Results and Discussion

Table 5: Reaction conditions for the synthesis of *racemic* **64j** which also gave an unknown complex, here called Dia X.



Entry	99	Step 1		Step 3 <i>t</i> /h	ratio ^a		yield ^b	
		<i>t</i> /h	<i>T</i> /°C		64j	Dia X	64j	Dia X
1	a	19	170	5	100	0	43	0
2	b	18	175	5	100	0	50	0
3	c	21	180	3	73	27	56	0
4	a	18	175	21	100	0	58	0
5	b	18	175	24	0	100	0	87 ^c
6	a	21	120	1	> 95	< 5	58	0
7	c	16	175	18	0	100	0	30 ^c

^a Calculated from ¹H-NMR of the crude mixture after the third step.

^b Isolated yields after column chromatography. ^c Estimated yield assuming similar molecular weight as **64j** including impurities.

The major contributions to the formation are the reaction time of the third step and the nature of the counteranion of the ligand precursor. As the ¹H-NMR spectrum (Figure 10) shows twice the amount of signals compared to **64j**, a non-C₂-symmetric geometry is assumed so far.

Crystals suitable for single X-ray diffraction were obtained by slow diffusion of Et₂O into a solution of **64j** in CH₃CN, crystallizing in the monoclinic *P*2₁/*c* spacegroup. With CH₃CN, complex **64j** crystallizes as yellow plates^[126] whereas CH₂Cl₂ led to crystallisation as green needles.^[127] Both crystals were measured and refined (Figure 11), verifying the expected coordination mode with the pyridine moieties in a *trans* fashion as well as the NHC moieties *trans* to the labile CH₃CN ligands. The distance of the mesityl and pyridine moiety of 3.484 Å and 3.562 Å is similar to the previous obtained distances of 3.511 Å for complex **64i** (Figure 6), thus a π-π interaction of the ligands is assumed.

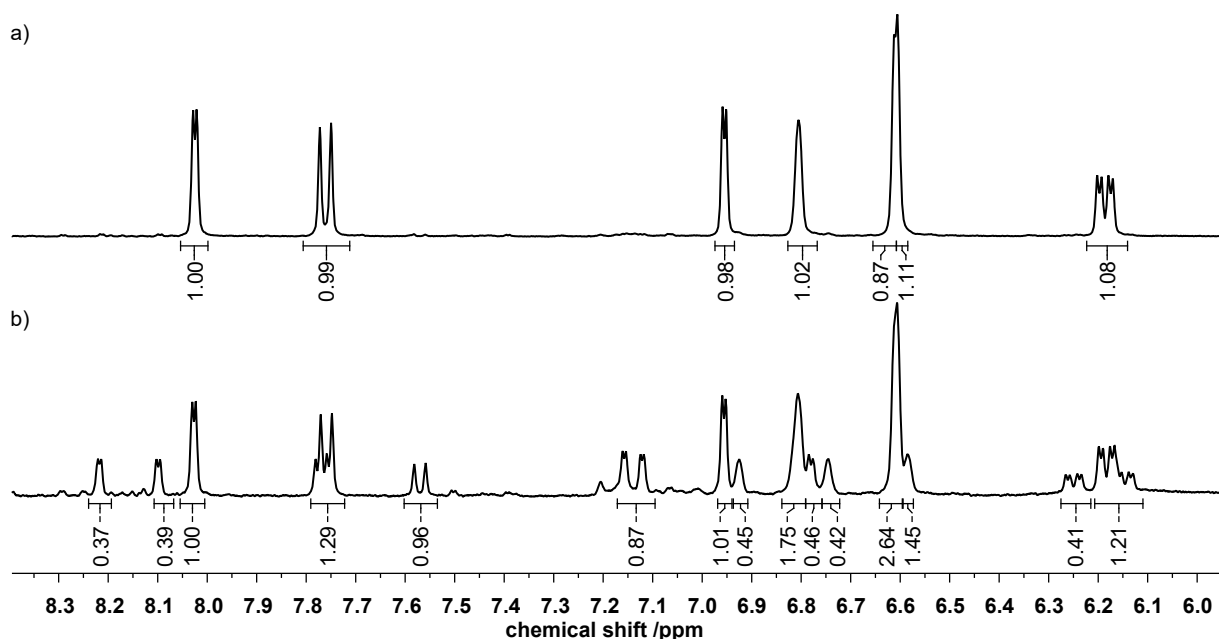


Figure 10: Excerpt of the ^1H -NMR spectrum of a) clean complex **64j** and b) the observed mixture with an unknown complex as shown in Table 5, entry 3. Spectra were recorded in CD_3CN .

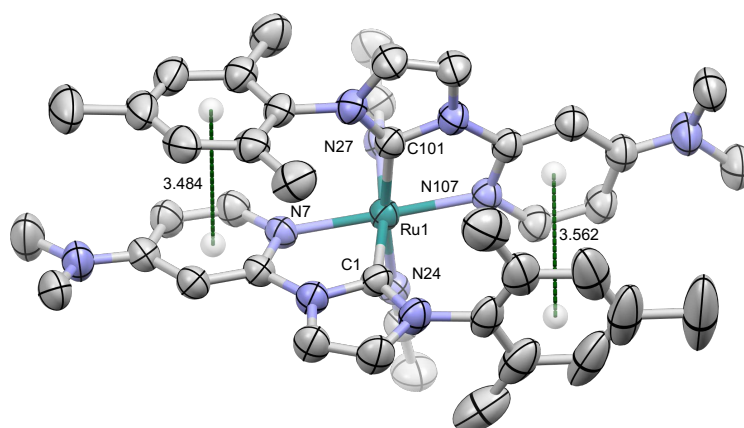


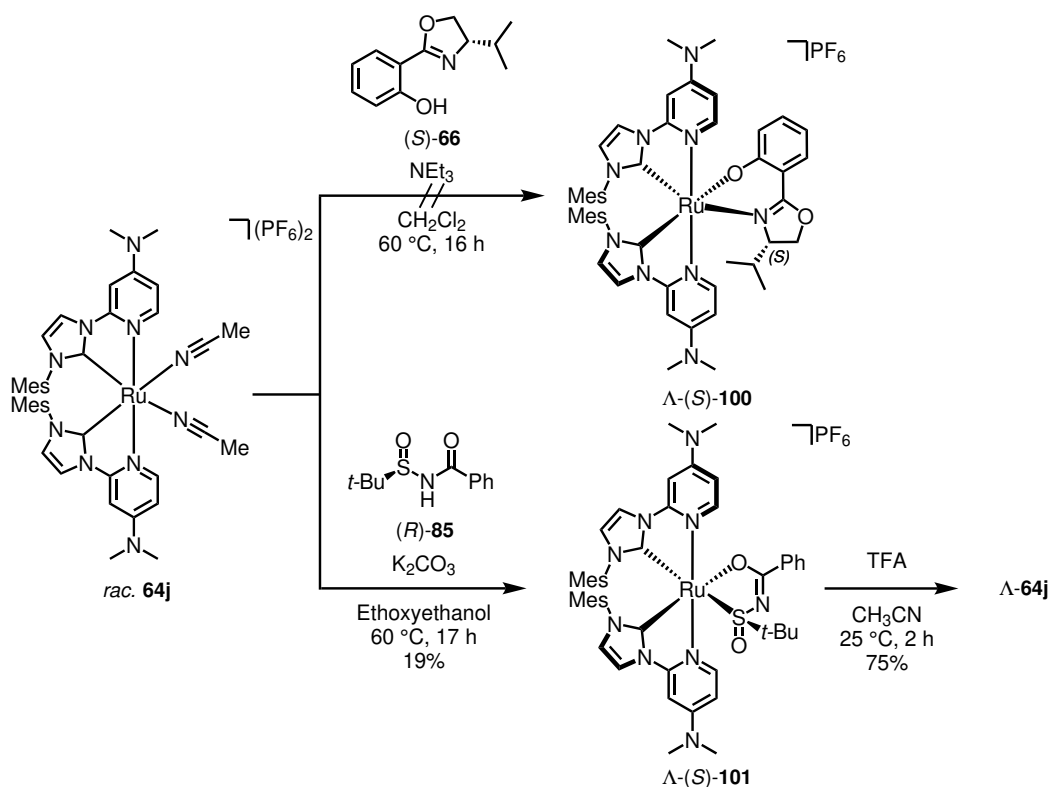
Figure 11: Crystal structure of complex **64j**. ORTEP drawing with 50% probability thermal ellipsoid. The PF_6^- counteranion and the solvent molecules are omitted for clarity. Selected bond lengths [\AA] and angles [$^\circ$]: Ru1-C1 1.979(2), Ru1-N7 2.093(2), Ru1-N24 2.112(2), Ru1-N27 2.109(2), Ru1-C101 1.978(2), Ru1-N107 2.087(2), C1-Ru1-N7 77.62(9), C1-Ru1-N24 94.03(9), C1-Ru1-N27 173.34(9), C1-Ru1-C101 88.9(1), C1-Ru1-N107 100.38(9), N7-Ru1-N24 89.24(8), N7-Ru1-N27 95.85(8), N7-Ru1-C101 99.20(9), N7-Ru1-N107 176.52(8), N24-Ru1-N27 87.08(9), N24-Ru1-C101 171.5(1), N24-Ru1-N107 93.75(8), N27-Ru1-C101 90.88(9), N27-Ru1-N107 86.09(8), C101-Ru1-N107 77.85(9). The distance of the centroids is indicated with a dotted green line and given in \AA .

With the desired complex **64j** in hand, the reported chiral auxiliary mediated procedure by the Meggers group^[114] was applied by reacting complex **64j** with a slight excess salicyl oxazoline (*S*)-**66** in presence of

3. Results and Discussion

NEt₃ in CH₂Cl₂ at 60 °C (Scheme 32). ¹H-NMR analysis of the crude product indicated the formation of complexes Δ-(*S*)-**100** and Λ-(*S*)-**100**, however a sufficient resolution of the two diastereomers via column chromatography could not be achieved. At this time, the Meggers group successfully applied a chiral (*R*)-sulfinyl benzamide **85** as chiral auxiliary.^[119] With this auxiliary, a resolution of the diastereomers was feasible obtaining the corresponding complex Λ-(*S*)-**101**¹ in 19% yield as green solid. Due to insufficient separation of the two diastereomers Δ-(*S*)-**101** and Λ-(*S*)-**101**, no higher yields were accomplished.

After the resolution, complex Λ-(*S*)-**101** was treated with TFA in CH₃CN at 25 °C for 2 h to replace the coordinated auxiliary with CH₃CN ligands (Scheme 32). The enantiomerically enriched complex Λ-**64j** was obtained in 75% yield as a yellow solid which turns green in presence of CH₂Cl₂. The assignment of the absolute configuration was according to the results of previously reported results^[119] and by subjecting complex Λ-**64j** for the reported alkylation of trifluoromethyl ketones.^[114] Comparison of the obtained results with the reported data suggested Λ-configuration and will be shown later in this work (Chapter 3.2.3).

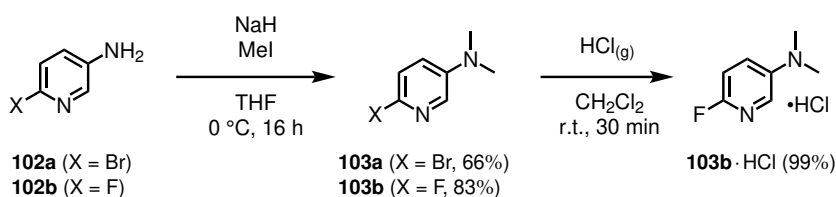


Scheme 32: Top: Attempted chiral resolution of *racemic* **64j** using salicyl oxazoline auxiliary (*S*)-**66**. Bottom: Chiral resolution of *racemic* **64j** using sulfinyl benzamide (*R*)-**101** followed by TFA induced ligand replacement provided complex Λ-**64j**.

¹The formal assignment of the absolute stereochemistry at the sulfur according to the Cahn-Ingold-Prelog priority rules changes from *R* to *S* upon coordination.

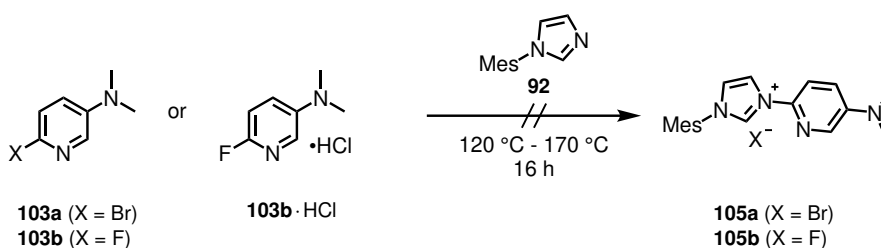
Synthesis of the Dimethylamino Substituted Derivative in C-5 Position.

Following a modified reported procedure by Bejoymohandas *et al.*^[128], 6-bromo-3-aminopyridine (**102a**) was reacted with NaH and methylene iodine in THF at 0 °C, provided the dimethylated product **103a** in 66% yield as a yellow solid. The fluorine derivative **102b** was subjected to the same procedure which provided the corresponding dimethylated pyridine **103b** in 83% yield as a colorless liquid. This compound was later converted into its hydrochloride salt **103b**·HCl by precipitation from a CH₂Cl₂ solution and HCl(g) in near quantitative yield as a colorless crystalline solid (Scheme 33).



Scheme 33: Synthesis of the 3-NMe₂ substituted pyridines **103a**, **103b** and **103b**·HCl.

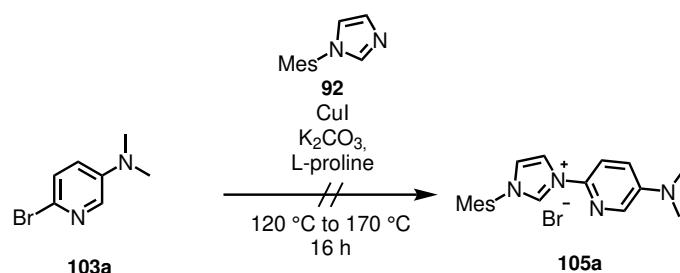
Similar to the previous imidazolium salts **93**, **99** or **104**, the pyridines **103a** and **103b** were heated to 120 °C with imidazole **92** under solvent free conditions (Scheme 34). Neither for bromine derivative **103a** nor the fluorine derivative **103b** showed formation of the product **105a** or **105b**. The temperature was raised to 170 °C for additional 24 h which did not result in product formation. To decrease the electron density of the pyridine system and therefore increase the reactivity towards a S_NAr reaction, the pyridine hydrochloride **103b**·HCl was synthesized as shown earlier. The protonation of the pyridine should therefore counter the +M-effect of the NMe₂-group. The hydrochloride salt **103b**·HCl was heated under solvent free conditions with imidazole **92** to 170 °C for 17 h which provided a mixture of compounds. Purification neither by fractional precipitation nor by column chromatography provided a clean product.



Scheme 34: Attempted synthesis of the 5-NMe₂ substituted ligand precursor **105**.

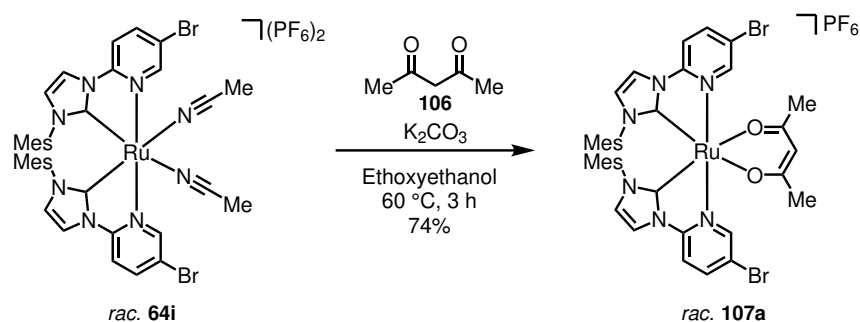
The bromine derivative **103a** was also subjected to Ullmann conditions with CuI, K₂CO₃ and L-proline in DMSO at 90 °C for 18 h (Scheme 35). After TLC indicated incomplete conversion, the reaction was stirred for additional 48 h at 90 °C, but no product formation was observed.

3. Results and Discussion



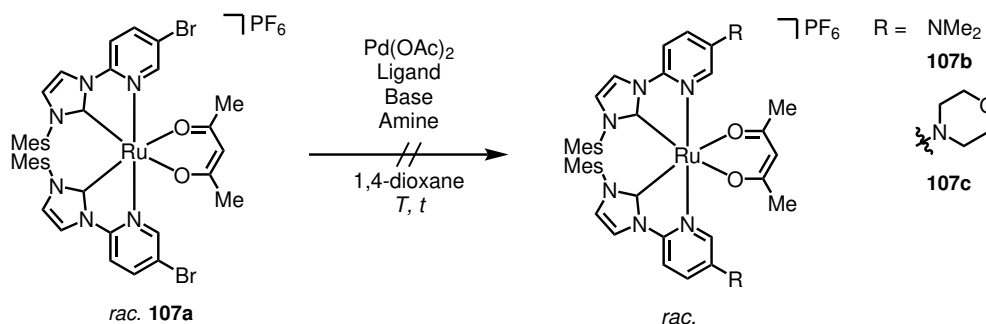
Scheme 35: Attempted synthesis of the 5-NMe₂ substituted ligand precursor **105** with a copper catalyzed Ullmann coupling reaction.

To circumvent the possible complex formation of the used transition metal, a post-complexation derivatization approach, inspired by the previous work in the Meggers group, was investigated.^[129] As starting material, the ruthenium complex **64i** was chosen as it bears a halogen atom at the desired position of the ligand. The complex **64i** was reacted with acetylacetonone (acac, **106**) in ethoxyethanol at 60 °C for 3 h which provided the target complex **107a** in 74% yield as an orange to red solid (Scheme 36).



Scheme 36: Synthesis of the ruthenium complex **107a**.

The complex **107a** has increased solubility in less polar solvents compared to the bis-acetonitrile complex **64i**, resulting in a wider applicable range of solvents for the post complexation derivatization. With the complex **107a** in hand, the late stage Buchwald Hartwig cross coupling was investigated (Scheme 37).



Scheme 37: Tested Buchwald conditions for the late stage modification of **107a**.

The complex **107a**, 10 mol% Pd(OAc)₂ as catalyst, equal amount of SPhos as ligand, 4 eq of Cs₂CO₃ and 3 eq of NMe₂·HCl (**108**) were reacted in 1,4-dioxane at 60 °C for 24 h in a pressure tube (Table 6, entry 1), but no product complex **107b** was observed. Increasing the catalyst and ligand loading to 40 mol% (entry 2) showed also no conversion of the complex **107a**. The amine was changed to morpholine (**109**) as the major amount NMe₂ might be in the gas phase at 80 °C, but still no conversion was observed (entry 3). The catalyst loading was increased to 30 mol%, the ligand to 40 mol% and the reaction temperature to 100 °C (entry 4) but no conversion was observed within 24 h. The base was changed to NaOt-Bu, which is a reported alternative used for lower catalyst loadings (entry 5).^[130] This showed no conversion to the desired complex **107c**. A change of the ligand to RuPhos (entry 6) also showed no conversion.

Table 6: Tested conditions for the Buchwald Hartwig cross coupling of complex **107a**.

Entry	Pd(OAc) ₂ /mol%	Ligand	loading /mol%	Base	Amine /eq.	<i>T</i> / °C	<i>t</i> / h	
1	10	SPhos	10	Cs ₂ CO ₃	4 108	3	60	24
2	40	SPhos	40	Cs ₂ CO ₃	4 108	3	60	20
3	10	SPhos	15	Cs ₂ CO ₃	3 109	3	80	18
4	30	SPhos	40	Cs ₂ CO ₃	3 109	3	100	24
5	10	SPhos	20	NaOt-Bu	3 109	3	80	18
6	10	RuPhos	10	NaOt-Bu	1.3 109	3	80	16

After evaluation of the topology of a putative oxidative addition product,² the palladium is shielded from either direction by the phosphine ligand, the mesityl moiety of the ruthenium complex or the bromine (Figure 12). With this, a coordination of the amine to the palladium would be unlikely and therefore explains the results of the attempted cross coupling as the amine coordination is inhibited.

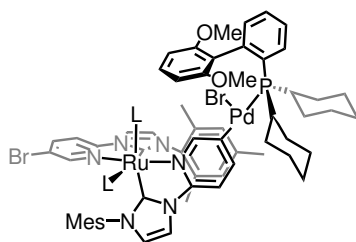
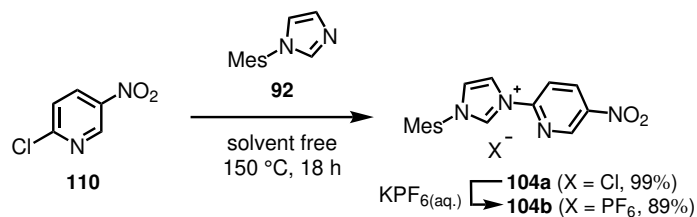


Figure 12: ChemDraw representation of a putative intermediate after oxidative addition of palladium into the C–Br bond and coordinated SPhos ligand with the back orientated ligand in grey.

²Based on calculations from ref. [131] and X-ray structure from ref. [132]. For a three dimensional projection with added Van der Waals spheres, see Figure 40 in Chapter A

Synthesis of the NO₂ Substituted Derivative in C-5 Position

Following modified literature conditions,^[122] commercially available 2-chloro-5-nitropyridine (**110**) was heated with imidazole **92** under solvent free conditions to 150 °C for 18 h provided the target imidazolium salt **104a** in near quantitative yield as a beige solid (Scheme 38). The PF₆ salt **104b** was precipitated by treating an aqueous solution of **104a** with a saturated aqueous solution of KPF₆, providing the target product in 89% yield as an off white solid.

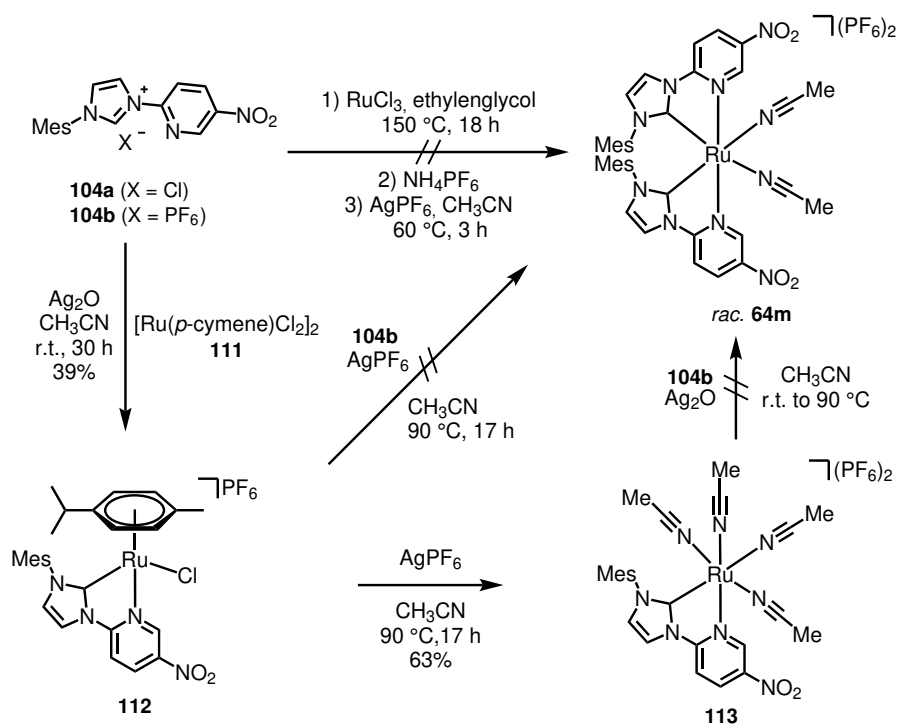


Scheme 38: Synthesis of the 5-NO₂ substituted ligand precursors **104a** and **104b**.

The two imidazolium salts **104a** and **104b** were reacted with RuCl₃ under conditions shown previously (Scheme 39), but according to ¹H-NMR analysis the target complex **64m** was not formed. Neither imidazolium salt **104a** nor **104b** were detected by ¹H-NMR or TLC, indicating complete decomposition of the imidazolium salts, rendering this synthesis approach unsuitable.

In 2011, Bernet *et al.* reported a synthesis route which included the synthesis of a piano-chair complex with a bidentate triazole ligand which was converted into a tetra acetonitrile complex. So it was envisioned that the imidazolium salts **104a** and **104c** might behave similarly.^[133] To circumvent a direct metalation, the transmetallation procedure reported by Bernet *et al.* was applied by reacting [Ru(*p*-cymene)Cl₂]₂ (**111**) with the imidazolium salt **104b** and Ag₂O as transmetallation reagent in CH₃CN at an ambient temperature for 30 h. The *p*-cymene NHC complex **112** was obtained in 39% yield as a yellow solid. The complex **112** was reacted with the imidazolium salt **104b** in CH₃CN at 90 °C for 17 h using a pressure tube but the target complex **64m** was not obtained. Instead, the tetra acetonitrile complex **113** was obtained in 63% yield as a yellow solid. The complex **113** was reacted in presence of Ag₂O and the imidazolium salt **104b** in CH₃CN first at room temperature and subsequent heating to 90 °C using a pressure tube, however the target complex **64m** was not obtained under these conditions.

3.1. Synthesis of Modified Chiral-at-Ruthenium Complexes



Scheme 39: Tested conditions for the synthesis of complex *racemic* **64m**.

Parallel to this investigation, a more promising discovery was made, so the investigation of the 5-NMe₂ and 4-NO₂ substitution was discontinued at this point.

3.1.3. Synthesis of aNHC Complexes 114a and 114b

During the investigation of the modified catalysts, a new complex was formed by reducing the temperature from 200 °C to 150 °C besides the known complex **64i** which was obtained in 39% yield. ^1H -NMR analysis showed two species, which were collected as one fraction during column chromatography, in a 1:2.1 ratio. The minor compound was identified as unreacted imidazolium salt **93b** by the characteristic signals at 7.51, 8.41 and 9.26 ppm for the uncoordinated imidazol moiety (Figure 13). The major compound showed twice the amount of expected signals for the target ruthenium complex **64i**, so a non- C_2 -symmetric complex was proposed (Scheme 40).

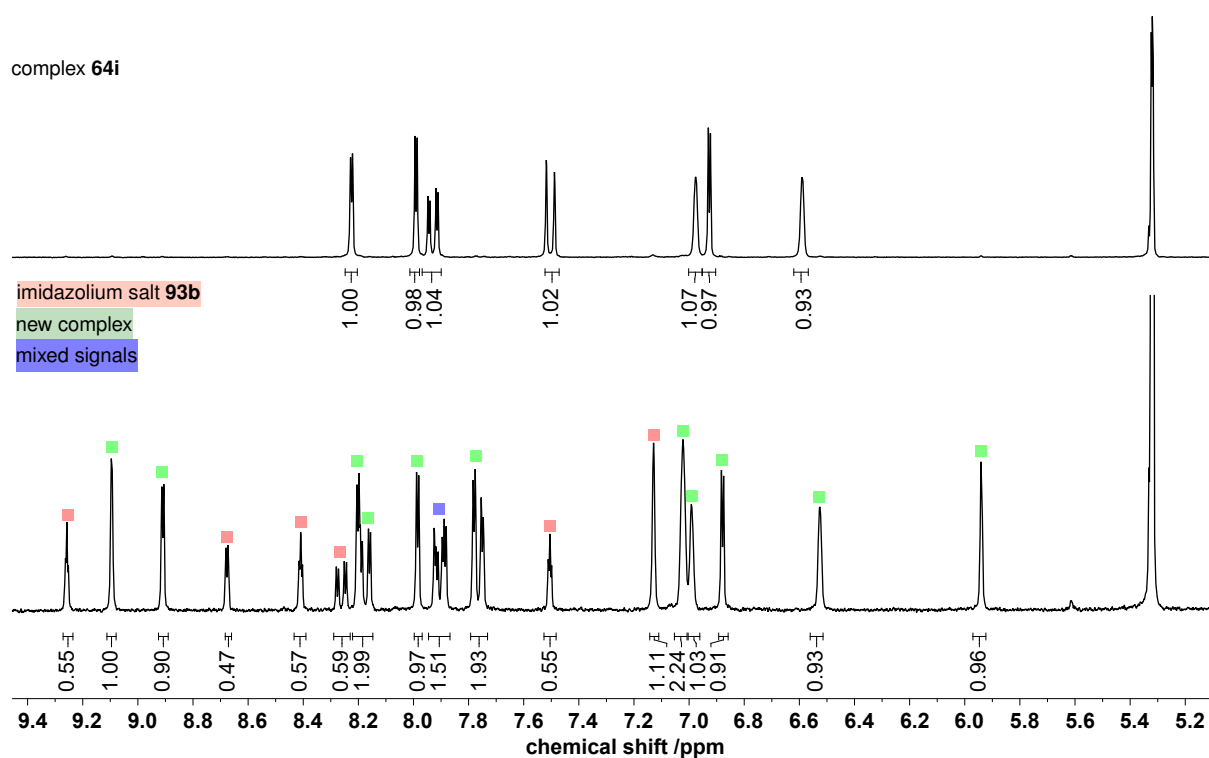
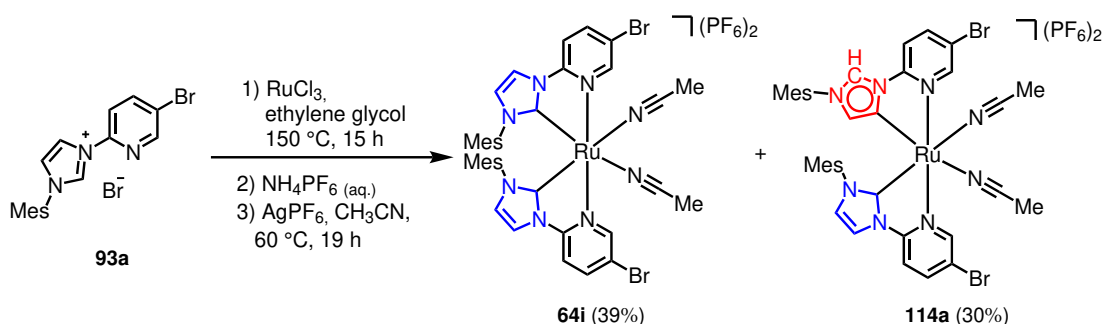


Figure 13: Comparison of the ^1H -NMR (measured in CD_2Cl_2 , 300 MHz at 300 K) of complex **64i** (top) with a new species (highlighted in green), obtained in a 1:2.1 mixture with imidazolium salt **93b** (highlighted in red,). Indistinct signals resulting from both compounds are highlighted in blue.



Scheme 40: First occurrence of non- C_2 -symmetric aNHC complex **114a**.

Single crystal analysis provided final proof for the non- C_2 -symmetric complex where one NHC ligand coordinates with the abnormal C4 carbon (Figure 14). This new complex features two coordination modes, a nNHC and an aNHC ligand, which was expected to have unique catalytic properties. The mesityl moiety of the nNHC and the pyridin moiety of the aNHC ligand were, in a parallel orientation with a distance of 3.489 Å, similar to the bis-nNHC complex **64i**. The mesityl moiety of the abnormal bound ligand points away from the metal center.

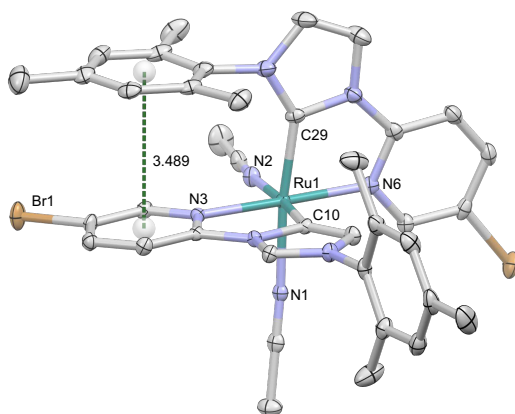
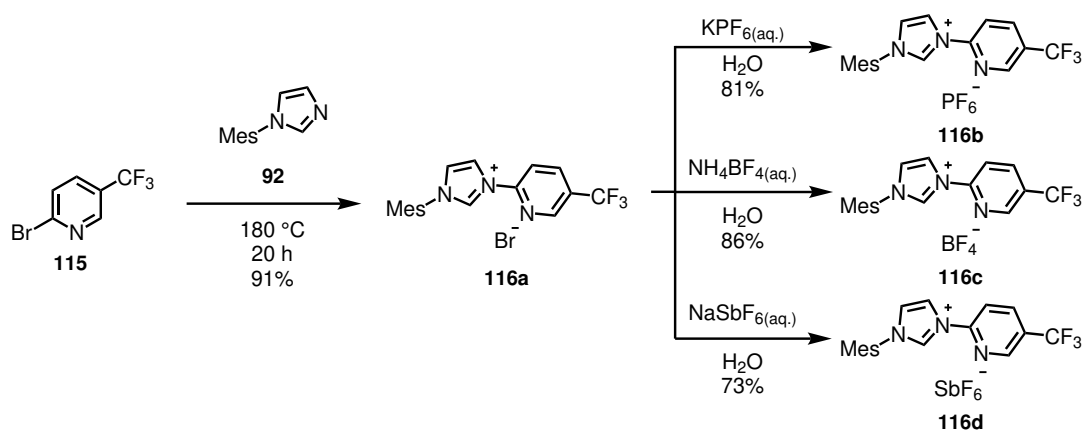


Figure 14: Crystal structure of complex **114a**. ORTEP drawing with 50% probability thermal ellipsoid. The PF_6^- counteranion and the solvent molecules are omitted for clarity. One imidazole part of the ligand coordinates with the abnormal C4 carbon.^[134] Selected bond lengths [Å] and angles [°]: Ru1-C10 2.012(3), Ru1-C29 1.983(2), Ru1-N1 2.114(2), Ru1-N2 2.104(2), Ru1-N3 2.084(2), Ru1-N6 2.072(2), N2-Ru1-N3 96.11(8), N2-Ru1-N6 89.38(8), N2-Ru1-C2 992.8(1), N2-Ru1-C1 0175.27(9), N2-Ru1-N1 88.85(8), N3-Ru1-N6 173.96(8), N3-Ru1-C2 999.2(1), N3-Ru1-C1 079.21(9), N3-Ru1-N1 86.87(8), N6-Ru1-C2 978.0(1), N6-Ru1-C1 095.33(9), N6-Ru1-N1 95.77(8), C29-Ru1-C1 088.7(1), C29-Ru1-N1 173.5(1), C10-Ru1-N1 90.19(9). The distance of the centroids is indicated with a dotted green line and given in Å.

Besides the shown complex **114a**, the corresponding CF_3 derivative **114b** was obtained as well and used for further investigation as $^1\text{H-NMR}$ analysis of the crude mixture allowed clear identification of individual signals for each compound (Figure 37, Chapter A).

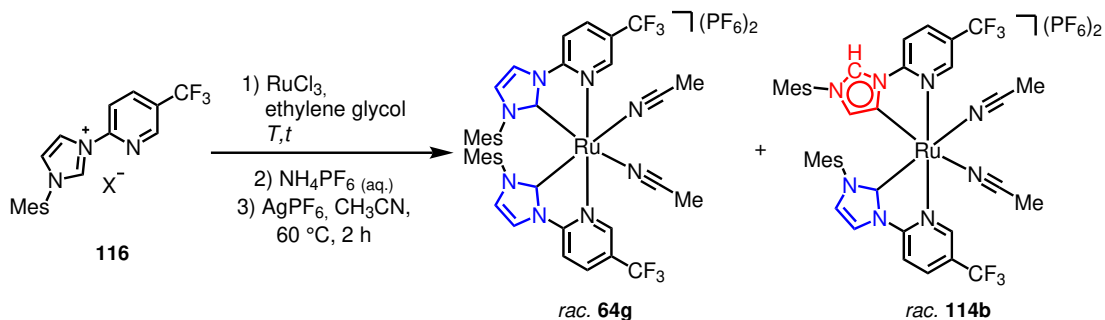
3. Results and Discussion

As mentioned earlier (Chapter 1.1.2), a preference of aNHC to nNHC depended on the anion of the used ligand precursor was reported by Crabtree *et al.* for their iridium complex.^[48] Therefore, the influence of Br⁻, PF₆⁻, BF₄⁻ and SbF₆⁻ as anion for this system was investigated. The synthesis of these ligands followed the previous reported procedure for the CF₃ ligand and counteranion exchange in similar fashion to the previous ligands. 2-Bromo-5-(trifluoromethyl)pyridine (**115**) was reacted with imidazole **92** under solvent free conditions at 180 °C for 20 h. This provided the imidazolium salt **116a** in 91% yield as a off white crystalline solid. Precipitation from an aqueous solution either with aqueous KPF₆, NH₄BF₄ or NaSbF₆ provided the corresponding imidazolium salt **116b** (81%), **116c** (86%) and **116d** (73%) as off white crystalline solids (Scheme 41).



Scheme 41: Synthesis of the CF₃ substituted imidazolium salts **116a**, **116b**, **116c** and **116d**.

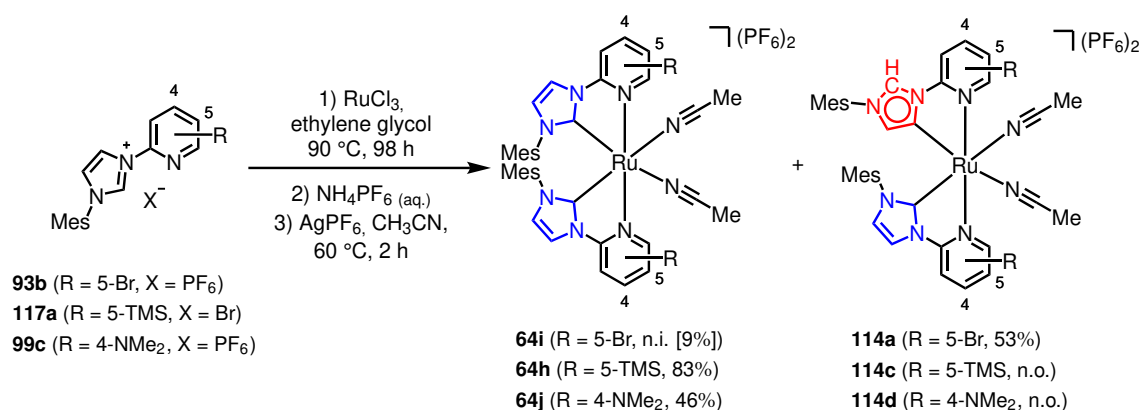
With the imidazolium salts in hand, the synthesis of the aNHC complex was investigated (Table 7). At 200 °C and the bromide salt **116a** as ligand precursor, only the formation of the nNHC complex **64g** was observed (entry 1). Lowering the temperature to 120 °C with an increased reaction time of 63 h provided a NMR yield for **64g** of 19.4% and for **114b** of 48.7% resulting in a ratio of 2.5 : 1 in favor of the aNHC complex **114b** (entry 2). Using the PF₆ salt **116b** under this conditions, a NMR yield of 9.7% for the nNHC complex **64g** and 55.0% for aNHC complex **114b** was obtained (entry 3). This resulted in an improved ratio of 5.7 : 1 in favor of the aNHC complex **114b**. Similar results were obtained with the BF₄ salt **116c** with a NMR yield of 10.2% for **64g**, 55.9% for **114b** and a resulting ratio of 5.5 : 1 (entry 4). A further improved ratio of 6.9 : 1 was observed using the SbF₆ salt **116d** with a NMR yield of 6.9% for nNHC complex **64g** and 47.8% for **114b** (entry 5). Although using the SbF₆ salt provided the best ratio in favor of the aNHC complex **114b**, the PF₆ salt **116b** was used for further optimization as it showed the most desirable ratio and yield. Decreasing the temperature to 100 °C with a prolonged reaction time of 89 h led to a NMR yield of 6.9% for nNHC **64g** and 55.9% for aNHC **114b**, resulting in a ratio of 8.2 : 1 (entry 6). The most desirable results were obtained at 90 °C for 89 h with a NHC yield of 6.4% for nNHC **64g**, 62.2% aNHC **114b**, resulting in a ratio of 9.8 : 1 (entry 7). Further increase of reaction time to 135 h at 90 °C led to a decreased NMR yield of 5.9% for nNHC complex **64g** and 54.8% for aNHC **114b**, resulting in a ratio of 9.3 : 1 (entry 8).

Table 7: Synthesis optimization of mixed normal/abnormal NHC complex **114b**.

entry	conditions (first step)			NMR yields ^a		ratio
	X	T / °C	t / h	64g / %	114b / %	114b:64g
1	Br	200	6	66.9	0	only 64g
2	Br	120	63	19.4	48.0	2.5:1
3	PF ₆	120	63	9.7	55.0	5.7:1
4	BF ₄	120	63	10.2	55.9	5.5:1
5	SbF ₆	120	63	6.9	47.8	6.9:1
6	PF ₆	100	89	6.9	55.9	8.2:1
7	PF ₆	90	89	6.4	62.2	9.8:1
8	PF ₆	90	135	5.9	54.8	9.3:1

^aSee chapter A.2 for details.

The corresponding bromine complex **114a** was obtained under these conditions with an isolated yield of 53% as a yellow solid. As sterics were expected to play a crucial role in the formation of the abnormal coordination, the imidazolium salts **117a** and **99c** were tested under the optimized conditions. Surprisingly, no aNHC derivatives were observed in both cases (Scheme 42).



Scheme 42: Tested conditions for aNHC formation using imidazolium salts **93b**, **117a** and **99c**. n.i. = not isolated, n.o. = not observed, calculated NMR yields are given in parenthesis.

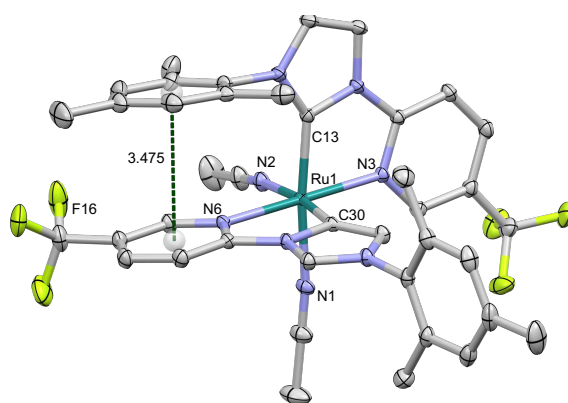


Figure 15: Crystal structure of complex **114b**. ORTEP drawing with 50% probability thermal ellipsoid. The PF₆⁻ counteranion and the solvent molecules are omitted for clarity. One imidazole part of the ligand coordinates with the abnormal C-4 carbon. Selected bond lengths [Å] and angles [°]: Ru1-N1 2.091(1), Ru1-N2 2.103(1), Ru1-N3 2.069(1), Ru1-N6 2.088(1), Ru1-C13 1.969(2), Ru1-C30 2.005(1), N1-Ru1-N2 84.92(5), N1-Ru1-N3 95.02(5), N1-Ru1-N6 86.65(5), N1-Ru1-C13 173.41(6), N1-Ru1-C30 90.46(6), N2-Ru1-N3 88.78(5), N2-Ru1-N6 94.96(5), N2-Ru1-C13 95.22(6), N2-Ru1-C30 172.68(6), N3-Ru1-N6 176.03(5), N3-Ru1-C13 78.41(5), N3-Ru1-C30 97.30(5), N6-Ru1-C13 99.89(5), N6-Ru1-C30 79.07(5), C13-Ru1-C30 90.02(6). The distance of the centroids is indicated with a dotted green line and given in Å

Stability of the Abnormal Complexes **114a** and **114b**

aNHC complexes are known to be the kinetically favored product of the complexation and are energetically estimated 23 kcal/mol higher in energy compared to their nNHC analogs.^[46] This might lead to a rearrangement of the aNHC complexes into the favored nNHC at elevated temperatures. The rigid coordination of the ligands and a stable arrangement around the metal center is crucial for the catalyst design as a rearrangement of the ligands would result in *racemic* mixtures of the corresponding complex or mixtures of **114b** and **64g**. This could interfere with the catalytic activity and selectivity of these complexes thus rendering them unsuitable as asymmetric catalysts. In order to gain insight into the thermal stability

of these complexes, the aNHC complex **114b** was dissolved in CD₃CN and heated to 80 °C for 24 h and 48 h under an N₂ atmosphere. ¹H-NMR analysis showed slight decomposition of the complex, but no detectable rearrangement of the aNHC complex **114b** into its nNHC counterpart **64g** (Figure 16). This implies a significant energy barrier for the interconversion into the thermodynamic more stable nNHC **64g**.

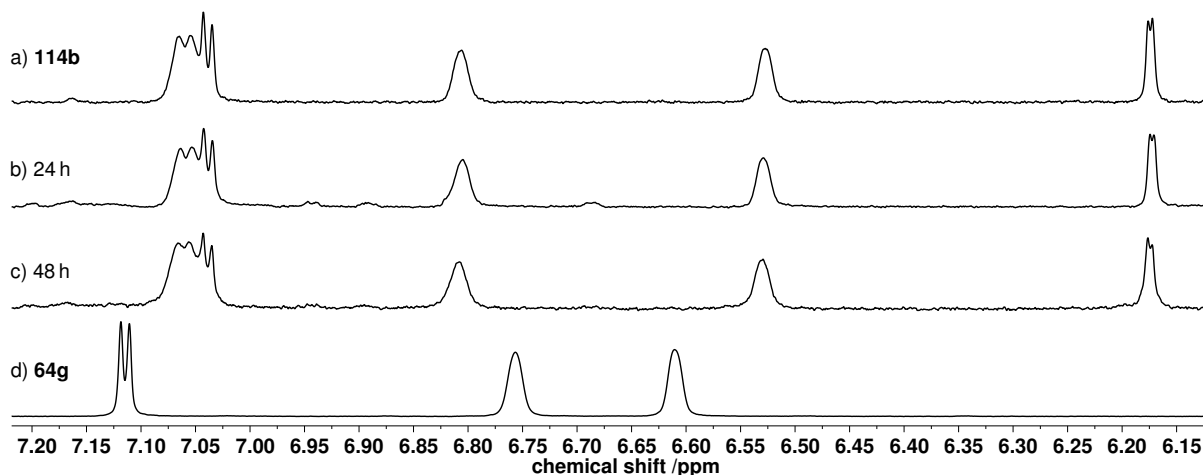


Figure 16: Investigation of the thermal stability of the non-*C*₂-symmetric complex **114b** which contains a normal as well as an abnormal NHC. Excerpts of ¹H-NMR spectra are shown for the complex **114b** in CD₃CN after heating at 80 °C under N₂ atmosphere for 24 h (b) and 48 h (c). Reference spectra of a freshly prepared solution of **114b** (a) and **64g** (d) are also provided for comparison.

A similar experiment carried out in CD₂Cl₂ showed no decomposition of aNHC **114a** after 24 h at 4 °C while at 20 °C the complex starts to decompose (Figure 17). After 72 h at 20 °C, the ¹H-NMR spectrum showed no significant changes compared to the measurement after 24 h. The signal at 9.1 ppm is affected by this decomposition and shifted downfield to 9.3 ppm. This signal corresponds to the C-2 proton of the abnormal bound imidazole. Comparison to the nNHC complex **114a** showed no detectable rearrangement. As the decomposition does not progress further, a reaction of the complex with the solvent can be assumed and for catalytic applications, chlorinated solvents might show side reactions or lead to catalyst inhibition by poisoning.

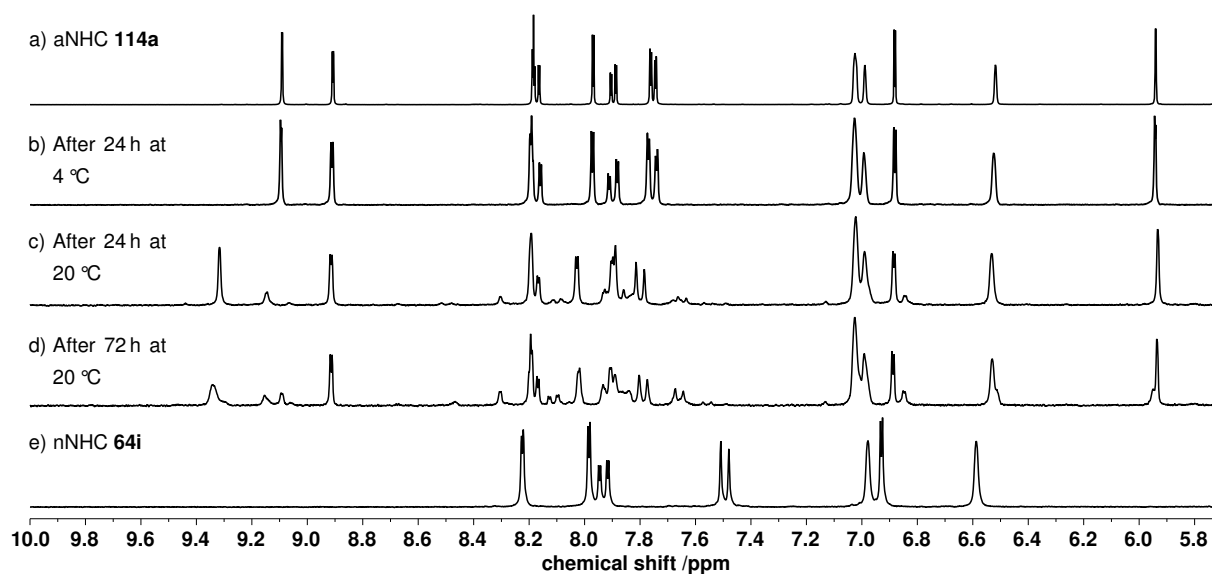


Figure 17: Investigation of solvent stability of the non- C_2 symmetric complex **114a**. Excerpts of ^1H -NMR spectra are shown for the complex **114a** in CD_2Cl_2 after 24 h at 0 °C (b), 24 h at 20 °C (c), 72 h at 20 °C (d). Reference spectra of freshly prepared solution of **114a** (a) and its C_2 symmetric counterpart **64i** (e) are also provided for comparison.

Synthesis of Non-*racemic* Complexes **114a** and **114b**

For the synthesis of the non-*racemic* complexes, the same approach as for the normal NHC complexes was applied by reacting the complex with the chiral salicyl oxazolidin (*S*)-**66**. Due to insufficient separation, the corresponding diastereomeric complexes were not obtained as single diastereomers. The number of potential diastereomers for a non- C_2 -symmetric auxiliary is increased from two to four for these complexes, as the ligands coordinate around the metal-center in a non- C_2 -symmetric fashion. Therefore, a C_2 -symmetric auxiliary was highly favorable. One recent example from the Meggers group employed bisoxazoline (BOX) ligands as C_2 -symmetric auxiliaries to achieve the separation of heteroleptic chiral-at-rhodium complexes.^[135] Two BOX derivatives bearing a phenyl moiety (**118a**) at the chiral center were tested and one was further functionalized with a nitrile group (**118b**) located at the bridging carbon atom. Although full conversion was observed, the separation via column chromatography was unsuccessful for all combinations of ruthenium complexes **114b** and **114a** and BOX derivatives **118a** and **118b**. The screening of suitable auxiliary was continued with the *N*-(*tert*-butylsulfonyl)benzamide **85**. Although the auxiliary is not C_2 -symmetric, one diastereomer could be isolated and is highly favored over the diastereomer with a 180° flipped auxiliary indicated by a yield of 37% for **119** (Figure 18).

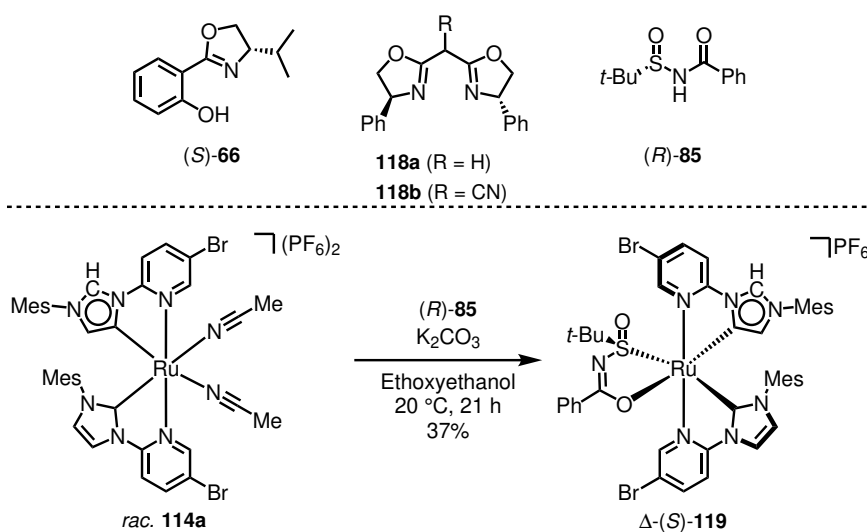


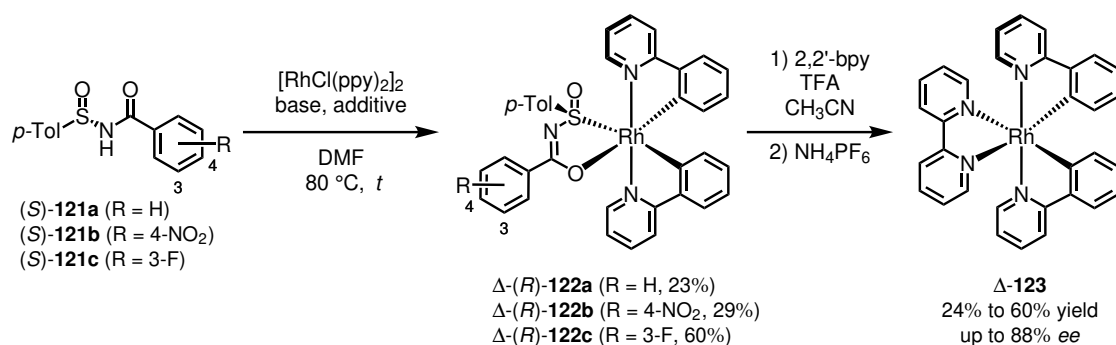
Figure 18: Tested auxiliaries for the resolution of **114a**. With **120** as well as the C_2 -symmetric BOX derivatives **118a** and **118b** no separation of the diastereomers was achieved, while the resolution with **85** was successful.

Although the synthesis provided satisfying results in terms of yield and quality, the separation was not always successful, resulting in inconsistent *ee* of the corresponding enantioenriched complex Δ -**114a**. In order to improve the synthesis and isolation, the coordination of auxiliary **85** to the metal complex was investigated in detail. The *tert*-butyl group induces steric repulsion, which favors one enantiomer over the other as well as favoring the one coordination mode. The phenyl moiety does not induce any type of attractive interaction. As the sulfinyl benzamide **85** was superior compared to the oxazoline **120**, this was maintained as the core functionality and center of chirality.

After re-evaluation of the previously applied auxiliaries in the Meggers group, *N*-(*para*-tolylsulfinyl)-benzamide **121** was selected. This type of auxiliary was applied in the Meggers group to separate bis(2-phenylpyridin)rhodiumchloride dimer ($[\text{RhCl}(\text{ppy})_2]_2$). The corresponding auxiliary complexes **122a**, **122b** and **122c** were subsequently treated with TFA in presence of 2,2'-bipyridine, which provided the enantioenriched complex **123** (Scheme 43).^[136]

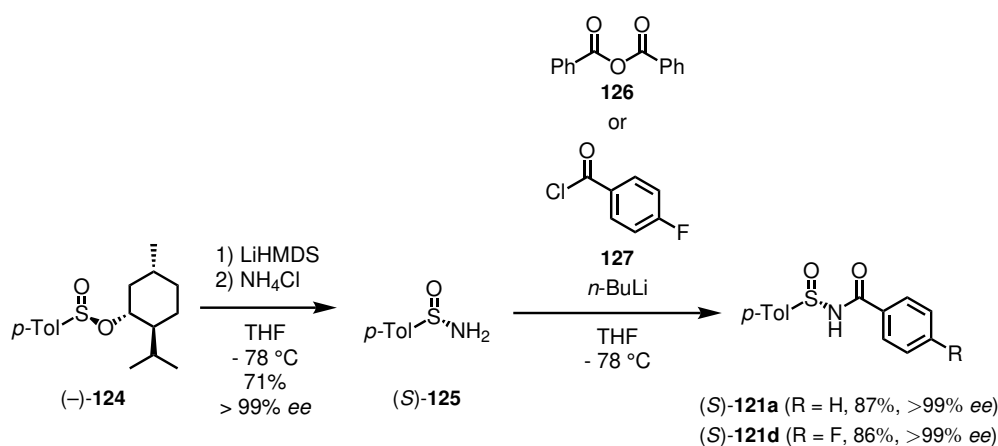
With commercially available starting materials and the possibility for late stage modifications using literature known synthetic methods, this auxiliary system was well suited for further investigations. The *para*-tolyl (*p*-Tol) group was assumed to differentiate between the two enantiomeric complexes by steric repulsion in a mismatch pair and attractive π - π interactions in a matching pair. Similar to the design of M. Helms, the phenyl moiety can be electronically fine-tuned if necessary.

With these promising considerations, the synthesis was performed according to literature conditions (Scheme 44).^[137,138] Commercially available (1*R*,2*S*,5*R*)-(-)-menthyl (*S*)-*p*-toluenesulfinate (**124**) was



Scheme 43: Separation of chiral-at-metal rhodium complex **123** using chiral sulfinyl-benzamides **121a**, **121b** and **121c** by M. Helms.^[136]

treated with lithium bis(trimethylsilyl)amide (LiHMDS) at $-78\text{ }^{\circ}\text{C}$ and subsequently treated with aqueous NH_4Cl at $0\text{ }^{\circ}\text{C}$ which provided sulfinamide (S) -**125** with yields up to 71% and $>99\%$ ee. Sulfinamide **125** was treated with *n*-BuLi and benzoic anhydride (**126**) which provided the final auxiliary **121a** with 87% yield and $>99\%$ ee. Using *para*-fluorobenzoylchloride (**127**), the fluorine derivative **121d** was obtained in 86% yield and $>99\%$ ee.

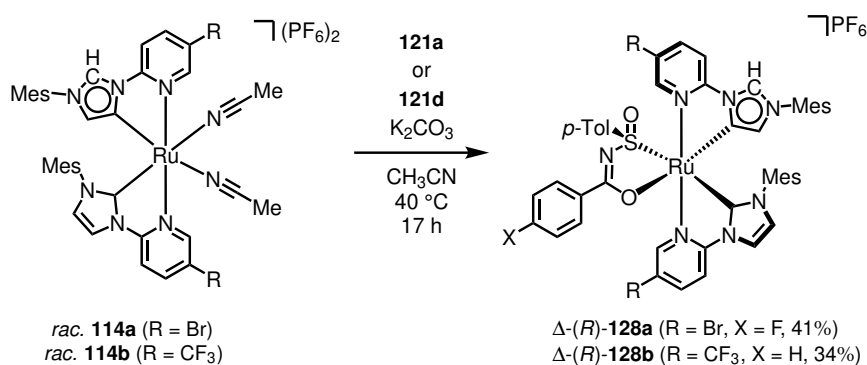


Scheme 44: Synthesis of the auxiliary **121a** and **121d** starting from commercially available menthyl sulfinate **124**.

With the auxiliaries **121a** and **121d** in hands, they were reacted with the *racemic* complexes **114a** and **114b** under basic conditions in CH_3CN at elevated temperatures of $40\text{ }^{\circ}\text{C}$ over night (Scheme 45). The resulting complexes **128a** and **128b** were isolated in 29% and 26% yield respectively. The reaction of *racemic* complex **114b** with the fluorinated auxiliary **121d** provided two inseparable diastereomeric complexes with a combined yield of 34% and a *dr.* of 1:3.6, therefore the combination with **121a** was more favorable. For complex **114a**, the opposite trend was observed as with auxiliary **121a** only mixtures of inseparable diastereomers were obtained. Further purification was observed to be challenging due to insufficient stability of this complex on silica, resulting in a partial removal of the auxiliary during column

chromatography. This indicates a matching pair with either a fluorine in the ligand or in the auxiliary results in stable complexes which are easier to separate. This might be a result of a slight reduced electron density, either pulled away from the metal through the CF₃ group or the fluorine of the auxiliary complex while both being present results in hard to separate diastereomers, leaving only a narrow band for optimal separation and stability.

For both complexes, a yellow compound was observed during column chromatography, which eluted after addition of NH₄PF₆ as solid on top of the stationary phase. ¹H-NMR analysis showed major amounts of the corresponding bis-acetonitrile complex **114b** respectively **114a**. However, low enantiopurity of the complex was determined by HPLC analysis (Figure 41, Chapter A). The obtained, diastereomerically pure complexes Δ -(*R*)-**128b** and Δ -(*R*)-**128a** were used for further investigations.



Scheme 45: Synthesis of the auxiliary complexes Δ -(*R*)-**128a** and Δ -(*R*)-**128b** starting from the bis-acetonitrile complexes **114a** and **114b**.

A single crystal suitable for single crystal diffraction analysis was obtained by slow diffusion of *n*-hexane into a solution of **128a** in CD₂Cl₂ (Figure 19). After refinement, the absolute configuration was assigned as Δ -(*S*) with a flak³ parameter of $-0.003(3)$. The coordinating oxygen of the auxiliary is in *trans* position to the carbon of the aNHC ligand while the sulfur is *trans* to the nNHC carbon atom. A near parallel orientation of the *p*-tolyl group is also observed, which results in a centroid distance of 3.543 Å and 3.515 Å measuring from the central aromatic system, which is the pyridine of the aNHC ligand. A $\pi - \pi$ interaction is strongly assumed and could be one of the reasons for the stability of this complex.

Beside the shown complex Δ -(*S*)-**128b** (Scheme 45), another complex was obtained but a clear separation from Δ -(*S*)-**128b** was not achieved. A ¹H-NMR comparison of the isolated complex Δ -(*S*)-**128b** and a mixed fraction (*dr*: of 1:1.5) is shown in Figure 20. The combined yields did not exceed 50%, so a second Δ -configured diastereomer was hypothesized in which the auxiliary ligand is flipped by 180° (Scheme 46).

³Factor for estimation of the absolute configuration. Values close to 0 indicate correct configuration while values close to 1 indicate an inverted configuration.^[139]

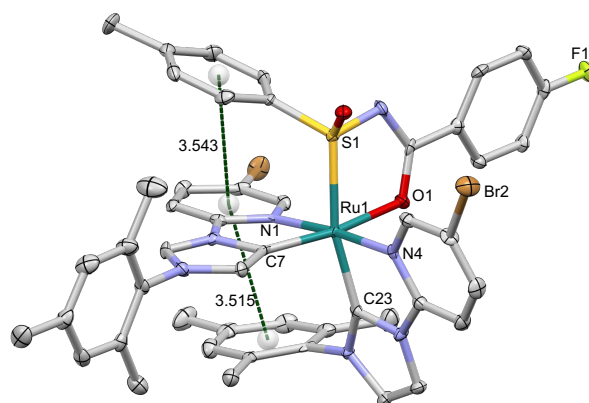


Figure 19: Crystal structure of complex Δ -(*S*)-**128a**. ORTEP drawing with 50% probability thermal ellipsoid. The PF_6^- counteranion and the solvent molecules are omitted for clarity. Selected bond lengths [\AA] and angles [$^\circ$]: Ru1-S1 2.297(1), Ru1-O1 2.131(5), Ru1-N4 2.083(5), Ru1-N1 2.067(5), Ru1-C7 2.002(7), Ru1-C23 2.006(6), S1-Ru1-N4 95.6(2), S1-Ru1-O1 78.8(1), S1-Ru1-C2 3165.5(2), S1-Ru1-C7 95.9(2), S1-Ru1-N1 89.0(2), N4-Ru1-O1 90.6(2), N4-Ru1-C2 377.7(2), N4-Ru1-C7 97.2(2), N4-Ru1-N1 174.6(2), O1-Ru1-C2 388.3(2), O1-Ru1-C7 171.0(2), O1-Ru1-N1 93.1(2), C23-Ru1-C7 97.7(3), C23-Ru1-N1 98.4(2), C7-Ru1-N1 79.4(2). The distances of the centroids are indicated with a dotted green line and given in \AA .

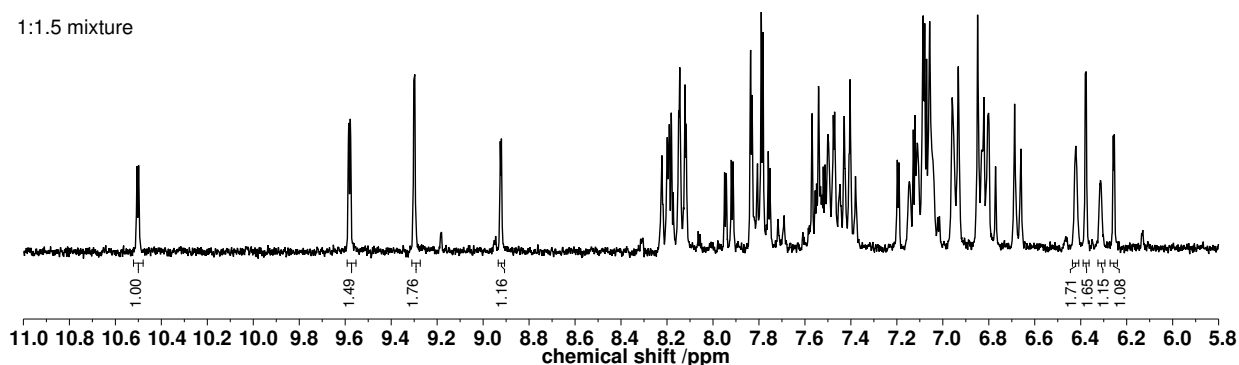
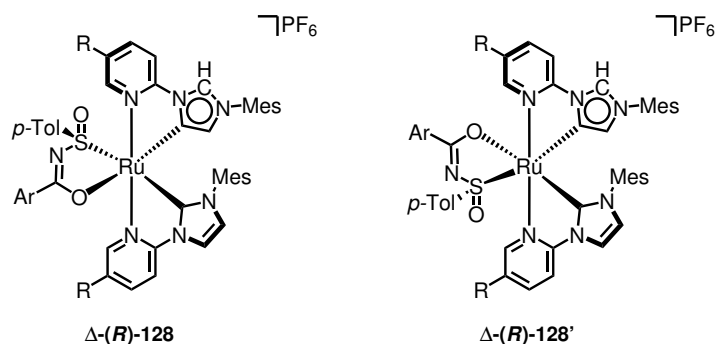


Figure 20: ^1H -NMR spectrum of Δ -(*R*)-**128a** 1:1.5 mixture accompanied by another complex, presumably with a 180° flipped auxiliary.



Scheme 46: The isolated diastereomers Δ -(*R*)-**128** and the assumed diastereomer Δ -(*R*)-**128'** with a 180° flipped auxiliary, deriving from the same metal centered geometry.

In order to investigate the metal centered configuration of the obtained complex, the auxiliary was removed by treating with TFA and the resulting complexes were analyzed by HPLC (Figure 21). The sample deriving from the 1:1.5 mixture of Figure 20 (Figure 21 a) shows a major signal at 55.87 min and a minor signal at 61.32 min. A sample taken from the decomposition product during the column chromatography, which consists of the Λ -configured metal complex with 90.6 % *ee*, was subjected to the same procedure (Figure 21 b) and shows a major signal at 51.28 min and a minor signal at 57.54 min. In order to verify the opposite configuration of these two samples, a third sample (Figure 21 c) was generated by mixing samples a) and b) and was analyzed by HPLC. Two major signals were observed at 54.35 min and 57.33 min with a near 1:1 ratio as well as a minor signal at 62.10 min. As the retention times were different compared to the measurements a) and b), a freshly prepared sample from *racemic* **114a** (Figure 21 d) was analyzed and verified the retention times from sample c).

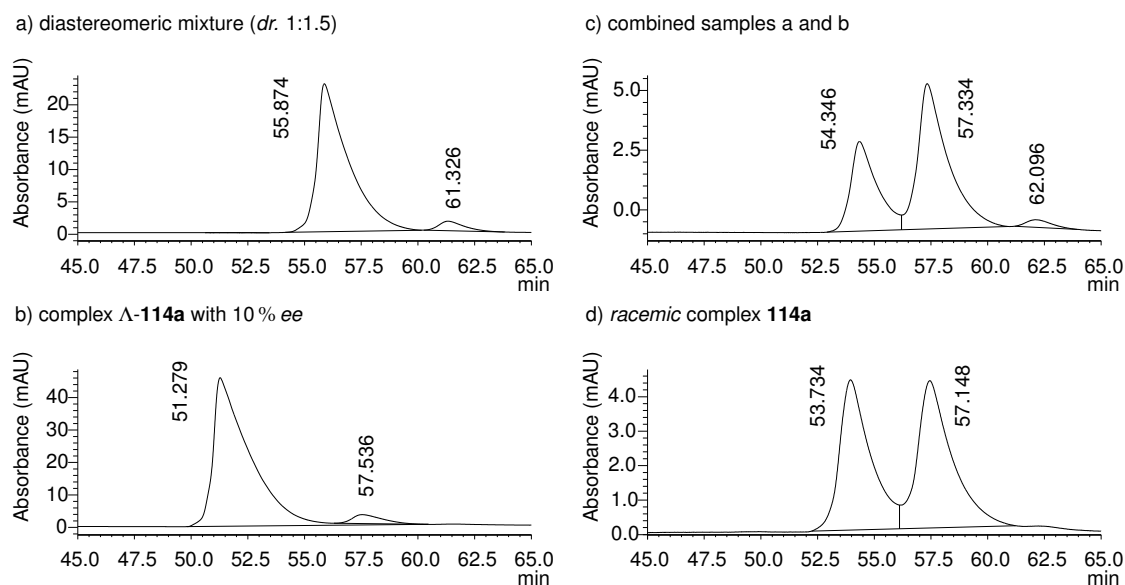


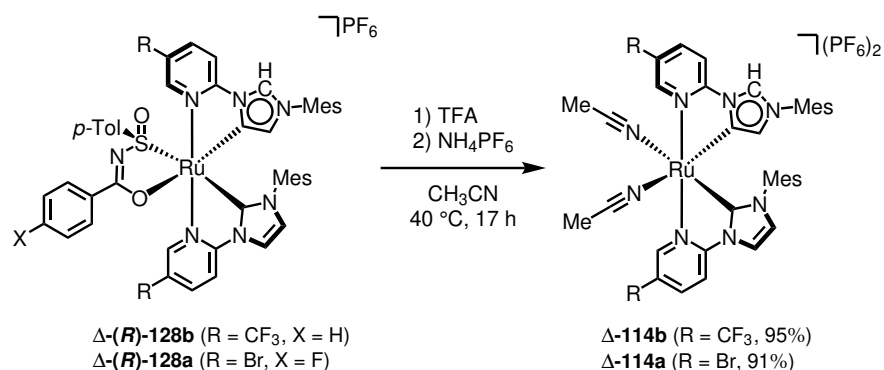
Figure 21: HPLC Traces of the diastereomeric mixtures from the synthesis of **128a**. a) Sample resulting from *dr.* 1:1.5, b) HPLC Trace of remaining bis-acetonitrile complex Λ -**114a** with 90.6% resulting from decomposition during column chromatography c) 1:1 mixture of samples a and b. d) *racemic* **114a**. Conditions: Chiralpak IB-N5 (250 x 4.6 mm), 1.0 mL min⁻¹, H₂O+0.1% TFA/CH₃CN 70:30 for 15 min, gradient to 63:37 in 55 min, 25 °C, 254 nm.

These experiments verify complexes of opposite configuration in sample a) and b) as well as enantio enriched samples of the complex **114a** show lower retention times compared to (near) *racemic* samples. The signal at 61.32 min is assumed to correspond to an unknown impurity, which was not observed in ¹H-NMR spectra. This indirect method shows that these two diastereomers Δ -(*R*)-**128a** and Δ -(*R*)-**128a**' result in the same enantiomeric complex Δ -**114a**. As such, these can be combined resulting in a total yield of 48%.

With the clean auxiliary complexes Δ -(*R*)-**128b** and Δ -(*R*)-**128a** in hand, the auxiliary cleavage was performed following modified literature conditions (Scheme 47).^[114] The complexes were dissolved in

3. Results and Discussion

CH₃CN, treated with 10 eq of TFA and heated to 40 °C over night. Further treatment with NH₄PF₆ and purification via column chromatography provided the pure, non-*racemic* complexes Δ -**114b** and Δ -**114a** with 95% and 91% yield respectively. Compared to the previously shown nNHC complexes **64i** and **64j**, the temperature increase from 20 °C to 40 °C and increase reaction time from 20 min to 16 h were needed for full conversion. Compared to the *t*-butyl substituted auxiliary **85**, which was removed at 20 °C within 2 h, the changes in stability of the auxiliary complexes is noteworthy. This indicates a positive effect of the *p*-tolyl group over the *t*-butyl, a further indication of the $\pi - \pi$ interaction.



Scheme 47: TFA induced protonation of the auxiliary complexes Δ -(*R*)-**128b** and Δ -(*R*)-**128a** yielding the corresponding non-*racemic* complexes Δ -**114b** and Δ -**114a**.

With the increased reaction temperature and time, the enantiopurity of the resulting complexes was questioned, therefore chiral HPLC analysis were performed (Figure 22). HPLC traces of the corresponding *racemic* complexes **114b** and **114a** are shown for comparison. For both complexes only the signal corresponding to the Δ complex could be observed. The absolute metal-centered configuration was assigned according to the configuration of crystal structure **128a** (Figure 19).

CD-spectra measured in MeOH (Figure 23a) shows an overall similarity of the new aNHC complexes Δ -**114b** and Δ -**114a**. A comparison of aNHC complex Δ -**114a** with its nNHC analog Δ -**64i** (Figure 23b) further supports the Δ -geometry as their spectra are close to mirror images with minor differences as expected from constitutional isomers.

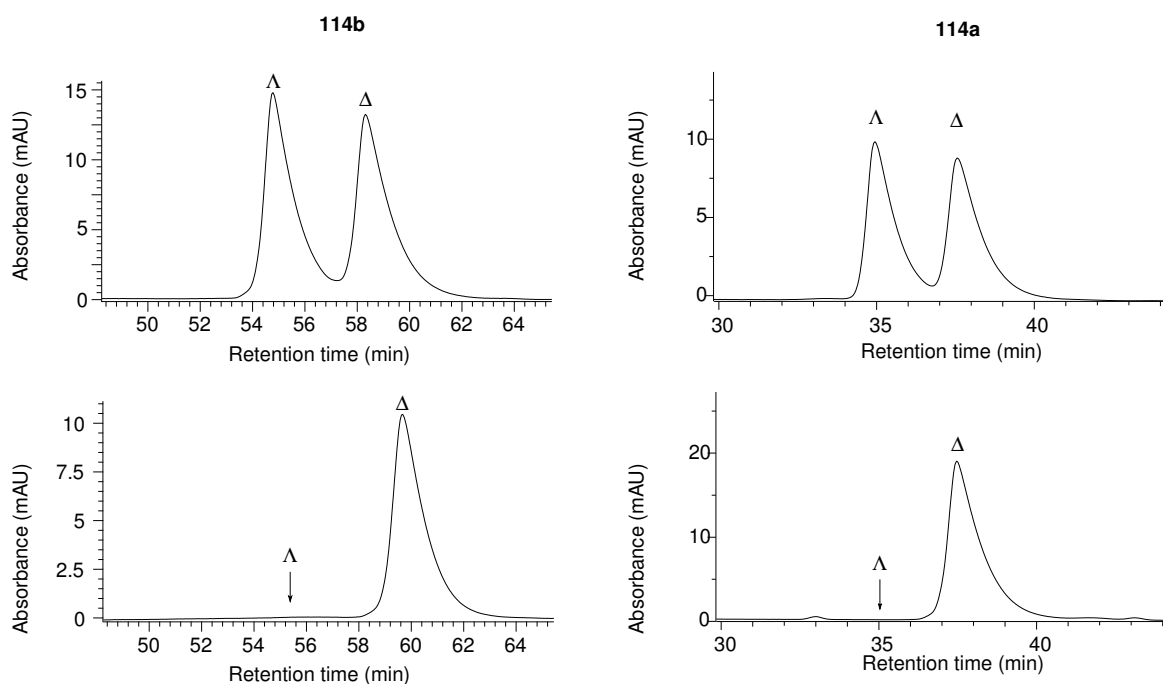


Figure 22: HPLC Traces of the *racemic* (top) and *non-racemic* (bottom) complexes **114b** (left) and **114a** (right). Chiralpak IB-N5 (250 x 4.6 mm), 1.0 mL min⁻¹, H₂O+0.1% TFA/CH₃CN 70:30 for 15 min, gradient to 63:37 in 55 min, 25 °C, 254 nm.

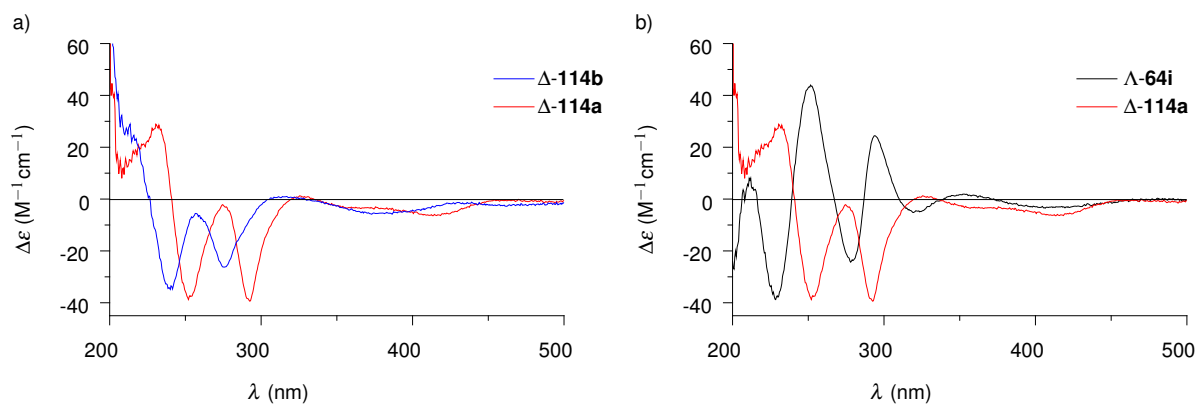
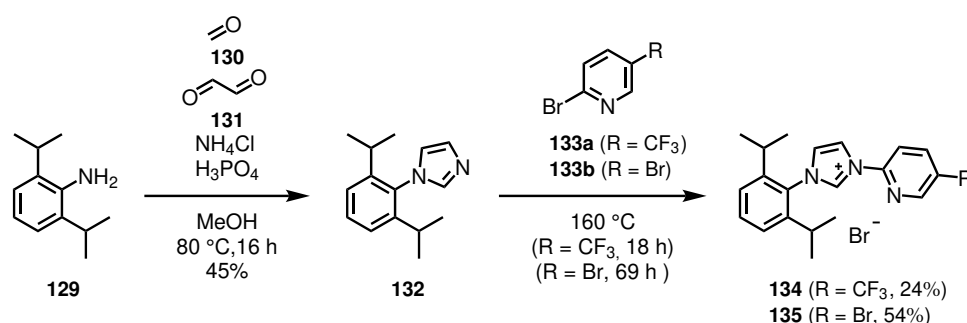


Figure 23: a) CD-spectra of aNHC complexes Δ -**114b** (blue) and Δ -**114a** (red) 0.2 mM in MeOH. b) CD-spectra of aNHC complex Δ -**114a** (red) and nNHC complex Λ -**64i** (black) 0.2 mM in MeOH.

Synthesis of Diisopropylphenyl Derivatives **137a** and **137b**

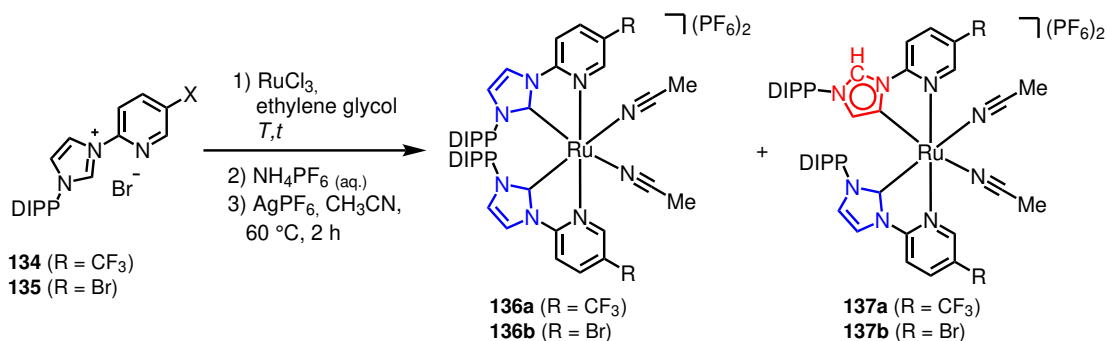
In the following, the influence of the steric properties of the ligand on the selectivity towards the abnormal binding mode and on the stereoinduction of the resulting complexes was investigated further.

The mesityl group was replaced by a 2,6-di(*iso*-propylphen-1-yl) (DIPP) group. The overall synthesis was planned analogously to the imidazolium salts shown previously (Scheme 48). Starting from 2,6-di-*iso*-propylaniline (**129**), which was reacted with aqueous formaldehyde (**130**, 37 wt %), aqueous glyoxal (**131**, 40 wt %) and NH₄Cl in MeOH. 1-(2,6-diisopropylphenyl)-1*H*-imidazole (**132**) was obtained in 45% yield as a colorless liquid. Subsequently, imidazole **132** was reacted with either pyridine **133a** or **133b** under solvent free reaction conditions at 160 °C and the corresponding imidazolium-salts **134** and **135** were obtained in 24% and 54% yield, respectively (Scheme 48). The decreased yield of the CF₃ derivative **134** was likely caused by the sterically demanding DIPP group. Subsequently, the reaction time of the bromine derivative **135** was adjusted accordingly and a higher yield was obtained. In both cases, the obtained quantity was sufficient for the following experiments and the reaction conditions were not further optimized.



Scheme 48: Synthesis of the imidazolium-salts **134** and **135**.

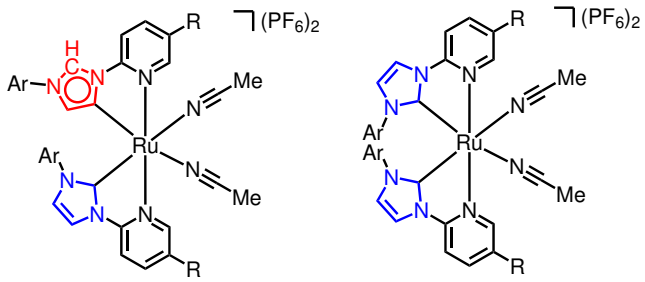
With the sterically more demanding imidazolium salts **134** and **135** in hand, the synthesis of nNHC and aNHC complexes was investigated (Table 8). Stirring imidazolium-salt **134** with RuCl₃ at 120 °C showed traces of the corresponding nNHC complex **136a** even after 46 h. However, the aNHC complex **137a** was obtained in 63% yield (entry 1). Under the same reaction conditions using imidazolium salt **135** (entry 2), nNHC complex **136b** was obtained in 26% yield as well as aNHC complex **137b** in 68% yield. Higher reaction temperatures of 180 °C resulted in the nNHC complex **136b** in 40% yield while its aNHC analogue **137b** was only detected in traces.

Table 8: Conditions for the synthesis of nNHC and aNHC DIPP ruthenium complexes **136** and **137**.

entry	conditions (first step)			Yield	
	R	<i>T</i> / °C	<i>t</i> / h	136 / %	137 / %
1	CF ₃	120	46	n.o.	63
2	Br	120	46	26	68
3	Br	180	24	40	traces

n.o. = not observed

The obtained yields under these conditions were compared to the previously synthesized complexes **64g**, **64i**, **114b** and **114a** (Table 9). In detail, the CF₃-derivatives showed a yield increase of the corresponding aNHC complex from 48% (entry 1) to 63% (entry 2), while the bromine derivative showed a yield increase from 48% (entry 3) to 68% (entry 4). The same trend was also observed for the nNHC complex **136b** with the higher yield of 26% (entry 4) compared to 21% yield for its mesityl analog **64i** (entry 3). As the aNHC derivatives **137a** and **137b** were the focus of research and satisfying yields were obtained, no further optimization was conducted.

Table 9: Comparison of the obtained yields for the nNHC and aNHC ruthenium complexes.^a


Entry	R	Ar	nNHC ^b	aNHC ^b
1	CF ₃	Mes	64g (19)	114b (48)
2	CF ₃	DIPP	136a (n.o.)	137a (63)
3	Br	Mes	64i (21)	114a (48)
4	Br	DIPP	136b (26)	137b (68)

^aConditions: 120 °C for 46 h. ^bYield given in parenthesis. n.o. = not observed.

A crystal suitable for X-ray analysis was obtained by slow diffusion of Et₂O into a saturated solution of *racemic* **137b** in CH₃CN (Figure 24), verifying the mixed nNHC/aNHC binding mode while retaining the overall geometry. The distance of the π - π stacking is increased to 3.687 Å, presumably due to the sterically more demanding DIPP moiety.

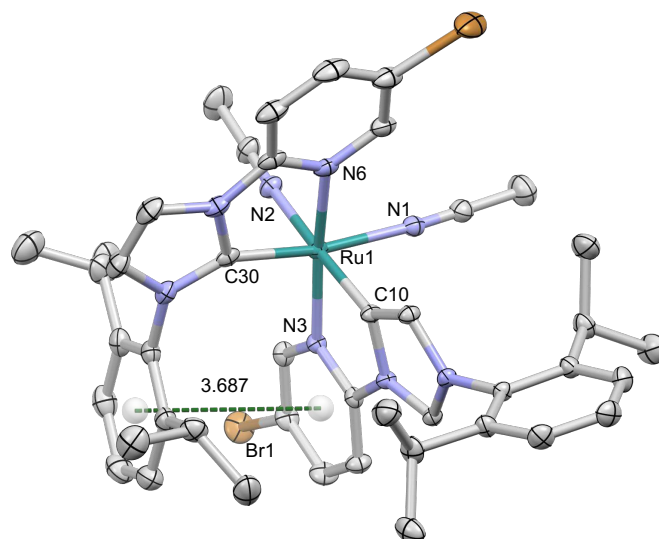
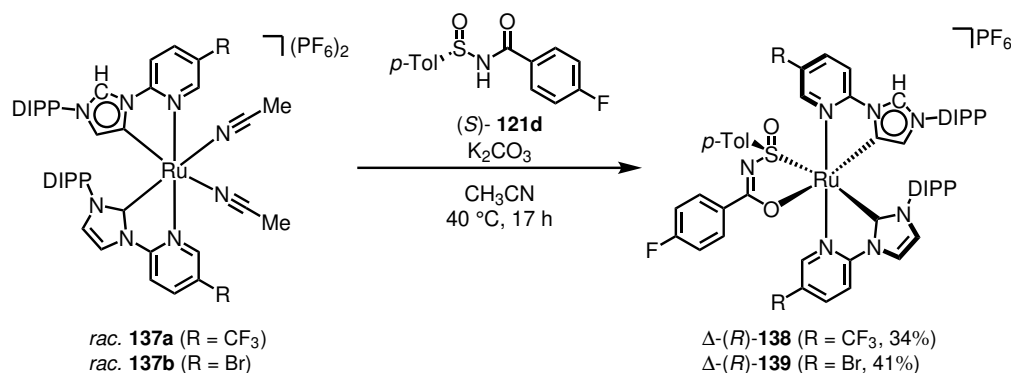


Figure 24: Crystal structure of **137b**. ORTEP drawing with 50% probability thermal ellipsoid. The PF₆⁻ counteranion and the solvent molecules are omitted for clarity. The distance of the centroids is indicated with a dotted green line and given in Å.

3.1. Synthesis of Modified Chiral-at-Ruthenium Complexes

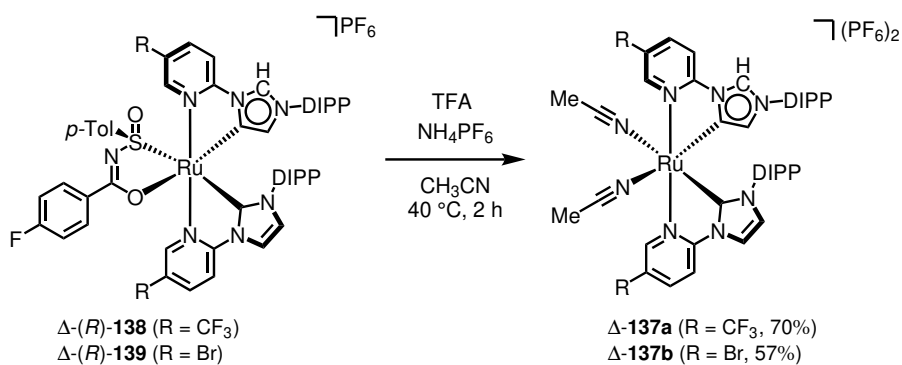
In order to obtain non-*racemic* complexes, the *racemic* complexes **137a** and **137b** were reacted with the chiral auxiliary (*S*)-**121d** under basic conditions at 40 °C in CH₃CN (Scheme 49). The resulting complex Δ -(*R*)-**138** was obtained in 34% yield with traces of a second diastereomer. Application of the reaction conditions using complex **137b** resulted in the corresponding complex **139** as an inseparable mixture of two diastereomers (*dr* 1:4) with a combined yield of 41%. Analogous to previous results, the second diastereomer was assumed to be formed by a rotation of the auxiliary by 180°.



Scheme 49: Synthesis of the DIPP derivatives **139** and **142** using the optimized conditions for the mesityl derivatives.

Similar to the previously shown non-*racemic* complexes, the auxiliary complexes **139** and **142** were dissolved in CH₃CN and treated with TFA at an elevated temperature of 40 °C for 2 h (Scheme 50). The enantiomerically enriched complexes **137a** and **137b** were obtained in 70% and 57% yield, respectively.

The, in comparison to the mesityl analogues **114b** and **114a**, lower yield could indicate a decrease in stability of the complexes **137a** and **137b** under the acidic conditions paired with higher temperature.



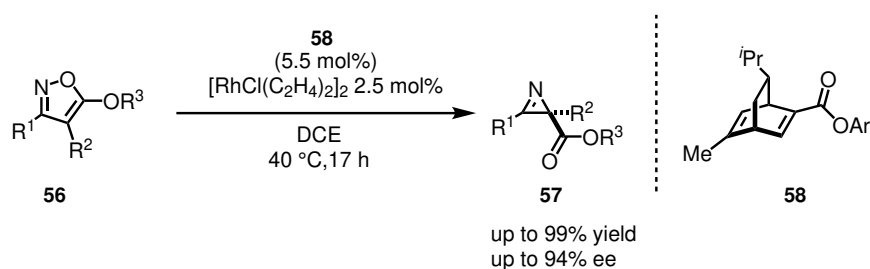
Scheme 50: Removal of the auxiliary, which provided the enantiopure Δ -configured complexes **137a** and **137b**.

3.2. Comparison of the Ruthenium Complexes

3.2.1. Ring Contraction of Isoxazolones to 2*H*-Azirines

Research Background

As mentioned earlier (Chapter 1.2), in 2018 the Okamoto group showed an asymmetric ring contraction of isoxazoles **56** using a chiral diene ligand **58**/ rhodium system as the catalyst for synthesis of 2*H*-azirines **57** (Scheme 51).^[77]

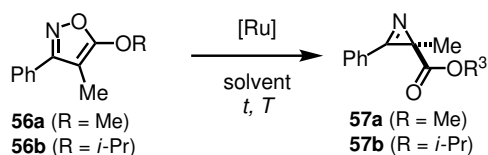


Scheme 51: Previous results by Okamoto *et al.* using a chiral diene/rhodium catalyst system for a ring contraction of isoxazoles (**56**) to chiral 2*H*-azirines (**57**).^[77]

As Qin and Zhou of the Meggers group have previously shown an enantioselective intramolecular C(sp³)-H amination reaction catalyzed by a ruthenium complex, a similar application by the previously discussed ruthenium complexes was proposed.^[117,121]

Substrate Synthesis

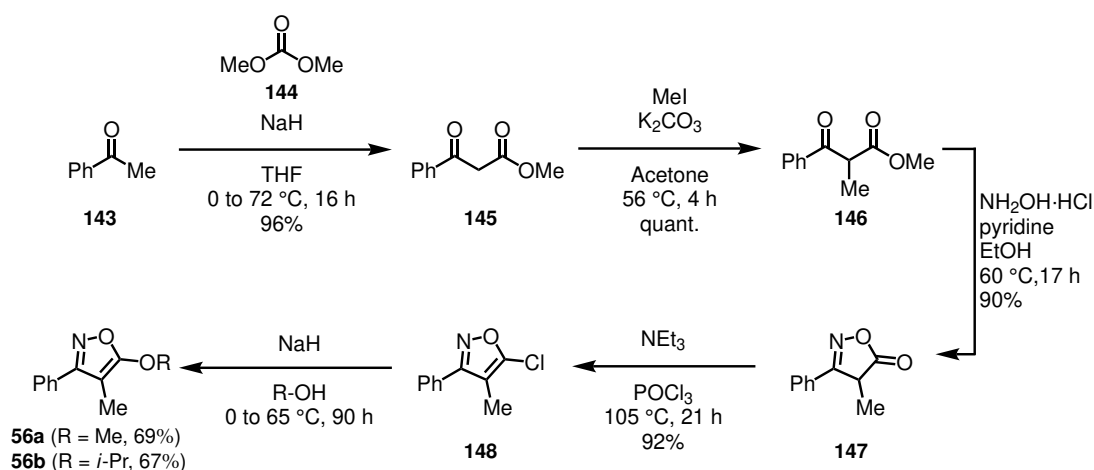
As a test system, the isoxazoles **56a** and **56b** were chosen for simplicity for a proof of concept study (Scheme 52).



Scheme 52: Initial test system starting from the isoxazoles **56a** and **56b**.

Isoxazoles **56a** and **56b** were synthesized according to literature conditions.^[77,140,141] Acetophenone (**143**) was reacted with dimethylcarbonate (**144**), providing the corresponding β -ketoester **145** with 96% yield as a colorless oil. Based on a published procedure by Okamoto *et al.*, β -ketoester **145** was treated with iodomethane in presence of K₂CO₃ in boiling acetone.^[77] After full conversion was observed, the reaction mixture was filtered, the solvent removed under reduced pressure. The methylated β -ketoester **146** was

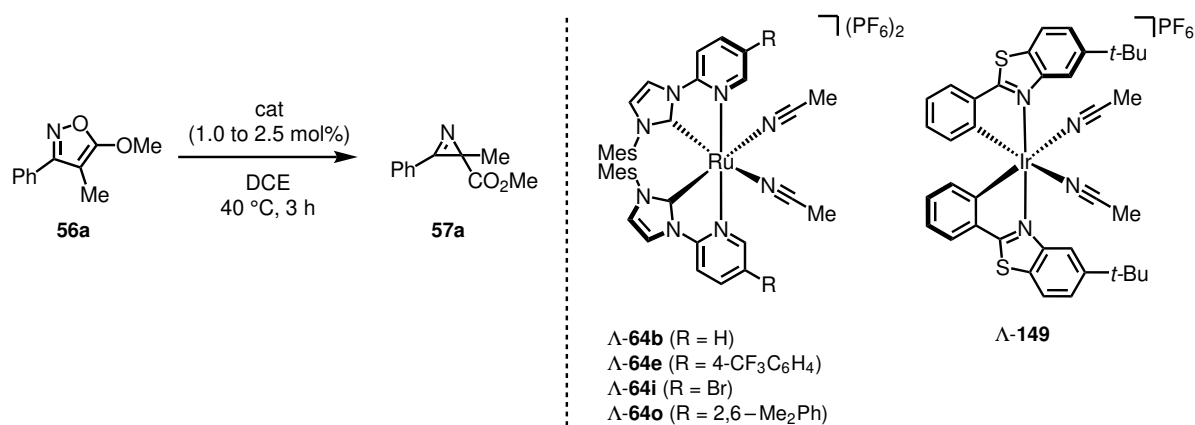
obtained in quantitative yield as a colorless liquid and was used without further purification. Following a reported procedure by Hellmuth *et al.*, β -ketoester **146** was reacted with hydroxylamine hydrochloride ($\text{NH}_2\text{OH}\cdot\text{HCl}$) under basic conditions and the isoxazolone **147** was obtained in 90% yield.^[141] Isoxazolone **147** was dissolved with NEt_3 in POCl_3 and heated to $105\text{ }^\circ\text{C}$ for 21 h, providing the chlorinated isoxazole **148** in 92% yield as a yellow oil. Depending on the desired substitution, sodium hydride (NaH) was added at $0\text{ }^\circ\text{C}$ to either MeOH or *i*- PrOH , generating the corresponding alcoholate. Isoxazole **148** was added to this mixture and heated to $65\text{ }^\circ\text{C}$ for 90 h. The target products **56a** and **56b** were obtained as colorless oils in 69% and 67% yield, respectively (Scheme 53).



Scheme 53: Synthesis of the isoxazoles **56a** and **56b**.

Catalyst Screening

With the isoxazoles **56a** and **56b** in hand, the reaction conditions by Okamoto *et al.* were applied. The catalyst screening involved ruthenium complexes **64o**,^[114] **64e**,^[117] **64b**,^[114] and the newly synthesized complex **64i** as well as the iridium catalyst Λ -**149**^[142] for comparison (Scheme 54).



Scheme 54: Ring contraction of **56a** to **57a** with different chiral-at-metal catalysts.

With ruthenium catalyst Λ -**64o** (2.5 mol%) at 40 °C, full conversion was observed within the first 3 h and the product **57a** was isolated in 94% yield and 32% *ee* (Figure 25, for a detailed list of all screening data, see Table 16 in chapter A). Under the same conditions with complex Λ -**64e**, the product was obtained in 92% yield and 41% *ee*. An increased yield of 96% was observed using complex Λ -**64b**, but the enantioselectivity decreased to 8% *ee*. With the new complex Λ -**64i**, the yield decreased to 76% while the enantioselectivity increased to 45% *ee*. Iridium complex Λ -**149** showed also full conversion within 3 h and the product **57a** was obtained in 85% yield and 8% *ee*. Compared with the rhodium system applied by Okamoto *et al.*, the activity of the ruthenium as well as the iridium catalyst system was higher and the reaction time could be lowered to 3 h. A control reaction without catalyst showed no conversion of **56a**, indicating no racemic background reaction. The catalyst loading for Λ -**64o** and Λ -**64i** could be lowered to 1.0 mol% and full conversion was observed within 3 h. The obtained yield were within the same range $86\pm 7\%$ and $87\pm 9\%$, respectively, as well as the enantioselectivity with $36\pm 3\%$ *ee* and $43\pm 3\%$ *ee*. Overall, the catalyst **64i** showed the best results and was used for further investigations. These conditions were also applied for isoxazole **56b**, which provided the corresponding 2*H*-azirine **57b** in 87% yield and 32% *ee* (data not shown). The increased steric demand of the *i*-Pr group affects the enantioselectivity in a less favorable fashion and further analysis was performed with the methyl derivative **56a**.

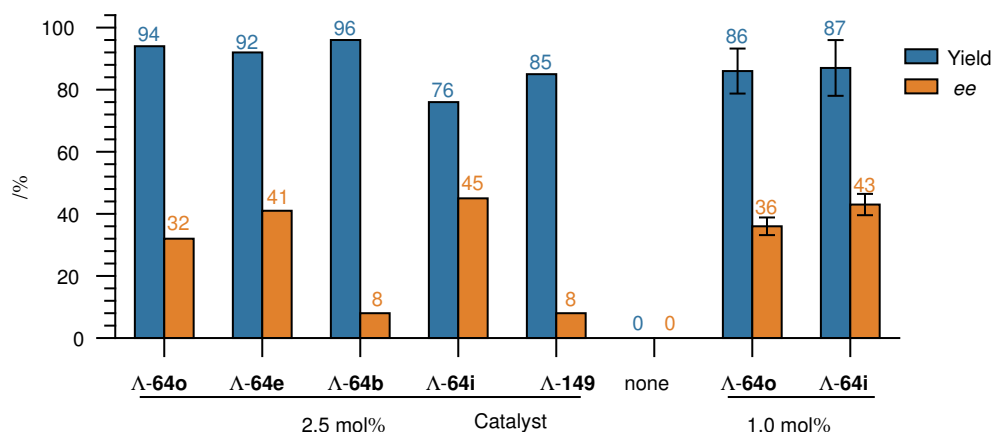


Figure 25: Initial catalyst screening for the ring contraction of **56a**. Conditions: 40 °C, 0.1 M, 3 h in DCE.

Solvent Screening

A wide variety of solvents were screened for their effect on catalytic activity (Figure 26, for a full list of obtained data, see Table 16 in chapter A). These experiments were performed at room temperature (25 °C), which allowed a comparison of the conversion rate, even though full conversion was not achieved.

In terms of yield, 1,2-dichlorobenzene (1,2-DCB) showed the least favorable result with 18% yield and numerous side products which were not identified. CH₃CN showed slow conversion of 12% with a yield

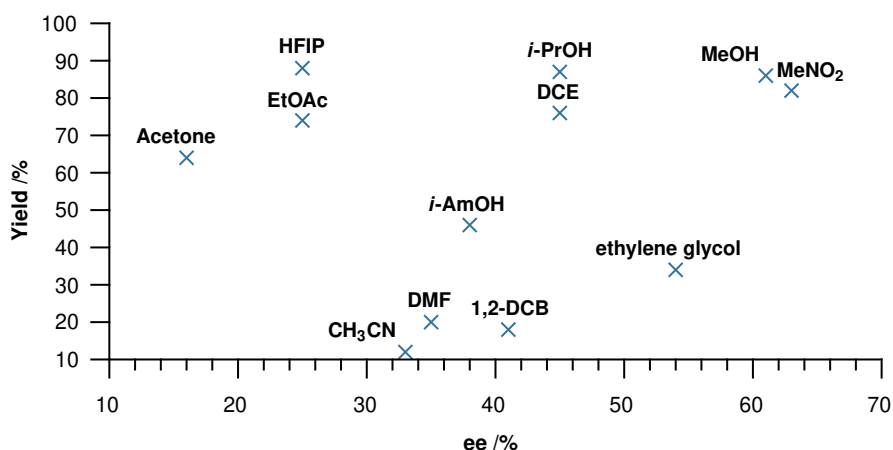


Figure 26: Screening of different solvents for the ring contraction of **56a** and their effect on yield and enantioselectivity.

of 12%. The slow conversion is likely due to CH₃CN being a competing ligand and thereby reducing the exchange rate. For both, MeNO₂ and HFIP, this represents the maximal achievable yield as full conversion was achieved, however numerous side products were formed. In contrast to this only low amounts of side products were observed in DCE, MeOH and *i*-PrOH and full conversion was not achieved within this time frame. As such, higher yields can be expected at full conversion.

In the following, only the solvents with high yield will be discussed. Acetone, EtOAc and HFIP provided poor enantioselectivity from 16% *ee* to 25% *ee*, *i*-PrOH and DCE resulted in intermediate enantioselectivity ranging from 41% *ee* to 45% *ee*. MeOH and MeNO₂ showed the highest enantioselectivity in this screening with 61% *ee* and 63% *ee*, respectively. Generally, solvents capable of forming H-bonds performed better with the exception of acetone. HFIP and *i*-PrOH showed similar yields, but differ drastically in enantioselectivity. This together with the formation of side products in HFIP indicates either *racemisation* of the product after formation or decomposition under acidic conditions. An increased enantioselectivity was observed which was an unclear result at this time and will be addressed later in this work.

The best enantioselectivity was observed in MeNO₂, however this came at the cost of side reactions which were not observed in MeOH, *i*-PrOH or DCE. With this consideration, MeOH showed the best performance with 86% yield and 61% *ee* and will be used together with DCE for further screenings to cover protic polar as well as aprotic polar solvents.

Additive Screening

Okamoto *et al.* reported DFT calculations, which suggested that one free coordination site is needed at the catalytic center for this transformation.^[77] The used chiral-at-ruthenium complexes, such as Λ -**64i**, contain two labile CH₃CN ligands and therefore also two possible reaction sites. As the complexes are C₂-symmetric, both sites are equal for enantioselectivity upon the first coordinate. However, a possible second coordination, either of the substrate **56a** or the finished product **57a** could influence the outcome of the catalysis. Therefore, different additives were added with the intend of reducing the likelihood of a second coordination.

For testing, trimethylphosphine (PMe₃), triphenylphosphine (PPh₃), imidazole and pyridine-*N*-oxide were used as additives. As another method, encapsulation^[143] was also tested for this purpose (Figure 27, for a detailed list see Table 16 in chapter A). However, none of the tested additives showed a positive effect. In cases of pyrazole and imidazole the yield fell below 20%, while the phosphines PMe₃ and PPh₃ decreased the enantioselectivity at similar yields as without additives. Addition of the amine base triethylamine (NEt₃) also gave inferior results, decreasing the yield to 69% and the enantioselectivity to 40% *ee*.

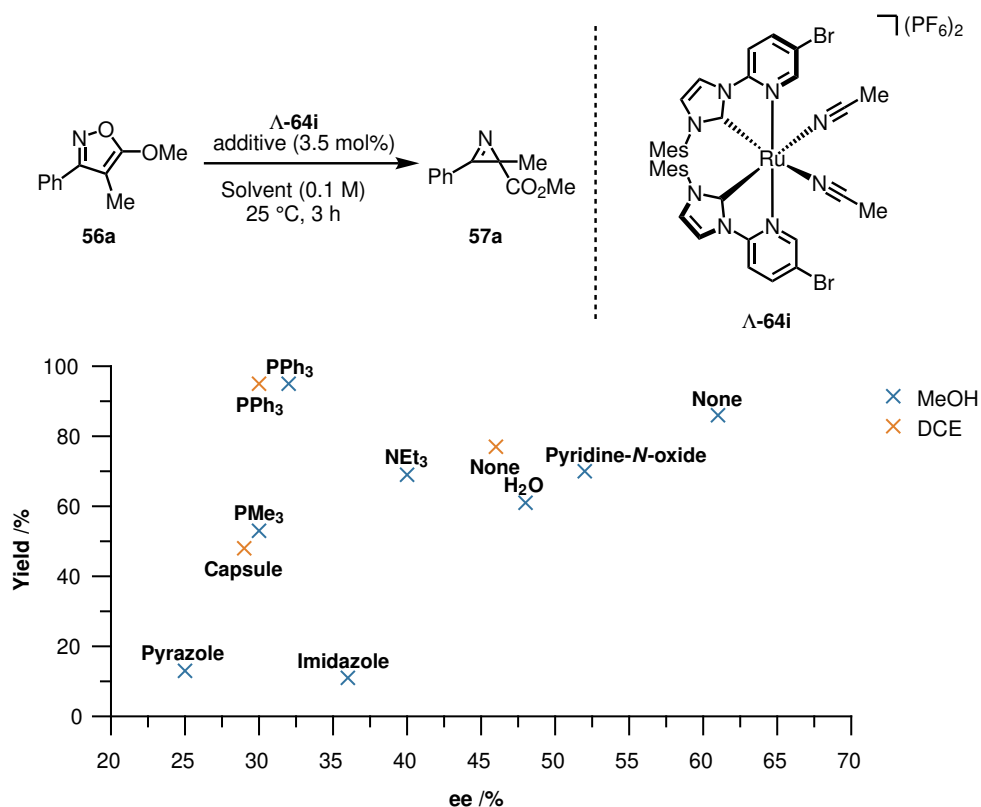


Figure 27: Effect of different additives towards the yield and *ee* of the asymmetric ring contraction in MeOH (blue) or DCE (orange). Conditions: 0.1 mmol isoxazole **56a**, 0.1 M, 3.5 mol% additive, 1 mol% Λ -**64i**, 1 mL MeOH or DCE.

Influence of Light

During the investigations shown above, the observed *ee* were not clearly consistent under the same conditions. Drastic drops in enantioselectivity were observed although the obtained yields were comparable. After re-evaluation, a correlation of the *ee* with the time of day during the reaction was discovered. As such, the influence of light was investigated as a parameter. In order to control the amount of light during the experiment, the reaction was performed in reaction vessels wrapped with aluminium foil to shield them from light and yield and *ee* monitored over time (Figure 28). While the conversion increased steadily, the *ee* values rose steeply within the first hour, forming a plateau between two and six hours at 67% *ee* and subsequently decrease slowly afterwards. After 50 and 70 h the *ee* values dropped to 52% and 46%, respectively. With these non-linear effects, the system increased in complexity as a re-coordination of the product cannot be excluded.

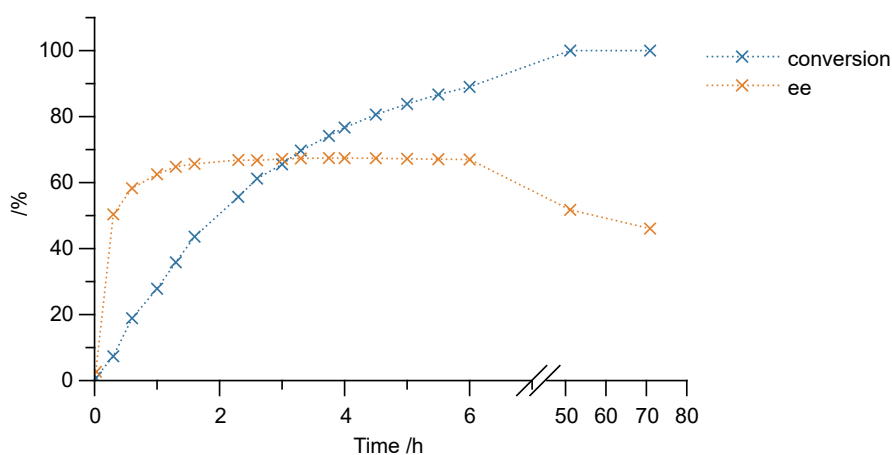
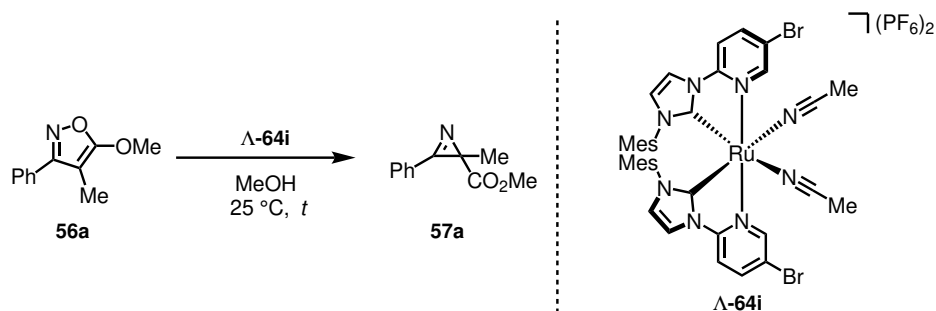


Figure 28: Measured conversion and *ee* over the time during the ring contraction of **56a**. Conditions: 0.1 mmol isoxazole **56a**, 0.1 M, 1 mol% **Λ -64i**, 1 mL MeOH.

This indicated a slow *racemisation* even though the reaction was shielded from light. With the steep rise of *ee* within the first hour, a product concentration dependent enantioselectivity was proposed. In order to investigate the influence of the product, 0.1 eq of purified product **57a** with 45% *ee* was added to the catalyst solution prior the substrate **56a** (entry 2). Interestingly, the *ee* value reached only 51% after 2 h, which indicates a negative effect of the product **57a** upon coordination. Repeating the conditions of entry 1 gave similar results in terms of *ee* (entry 3). This indicates that a high concentration of the major enantiomer slows down the corresponding pathway, therefore preventing a high *ee*. Entry 4 to 7 represent individual values of repeated experiments and the amount of variation occurring even while the reaction was shielded from light. This indicates additional unknown influences. For a better understanding, the reaction was irradiated with a 24 W blue LED at a wavelength of 455 nm (entry 8). After 6 h, full conversion was observed and the enantioselectivity was determined with 0% *ee*, indicating full racemisation.

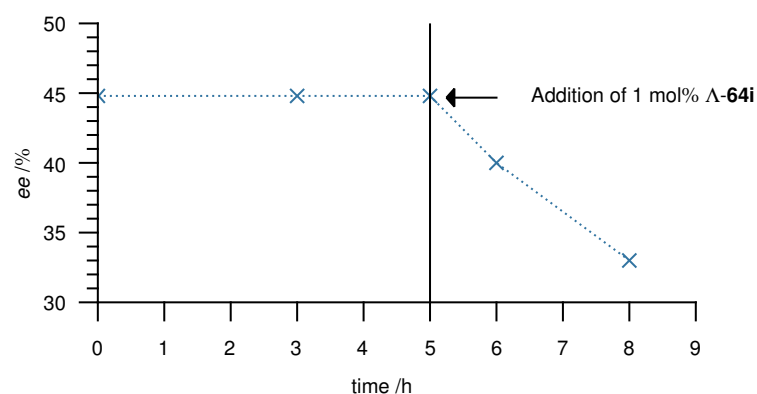
Table 10: Influence of light on the ring contraction of isoxazole **56a**.^a

Entry	cat. loading /mol%	t /h	yield /%	ee /%
1 ^b	1	6.0	90	67
2 ^c	1	2.5	90	51
3	1	6.0	65	67
4	0.5	6.0	81	61
5	0.5	6.0	66	53
6	1	5.0	65	67
7	1	5.0	69	59
8 ^d	1	6.0	n.d.	0

^a reactions shielded from light, ^b values taken from experiment shown in Figure 28 for comparison, ^c added 0.1 eq purified product with 45% *ee*.

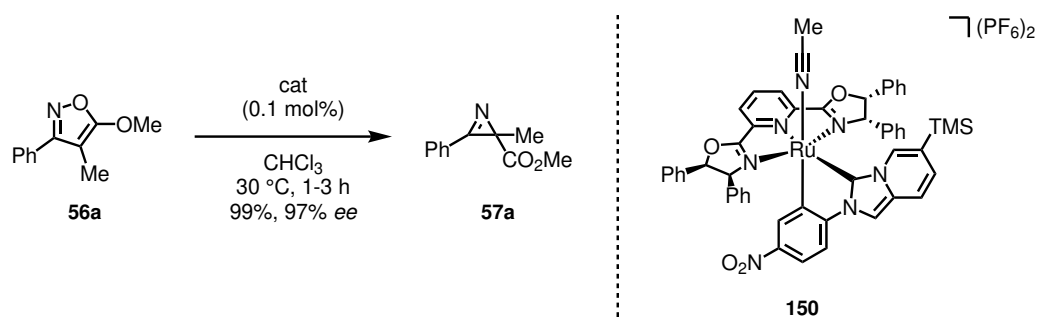
^d irradiated with 24 W blue LED (455 nm). n.d. = not determined.

As a photoinduced ring opening of *2H*-azirine is known to literature,^[99] isolated product with 45% *ee* was dissolved in MeOH, and irradiated with a blue LED, replicating the same conditions as used previously. (Figure 29). The *ee* was determined after 3 h and 5 h, indication that no *racemisation* occurred. Addition of 1 mol% catalyst and irradiation for 1 h decreased the *ee* by 5% (from 45% *ee* down to 40% *ee*). After further 2 h of irradiation, the *ee* fell to 33% providing proof for a photo-racemisation, catalyzed by the ruthenium complex **64i**.

**Figure 29:** Irradiation of **57a** in MeOH and after 5 h addition of 1 mol% $\Delta\text{-64i}$.

Conclusion

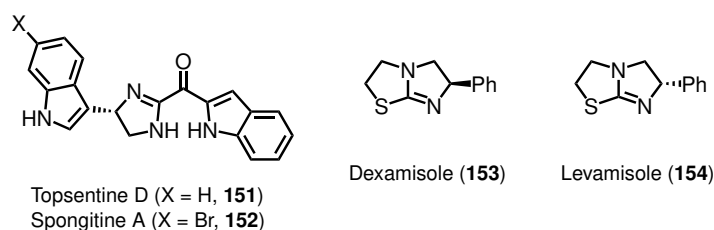
Summarized, the chiral-at-metal ruthenium complexes **64** are able to catalyze the asymmetric ring contraction of **56a**, which was reported by Okamoto *et al.* The complexes bearing steric demanding moieties like Bromine (**64i**), 4-CF₃-phenyl (**64e**) and dimethyl-phenyl (**64o**) showed in the initial catalyst screening enantioselectivities between 32% *ee* (**64o**) and 45% *ee* (**64i**), surpassing the unsubstituted complex **64b**, which provided the product **57a** with 8% *ee*. The catalyst loading was lowered from 2.5 mol% down to 1.0 mol% without significant losses in *ee* or yield. A broad solvent screening showed MeOH and MeNO₂ as the solvents resulting in the highest *ee*, but side products were observed in MeNO₂, leaving MeOH as the solvent of choice with 86% yield and 61% *ee*. A screening of different additives showed no positive effects towards *ee*. Later on, it was revealed that the *ee* is not linear over the time of the reaction, and the combination of ruthenium complex **64** and light leads to a slow but steady *racemisation*. At this point, the investigations was discontinued. With a new catalyst design based on a pyridine-2,6-bis(oxazoline) (**150**), Li from the Meggers group was able to improve the results with up to 97% *ee* and very good yields above 90% (Scheme 55).^[144]



Scheme 55: Ring contraction of **56a** to **57a** accomplished by Li from the Meggers group with a new catalyst design.^[144]

3.2.2. Asymmetric Ring-Closing C(sp³)-H Amination

As mentioned earlier (Chapter 1.3.1), the direct amidation of prochiral C(sp³)-H bonds has gained a lot of attention and several methods and systems have been developed. Besides cyclic sulfinamidates, sulfamides, sulfonamides, carbamates, lactams and Boc-protected pyrrolidines, the asymmetric synthesis of cyclic urea substrates was developed in the Meggers group using the nNHC chiral-at-metal ruthenium catalysts.^[117–119,121,144–146] Subsequently, these can be converted to biological active compounds like Tospentine D (**151**), Spongistine A (**152**), Dexamisole (**153**) and Levamisole (**154**), providing a new tool for asymmetric catalysis (Scheme 56).



Scheme 56: Natural products deriving from chiral 1,2-diamines synthesized by asymmetric ring-closing C(sp³)-H amination.^[118]

In order to gain further insight into the effects towards catalytic activity and selectivity, the aNHC complexes Δ -**114b** and Δ -**114a** were applied in this reaction (Table 11).

Table 11: Mixed normal and abnormal NHC Ruthenium complexes for C(sp³)-H amination of *N*-benzoylurea **76**.^a

entry	catalyst	loading /mol%	<i>t</i> /h	yield /%	TON	TOF /h ⁻¹	ee ^b /%
1	Δ - 114b	1.1	0.18	98	90	490	71 (<i>R</i>)
2	Δ - 114a	0.9	0.18	99	110	670	86 (<i>R</i>)
3 ^c	Δ - 114a	0.05	16	97	1940	110	60 (<i>R</i>)
4 ^c	Δ - 114a	0.01	24	33	3360	140	48 (<i>R</i>)
5 ^d	Λ - 64g	1.0	16	quant	100	6	94 (<i>S</i>)
6	Λ - 64i	1.0	24	95	95	4	90 (<i>S</i>)
7 ^{c,d}	Λ - 64h	0.1	24	quant	1000	40	94 (<i>S</i>)
8 ^{c,d}	Λ - 64h	0.05	24	66	1320	55	93 (<i>S</i>)

^a Standard conditions: Urea **76** (0.2 mmol), K₂CO₃ (0.6 mmol), Ru catalyst (0.02 μ mol – 2.2 μ mol) in CH₂Cl₂ (2.0 mL) ^b Determined by HPLC on a chiral stationary phase. ^cTemperature increased to 40 °C. ^dTaken from ref. [118]

With 1.1 mol% of Δ -**114b** (entry 1), full conversion was observed within 10 min and the target product **77** was obtained in 98% yield and 71% *ee*, which results in a turnover number (TON) of 90 and a turnover frequency (TOF) of 490 h⁻¹. Under similar conditions, the catalyst Δ -**114a** (entry 2) showed also full conversion, providing the target product in near quantitative yield and an enantioselectivity of 86% *ee* with a TOF of 670 h⁻¹. With greatly increased activity, the catalyst loading was lowered to 0.05 mol% (entry 3), which achieved full conversion after 16 h at 40 °C. The product was isolated in 97% yield and a TON of 1940 and a TOF of 110 h⁻¹ was determined. However the *ee* value dropped from 86% down to 60%. Subsequently, the catalyst loading was further reduced to 0.01 mol% (entry 4) with an elongation of the reaction time to 24 h. This resulted in a drastic diminished yield of 33%, incomplete conversion, reduced enantioselectivity of 48% *ee*, TON of 3360 and TOF of 140 h⁻¹.

Application of the nNHC complexes **64g**, **64i** and **64h** (entry 5 to 7) resulted in near quantitative formation of the product, but lower TOF values of 6, 4 and 40 h⁻¹, respectively. With a low catalyst loading of 0.05 mol%, the product was obtained in 66% yield (entry 8), TON of 1320 and TOF of 55 h⁻¹. The *ee* values were overall above 90%, outperforming the aNHCs. In terms of TOF, the maximum value for the nNHC catalysts was determined with 55 h⁻¹ (entry 8), while the lowest TOF determined for the aNHCs was 110 h⁻¹ (entry 3) and up to 670 h⁻¹ (entry 2).

With these results, the aNHCs Δ -**114b** and Δ -**114a** showed a two to tenfold increase of TOF with a trade-off a lower enantioselectivity as it dropped by at least 4% *ee*. The increased reaction rate could indicate less steric hindrance of the abnormal binding mode around the catalytic site and/or be a result of the higher σ -donor strength of the aNHC ligand, increasing the electron density at the metal center. This might further destabilize the CH₃CN ligands in the *trans* position and therefore increase the ligand exchange rate. The decreased sterics and the resulting decreased steric induction on the other hand might also be responsible for the loss of *ee* for this catalysis.

3.2.3. Alkynylation

The alkynylation of trifluoroacetophenone (**68**) with phenylacetylene (**69**) can be catalyzed by the chiral-at-metal ruthenium complexes as shown by Zheng from the Meggers group who achieved outstanding 98% yield and 99% *ee* with low catalyst loading as low as 0.2 mol%.^[114] The reaction features easy accessible starting materials, low reaction times and only one minor side product. With this, the reaction was used as internal reference and as a test system for new ruthenium complexes in the Meggers group (Table 12). As reference, the unsubstituted complex Λ -**64b** with the results taken from reference [114] is shown in entry 1, providing the product **70** in 95% yield, 97% *ee*, TON of 190 and TOF of 12 h⁻¹. Complex Λ -**64j**, with the NMe₂ substitution (entry 2), showed full conversion within the same time using

3. Results and Discussion

a catalyst loading of 0.7 mol%. The yield was decreased from 95% to 84%, which also lowered the TON and TOF to 114 and 7 h⁻¹ respectively, while the enantioselectivity was comparable with 96% *ee*. The bromine derivative Λ -**64i** (entry 3) showed a higher yield of 99%, TON and TOF of 210 and 14 h⁻¹ and also an increased enantioselectivity of 98% *ee*. The aNHC Δ -**114b** showed a lower yield of 82% within 23 h, with a resulting TON and TOF of 152 and 7 h⁻¹ (entry 4). The enantioselectivity with 96% *ee* was similar to the previous results. A replicate of the same conditions indicated full conversion of acetylene **69** within 6 h (entry 5). The product **70** was isolated with 85% yield and 97% *ee*. Due to the drastically reduced reaction time, the TOF accelerated to 22 h⁻¹.

The side reaction, a dimerisation of acetylene **69**, which forms the head-to-head dimerisation product, the en-yn system **155**, was more prominent compared to the nNHCs. Only complex Λ -**64j** showed also an increased yield of this side product. The aNHC with the bromine derivative Δ -**114a** generated both a lower yield (80%) and enantioselectivity (87% *ee*, entry 6). Using the unfluorinated acetophenone **143** instead of **68** (entry 7) did not lead to product formation.

Table 12: Overview of catalytic activity of different ruthenium catalysts, both nNHCs and aNHCs for the asymmetric alkynylation of trifluoromethyl acetophenone **68**.^a

Entry	Cat	Cat loading /mol%	Time /h	Yield ^b /%	TON	TOF / h ⁻¹	<i>ee</i> /%
1	Λ - 64b	0.5	16	95	190	12	97 (<i>S</i>)
2	Λ - 64j	0.7	16	84	114	7	96 (<i>S</i>)
3	Λ - 64i	0.5	16	99	210	14	98 (<i>S</i>)
4	Δ - 114b	0.5	23	82	152	7	96 (<i>R</i>)
5	Δ - 114b	0.6	6	85	135	22	97 (<i>R</i>)
6	Δ - 114a	0.5	19	80	170	9	87 (<i>R</i>)
7 ^c	Δ - 114a	0.5	19	0	n.d.	n.d.	n.d.

^astandard conditions: Substrate **68** (0.2 mmol), alkyne **69** (0.6 mmol), NEt₃ (0.04 mmol), Ru catalyst (0.5 mol%-0.7 mol%) in THF (0.5 M) stirred at 60 °C for the indicated time under N₂ unless noted otherwise.

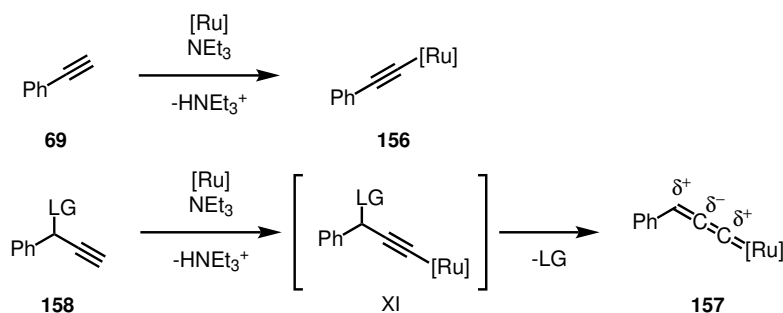
^bbased on isolated **70**. ^c**143** used instead of **68**.

Comparing these results, the nNHCs showed high enantioselectivities similar to the published catalysts, while the aNHCs and **64j** displayed lower yields in the range of 80% to 85%. The aNHCs as well as the electron donating NMe₂-group can be considered more electron rich in comparison to the CF₃ and bromine derivatives, which gives insight into the relative kinetics of the two possible reactions. As the dimerisation reaction to **155** is favored more by the electron rich complexes, a higher yield might be achieved by a even higher quantity of acetylene **69**. As unfluorinated substrates such as **143** were not converted and only electron deficient aromatic systems led to product formation, it is clear that electron deficient catalysts are more suitable for this type of conversion. This might be caused by the carbonyl carbon atom of the coordinated ketone being more electrophilic with electron deficient catalysts. As such, these catalysts are more efficient in the transfer of the alkenyl as nucleophile. In contrast to the asymmetric amination reaction shown earlier (3.2.2), the aNHCs showed no significantly increased Turnover frequency (TOF) for this type of reaction.

3.2.4. Propargylic Substitution

Research Background

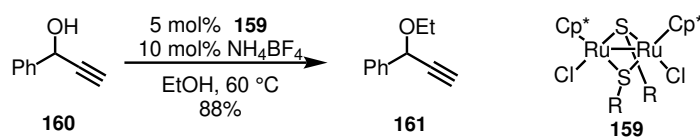
As shown in chapter 3.2.3, the complexes bearing the abnormal type binding mode showed a higher activity towards the dimerisation of acetylene **69**, which formed the en-yn system **155**. Based on DFT calculations Chen *et al.* proposed a ruthenium acetylide **156** (Scheme 57) as a possible intermediate for the transformation.^[115] With this in mind, a leaving group at the C-3 atom was hypothesized for a metal allenyliden complex **157** via a acetylide intermediate **XI**. This could be used as the reactive intermediate, for example a enantioselective propargylic substitution.



Scheme 57: Research background propargylic substitution.

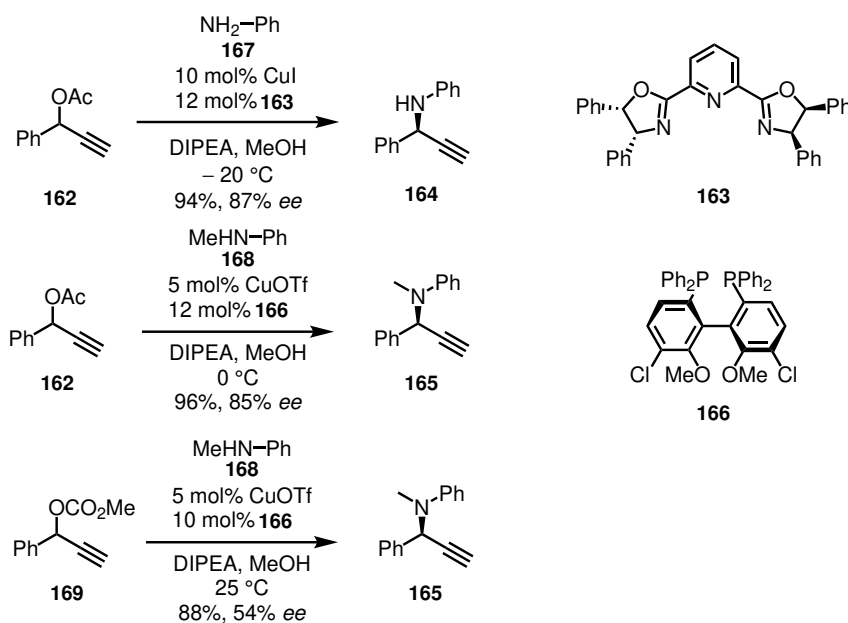
Such reactions of propargylic substrates are known to be catalyzed by ruthenium and copper complexes, especially a γ -selective nucleophilic additions of heteroatom nucleophiles (Scheme 58). Early examples employing diruthenium catalysts like **159**, to convert phenylpropargylic alcohol **160** in presence of EtOH into the ether **161**.^[147,148] NH₄BF₄ was employed for activation of the diruthenium catalyst by removal of a chlorido ligand to open up a coordination site.

3. Results and Discussion



Scheme 58: Literature known propargylic substitution reactions via a metal allenyliden intermediate.^[147,149,150]

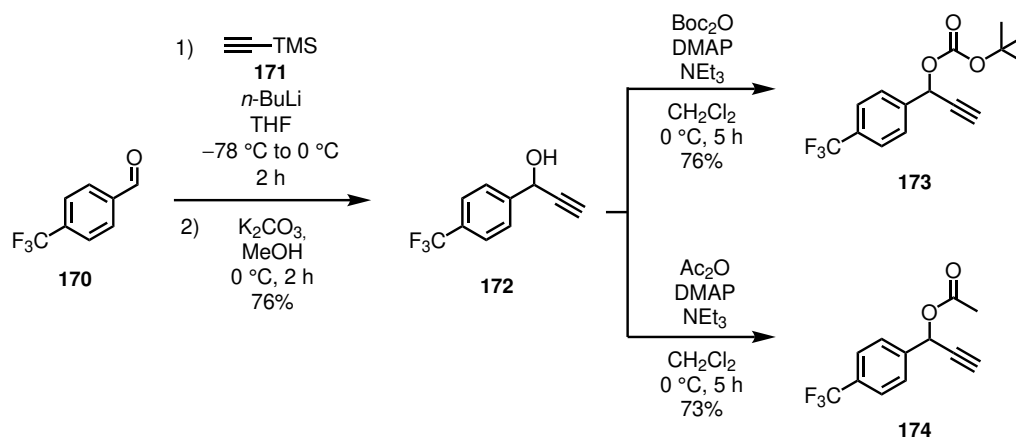
In terms of asymmetric reaction development, significant advances were made using different chiral copper catalysts in 2008 by the groups of Maarseveen and Nishibayashi (Scheme 59).^[149–152] Both systems used acylated phenylpropargyl alcohol **162** as the starting material, which was reacted with either aniline (**167**) or methylaniline (**168**). The group of van Maarseveen used CuI with the pybox **163** as the source of chirality, while Nishibayashi used the chiral bis-phosphine **166**. Both groups achieved comparable results with yields around 95% yield and 86% *ee*. These conditions were also successfully applied for propargylic carbamates **169** as substrates for such copper catalyzed asymmetric substitution reactions, providing propargylic amines under extrusion of CO_2 .^[151]



Scheme 59: Literature known propargylic substitution reactions via a metal allenyliden intermediate.^[147,149,150]

Based on these results, a proof of concept study was initiated. In order to increase the electrophilic character of the ruthenium allenyliden intermediate **157** (Scheme 57), a *p*- CF_3 substituted phenyl moiety was used. As a leaving group, the Boc group was selected for its established synthesis and the irreversible extrusion of CO_2 during the formation of the intermediate **157**. The synthesis^[153] (Scheme 60) started from *p*- CF_3 benzaldehyde (**170**), which was reacted with TMS-acetylene (**171**) in a two step procedure. The corresponding propargylic alcohol **172** was obtained in 76% yield over two steps. Subsequent treatment

with Boc₂O produced the Boc-protected propargylic alcohol **173** in 76% yield. In addition, the acetylated propargyl alcohol **174** was synthesized from the propargylic alcohol **172** in 73% yield.

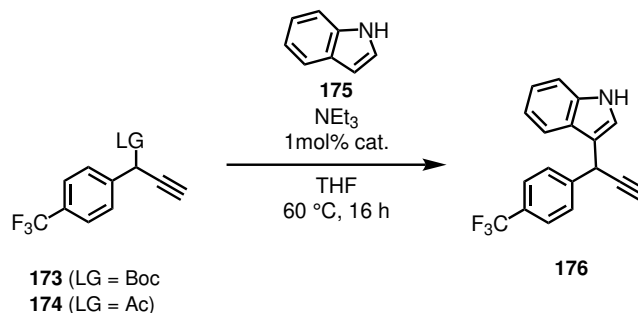


Scheme 60: Synthesis of Boc protected propargyl alcohol **173**.

With the desired protected propargyl alcohols **173** and **174** in hand, the aNHC complex *rac.* **114b** was selected to further increase the electrophilicity of the proposed allenyliden intermediate. Starting with the conditions used for the alkynylation (Chapter 3.2.3), the two substrates were reacted with indole (**175**). The acylated substrate **174** (Table 13, entry 1) showed no conversion at 25 °C and 60 °C after 24 h, although the color of the solution changed to a deep red after addition of the base. Under the same conditions, the Boc-protected substrate **173** (entry 2) showed no conversion at 25 °C. After heating to 60 °C for 24 h, the product **176** was obtained in 16% yield. With the proof of activity, the reaction was performed using non-*racemic* catalyst Δ -**114b** (entry 3), which provided the product **176** in 14% yield and 11% *ee*.

For comparison, the nNHC complex Λ -**64g** (entry 4) was applied as catalyst, which resulted in a higher yield of 40% but no enantioselectivity. In order to exclude a *racemic* background reaction, the experiment was performed without addition of catalyst (entry 5) and no conversion of the starting material was observed after 20 h. As the formed chiral center is located at the C-3 atom is rather distant from the metal center, a low asymmetric induction was assumed, thus leading to the low *ee* values. To reduce this effect, the sterically more demanding complexes Δ -**137a** and Δ -**137b** were synthesized and applied to this reaction. The CF₃ complex Δ -**137a** (entry 6) showed a NMR yield of 12% with an increased enantioselectivity of 38% *ee* after 17 hour. The corresponding bromine complex Δ -**137b** (entry 7) was found to be active at 25 °C and the target product was obtained in 8% yield and 55% *ee*.

In this proof of principle study the Boc protected substrate **173** showed higher activity compared to the acylated substrate **174**. The nNHC complex **64g** showed the highest yield of 40% but without any asymmetric induction, while its aNHC counterpart **114b** produced the target product with a diminished yield

Table 13: Catalyst and LG screening for the propargylic substitution reaction.

Entry	cat.	LG	T / $^\circ\text{C}$	t /h	NMR yield / $\%$	ee / $\%$
1	<i>rac.</i> 114b	OAc	25 to 60	24	0	–
2	<i>rac.</i> 114b	OBoc	25 to 60	24	16 ^a	–
3	Δ - 114b	OBoc	60	18	14	11
4	Λ - 64g	OBoc	60	16	40	0
5	–	OBoc	60	20	0 ^b	–
6	Δ - 137a	OBoc	60	17	12	38
7	Δ - 137b	OBoc	25	24	8	55

^a isolated Yield, ^b no conversion

of 14% but an increased enantioselectivity of 11% *ee*. The sterically more demanding DIPP derivatives **137a** and **137b** were found to provide higher enantioselectivity and showed activity at 25 °C. These results provide the foundation for further investigations as the newly developed non- C_2 -symmetric aNHC complexes allow the asymmetric transformation while the C_2 -symmetric nNHCs failed to provide asymmetric induction.

3.3. UV-Vis Absorption

3.3.1. UV-Vis Absorption Measurements

As part of the investigations with the substituted ruthenium complexes, UV-Vis absorption spectra were measured to explore the possibility of photoredox catalysis. Similar to previous photo redox catalysis in the Meggers group, the concept is based on absorption of the metal-substrate complex **177** or **178** at a certain wavelength while the substrate alone does not show any absorption. This minimizes the probability of an unwanted excitement of the substrate without being bound to the chiral catalyst, therefore preventing a *racemic* background reaction. 2-Acylimidazole **179** was chosen as a substrate since it showed activity for a [2+2] cycloaddition with rhodium complexes.^[154] This was compared to the saturated acylimidazole **180** and the solvents CH_3CN and MeOH were used for this investigation (see Scheme 61). Although

3. Results and Discussion

In a similar manner, the spectra recorded with the CF₃ derivatives **64g** and **114b** are shown in Figure 31. The spectra overall are similar to the previous spectra with numerical shifts of the maxima. Complex **64g** showed with both substrates no changes in MeOH, while in CH₃CN the same broad absorption band for **179** with the maximum at 520 nm was observed. For the abnormal variant **114b**, this band is visible in both solvents with the maximum at 558 nm in MeOH and 570 nm in CH₃CN with a slightly more prominent absorption in the CH₃CN. For the saturated substrate **180** the absorption with the aNHC complex **114b** showed two less distinct, broad absorption bands around 490 nm without a clear maximum.

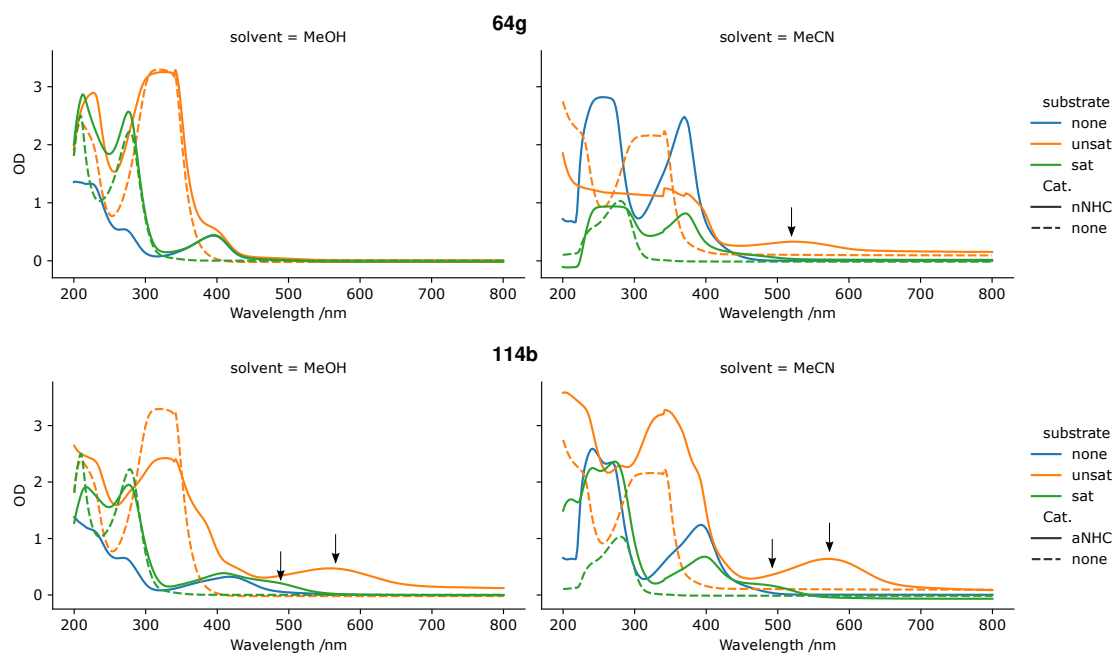


Figure 31: UV-Vis absorption spectra of **64g** (top row) and **114b** (bottom row) in MeOH (left column) and CH₃CN (right column). The metal complex alone is shown as a solid blue line, addition of **179** is displayed in orange, **180** in green. Both substrates are also shown in the corresponding color without the metal complex as dashed lines. Points of interests are marked with arrows.

The electron rich complex **64j** with the dimethyl amino substitution showed the broad absorption band at 632 nm with the unsaturated substrate **179**, which was previously only seen for aNHC complexes (Figure 32). However this broad band is barely visible around 644 nm in CH₃CN. With the saturated imidazole **180**, a similar and barely visible broad band at 510 nm was visible in MeOH, while in CH₃CN no absorption band was observed. The general intensity with this complex is lower compared to the previous complexes.

The wavelengths for the local maxima are summarized in Table 14 for easier comparison. The aNHC complexes **114a** and **114b** generally have a red-shifted absorption maximum of around +45 nm compared to their nNHC counterparts. This red shift is more pronounced for **64j** with +74 and +58 nm. Therefore,

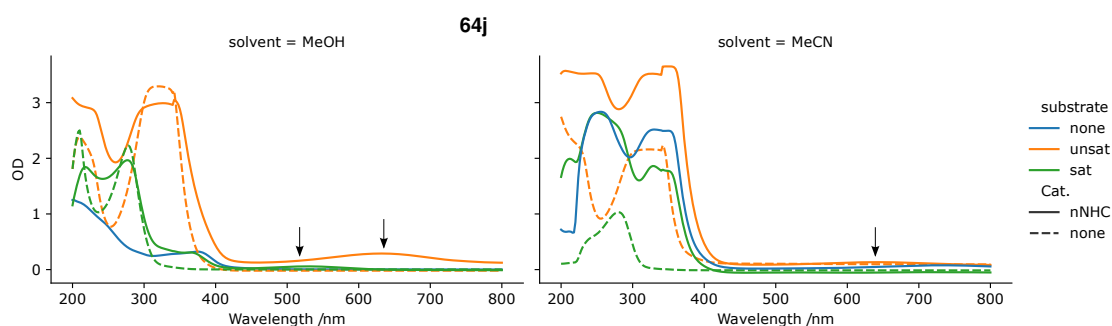


Figure 32: UV-Vis absorption spectra of **64j** in MeOH (left) and CH₃CN (right). The metal complex alone is shown as a solid blue line, addition of **179** is displayed in orange and **180** in green. Both substrates are also shown in the corresponding color without the metal complex as dashed lines. Points of interests are marked with arrows.

the maxima can be ordered by the binding mode of the complex and the modification in the following order:



This corresponds with the estimated ability to act as a electron donor of the ligands. Changing the solvent from MeOH to CH₃CN results in an estimated shift of +10 nm. Compared to the known behavior of the Rh complexes by the Meggers group, which showed an emerging band around 375 nm, the broad absorption bands between 500 and 650 nm was not expected. Potentially, this could enable new synthetic applications utilizing the longer wavelengths, which were not accessible with the known Rh complexes so far. Further studies could include DFT calculations to support the spin densities of the triplet state.^[154]

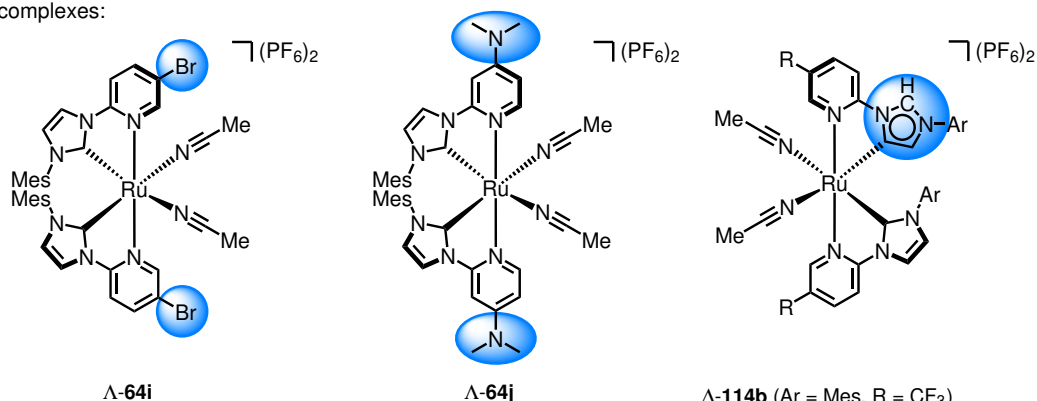
Table 14: Summarized wavelengths of the local maxima as a result of coordination of the substrate **179** and the metal complexes either in MeOH or CH₃CN.

Entry	Cat	λ_{max} /nm	
		MeOH	CH ₃ CN
1	64i	–	546
2	114a	572	586
3	64g	–	520
4	114b	558	570
5	64j	632	644

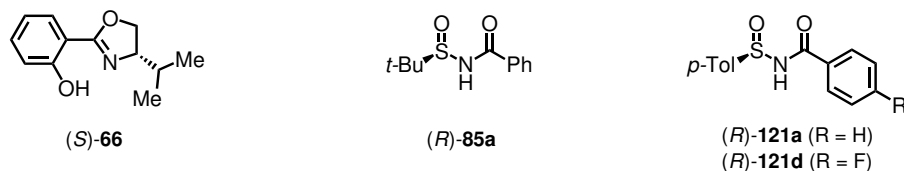
4. Summary and Outlook

Within this thesis, modified chiral-at-metal ruthenium complexes have been developed through a chiral auxiliary mediated synthesis (Scheme 62). The complexes consist of two chelating NHC ligands, generating a helical chirality with a formal stereogenic metal center, and two labile acetonitrile ligands. The main focus was set towards modifications of the pyridine moiety. During the investigation, a synthesis for the 5-Br derivative **64i** as well as the 4-NMe₂ derivative **64j** was successfully developed. The three modifications 4-NO₂, 5-NO₂ and 5-NMe₂ on the other hand remained inaccessible.

New complexes:



Matching auxiliaries:



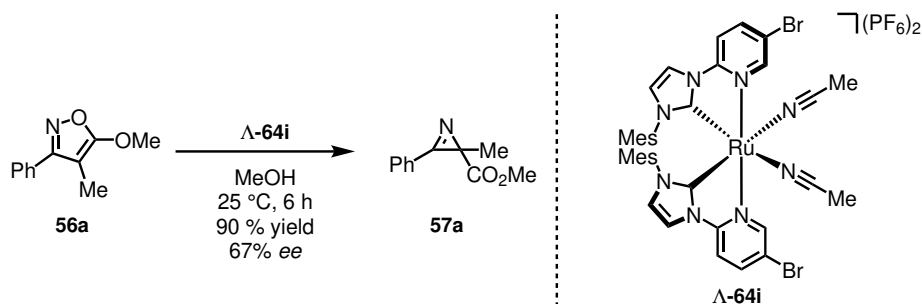
Scheme 62: Overview of the synthesized chiral-at-metal ruthenium complexes within this thesis, the successful applied auxiliary's below and the modified moieties highlighted in blue.

As part of the investigation, lowering the reaction temperature from 200 °C to 90 °C resulted in a new type of complex containing a nNHC as well as an aNHC ligand. This was exclusive for the 5-CF₃ and 5-Br derivatives, resulting in the complexes Δ -**114b** and Δ -**114a**. Furthermore, the Mes group of the mixed complexes Δ -**114b** and Δ -**114a** was successfully replaced by the sterically more demanding DIPP group, resulting in the complexes Δ -**137a** and Δ -**137b**.

For each of the newly synthesized complexes, the choice of the auxiliary had to be adjusted to achieve stable diastereomeric complexes and sufficient resolution during column chromatography. These requirements were satisfied for complex **64i** with the established salicyl oxazoline auxiliary (S) -**66**, while the new sulfinyl benzamide (R) -**85** was a match for complex **64j**. On the other hand, these auxiliaries did not

fulfill the requirements for any of the new mixed normal/abnormal NHC complexes. In a first approach, a C_2 -symmetric auxiliary, such as the PyBOX systems **118a** and **118b**, was used to keep the number of possible diastereomeric complexes low, but resulted in stability issues and/or insufficient separation. The modified sulfinamides **121a** and **121d** were designed to increase the differences in energy by enabling $\pi - \pi$ stacking for a matched pair and repulsive interactions for a mismatched pair. This allowed a simplified separation as the two stable diastereomeric complexes contain the same configuration at the metal center.

The ring contraction reaction of isoxazole **56a** to 2*H*-azirine **57a** was investigated (Scheme 63). A initial catalyst screening revealed the newly synthesized ruthenium complex Λ -**64i** to provide a high yield of 76% and moderate enantioselectivity of 45% *ee*. After a broad screening of solvents, polar solvents such as MeOH, MeNO₂, *i*-PrOH and DCE showed high yields (above 70%) while DMF, CH₃CN, ethylene glycol and *i*-AmOH led to either low conversion and/or low yields (below 50%). In terms of enantioselectivity, MeOH, MeNO₂ and DCE showed the best results with up to 63% *ee*. As only one coordination site was needed for this transformation and the complexes provide two labile CH₃CN ligands, a screening of coordinating additives such as PPh₃ and imidazole was performed. However, none of these additives showed a positive effect. Further investigations revealed a non-linear dependency of *ee* over time as well as a light induced *racemisation*. Overall, a maximum of 90% yield and 67% *ee* was achieved.



Scheme 63: Ring contraction of isoxazole **56a** catalyzed by Λ -**64i**.

Besides the ring contraction reaction, the newly synthesized complexes were also investigated for differences in the catalytic properties of an alkynylation of trifluoroacetophenone (**68**) and the C(sp³)-H amination reaction of benzoyl urea **76** (Figure 33). It was discovered that the TOF for alkynylation of **68** are in a similar range for nNHCs (14 h⁻¹ for Λ -**64i**) and the aNHCs (9 h⁻¹ for Δ -**114a**). Interestingly, the ratio of the target alkynylation compared to the head-to-head dimerisation of the alkyne **69** was shifted towards the dimerisation in case of the aNHCs complexes. This consumes the alkyne faster, resulting in lower yields of the target product **70**.

For the C(sp³)-H amination reaction of urea **76**, the TOF were quite different with 4 h⁻¹ using nNHC complex Λ -**64i** and 670 h⁻¹ using aNHC complex Δ -**114a**. This denotes a 160-fold increase however the asymmetric induction is decreased, resulting in a lowered enantioselectivity of 86% *ee*.

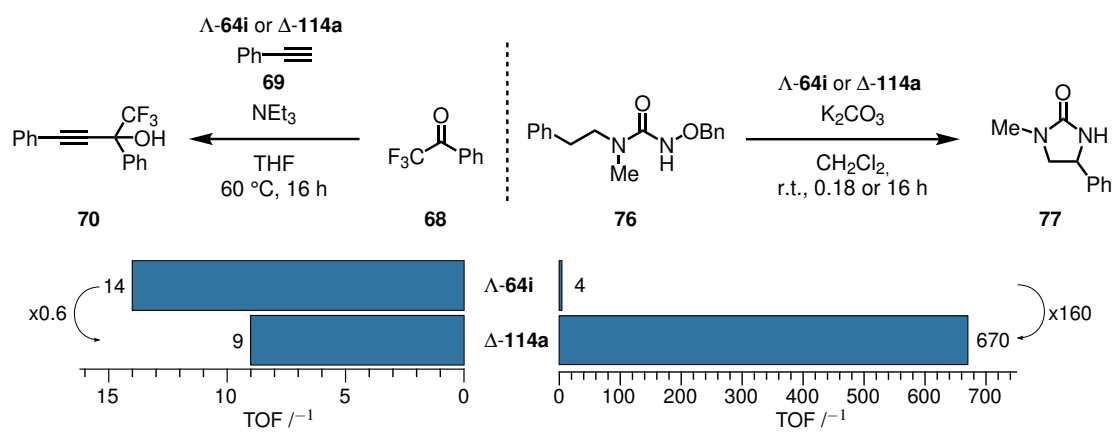


Figure 33: Comparison of the two investigated reactions, the alkylation of **68** (left) and the C(sp³)-H amination reaction of benzoyl urea **76** (right) exemplary shown for nNHC complex $\Delta\text{-64i}$ and aNHC $\Delta\text{-114a}$.

Outlook

In this work aNHC complexes showed significantly faster kinetics for nitrene based conversions, which is an ideal starting point for further investigations concerning C(sp³)-H amination reactions. The issue of lower *ee* likely arises from the less sterically demanding coordination as the aryl moiety of the abnormal bond ligand points away from the metal-center. A modified ligand **181**, which maintains the abnormal binding mode and provides the same orientation as a nNHC could inherit the positive effects from both, a high enantioselectivity combined with high activity (Figure 34).

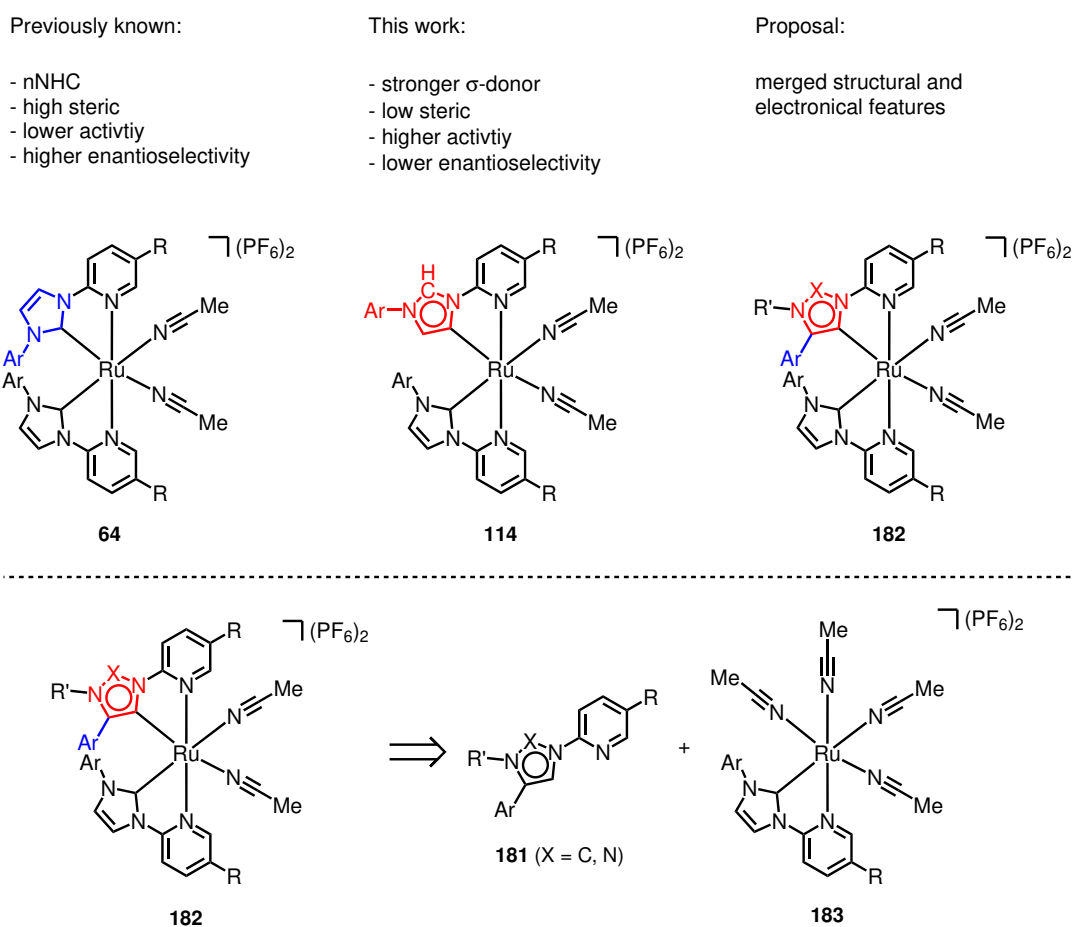


Figure 34: Synthesis plan for modified complexes for substituted triazole (X=N) or imidazole (X=C) ligands.

Ligand precursor **181**, either as triazole (X = N)^[13,155,156] or imidazole (X = C),^[157] with synthesis and complexation protocols is literature known. A complex similar to **183** was already reported by Bernet *et al.* in 2011 and was successfully synthesized in this work as complex **113** (Scheme 39), providing a starting point for further modifications.^[133] The resulting system features a modular synthesis, which allows the introduction of different substitutions thereby providing a wide range of possible modifications.

5. Experimental Part

5.1. General Materials and Methodes

All reactions were carried out under nitrogen atmosphere in oven-dried glassware unless noted otherwise. All reagents and reaction solvents (HPLC-grade) were purchased from *Acros*, *Merck* or *Alfa Aesar* and used without further purification unless noted otherwise. Dry solvents were distilled under nitrogen from calcium hydride (CH_3CN , CH_2Cl_2) or sodium/benzophenone (tetrahydrofurane) prior to use. Solvents for column chromatography were purified by distillation. Mesitylimidazole (**92**) was synthesized by Marcel Hemming according to published procedures.^[158] (*S*)-salicyl oxazoline **66**^[114], $[\text{RuCl}(p\text{-cymene})]_2$ (**111**)^[159], ruthenium complexes Λ -**64b** and Λ -**64o** were prepared according to published procedures.^[114] Complex Λ -**64e** was kindly provided by Zijun Zhou.

Thin Layer Chromatography: TLC was performed on *Merck KGaA* precoated TLC-sheets (Silica gel 60 F₂₅₄, layer thickness 210–270 μm). TLC spots were detected by irradiation with UV-light ($\lambda = 254 \text{ nm}$ and $\lambda = 366 \text{ nm}$). Non aromatic compounds were stained using a Cer-Dip (0.5 g $\text{Ce}(\text{NH}_4)(\text{NO}_3)_6$, 24 g $(\text{NH}_4)_6\text{Mo}_7\text{O}_{24} \cdot 4\text{H}_2\text{O}$, 28 mL H_2SO_4 in 150 mL water) or MnO_4 -Dip (3 g KMnO_4 , 20 g Na_2CO_3 , 0.5 g NaOH in 240 mL water).

Column Chromatography: *Macherey-Nagel* (irregularly shaped, 230–400 mesh, pH 6.8, pore volume 0.81 mL g^{-1} , mean pore size 66 \AA , specific surface 492 $\text{m}^2 \text{g}^{-1}$, particle size distribution 0.5% < 25 μm and 1.7% > 71 μm , water content 1.6%) was used as the stationary phase. Compressed air was utilized to build up the pressure for flash column chromatography.

Analytic Section

Nuclear Magnetic Resonance Spectroscopy: ^1H -NMR, $^{13}\text{C}\{^1\text{H}\}$ NMR and $^{19}\text{F}\{^1\text{H}\}$ NMR spectra were recorded at 300 K on *Bruker AV II 300* (300 MHz) and *AV III HD 250* (250 MHz) in automation or on *Bruker AV NEO 300* (300 MHz), *AV III 500* (500 MHz) or *AV III HD 500* (500 MHz) spectrometer by the members of the NMR service department of the Philipps-Universität Marburg. Chemical shifts values δ are reported in ppm relative to tetramethylsilane (TMS, $\delta = 0 \text{ ppm}$) with the solvent resonance as internal reference (Table 15). ^1H -NMR spectra multiplicities are indicated as singlets (s), broad singlet (s, br), doublet (d), triplet (t), quartet (q), multiplet (m) and combinations thereof.

Table 15: Chemical shifts of the residual signals of the used NMR solvents.^[160]

Solvent	¹ H NMR	¹³ C NMR
CDCl ₃	7.26 ppm	77.16 ppm
CD ₂ Cl ₂	5.32 ppm	53.84 ppm
CD ₃ CN	1.94 ppm	1.32 ppm
MeOD	3.31 ppm	49.00 ppm
DMSO- <i>d</i> ₆	2.50 ppm	39.52 ppm

High-Performance Liquid Chromatography (HPLC): HPLC-measurements were performed on an *Agilent* 1200, 1260 or on a *Shimadzu* LC-2030C. The used chiral stationary phase and detailed procedures are given for each compound individually.

Gas Chromatography (GC and GC/MS): GC analysis were recorded on an *Agilent* 7890A gas chromatograph equipped with an flame ionization detector (FID). Carrier gas: N₂, Inlet temperature: 250 °C, FID temperature: 300 °C. Column conditions are given for each compound individually. GC/MS spectra were recorded on an *Agilent* 6890 gas chromatograph coupled with a *Hewlett Packard* 5973 mass selective detector. Carrier gas: He, total flow 15.1 mL min⁻¹, column: *Macherey Nagel* Optima 5 HT (30 m x 0.25 mm x 0.25 μm).

Mass Spectrometry: Mass spectra were recorded on a *Thermo Fischer Scientific* Finnigan LTQ-FT Ultra mass spectrometer using ESI or APCI as ionization source. The ionic masses are given as *m/z* and refer to the isotope with the highest natural occurrence. The measurement was performed by the members of the mass spectrometry department of the Philipps-Universität Marburg.

Infrared Spectroscopy: IR-spectra were recorded on a *Bruker* Alpha FT-IR spectrometer using ATR (attenuated total reflection) mode. Absorption bands are given as wave numbers $\tilde{\nu}$ in the unit of cm⁻¹. All substances were measured as films or solids.

UV-Vis Spectroscopy: UV-Vis absorbance spectra were recorded on a *JASCO* V-650 spectro photometer equipped with a *JASCO* PAC 743 Peltier cell changer at constant temperature of 20 °C in a quartz cuvette with a path length of 10 mm and a volume of 1 mL.

Circular Dichroism Spectroscopy: CD-spectra were recorded on a *JASCO* J-810 CD spectropolarimeter in a quartz cuvette with a path length of 1 mm, 600–200 nm, 1 nm bandwidth, 1 s response time, 50 nm min⁻¹ scanning speed, accumulation of 3 scans.

Single-Crystal X-ray Diffraction: X-ray data were collected with a *Stoe* Stadivari diffractometer or with a *Bruker* AXS D8 Quest diffractometer. Measurement and evaluation of the data were conducted by Mr. Riedel, Mr. Marsch, Dr. Harms or Dr. Ivlev of the department for crystal structure analysis of the Philipps-Universität Marburg. The obtained data were solved and refined by Dr. Harms or Dr. Ivlev. The data of all published structures have been deposited in the Cambridge Crystallographic Data Center (CCDC). The CIF files can be obtained from the CCDC free of charge via http://www.ccdc.cam.ac.uk/data_request/cif.

Melting Points: Melting points were determined on a *Mettler Toledo* MP70 using one end closed capillary tubes.

5.2. General Procedures

Procedure A: Synthesis of Imidazolium Salts

Following a published and modified procedure,^[122] a flame dried 10 mL PTFE sealed pressure tube was charged with imidazole derivative (1 eq), 2-halogen pyridine (1 eq) and a magnetic stirring bar under an atmosphere of N₂. The pressure tube was fully immersed in a preheated oil bath. The solvent-free reaction mixture was stirred for the indicated time and temperature. After cooling to room temperature, Et₂O (5 mL) was added and the solid triturated and further treated with an ultrasonic bath for 10 min. The obtained slurry was filtrated and the resulting solid subsequently redissolved in the least possible amount of CH₂Cl₂, precipitated with excess amount of Et₂O and filtrated. The desired imidazolium salt was obtained usually in sufficient purity.

Procedure B: Anion Metathesis of Imidazolium Salts

Following a reported procedure,^[161] the obtained imidazolium salt (1 mmol) was dissolved in water (50 mL) at room temperature. A solution of the desired salt (1-2 eq of either NH₄PF₆, NH₄BF₄ or NaSbF₆) in water (5 mL) was added. The mixture was stirred for 5 min and the precipitation collected by filtration, washed with water and dried under reduced pressure.

Procedure C: Direct Metalation

Based on a modified reported procedure,^[114] a oven dried 10 mL PTFE sealed pressure tube was charged with RuCl₃ (1 eq), imidazolium salt (2 eq) and ethylene glycol (0.1 mL mg⁻¹ of RuCl₃). The solution was degassed by applying high vacuum for 30 min, flushed with N₂, and stirred at the indicated temperature and time. The reaction mixture was cooled to room temperature, and a saturated aqueous solution of NH₄PF₆ (10 eq) was added. The precipitation was filtrated and rinsed with water. The solid was re-

dissolved in a small amount of CH₃CN (ca. 10 mL), transferred into a new flask, and the solvent was removed under reduced pressure to dryness. AgPF₆ (2 eq) and CH₃CN (2.5 mL) were added under N₂ atmosphere and heated to 60 °C for 2 h. The mixture was cooled to room temperature, filtrated through a pad of Celite, rinsed with CH₃CN and the solvent was removed under reduced pressure. Purification of the obtained brown solid by column chromatography (CH₂Cl₂/CH₃CN 10:1 → 5:1) afforded the complex as a mixture with the free ligand, both as hexafluorophosphate salts. The mixture was dissolved in CH₃CN (ca. 1.5 mL) and precipitated with Et₂O (ca. 20 mL) at -20 °C overnight. The resulting pale yellow crystalline solid was collected via filtration and dried under high vacuum.

Procedure D: Enantioselective C-H Amination

Following a published procedure,^[118] an oven dried 10 mL PTFE sealed pressure tube was charged with *N*-benzoyloxyurea (55.6 mg, 0.2 mmol, 1.0 eq), catalyst (0.9 mol%) and K₃CO₃ (83.5 mg, 0.60 mmol, 3.1 eq) under an atmosphere of N₂. Freshly distilled CH₂Cl₂ (2 mL) was added under positive N₂ pressure and stirred at room temperature and monitored by TLC (elution with pure EtOAc). After full conversion of the starting material was observed, the reaction mixture was directly purified by flash chromatography on silica gel (EtOAc to EtOAc/MeOH 20:1).

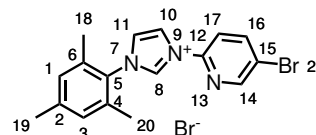
Procedure E: Enantioselective Ring Contraction of Isoxazoles

Following a published procedure,^[77] the catalyst (1.0 mol%) was dissolved in CH₂Cl₂ (1 mL), substrate (0.10 mmol) was added and stirred at the indicated temperature and time. After full conversion was observed via TLC, the mixture was filtered through a small silica pad with CH₂Cl₂. The solvent was removed under reduced pressure which provided the target product as a yellow oil.

5.3. Synthesis of Imidazolium Salts

Synthesis of 3-(5-bromopyridin-2-yl)-1-mesityl-1*H*-imidazolium bromide (**93a**)

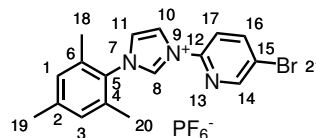
According to general procedure A, imidazole **92** (1576 mg, 8.46 mmol, 1.02 eq) and 2,5-dibromopyridine (**91**, 1990 mg, 8.40 mmol, 1.00 eq) were heated to 190 °C for 19 h. After purification, target product **93a** (3270 mg, 7.73 mmol, 92 %) was obtained as an off-white solid.



¹H-NMR (250 MHz, CDCl₃): δ = 9.28 (dd, 1H, *J* = 1.8, 1.8 Hz, *H*₈), 8.60 (d, 1H, ⁴*J* = 2.3 Hz, *H*₁₄), 8.45 (dd, 1H, *J* = 1.8, 1.8 Hz, *H*_{imidazole}), 8.18 (dd, 1H, ³*J* = 8.7 Hz, ⁴*J* = 2.3 Hz, *H*₁₆), 8.02 (d, 1H, ³*J* = 8.6 Hz, *H*₁₇), 7.42 (dd, 1H, *J* = 1.8, 1.8 Hz, *H*_{imidazole}), 7.07 (s, 2H, *H*_{1,3}), 2.38 (s, 3H, *H*₁₉), 2.12 (s, 6H, *H*_{18,20}) ppm. **¹³C-NMR** (75 MHz, CDCl₃): δ = 150.4, 143.7, 142.2, 134.6, 134.2, 130.5, 130.2 (2C), 125.0, 122.6, 120.7, 116.5, 21.3, 17.5 (2C) ppm. **¹⁹F-NMR** (235 MHz, CDCl₃): δ = -72.4 (d, ¹*J*_{P,F} = 712.9 Hz, M-PF₆⁻) ppm. **HRMS (ESI)**: *m/z* calcd. for C₁₇H₁₇Br₁N₃ [M-Br⁻]⁺: 342.0600, found: 342.0608. **IR** (film): $\tilde{\nu}$ = 1591, 1539, 1465, 1387, 1332, 1237, 1089, 1056, 1014, 822, 745, 666, 554, 516, 414 cm⁻¹. **M.p.**: 210 °C (CH₂Cl₂).

Synthesis of 3-(5-bromopyridin-2-yl)-1-mesityl-1*H*-imidazolium bromide (**93b**)

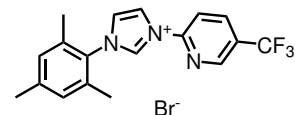
According to general procedure B, **93a** (426 mg, 1.00 mmol, 1.00 eq) was dissolved in water (50 mL) and a solution of NH₄PF₆ (300 mg, 1.84 mmol, 1.8 eq) in water (5 mL) was added, providing the target product **93b** (618 mg, 1.27 mmol, 69 %) as a colorless solid.



¹H-NMR (250 MHz, CDCl₃): δ = 9.28 (dd, 1H, ⁴*J* = 1.8, 1.8 Hz, *H*₈), 8.60 (d, 1H, ⁴*J* = 2.3 Hz, *H*₁₄), 8.45 (dd, 1H, *J* = 1.8, 1.8 Hz, *H*_{imidazole}), 8.18 (dd, 1H, ³*J* = 8.7 Hz, ⁴*J* = 2.3 Hz, *H*₁₆), 8.02 (d, 1H, ³*J* = 8.6 Hz, *H*₁₇), 7.42 (dd, 1H, *J* = 1.8, 1.8 Hz, *H*_{imidazole}), 7.07 (s, 2H, *H*_{1,3}), 2.38 (s, 3H, *H*₁₉), 2.12 (s, 6H, *H*_{18,20}) ppm. **¹³C-NMR** (75 MHz, CDCl₃): δ = 150.4, 143.7, 142.2, 134.6, 134.2, 130.5, 130.2 (2C), 125.0, 122.6, 120.7, 116.5, 21.3, 17.5 (2C) ppm. **¹⁹F-NMR** (235 MHz, CDCl₃): δ = -72.4 (d, ¹*J*_{P,F} = 712.9 Hz, PF₆⁻) ppm. **HRMS (ESI)**: *m/z* calcd. for C₁₇H₁₇Br₁N₃ [M-PF₆⁻]⁺: 342.0600, found: 342.0608. **IR** (film): $\tilde{\nu}$ = 1591, 1539, 1465, 1387, 1332, 1237, 1089, 1056, 1014, 822, 745, 666, 554, 516, 414 cm⁻¹. **M.p.**: 210 °C (CH₂Cl₂).

Synthesis of 3-(5-trifluoromethylpyridin-2-yl)-1-mesityl-1*H*-imidazolium bromide (116a)

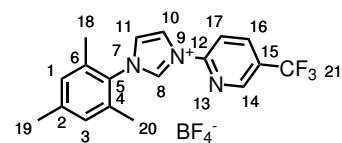
According to general procedure A, **92** (844 mg, 4.53 mmol, 1.02 eq) and 2-bromo-5-trifluoromethylpyridine (**115**, 1003 mg, 5.44 mmol, 1.00 eq) were heated to 180 °C for 20 h, providing the target product **116a** (1671 mg, 4.05 mmol, 91 %) as an off-white solid.



¹**H-NMR** (300 MHz, CDCl₃) δ = 11.58 (dd, ⁴*J* = 1.6, 1.6 Hz, 1H, *H*₈), 9.56 (d, ³*J* = 8.6 Hz, 1H, *H*₁₇), 8.90 (dd, *J* = 1.9 Hz, 1H, *H*_{imidazole}), 8.79 (s, br, 1H, *H*₁₄), 8.30 (dd, ³*J* = 8.6 Hz, ⁴*J* = 2.3, 1H, *H*₁₆), 7.41 (dd, *J* = 1.8 Hz, 1H, *H*_{imidazole}), 7.04 (s, 2H, *H*_{1,3}), 2.34 (s, 3H, *H*₁₉), 2.19 (s, 6H, *H*_{18,20}) ppm. ¹³**C-NMR** (126 MHz, CDCl₃): δ = 148.2, 146.1 (q, ³*J*_{C,F} = 4.0 Hz), 141.9, 138.6 (q, ⁴*J*_{C,F} = 3.3 Hz), 137.1, 134.0, 130.5, 130.2, 128.5 (q, ²*J*_{C,F} = 34.1 Hz), 124.4, 122.7 (q, ¹*J*_{C,F} = 272.8 Hz), 120.3, 117.0, 21.3, 18.0 ppm. ¹⁹**F-NMR** (235 MHz, CDCl₃): δ = -62.4 ppm. **HRMS (ESI)**: *m/z* calcd. for C₁₈H₁₇F₃N₃ [M+Br⁻]⁺: 332.1369, found: 332.1371. **IR** (film): $\tilde{\nu}$ = 3196, 3056, 2970, 1603, 1534, 1490, 1406, 1327, 1267, 1243, 1170, 1130, 1069, 1017, 963, 936, 861, 835, 765, 708, 665, 635, 608, 580, 507, 467, 425 cm⁻¹.

Synthesis of 3-(5-trifluoromethylpyridin-2-yl)-1-mesityl-1*H*-imidazolium tetrafluoroborate (116c)

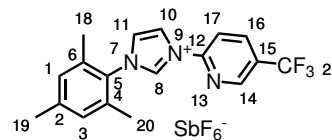
According to general procedure B, **116a** (204.6 mg, 0.49 mmol, 1.00 eq) was dissolved in water and precipitated with NH₄BF₄ (294 mg, 2.80 mmol, 5.65 eq). The target product **116c** was obtained as a crystalline, colorless solid (179 mg, 0.43 mmol, 86 %).



¹**H-NMR** (300 MHz, CDCl₃): δ = 9.73 (s, br, 1H, *H*₈), 8.66 (s, br, 1H, *H*_{imidazole}), 8.53 (d, 1H, ³*J* = 8.6 Hz, *H*₁₇), 8.31 (dd, 1H, ³*J* = 8.7 Hz, ⁴*J* = 2.3 Hz, *H*₁₆), 7.44 (dd, 1H, ⁴*J* = 1.9, 1.9 Hz, *H*_{imidazole}), 7.06 (s, 2H, *H*_{1,3}), 2.37 (s, 3H, *H*₁₉), 2.14 (s, 6H, *H*_{18,20}) ppm. Note: only one out of three couplings of the imidazole is clearly visible. ¹³**C-NMR** (126 MHz, CDCl₃): δ = 148.2, 146.4 (q, ³*J*_{C,F} = 4.1 Hz, *C*₁₄), 142.1, 138.8 (q, ³*J*_{C,F} = 3.4 Hz, *C*₁₆), 135.2, 134.2, 130.5, 130.2 (2C), 128.7 (q, ²*J*_{C,F} = 34.1 Hz, *C*₁₅), 125.0, 122.7 (q, ¹*J*_{C,F} = 272.8 Hz, *C*₂₁), 120.8, 115.7, 21.3, 17.5 (2C) ppm. ¹⁹**F-NMR** (282 MHz, CDCl₃): δ = -62.4 (s, CF₃), -151.4 (BF₄⁻) ppm. **HRMS (ESI)**: *m/z* calcd. for C₁₈H₁₇F₃N₃ [M-BF₄⁻]⁺: 332.1369, found: 332.1371. **IR** (film): $\tilde{\nu}$ = 3161, 1604, 1539, 1489, 1402, 1327, 1241, 1174, 1138, 1101, 1063, 1011, 844, 754, 666, 636, 618, 580, 519, 465, 433 cm⁻¹. **M.p.**: 236 °C (CH₂Cl₂).

Synthesis of 3-(5-trifluoromethylpyridin-2-yl)-1-mesityl-1*H*-imidazolium hexafluoroantimonate (**116d**)

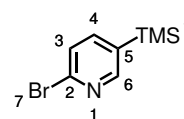
According to general procedure B, **116a** (2433 mg, 5.92 mmol, 1.00 eq) was dissolved in water and precipitated with NaSbF₆ (2550 mg, 9.86 mmol, 1.66 eq). The target product **116d** was obtained as a crystalline, colorless solid (2452 mg, 4.32 mmol, 73%).



¹H-NMR (300 MHz, CDCl₃): δ = 9.38 (dd, 1H, ⁴J = 1.7, 1.7 Hz, H₈), 8.80 (s, br, 1H, H_{Ar}), 8.55 (dd, 1H, J = 1.9, 1.9 Hz, H_{imidazole}), 8.33 (dd, 1H, ³J = 8.6 Hz, ⁴J = 2.3 Hz, H_{Ar}), 8.25 (d, 1H, ³J = 8.6 Hz, H_{Ar}), 7.47 (dd, 1H, J = 1.9, 1.9 Hz, H_{imidazole}), 7.07 (s, 2H, H_{1,3}), 2.38 (s, 3H, H₁₉), 2.12 (s, 6H, H_{18,20}) ppm. HRMS (ESI): *m/z* calcd. for C₁₈H₁₇F₃N₃ [M–SbF₆[–]]⁺: 332.1369, found: 332.1371. IR (film): $\tilde{\nu}$ = 1603, 1540, 1488, 1328, 1240, 1172, 1137, 1102, 1070, 1018, 945, 863, 843, 759, 658, 633, 578, 428 cm^{–1}. M.p.: 186 °C (CH₂Cl₂).

Synthesis of 2-bromo-5-(trimethylsilyl)pyridin (**184**)

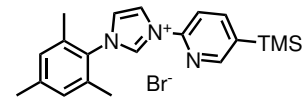
Following a published procedure,^[162] a flame-dried 50 mL N₂ round-bottom flask was charged with 2,5-dibromopyridine (**91**, 2105 mg, 8.89 mmol, 1.00 eq) under N₂-atmosphere, dissolved in Et₂O (20 mL) and cooled to –78 °C. Over a period of 30 min, a solution of *n*-BuLi (1.6 M in *n*-hexane) was added and stirred at this temperature for additional 80 min. After full conversion of the starting material was observed via TLC, a solution of TMS-chloride (1.1 mL, 8.6 mmol, 0.97 eq) in Et₂O (3.0 mL) was added slowly over a period of 5 min. The reaction mixture was allowed to warm up to –20 °C. Full conversion of the intermediate was observed via TLC after 1.5 h. The reaction was stopped via addition of water (20 mL) and stirred for further 5 min. The bi-phasic solution was extracted with Et₂O (3x30 mL), the combined organic phases were dried over Na₂SO₄ and evaporated. The crude product was purified via flash chromatography (*n*-pentane/ EtOAc 20:1) providing the target product **184** (1606 mg, 6.98 mmol, 78%) as a yellow oil.



¹H-NMR (300 MHz, CDCl₃): δ = 8.40 (dd, 1H, ⁴J = 2.1, 0.9 Hz, H₆), 7.61 (dd, 1H, ³J = 7.9, ⁴J = 2.1 Hz, H₄), 7.45 (dd, 1H, ³J = 7.8, ⁴J = 0.9 Hz, H₃), 0.29 (s, 9H, SiMe₃) ppm.

Synthesis of 3-(5-(trimethylsilyl)pyridin-2-yl)-1-mesityl-1*H*-imidazolium bromide (117a)

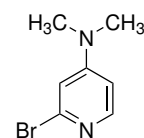
According to general procedure A, imidazole **92** (804.5 mg, 4.32 mmol, 1.0 eq) and pyridine **184** (968.9 mg, 4.21 mmol, 1.0 eq) were heated to 170 °C for 22 h, providing the target product **117a** (909 mg, 2.18 mmol, 51%) as an off-white solid.



¹H-NMR (300 MHz, CDCl₃) δ = 11.30 (dd, ⁴*J* = 1.6, 1.6 Hz, 1H, *H*₈), 9.15 (dd, ³*J* = 8.2 Hz, ⁴*J* = 0.9, 1H, *H*₁₇), 8.92 (dd, *J* = 1.8, 1.8 Hz, 1H, *H*_{imidazole}), 8.54 (d, ⁴*J* = 1.8 Hz, 1H, *H*₁₄), 8.19 (dd, ³*J* = 8.1 Hz, ⁴*J* = 1.9 Hz, 1H, *H*₁₆), 7.35 (dd, *J* = 1.8, 1.8 Hz, 1H, *H*_{imidazole}), 7.03 (s, 2H, *H*_{1,3}), 2.33 (s, 3H, *H*₁₉), 2.17 (s, 6H, *H*_{18,20}), 0.32 (s, 9H, SiMe₃) ppm. **¹³C-NMR** (75 MHz, CDCl₃): δ = 152.8, 146.4, 146.3, 141.8, 138.5, 136.2, 134.1, 130.7, 130.2 (*C*_{1,3}), 123.9, 120.2, 115.6, 21.3(*C*₁₉), 18.0 (*C*_{18,20}), -1.3 (SiMe₃) ppm. **HRMS (ESI):** *m/z* calcd. for C₂₀H₂₆N₃Si₁ [M-Br⁻]⁺: 336.1891, found: 336.1895. **IR** (film): $\tilde{\nu}$ = 3410, 3032, 2954, 1618, 1578, 1534, 1477, 1365, 1327, 1246, 1127, 1102, 1057, 1028, 965, 837, 757, 698, 661, 627, 581, 532, 472, 408 cm⁻¹.

Synthesis of 2-bromo-4-*N,N*-dimethylamino-pyridin (98a)

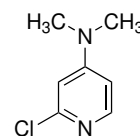
Following a modified literature procedure,^[125] a flame-dried 100 mL round-bottom flask was charged with *N,N*-dimethylethanol (0.8 mL, 7.99 mmol, 2.0 eq) and *n*-hexane (10 mL) and cooled to -3 °C. Over a period of 3 min, a solution of *n*-BuLi (6.4 mL, 2.5 M, 15 mmol, 4.0 eq) was added and the solution turned bright yellow. After stirring for 20 min, 4-dimethylaminopyridine (**97**, 484 mg, 3.96 mmol, 1.0 eq) was added in one portion and stirred for additional 5 min. The flask was equipped with a dropping funnel, cooled to -78 °C and a solution of CBr₄ (3300 mg, 9.95 mmol, 2.5 eq) in *n*-hexane (30 mL) was added over a period of 80 min. The reaction mixture was allowed to warm up to 0 °C and stirred for 30 min. After full conversion was observed via TLC, water (20 mL) was added, the biphasic mixture extracted with Et₂O (20 mL) and CH₂Cl₂ (30 mL). The combined organic phases were dried over Na₂SO₄, adsorbed on silica and purified via flash chromatography (*n*-pentane/EtOAc 1:1). The title compound **98a** (398 mg, 1.98 mmol, 50%) was obtained as a brown solid.



¹H-NMR (300 MHz, CDCl₃): δ = 7.9 (d, 1H, ³*J* = 6.0 Hz, *H*₆), 6.6 (d, 1H, ⁴*J* = 2.4 Hz, *H*₃), 6.4 (dd, 1H, ³*J* = 6.0, ³*J* = 2.4 Hz, *H*₅), 3.0 (s, 6H, 2xCH₃) ppm. **¹³C-NMR** (75 MHz, CDCl₃): δ = 155.9, 149.5, 143.3, 109.4, 106.3, 39.4 (2C, 2x CH₃) ppm. **HRMS (ESI):** *m/z* calcd. for C₇H₁₀Br₁N₂ [M⁺H⁺]⁺ 203.0001, found: 203.0001. **R_f** = 0.2 (*n*-pentane/ EtOAc 1:1).

Synthesis of 2-chloro-4-*N,N*-dimethylamino-pyridin (**98b**)

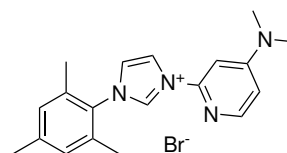
Following a modified literature procedure,^[125] a flame-dried 100 mL round-bottom flask equipped with nitrogen inlet was charged with *N,N*-dimethylaminoethanol (0.8 mL, 7.99 mmol, 2.00 eq) and *n*-hexane (10 mL) and cooled to -3°C . Over a period of 3 min, a solution of *n*-BuLi (6.5 mL, 2.5 M, 16 mmol, 4.08 eq) was added and the solution turned bright yellow. After stirring for 20 min, 4-dimethylaminopyridine (**97**, 487 mg, 3.98 mmol, 1.00 eq) was added in one portion and stirred for additional 5 min. The flask was equipped with a dropping funnel, cooled to -78°C and a solution of C_2Cl_6 (2299 mg, 9.71 mmol, 2.4 eq) in *n*-hexane (20 mL) was added over a period of 40 min. The reaction mixture was allowed to warm up to room temperature over night. After full conversion was confirmed by TLC, Water (20 mL) was added and the biphasic mixture was extracted with CH_2Cl_2 (3x60 mL). The combined organic phases were dried over Na_2SO_4 , adsorbed on silica and purified via flash chromatography (*n*-pentane/EtOAc 1:3). The title compound **98b** (453 mg, 2.89 mmol, 72%) was obtained as a brown solid.



$^1\text{H-NMR}$ (300 MHz, CDCl_3): $\delta = 7.96$ (d, 1H, $^3J = 6.0$ Hz, H_6), 6.46 (d, 1H, $^4J = 2.4$ Hz, H_3), 6.40 (dd, 1H, $^3J = 6.0$, $^4J = 2.4$ Hz, H_5), 2.99 (s, 6H, 2x CH_3) ppm. **$^{13}\text{C-NMR}$** (75 MHz, CDCl_3): $\delta = 156.2$, 152.4, 149.2, 106.0, 105.6, 39.4 (2C, 2x CH_3) ppm. **HRMS (ESI)**: m/z calcd. For $\text{C}_7\text{H}_{10}\text{Cl}_1\text{N}_2$ [M^+H^+] $^+$: 157.0527, found: 157.0531. **IR** (film): $\tilde{\nu} = 2924, 2810, 1589, 1514, 1423, 1379, 1295, 1265, 1219, 1131, 1073, 974, 804, 693, 612, 449, 417$ cm^{-1} . $R_f = 0.5$ (*n*-pentane/EtOAc 5:1).

Synthesis of 3-(4-(*N,N*-dimethylamino)pyridin-2-yl)-1-mesityl-1*H*-imidazolium bromide (**99a**)

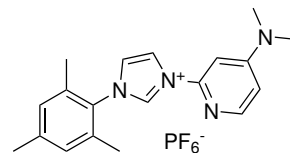
According to general procedure A, imidazole **92** (234 mg, 1.25 mmol, 1.01 eq) and pyridine **98a** (251 mg, 1.25 mmol, 1.00 eq) were heated to 160°C for 20 h, providing the target product **99a** (465 mg, 1.20 mmol, 96%) as an off-white solid.



$^1\text{H-NMR}$ (500 MHz, MeOD) $\delta = 8.62$ (d, $^4J = 2.1$ Hz, 1H, $H_{\text{imidazole}}$), 8.15 (d, $^3J = 6.1$ Hz, 1H, H_{14}), 7.91 (d, $^4J = 2.1$ Hz, 1H, $H_{\text{imidazole}}$), 7.18 (s, 2H, $H_{1,3}$), 7.13 (d, $^4J = 2.3$ Hz, 1H, H_{17}), 6.82 (dd, $^3J = 6.1$ Hz, $^4J = 2.3$ Hz, 1H, H_{15}), 3.16 (s, 6H, $H_{22,23}$), 2.39 (s, 3H, H_{19}), 2.16 (s, 6H, $H_{18,20}$) ppm. Note: 1H signal of H_8 is missing due to H/D exchange. **$^{13}\text{C-NMR}$** (126 MHz, MeOD): $\delta = 158.5, 149.8, 149.0, 142.8, 135.8, 132.6, 130.8$ (2C, $C_{1,3}$), 126.1, 121.7, 109.1, 97.2, 39.7 (2C, $C_{22,23}$), 21.1 (C_{19}), 17.4 (2C, $C_{18,20}$) ppm. **HRMS (ESI)**: m/z calcd. For $\text{C}_{19}\text{H}_{23}\text{N}_4$ [$\text{M}-\text{Br}^-$] $^+$: 307.1917, found: 307.1914. **IR** (film): $\tilde{\nu} = 3161, 3126, 2910, 2777, 1611, 1523, 1446, 1395, 1323, 1259, 1227, 1172, 1135, 1085, 1058, 978, 943, 908, 866, 821, 759, 729, 700, 669, 578, 528, 464, 413$ cm^{-1} .

Synthesis of 3-(4-(*N,N*-dimethylamino)pyridin-2-yl)-1-mesityl-1*H*-imidazolium hexafluorophosphate (**99c**)

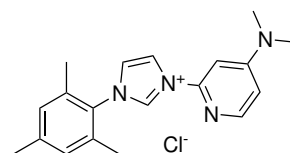
According to the general procedures A and B, pyridine **98b** (412 mg, 2.63 mmol, 1.00 eq) and imidazole **92** (489 mg, 2.62 mmol, 1.00 eq) were stirred at 175 °C for 16 h, precipitated and redissolved in water (20 mL). The product **99c** was precipitated with a aqueous solution of NH_4PF_6 (755 mg, 4.63 mmol, 1.76 eq). The title compound **99c** (956 mg, 2.12 mmol, 81% over two steps) was obtained as an off-white solid.



$^1\text{H-NMR}$ (300 MHz, CDCl_3) δ = 9.29 (dd, 4J = 1.9, 1.7 Hz, 1H, H_8), 8.56 (dd, J = 1.9, 1.7 Hz, 1H, $H_{\text{imidazole}}$), 8.08 (d, 3J = 6.1 Hz, 1H, H_{14}), 7.37 (dd, J = 1.9, 1.7 Hz, 1H, $H_{\text{imidazole}}$), 7.15 (d, 4J = 2.3 Hz, 1H, H_{17}), 7.10 (s, 2H, $H_{1,3}$), 6.61 (dd, 3J = 6.1 Hz, 4J = 2.3 Hz, 1H, H_{15}), 3.19 (s, 6H, $H_{22,23}$), 2.41 (s, 3H, H_{19}), 2.15 (s, 6H, $H_{18,20}$) ppm. $^{19}\text{F-NMR}$ (282 MHz, CDCl_3): δ = -72.4 (d, $^1J_{\text{P,F}}$ = 712.9 Hz) ppm. **HRMS (ESI)**: m/z calcd. for $\text{C}_{19}\text{H}_{23}\text{N}_4 [\text{M}-\text{PF}_6^-]^+$: 307.1917, found: 307.1917. **IR** (film): $\tilde{\nu}$ = 3189, 3154, 2927, 1611, 1525, 1444, 1385, 1284, 1226, 1165, 1095, 1061, 1008, 979, 948, 822, 733, 665, 584, 551, 466, 412 cm^{-1} .

Synthesis of 3-(4-(*N,N*-dimethylamino)pyridin-2-yl)-1-mesityl-1*H*-imidazolium chloride (**99b**)

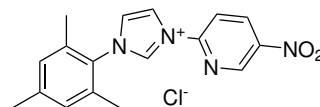
According to general procedure A, imidazole **92** (320 mg, 1.72 mmol, 1.03 eq) and pyridine **98b** (261 mg, 1.66 mmol, 1.00 eq) were heated to 170 °C for 24 h, providing the target product **99b** (250 mg, 0.73 mmol, 44%) as an off-white solid.



$^1\text{H-NMR}$ (300 MHz, MeOD): δ = 8.63 (d, 1H, 4J = 2.2 Hz, $H_{\text{imidazole}}$), 8.15 (d, 1H, 3J = 6.1 Hz, H_{14}), 7.92 (d, 1H, 4J = 2.2 Hz, $H_{\text{imidazole}}$), 7.18 (s, 2H, $H_{1,3}$), 7.14 (d, 1H, 4J = 2.3 Hz, H_{17}), 6.82 (dd, 1H, 3J = 6.1 Hz, 4J = 2.3 Hz, H_{15}), 3.16 (s, 6H, $H_{22,23}$), 2.39 (s, 3H, H_{19}), 2.16 (s, 6H, $H_{18,20}$) ppm. Note: 1H signal of H_8 is missing due to H/D exchange.

Synthesis of 3-(5-nitropyridin-2-yl)-1-mesityl-1*H*-imidazolium chloride (104a)

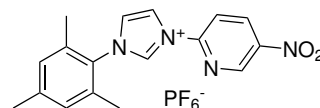
According to the general procedure A, imidazole **92** (359 mg, 1.92 mmol, 1.00 eq) and 2-chloro-5-nitropyridine (**185**, 313 mg, 1.97 mmol, 1.00 eq) were heated to 150 °C for 1 h, providing the target product **104a** (602 mg, 1.75 mmol, 88%) as a brown solid.



¹H-NMR (300 MHz, MeOD): δ = 10.38 (dd, 1H, 4J = 1.6, 1.6 Hz, H_8), 9.47 (d, 1H, 4J = 2.6 Hz, H_{14}), 8.99 (dd, 1H, 3J = 9.0 Hz, 4J = 2.7 Hz, H_{16}), 8.81 (d, 1H, 4J = 2.2 Hz, $H_{imidazole}$), 8.32 (d, 1H, 3J = 8.9 Hz, H_{17}), 8.07 (d, 1H, 4J = 2.2 Hz, $H_{imidazole}$), 7.21 (s, 2H, $H_{1,3}$), 2.41 (s, 3H, H_{19}), 2.20 (s, 6H, $H_{19,20}$) ppm. **¹³C-NMR** (75 MHz, MeOD): δ = 151.0, 146.4, 143.1, 137.1, 135.7, 132.3, 130.9 (2 C, $C_{1,3}$), 126.9, 121.8, 116.2, 21.2, 17.4 (2 C, $C_{18,20}$) ppm. **HRMS (ESI)**: m/z calcd. for $C_{17}H_{17}N_4O_2 [M-Cl]^{+}$: 309.1346, found: 309.1348. **IR** (film): $\tilde{\nu}$ = 3185, 3080, 2946, 2798, 1609, 1586, 1529, 1475, 1412, 1351, 1330, 1277, 1244, 1120, 1083, 1052, 1016, 959, 932, 853, 766, 665, 627, 585, 548, 499, 408 cm^{-1} .

Synthesis of 3-(5-nitropyridin-2-yl)-1-mesityl-1*H*-imidazolium hexafluorophosphate (104b)

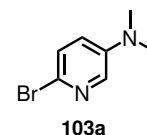
Following the general procedures A and B, **92** (352 mg, 1.89 mmol, 1.00 eq) and 2-chloro-5-nitropyridine **185** (298 mg, 1.88 mmol, 1.00 eq) were heated to 150 °C for 22 h. Treatment with an aqueous solution of KPF_6 (360 mg, 1.82 mmol, 1.0 eq) provided the title compound **104b** (762 mg, 1.68 mmol), 89%) as a brown solid.



¹H-NMR (300 MHz, MeOD): δ = 9.5 (d, 1H, 4J = 2.6 Hz, H_{14}), 9.0 (dd, 1H, 3J = 9.0, 4J = 2.7 Hz, H_{16}), 8.8 (d, 1H, 3J = 2.2 Hz, $H_{imidazole}$), 8.3 (d, 1H, 3J = 8.9 Hz, H_{17}), 8.0 (d, 1H, 3J = 2.2 Hz, $H_{imidazole}$), 7.2 (s, 2H, $H_{1,3}$), 2.4 (s, 3H, H_{19}), 2.2 (s, 6H, $H_{18,20}$) ppm. Note: 1H signal of H_8 is missing due to H/D exchange. **¹⁹F-NMR** (282 MHz, MeOD): δ = -74.6 (d, $^1J_{P,F}$ = 708.1 Hz) ppm. **HRMS (ESI)**: m/z calcd. for $C_{17}H_{17}N_4O_2 [M-PF_6]^{+}$ 309.1346, found: 309.1346.

Synthesis of 6-Bromo-*N,N*-dimethyl-3-pyridinamine (103a)

Following a modified reported procedure by Bejoymohandas *et al.*^[128], NaH (60 wt%, 707 mg, 29.5 mmol, 5.0 eq) was suspended in THF (6 mL), cooled to 0 °C and a solution of 6-bromo-3-pyridinamine (**102a**, 1000 mg, 5.85 mmol, 1.00 eq) in THF (5 mL) was added dropwise over a period of 10 min. The mixture was stirred for 2 h at 0 °C followed by slow addition of methylene iodine (0.9 mL, 14.4 mmol, 2.5 eq) and stirred at r.t. for 1 h. The reaction was stopped via addition of water (10 mL), extracted with EtOAc (3x 15 mL). The combined organic phases



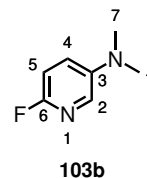
5. Experimental Part

were dried over Na_2SO_4 , adsorbed on silica and purified via flash chromatography (*n*-pentane/EtOAc 3:1 \rightarrow 1:1). The title compound **103a** (336 mg, 1.67 mmol, 29%) was obtained as a yellow solid. Unreacted starting material ((200 mg, 1.15 mmol, 20%)) as well as mono methylated 6-bromo-*N*-methyl-3-pyridinamine (250 mg, 1.34 mmol, 23%) was recovered and the reaction conditions were applied a second time with and the reaction time after addition of methylene iodine was extended to 16 h, providing additional target product (438 mg, 2.18 mmol, 37%), increasing the combined yield to 66%.

$^1\text{H-NMR}$ (300 MHz, CDCl_3): δ = 7.83 (d, 4J = 3.3 Hz, 1H, H_2), 7.24 (d, 3J = 8.9 Hz, 1H, H_5), 6.86 (dd, 3J = 8.8 Hz, 4J = 3.3 Hz, 1H, H_4), 2.95 N(CH_3)₂ ppm. **$^{13}\text{C-NMR}$** (75 MHz, CDCl_3): δ = 145.6, 134.5, 127.6, 127.3, 121.8, 40.1 (2 C, N(CH_3)₂) ppm. **HRMS (ESI)**: *m/z* calcd. for $\text{C}_7\text{H}_{10}\text{Br}_1\text{N}_2$ [M^+H^+]⁺: 203.0001, found: 203.0000. R_f = 0.40 (*n*-pentane/EtOAc 2:1).

Synthesis of 6-Fluoro-*N,N*-dimethyl-3-pyridinamine (103b)

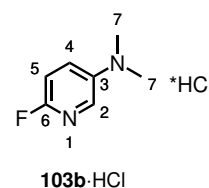
Following a modified reported procedure by Bejoymohandas *et al.*^[128], NaH (60 wt%, 539 mg, 13.5 mmol, 3.0 eq) was suspended in THF (5 mL), cooled to 0 °C and a solution of 6-fluoro-3-pyridinamine (**102b**, 497.5 mg, 4.44 mmol, 1.00 eq) in THF (5 mL) was added dropwise over a period of 5 min. The mixture was stirred for 2 h at 0 °C, allowed to warm to r.t. for 30 min and cooled to 0 °C. Methylene iodine (0.7 mL, 11.24 mmol, 2.5 eq) was added dropwise over a period of 5 min. The reaction mixture was stirred at 0 °C for 2 h and at r.t. for 16 h. After TLC showed full conversion (*n*-pentane/EtOAc 2:1), $\text{NH}_4\text{Cl}_{(\text{aq.})}$ was added, extracted with EtOAc (3x 20 mL), the combined organic phases were dried over Na_2SO_4 and purified by flash chromatography (*n*-pentane/EtOAc 2:1). The title compound **103b** (517 mg, 3.69 mmol, 83%) was obtained as a colorless oil.



$^1\text{H-NMR}$ (250 MHz, CDCl_3): δ = 7.60 (t, 4J = 2.5 Hz, 1H), 7.13 (ddd, 3J = 9.0, 6.7, 4J = 3.3, 1H), 6.78 (dd, 3J = 9.0, 4J = 3.5, 1H, H_2), 2.93 (s, 6H, N(CH_3)₂) ppm. **$^{13}\text{C-NMR}$** (75 MHz, CDCl_3): δ = 156.48 (d, 1J = 228.7, C_6), 145.10 (d, 4J = 3.6, C_3), 130.86 (d, 3J = 14.9), 125.22 (d, 4J = 6.8), 108.94 (d, 2J = 39.4, C_5), 41.00 (N(CH_3)₂) ppm. **$^{19}\text{F-NMR}$** (235 MHz, CDCl_3): δ = -83.6 ppm. **HRMS (ESI)**: *m/z* calcd. for $\text{C}_7\text{H}_{10}\text{F}_1\text{N}_2$ [M^+H^+]⁺: 141.0823, found: 141.0822. R_f = 0.40 (*n*-pentane/EtOAc 2:1).

Synthesis of 6-Fluoro-*N,N*-dimethyl-3-pyridinamine hydrochloride (**103b**·HCl)

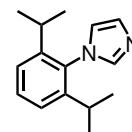
A three neck flask was charged with NaCl (813 mg, 13.9 mmol, 5.0 eq). A second two neck flask was charged with 6-Fluoro-*N,N*-dimethyl-3-pyridinamine (**103b**, 390 mg, 2.78 mmol, 1.00 eq), CH₂Cl₂ (28 mL). The two flasks were connected by a gas inlet build out of a quickfit connector and a Pasteur pipette. A constant slow flow of N₂ from the first to the second flask was applied while conc. H₂SO₄ (0.4 mL) was added dropwise to the NaCl flask over a period of 5 min. The flow was maintained for additional 30 min after full addition of H₂SO₄. The colorless precipitation was collected via suction, washed with CH₂Cl₂ and dried under high vacuum. The title compound **103b**·HCl (490 mg, 2.77 mmol, 99%) was obtained as a colorless crystalline solid.



¹H-NMR (250 MHz, DMSO-*d*₆): δ = 7.94 (s, 1H), 7.83-7.63 (m, 1H), 7.11 (dd, ³J = 9.0 Hz, ⁴J = 3.3 Hz, 1H), 5.92 (s, br, 5H), 2.96 (s, 6H) ppm. Note: The broad singlet at 5.92 ppm is expected to derive from water of the solvent.

Synthesis of 1-(2,6-diisopropylphenyl)-1*H*-imidazole (**132**)

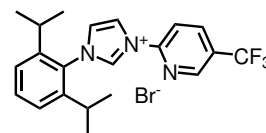
A round bottom 50 mL flask was charged with 2,6-diisopropylanilin (3700 mg, 20.9 mmol, 1.0 eq), MeOH (20 mL) and glyoxal (40 wt% in water, 2.5 mL, 21.8 mmol, 1.05 eq). The mixture was heated to 80 °C for 1 h followed by addition of aqueous NH₃-solution (25 wt%, 1.6 mL, 20.9 mmol, 1.0 eq) and aqueous formaldehyde (37 wt%, 1.6 mL, 20.9 mmol, 1.0 eq) and further stirred at 80 °C for 90 min and cooled to room temperature over night. The resulting solid, identified as *N*¹,*N*²-bis(2,6-diisopropylphenyl)ethane-1,2-diimine, 2556 mg was dissolved in MeOH (45 mL) and added NH₄Cl (1400 mg, 26 mmol, 1.2 eq), H₃PO₄ (1 mL) and heated to 80 °C for 45 min. After TLC indicated full conversion of the diimine, formaldehyde (37 wt%, 2.0 mL, 26.9 mmol, 1.3 eq) and glyoxal (40 wt% in water, 1.5 mL, 13.1 mmol, 0.63 eq) were added and stirred at 80 °C for 2 h. After cooling to room temperature, the solvents were removed *in vacuo*, adsorbed on silica and purified by flash chromatography (CH₂Cl₂/MeOH 100:1). The title compound **132** (1390 mg, 6.09 mmol 29%) was obtained as a brown oil.



¹H-NMR (300 MHz, CDCl₃): δ = 7.49 (t, 1H, ⁴J = 1.2 Hz, *H*_{Ar}), 7.47-7.43 (m, 1H, *H*_{Ar}), 7.30-7.25 (m, 3H, *H*_{Ar}), 7.0 (t, 1H, ⁴J = 1.3 Hz, *H*_{Ar}), 2.4 (hept, 2H, ³J = 6.9 Hz, 2xCH(CH₃)₂), 1.2 (d, 12H, ³J = 6.9 Hz, 2xCH(CH₃)₂) ppm. ¹³C-NMR (63 MHz, CDCl₃): δ = 146.7, 138.6, 129.9, 129.5, 123.9 (2C), 121.7, 28.2 (2C), 24.6 (2C), 24.5 (2C) ppm. HRMS (ESI): *m/z* calcd. for C₁₅H₂₁N₂ [M+H]⁺: 229.1699, found: 229.1704.

Synthesis of**3-(5-trifluoromethylpyridin-2-yl)-1-(2,6-diisopropylphenyl)-1H-imidazolium bromide (134)**

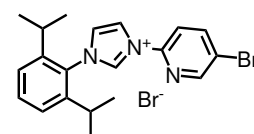
Following general procedure A, imidazole **132** (400 mg, 1.75 mmol, 1.0 eq) and pyridine **115** (399 mg, 1.76 mmol, 1.01 eq) were heated to 170 °C for 18 h. The title compound **134** (188 mg, 0.41 mmol, 24%) was obtained as a brown crystalline solid.



¹H-NMR (250 MHz, CDCl₃) δ = 11.37 (dd, ⁴J = 1.6, 1.6 Hz, 1H, H₈), 9.72 (d, ³J = 8.6 Hz, 1H, H₁₇), 9.29 (dd, ⁴J = 1.9 Hz, 1H, H_{imidazole}), 8.80 (d, ⁴J = 2.3 Hz, 1H, H₁₄), 8.38 (dd, ³J = 8.7 Hz, ⁴J = 2.4, 1H, H₁₆), 7.63-7.54 (m, 1H, H_{Ar}), 7.41 (dd, ⁴J = 1.8, 1H, H₈), 7.38 (s, br, 1H, H_{imidazole}), 7.35 (s, br, 1H, H_{imidazole}), 2.41 (hept, ³J = 6.8 Hz, 2H, H_{18,21}), 1.30 (d, ³J = 6.8 Hz, 6H, H_{19,23}), 1.18 (d, ³J = 6.8 Hz, 6H, H_{22,20}) ppm. ¹⁹F-NMR (235 MHz, CDCl₃): δ = -62.5 ppm.

Synthesis of 3-(5-bromopyridin-2-yl)-1-(2,6-diisopropylphenyl)-1H-imidazolium bromide (135)

Following general procedure A, imidazole **132** (364.5 mg, 1.59 mmol, 1.0 eq) and pyridine **91** (387 mg, 1.63 mmol, 1.0 eq) were heated to 160 °C for 69 h. The title compound **135** (398 mg, 0.86 mmol, 54%) was obtained as a brown crystalline solid.

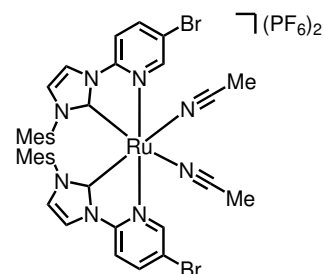


¹H-NMR (300 MHz, CDCl₃) δ = 11.18 (dd, ⁴J = 1.6, 1.6 Hz, 1H, H₈), 9.39 (d, ³J = 8.7 Hz, 1H, H₁₇), 9.21 (t, ⁴J = 1.8 Hz, 1H, H_{imidazole}), 8.57 (d, ⁴J = 2.3 Hz, 1H, H₁₄), 8.24 (dd, ³J = 8.7 Hz, ⁴J = 2.4 Hz, 1H, H₁₆), 7.58 (dd, J = 7.8 Hz, 1H, H₂), 7.42-7.32 (m, 3H, H_{Ar}), 2.41 (hept, ³J = 6.5 Hz, 2H, H_{18,21}), 1.29 (d, ³J = 6.8 Hz, 6H, H_{19,23}), 1.18 (d, ³J = 6.8 Hz, 6H, H_{20,22}) ppm. ¹³C-NMR (75 MHz, CDCl₃) δ = 149.9, 145.2, 144.7, 143.7, 136.1, 132.5, 130.0, 125.3, 125.0, 122.4, 120.9, 118.5, 29.1 (C(CH₃)₂), 24.5 (2C, CH₃), 24.4 (2C, CH₃) ppm. HRMS (ESI): *m/z* calcd. for C₂₀H₂₃Br₁N₃ [M-Br⁻]⁺: 386.1051, found: 386.1056. IR (film): $\tilde{\nu}$ = 3181, 3076, 2965, 2929, 2869, 1587, 1529, 1467, 1384, 1320, 1265, 1220, 1186, 1076, 1056, 1009, 956, 827, 805, 757, 735, 664, 624, 568, 509, 438, 411 cm⁻¹.

5.4. Synthesis of Ruthenium Complexes

Synthesis of *Racemic* Complex **64i**

Following the published procedure,^[114] with slight modifications, a flame-dried 10 mL PTFE sealed pressure tube was charged with RuCl₃ (101 mg, 0.49 mmol, 1.00 eq), **93a** (409 mg, 0.96 mmol, 2.0 eq) and ethylene glycol (10 mL). The mixture was degassed by applying high vacuum until no bubbles were visible, at least 30 min. Afterwards, the tube was flushed with N₂ and was fully immersed in a preheated oil bath (175 °C). The reaction mixture was stirred at this temperature for 15 h, cooled to room temperature, followed by treatment with NH₄PF₆ (855 mg, 5.2 mmol, 11 eq) in water (15 mL). The yellow precipitation was collected via filtration, rinsed firmly with water, redissolved in CH₂Cl₂ and transferred into a round-bottom flask equipped with nitrogen inlet. The solvent was removed under reduced pressure to dryness. AgPF₆ (282 mg, 1.1 mmol, 2.3 eq) and CH₃CN were added under a positive N₂ pressure, placed in a preheated oil bath (60 °C) and stirred for 5 h. The reaction time can also be increased up to 16 h with no drawbacks in terms of yield or purity. The reaction mixture was filtered through a pad of celite, rinsed with CH₂Cl₂ and the solvents were removed under reduced pressure. Purification of the crude product via flash chromatography (CH₂Cl₂/CH₃CN 50:1 → 2:1) provided the *racemic* target product **64i** (508 mg, 0.44 mmol, 90%) as a yellow solid.



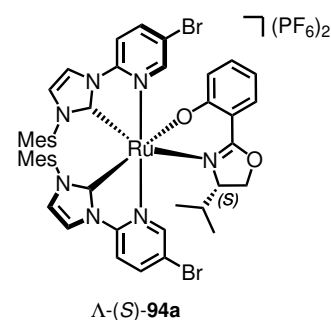
rac. **64i**

¹H-NMR (500 MHz, CD₂Cl₂): δ = 8.22 (d, *J* = 2.0 Hz, 1H, *H*_{Ar}), 7.98 (d, ⁴*J* = 2.3 Hz, 1H, *H*_{Ar}), 7.93 (dd, ³*J* = 8.8, ⁴*J* = 2.2 Hz, 1H, *H*_{Ar}), 7.50 (d, ³*J* = 8.8 Hz, 1H, *H*_{Ar}), 6.97 (s, 1H, *H*_{Ar}), 6.93 (d, ⁴*J* = 2.3 Hz, 1H, *H*_{Ar}), 6.58 (s, 1H, *H*_{Ar}), 2.32 (s, 3H, CH₃), 2.27 (s, 3H, CH₃), 2.01 (s, 3H, CH₃), 1.44 (s, 3H, CH₃) ppm. **¹³C-NMR** (126 MHz, CD₂Cl₂): δ = 189.0, 152.4, 152.3, 141.7, 140.9, 135.3, 134.1, 133.8, 130.4, 129.7, 126.1, 125.4, 118.2, 117.7, 112.8, 21.3, 17.5, 17.2, 4.2 ppm. **HRMS (ESI):** *m/z* calcd. for C₃₈H₃₈N₈Ru₁P₁F₆Br₂ [M⁺PF₆⁻]⁺: 1013.0259, found: 1013.0245. **IR** (film): $\tilde{\nu}$ = 1608, 1485, 1424, 1374, 1324, 1254, 1143, 1090, 1029, 933, 834, 807, 737, 695, 551, 517, 496 cm⁻¹. **M.p.:** 183 °C (decomp.). **HPLC:** CHIRALPAK IB (250 x 4.6 mm), 0.8 mL min⁻¹, H₂O+0.05% TFA/CH₃CN 75:25, gradient to 30:70 in 50 min, 40 °C, 254 nm, R_t (Λ) = 43.565 min, R_t (Δ) = 46.021 min.

Assignment of the HPLC traces to each enantiomer was done by comparison with enantioenriched complex Λ-**64i** (Figure 7, Chapter 3.1.1).

Synthesis of Auxiliary Complex Λ -(S)-94a

Following the published procedure,^[114] racemic **64i** (74.9 mg, 65.0 μmol , 1.0 eq) and (*S*)-oxazoline (**66**, 34.2 mg, 167.0 μmol , 2.6 eq) were dissolved in CH_2Cl_2 (1 mL). NEt_3 (90 μL , 0.65 mmol, 10.0 eq) was added to this mixture and stirred at 40 °C for 16 h hours. The mixture was cooled to room temperature, filtrated through a pad of celite, rinsed with CH_2Cl_2 and the solvent removed under reduced pressure. The crude product was purified via column chromatography ($\text{CH}_2\text{Cl}_2/\text{CH}_3\text{CN}$ 100:1 \rightarrow 20:1) and the title compound Λ -(*S*)-**94a** (36.0 mg, 0.032 mmol, 49%, *dr* > 20:1) was obtained as a red solid.

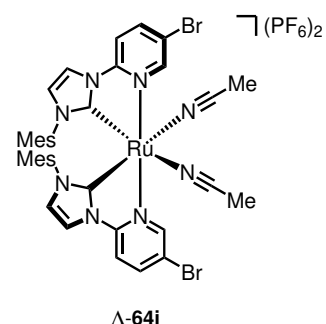


The configuration was assigned according to previous results where auxiliary (*S*)-**66** was found to form a stable complex with the Λ enantiomer.^[114]

¹H-NMR (300 MHz, CD_2Cl_2): δ = 8.49 (d, 4J = 2.2 Hz, 1H, H_{Ar}), 7.94 (d, 4J = 2.3 Hz, 1H, H_{Ar}), 7.81 (d, 4J = 2.2 Hz, 2H, H_{Ar}), 7.76 (dd, 3J = 8.8, 4J = 2.2 Hz, 1H, H_{Ar}), 7.60 (dd, 3J = 8.8, 4J = 2.2 Hz, 1H, H_{Ar}), 7.42 (dd, 3J = 8.1, 4J = 1.9 Hz, 1H, H_{Ar}), 7.37 (d, 3J = 8.8 Hz, 1H, H_{Ar}), 7.21 (d, 3J = 8.8 Hz, 1H, H_{Ar}), 7.01-6.89 (m, 4H, H_{Ar}), 6.84 (d, 4J = 2.3 Hz, 1H, H_{Ar}), 6.56 (s, 1H, H_{Ar}), 6.45 (s, 1H, H_{Ar}), 6.36 (d, 3J = 8.6 Hz, 1H, H_{Ar}), 6.21 (t, 3J = 7.5 Hz, 1H, H_{Ar}), 4.27 (dd, 3J = 9.4, 4J = 3.4 Hz, 1H, H_{aliph}), 4.16 (t, 3J = 9.1 Hz, 1H, H_{aliph}), 3.80-3.69 (m, 1H, H_{aliph}), 2.28 (s, 3H, CH_3), 2.26 (s, 3H, CH_3), 2.20 (s, 3H, CH_3), 2.12 (s, 3H, CH_3), 1.32 (s, 3H, CH_3), 0.52 (d, J = 6.5 Hz, CHCH_3), 0.07 (d, J = 5.9 Hz, 3H, CHCH_3), 0.04–0.07 (m, 1H= CHCH_3) ppm. **¹³C-NMR** (75 MHz, CD_2Cl_2): δ = 197.2, 195.6, 172.3, 165.7, 153.3, 152.9, 151.8, 151.2, 140.2, 140.1, 139.4, 138.8, 137.5, 135.1, 134.9, 134.7, 134.5, 134.2, 133.9, 130.3, 130.3, 130.0, 129.9, 129.4, 125.9, 125.6, 123.6, 116.9, 116.4, 116.3, 116.0, 113.2, 111.6, 111.1, 110.9, 74.8, 66.8, 30.5, 21.4, 21.2, 19.0, 18.4, 17.9, 17.8, 17.3, 13.6 ppm. **HRMS (ESI)**: m/z calcd. for $\text{C}_{46}\text{H}_{46}\text{Br}_2\text{N}_7\text{O}_2\text{Ru}_1$ [M^+]⁺: 990.1113, found: 990.1174. **IR** (film): $\tilde{\nu}$ = 2922, 2856, 1606, 1536, 1477, 1417, 1377, 1293, 1251, 1226, 1148, 1065, 1032, 952, 925, 835, 731, 689, 630, 583, 553, 528, 501, 459, 431 cm^{-1} . **M.p.**: 190 °C (decomp.).

Synthesis of Complex Λ -64i

Following the published procedure,^[114] auxiliary complex Λ -(*S*)-**94a** (75 mg, 0.066 mmol, 1.0 eq) was dissolved in CH₃CN (9 mL) and TFA (80 μ L, 1.04 mmol, 16 eq) was added at room temperature and stirred for 30 min. The solvent was removed under reduced pressure, NH₄PF₆ (340 mg, 2.1 mmol, 32 eq) and CH₃CN (9 mL) was added and stirred at room temperature for 16 h. Column chromatography (CH₂Cl₂/ CH₃CN 100:1 \rightarrow 5:1) provided complex Λ -**64i** (73 mg, 0.063 mmol, 95%) as a yellow solid.



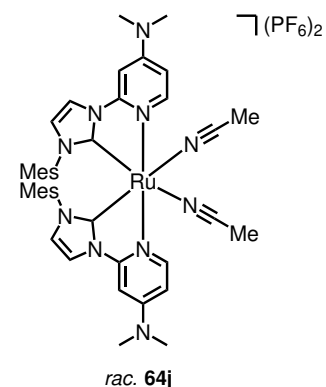
The absolute configuration was assigned based on the configuration of the auxiliary complex Λ -(*S*)-**94a** and verified by comparison of the observed enantioselectivity for asymmetric alkynylation of trifluoroacetophenone (Table 12, Chapter 3.2.3) with reported data.^[114]

Synthetic note: If the obtained solid is orange or red of color, the removal of the auxiliary was not successful and should be repeated. The color should be a bright straw-yellow.

CD (CH₃OH): λ , ($\Delta\epsilon$, M⁻¹ cm⁻¹): 353 (+2), 321 (−5), 293 (+24), 279 (−24), 252 (+44), 229 (−38), 211 (+7) nm. All other spectroscopic data are in agreement with *racemic* complex **64i**.

Synthesis of *Racemic* Complex **64j**

Following the published procedure^[114] with slight modifications, a flame-dried 10 mL PTFE sealed pressure tube was charged with RuCl₃ (49.5 mg, 238 μ mol, 1.00 eq), imidazolium salt **99a** (112.4 mg, 290 μ mol, 2.0 eq) and ethylenglycole (3.5 mL). The mixture was degassed by applying high vacuum until no bubbles were visible, at least 30 min. Afterwards, the tube was flushed with N₂ and was fully immersed in a preheated oil bath (175 °C). The reaction mixture was stirred at this temperature for 17 h, cooled to room temperature, followed by treatment with NH₄PF₆ (160 mg, 0.981 mmol, 5 eq) in water (3 mL). The yellow precipitation was collected via filtration, rinsed firmly with water, redissolved in CH₂Cl₂ and transferred into a round-bottom flask equipped with nitrogen inlet. The solvent was removed under reduced pressure to dryness. AgPF₆ (71.3 mg, 282 μ mol, 2.0 eq) and CH₃CN (3.5 mL) were added under a positive N₂ pressure, placed in a preheated oil bath (60 °C) and stirred for 24 h. The reaction mixture was filtrated through a pad of celite, rinsed with CH₃CN and the solvents were removed under reduced pressure. Purification of the crude product via flash chromatography (CH₂Cl₂/CH₃CN 50:1 \rightarrow 10:1) provided the *racemic* target product **64j** (95 mg, 90 μ mol, 58%) as a yellow solid. The product shows a solvatochromic effect: it appears yellow in combination with

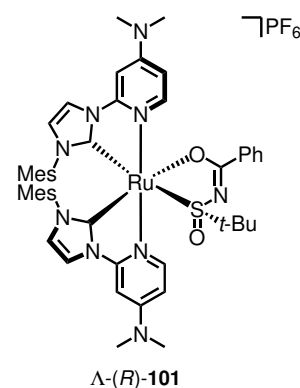


CH₃CN and turns to green/blue in CH₂Cl₂ solution. This also includes the solid after the evaporation of the solvent.

¹H-NMR (500 MHz, CD₃CN): δ = 8.00 (d, ⁴J = 2.3 Hz, 2H, H_{Ar}), 7.73 (d, ³J = 6.8 Hz, 2H, H_{Ar}), 6.93 (d, ⁴J = 2.3 Hz, 2H, H_{Ar}), 6.78 (dd, ⁴J = 2.2, 0.7 Hz, 2H, H_{Ar}), 6.58 (d, ⁴J = 2.5 Hz, 4H, H_{Ar}), 6.15 (dd, ³J = 6.8, ⁴J = 2.7 Hz, 2H), 3.11 (s, 12H, 2xNCH₃)₂, 2.17 (s, 6H, 2xCH₃), 2.15 (s, 12H, 4xCH₃), 1.98 (s, 6H, 2xCH₃) ppm. Note: The Signals for the CH₃-groups of the mesityl and coordinated CH₃CN overlap partial with the signals for HDO as well as free CH₃CN. ¹³C-NMR (126 MHz, CD₃CN): δ = 192.3, 156.3, 154.0, 153.4, 150.5, 149.9, 139.4, 136.2, 135.3, 134.8, 130.3, 129.9, 125.6, 124.4, 118.3, 117.7, 106.5, 93.6, 40.0, 20.9, 17.7, 17.5, 1.3 ppm.

Synthesis of Auxiliary Complex Λ-(S)-101

Following the published procedure,^[119] a 10 mL PTFE sealed pressure tube was charged with *racemic* complex **64j** (53.5 mg, 49.2 μmol, 1.00 eq), sulfinyl benzamide (*R*)-**85** (9.4 mg, 41.7 μmol, 0.85 eq) and K₂CO₃ (12.2 mg, 88.3 μmol, 1.80 eq), was evacuated for 5 min and flushed with N₂. Ethoxyethanol (2.3 mL) was added under positive N₂ pressure, evacuated via two cycles of freeze, pump, thaw (each cycle 10 min) and placed in a preheated oil bath (60 °C) and stirred for 17 h. After TLC indicated full conversion, the mixture was filtered through a pad of celite, rinsed with CH₂Cl₂ and the solvents removed under reduced pressure with a water bath (60 °C). Purification of the crude product via flash chromatography (CH₂Cl₂/MeOH 100:0 → 100:1 → 50:1) two times provided the target product Λ-(S)-**101** (10.2 mg, 9.4 μmol, 19%, *dr* > 20:1) as a green solid.

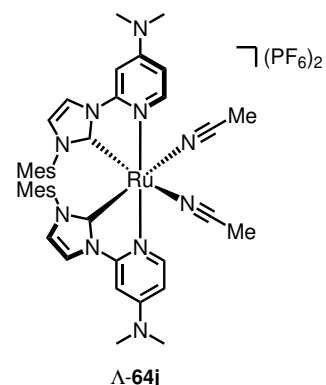


The absolute configuration was assigned analogously to previous results where auxiliary (*R*)-**85** forms a stable complex with the Λ enantiomer.^[119]

¹H-NMR (500 MHz, CD₂Cl₂): δ = 9.27 (d, ³J = 7.1 Hz, 1H, H_{Ar}), 8.13-8.06 (m, 2H, H_{Ar}), 7.89 (d, ⁴J = 2.2 Hz, 1H, H_{Ar}), 7.85 (d, ⁴J = 2.4 Hz, 1H, H_{Ar}), 7.43-7.36 (m, 1H, H_{Ar}), 7.36-7.28 (m, 2H, H_{Ar}), 7.12 (d, ³J = 6.9 Hz, 1H, H_{Ar}), 6.85 (d, ⁴J = 2.3 Hz, 1H, H_{Ar}), 6.79 (d, ⁴J = 2.2 Hz, 1H, H_{Ar}), 6.81-6.76 (m, 3H, H_{Ar}), 6.56-6.52 (m, 1H, H_{Ar}), 6.50 (d, ⁴J = 2.6 Hz, 1H, H_{Ar}), 6.50-6.45 (m, 1H, H_{Ar}), 6.40 (d, ⁴J = 2.8 Hz, 1H, H_{Ar}), 5.92 (dd, ³J = 7.1, ⁴J = 2.8 Hz, 1H, H_{Ar}), 5.64 (dd, ³J = 6.9, ⁴J = 2.6 Hz, 1H, H_{Ar}), 3.04 (s, 12H, 2x N(CH₃)₂), 2.31 (s, 3H, CH₃), 2.27 (s, 3H, CH₃), 2.19 (s, 3H, CH₃), 2.14 (s, 3H, CH₃), 1.54 (s, 3H, CH₃), 1.42 (s, 3H, CH₃), 0.74 (s, 9H, C(CH₃)₃) ppm. ¹³C-NMR (126 MHz, CD₂Cl₂): δ = 194.5, 192.2, 179.2, 155.6, 155.2, 153.9, 153.7, 153.4, 149.8, 138.8, 138.8, 136.8, 136.5, 135.8, 135.2, 135.2, 134.7, 134.4, 133.5, 131.3, 130.1, 130.1, 129.9, 129.7, 129.4, 129.1, 128.3, 126.0, 125.5, 116.8, 115.8, 105.9, 105.4, 92.8, 92.5, 65.1, 40.0, 39.8, 24.0, 23.2, 22.4, 21.3, 21.0, 18.8, 18.0, 17.6, 17.2, 15.6, 15.4, 14.4, 1.3 ppm.

Synthesis of Complex Λ -64j

A 10 mL round-bottom flask was charged with complex Λ -(*S*)-**101** (11.6 mg, 9.79 μ mol, 1.00 eq), CH₃CN (1.5 mL) and TFA (6.5 μ L, 84.3 μ mol, 8.60 eq) and stirred at room temperature for 2 h. The solvent was removed under reduced pressure, NH₄PF₆ (43.5 mg, 266.9 μ mol, 27 eq) and CH₃CN (1.5 mL) were added and stirred for 30 min. Purification of the crude product via flash chromatography (CH₂Cl₂/CH₃CN/MeOH 50:1:0 \rightarrow 50:1:1) provided the target product Λ -**64j** (8.0 mg, 7.4 μ mol, 75%) as a yellow solid which turned green after exposure to CH₂Cl₂.

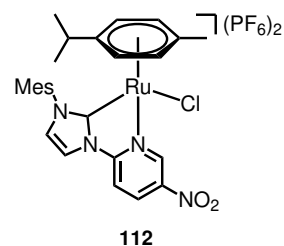


The absolute configuration was assigned based on the configuration of the auxiliary complex Λ -(*S*)-**101** and verified by comparison of the observed enantioselectivity for asymmetric alkylation of trifluoroacetophenone (Table 12, Chapter 3.2.3) with reported data.^[114]

The spectroscopic data are in agreement with *racemic* complex **64j**.

Synthesis of Complex **112**

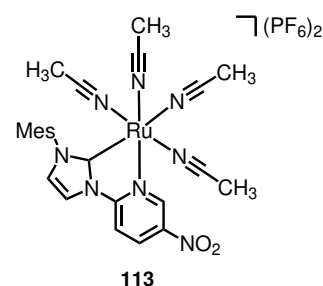
According to a published procedure by Bernet *et al.*,^[133] a 50 mL round-bottom flask equipped with nitrogen inlet was charged with complex **111** (100 mg, 163 μ mol, 1.00 eq), imidazolium salt **104b** (154.8 mg, 407 μ mol, 2.49 eq), Ag₂O (53.9 mg, 232 μ mol, 1.42 eq), evacuated for 20 min and flushed with N₂. CH₃CN (16 mL) was added, the mixture shielded from light with aluminum foil and stirred for 30 h at room temperature. After TLC indicated full conversion, the mixture was filtered through a pad of celite, rinsed with CH₃CN and the solvents were removed under reduced pressure. Purification of the crude product via flash chromatography (CH₂Cl₂/MeOH 50:1 \rightarrow 10:1) provided a 1:1 (n/n) mixture of the target product **112** (calculated 92.8 mg, 0.128 mmol, 39%) and remaining imidazolium salt **104b** and was used without further purification.



¹H-NMR (300 MHz, CD₂Cl₂): δ = 9.85 (d, ⁴*J* = 2.4 Hz, 1H), 8.89 (dt, ³*J* = 9.2 Hz, ⁴*J* = 1.7 Hz, 1H), 8.17 (d, ⁴*J* = 2.3 Hz, 1H), 8.05 (d, ³*J* = 9.2 Hz, 1H), 7.52 (d, ⁴*J* = 2.3 Hz, 1H), 7.29 (d, ⁴*J* = 1.8 Hz, 1H), 7.24 (s, 1H), 6.01 (d, ³*J* = 6.6 Hz, 1H), 5.83 (dd, ³*J* = 6.6 Hz, ⁴*J* = 1.3 Hz, 1H), 5.45 (s, 2H), 5.38 (dd, ³*J* = 6.0 Hz, ⁴*J* = 1.3 Hz, 1H), 4.42 (d, ³*J* = 5.9 Hz, 1H), 2.46 (s, 3H, CH₃), 2.24 (s, 3H, CH₃), 2.15 (s, 3H, CH₃), 1.87 (s, 3H, CH₃), 1.00 (d, ³*J* = 6.9 Hz, 3H, CHCH₃), 0.76 (d, *J* = 6.9 Hz, 3H, CHCH₃) ppm.

Synthesis of Complex 113

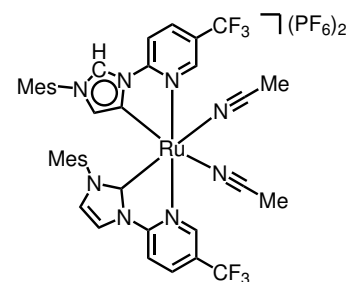
According to a published procedure,^[133] a flame-dried 10 mL PTFE sealed pressure tube was charged with complex **112** (71 mg, 98.6 μmol , 1.00 eq), AgPF_6 (36.1 mg, 142 μmol , 1.45 eq) and CH_3CN (7.5 mL). The mixture was placed in a preheated oil bath (90 °C) and stirred for 17 h. After the reaction mixture was cooled to room temperature, it was filtered through a pad of celite, rinsed with CH_3CN and the solvents removed under reduces pressure. Purification of the crude product via flash chromatography ($\text{CH}_2\text{Cl}_2/\text{CH}_3\text{CN}$ 10:1 \rightarrow 5:1) provided the target product **113** (53.4 mg, 60 μmol , 63%) as a orange to yellow solid.



$^1\text{H-NMR}$ (300 MHz, CD_2Cl_2): δ = 9.56 (d, 4J = 2.4 Hz, 1H, H_{Ar}), 8.81 (dd, 3J = 9.1 Hz, 4J = 2.4 Hz, 1H, H_{Ar}), 8.21 (d, 4J = 2.4 Hz, 1H, H_{Ar}), 8.06 (d, 3J = 9.1 Hz, 1H, H_{Ar}), 7.22 (d, 4J = 2.4 Hz, 1H, H_{Ar}), 7.15 (s, 2H, H_{Ar}), 2.64 (s, 3H, CH_3), 2.39 (s, 3H, CH_3), 2.22 (s, 6H, CH_3), 2.12 (s, 6H, CH_3), 1.95 (s, 3H, CH_3) ppm.

Synthesis of Racemic Complex 114b

According to general procedure C, RuCl_3 (27 mg, 130 μmol , 1.00 eq) and imidazolium salt **116b** (125 mg, 260 μmol , 2.0 eq) were reacted in ethylenglycole (2.5 mL) for 98 h at 90 °C, followed by treatment with NH_4PF_6 (200 mg, 1.23 mmol, 9.2 eq) and AgPF_6 (65 mg, 260 μmol , 2.0 eq). The resulting crude mixture was filtrated through a pad of celite and purified via flash chromatography ($\text{CH}_2\text{Cl}_2/\text{CH}_3\text{CN}$ 10:1 \rightarrow 5:1). The *racemic* target complex **114b** was obtained as a mixture with unreacted imidazolium salt **116b**. For further purification, the mixture was dissolved in CH_3CN (1.5 mL) and precipitated with Et_2O (20 mL) at -20 °C. The resulting pale yellow solid was collected via filtration and dried *in vacuo* which provided *racemic* complex **114b** (82 mg, 70 μmol , 54%) as a yellow crystalline solid.



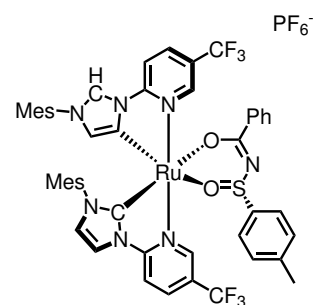
$^1\text{H-NMR}$ (500 MHz, CD_3CN): δ = 9.27 (d, 4J = 1.3 Hz, 1H, $H_{\text{imidazole}}$), 9.16-9.13 (m, 1H, H_{Ar}), 8.66-8.62 (m, 1H, H_{Ar}), 8.36 (dd, 3J = 8.8 Hz, 4J = 1.9 Hz, 1H, H_{Pyr}), 8.19-8.13 (m, 2H, H_{Ar}), 8.03 (d, 3J = 8.7 Hz, 1H, H_{Pyr}), 7.77 (d, 3J = 8.7 Hz, 1H, H_{Pyr}), 7.07 (s, br, 1H, H_{Ar}), 7.05 (s, br, 1H, H_{Ar}), 7.04 (d, 4J = 2.4 Hz, 1H, H_{Pyr}), 6.81 (s, br, 1H, H_{Ar}), 6.53 (s, br, 1H, H_{Ar}), 6.18 (d, 4J = 1.3 Hz, 1H, $H_{\text{imidazole}}$), 2.32 (s, 3H, CH_3), 2.13 (s, 3H, CH_3), 1.97 (s, 3H, CH_3), 1.96 (s, 6H, 2x CH_3), 1.34 (s, 3H, CH_3) ppm. Note: coordinated CH_3CN not visible. **$^{13}\text{C-NMR}$** (126 MHz, CD_3CN): δ = 196.2, 163.5, 157.5, 156.0, 150.2 (q, $^3J_{\text{C,F}}$ = 4.6 Hz), 150.1 (q, $^3J_{\text{C,F}}$ = 4.7 Hz), 141.9, 140.5, 136.7 (q, $^3J_{\text{C,F}}$ = 3.2 Hz), 136.3 (q, $^3J_{\text{C,F}}$ = 3.3 Hz), 136.0, 135.6, 135.5, 135.0, 134.9, 134.8, 132.4, 130.4, 130.3, 130.3, 130.1, 126.4 (q,

$^2J_{C,F} = 36.1$ Hz), 126.2, 125.9, 125.1 (q, $^2J_{C,F} = 34.3$ Hz), 124.5, 123.9 (q, $^1J_{C,F} = 271.5$ Hz), 123.3 (q, $^1J_{C,F} = 270.6$ Hz) 113.9, 112.6, 21.1, 20.9, 17.6, 17.5, 17.1, 16.5 ppm. $^{19}\text{F-NMR}$ (282 MHz, CD_3CN): $\delta = -62.1$ (s, CF_3), -62.6 (s, CF_3), -72.5 (d, $^1J_{P,F} = 706.4$ Hz, PF_6^-) ppm. **HRMS (ESI)**: m/z calcd. for $\text{C}_{38}\text{H}_{33}\text{F}_6\text{N}_7\text{Ru}_1$ $[\text{M}-(\text{CH}_3\text{CN})_2]^{2+}$: 401.5872, found: 401.5891. **IR** (film): $\tilde{\nu} = 3155, 2292, 1619, 1519, 1429, 1327, 1257, 1177, 1134, 1078, 929, 824, 706, 665, 628, 584, 553, 508, 462, 433$ cm^{-1} . **M.p.**: 204°C (decomp.). **HPLC**: Chiralpak IB-N5 (250 x 4.6 mm), 1.0 mL min^{-1} , $\text{H}_2\text{O}+0.1\%$ TFA/ CH_3CN 70:30 for 15 min, gradient to 63:37 in 55 min, 25°C , 254 nm, R_f (Λ) = 54.77 min, R_f (Δ) = 58.31 min.

The assignments of the individual signals was done after comparison with HPLC traces of complex Δ -**114a** (Figure 22, chapter 3.1.3).

Synthesis of Auxiliary Complex Δ -(*R*)-**128b**

An oven dried 50 mL round-bottom flask equipped with nitrogen inlet was charged with *racemic* complex **114b** (50 mg, 44 μmol , 1.00 eq), sulfinyl benzamide (*S*)-**121a** (13 mg, 51 μmol , 1.1 eq), K_2CO_3 (13 mg, 96 μmol , 2.2 eq) and CH_3CN (4.5 mL). The reaction mixture was stirred at 40°C for 17 h. After cooling to room temperature, the mixture was filtrated through a pad of celite, rinsed with CH_3CN and the solvents were removed under reduced pressure. Column chromatography ($\text{CH}_2\text{Cl}_2/\text{CH}_3\text{CN}$ 50:1 to 10:1) provided the title compound Δ -(*R*)-**128b** (13 mg, 11 μmol , 26%) as bright orange to red solid.



The absolute configuration was assigned analogously to literature^[119] data where the (*S*)-configured auxiliary forms a stable complex with the Δ enantiomer. This is further supported by X-ray diffraction data of the analogous complex Δ -(*R*)-**128a** (Table 22, Chapter B).

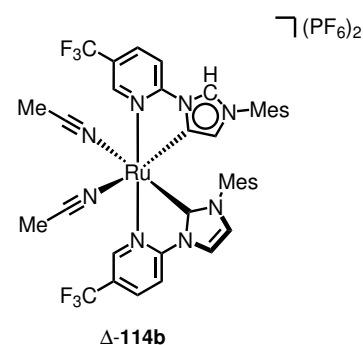
$^1\text{H-NMR}$ (500 MHz, CD_2Cl_2): $\delta = 10.94$ (s, br, 1H), 9.05 (d, 1H, $^4J = 1.4$ Hz, $H_{\text{imidazole}}$), 8.26-8.19 (m, 2H, H_{Ar}), 8.15 (dd, 1H, $^3J = 8.7$, $^4J = 2.1$ Hz, H_{Ar}), 8.05 (d, 1H, $^4J = 2.3$ Hz, H_{Ar}), 7.84 (d, 1H, $^3J = 8.7$ Hz, H_{Ar}), 7.62 (s, br, 1H, H_{Ar}), 7.57-7.48 (m, 2H, H_{Ar}), 7.47-7.40 (m, 2H, H_{Ar}), 7.34 (d, 1H, $^3J = 8.7$ Hz, H_{Ar}), 7.09 (s, br, 1H, H_{Ar}), 7.02-6.98 (m, 2H, H_{Ar}), 6.76-6.67 (m, 5H, H_{Ar}), 6.47 (s, 1H, H_{Ar}), 6.05 (d, 1H, $^4J = 1.3$ Hz, $H_{\text{imidazole}}$), 2.35 (s, 3H, CH_3), 2.34 (s, 3H, CH_3), 2.28 (s, 3H, CH_3), 2.21 (s, 3H, CH_3), 2.06 (s, 3H, CH_3), 1.89 (s, 3H, CH_3), 1.33 (s, 3H, CH_3) ppm. $^{13}\text{C-NMR}$ (126 MHz, CD_2Cl_2): $\delta = 197.5, 181.8, 164.0, 156.6, 154.6, 153.5$ (q, $^3J_{C,F} = 4.0$ Hz), 146.5 (q, $^3J_{C,F} = 4.5$ Hz), 142.2, 141.7, 140.6, 138.6, 135.5 (q, $^3J_{C,F} = 3.2$ Hz), 135.3, 134.6, 134.5, 134.4, 134.3, 134.3, 133.2, 132.2, 131.8, 130.2, 130.2, 130.1, 130.1, 129.6, 128.7, 126.1, 125.8 (q, $^2J_{C,F} = 34.0$ Hz), 124.9 (q, $^2J_{C,F} = 33.5$ Hz), 124.7, 124.6, 123.1 (q, $^1J_{C,F} = 272.4$ Hz), 123.3 (q, $^1J_{C,F} = 273.9$ Hz), 117.4, 112.7, 111.1, 21.4, 21.3, 20.9, 17.7, 17.7, 17.3, 16.2 ppm. $^{19}\text{F-NMR}$ (282 MHz, CD_2Cl_2): $\delta = -62.2$ (s, CF_3), -63.7

5. Experimental Part

(s, CF₃), -72.2 (d, ¹J_{P,F} = 711.7 Hz, PF₆⁻) ppm. **HRMS (ESI):** *m/z* calcd. for C₅₀H₄₄F₆N₇O₂Ru₁S₁ [M]⁺: 1022.2232, found: 1022.2240. **IR** (film): $\tilde{\nu}$ = 3142, 2923, 1618, 1516, 1476, 1434, 1363, 1324, 1258, 1174, 1134, 1079, 1038, 933, 833, 710, 668, 631, 584, 548, 480, 433 cm⁻¹. **M.p.:** 217 °C (decomp.) **CD** (CH₃OH): λ , ($\Delta\epsilon$, M⁻¹ cm⁻¹): 380 (-5), 341 (3), 283 (-18), 242 (-31), 226 (-26), 216 (-8) nm.

Synthesis of Complex Δ -114b

Following a modified procedure,^[117] auxiliary complex **128b** (11 mg, 9.0 μ mol, 1.00 eq) was dissolved in CH₃CN (2 mL), treated with TFA (7.4 μ L, 96 μ mol, 10 eq) and stirred at 40 °C for 16 h. After cooling to room temperature, the liquids were removed under reduced pressure, NH₄PF₆ (47 mg, 29 μ mol, 31 eq) added, and the mixture redissolved in CH₃CN (2 mL). After stirring for 20 min at room temperature, the solvent was removed under reduced pressure. Purification by column chromatography (CH₂Cl₂/CH₃CN 10:1 to 5:1) provided the enantiomerically enriched complex Δ -**114b** (10 mg, 8.9 μ mol, 95%) as bright yellow solid.



The absolute configuration was assigned based on the configuration of the auxiliary complex Δ -(*R*)-**128b**.

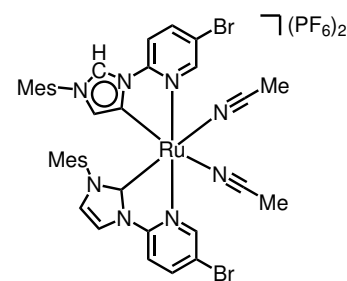
Synthetic note: If the obtained solid is of orange to red colour, the removal of the auxiliary was not successful and should be repeated as this impure complex shows far inferior catalytic activity.

CD (CH₃OH): λ , ($\Delta\epsilon$, M⁻¹ cm⁻¹): 375 (-6), 315 (+1), 276 (-26), 258 (-5), 239 (-34) nm. All other spectroscopic data were in agreement with *racemic* **114b**.

Synthesis of *Racemic* Complex **114a**

According to general procedure C, RuCl₃ (51 mg, 0.24 mmol, 1.00 eq) was reacted with imidazolium salt **93b** (241 mg, 0.49 mmol, 2.0 eq). The *racemic* title compound **114a** (174 mg, 0.15 mmol, 61%) was obtained as a yellow crystalline solid.

¹H-NMR (500 MHz, CD₂Cl₂): δ = 9.09 (d, ⁴J = 1.3 Hz, 1H, *H*_{imidazole}), 8.91 (dd, ⁴J = 2.2, 0.6 Hz, 1H, *H*_{imidazole}), 8.19-8.16 (m, 2H, *H*_{Ar}), 7.97 (d, ⁴J = 2.3 Hz, 1H, *H*_{Pyr}), 7.89 (dd, ³J = 8.8, ⁴J = 2.2 Hz, 1H, *H*_{Pyr}), 7.75 (ddd, ³J = 8.9, ⁴J = 2.6, 0.6 Hz, 2H, *H*_{Ar}), 7.03-7.01 (m, 2H, *H*_{Ar}), 6.99 (s, br, 1H, *H*_{Ar}), 6.88 (d, ⁴J = 2.3 Hz, 1H, *H*_{Ar}), 6.52 (s, br, 1H, *H*_{Ar}), 5.94 (d, ⁴J = 1.3 Hz, 1H, *H*_{imidazole}), 2.35 (s, 3H, CH₃), 2.32 (s,

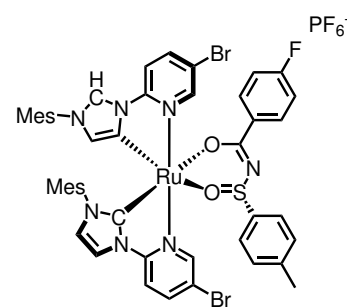


3H, CH₃), 2.28 (s, 3H, CH₃), 2.26 (s, 3H, CH₃), 2.14 (s, 3H, CH₃), 2.03 (s, 3H, CH₃), 1.90 (s, 3H, CH₃), 1.32 (s, 3H, CH₃) ppm. ¹³C-NMR (126 MHz, CD₂Cl₂): δ = 193.6, 162.4, 152.7, 152.4, 152.2, 151.0, 141.3, 141.1, 140.6, 140.1, 134.5, 134.4, 134.1, 133.8, 133.6, 132.6, 131.1, 129.7, 129.6, 129.4, 129.0, 124.6, 124.4, 123.3, 122.9, 118.7, 117.2, 116.5, 113.7, 112.1, 20.9, 20.8, 17.1, 16.9, 16.8, 15.8, 3.7, 3.6 ppm. HRMS (ESI): *m/z* calcd. for C₃₈H₃₈N₈Ru₁P₁F₆Br₂ [M⁺PF₆⁻]⁺: 1013.0259, found: 1013.0266. IR (film): $\tilde{\nu}$ = 3150, 1602, 1523, 1484, 1423, 1377, 1322, 1246, 1067, 1037, 931, 827, 699, 584, 552, 427 cm⁻¹. M.p.: 167 °C (decomp.). HPLC: Chiralpak IB-N5 (250 x 4.6 mm), 1.0 mL min⁻¹, H₂O+0.1% TFA/CH₃CN 70:30 for 15 min, gradient to 63:37 in 55 min, 25 °C, 254 nm, R_t (Λ) = 34.95 min, R_t (Δ) = 37.56 min.

The assignments of the individual signals was done after comparison with HPLC traces of complex Δ-**114a** (Figure 22, Chapter 3.1.3) and the corresponding auxiliary complex Δ-(*R*)-**128a**.

Synthesis of Auxiliary Complex Δ-(*R*)-**128a**

An oven dried 50 mL round-bottom flask equipped with nitrogen inlet was charged with *racemic* **114a** (209.3 mg, 0.18 mmol, 1.0 eq), **121d** (53.3 mg, 0.19 mmol, 1.1 eq), K₂CO₃ (51 mg, 0.37 mmol, 2.2 eq) and CH₃CN (18 mL). The reaction mixture was stirred at 40 °C for 17 h. After cooling to room temperature, the mixture was filtrated through a pad of celite, rinsed with CH₃CN and the solvents were removed under reduced pressure. Column chromatography (CH₂Cl₂/CH₃CN 40:1) provided auxiliary complex Δ-(*R*)-**128a** (64.8 mg, 0.054 mmol, 29%) as bright orange to red solid.



The assignment of configuration was based on X-ray diffraction data (Table 22, Chapter B).

¹H-NMR (500 MHz, CD₂Cl₂): δ = 10.60 (d, 1H, ⁴J = 1.9 Hz, *H*_{imidazole}), 8.89 (d, 1H, ⁴J = 1.4 Hz, *H*_{Ar}), 8.30-8.22 (m, 2H, *H*_{Ar}), 8.05 (dd, 1H, ³J = 8.8, ⁴J = 2.2 Hz, *H*_{Ar}), 7.94 (d, 1H, ⁴J = 2.3 Hz, *H*_{Ar}), 7.56 (d, 1H, ³J = 8.8 Hz, *H*_{Ar}), 7.43 (dd, 1H, ³J = 8.8, ⁴J = 2.2 Hz, *H*_{Ar}), 7.23 (d, 1H, ⁴J = 2.0 Hz, *H*_{Ar}), 7.15-7.08 (m, 2H), 7.09 (s, br 1H, *H*_{Ar}), 7.03 (d, 1H, ³J = 8.8 Hz), 6.99 (s, br 1H, *H*_{Ar}), 6.98 (d, 1H, ⁴J = 2.2 Hz), 6.94 (s, br 1H, *H*_{Ar}), 6.82-6.76 (m, 2H), 6.75-6.68 (m, 2H), 6.42 (s, br 1H, *H*_{Ar}), 6.02 (d, 1H, ⁴J = 1.3 Hz, *H*_{imidazole}), 2.35 (s, 3H, CH₃), 2.34 (s, 3H, CH₃), 2.27 (s, 3H, CH₃), 2.23 (s, 3H, CH₃), 2.16 (s, 3H, CH₃), 1.85 (s, 3H, CH₃), 1.31 (s, 3H, CH₃) ppm. ¹³C-NMR (126 MHz, CD₂Cl₂): δ = 196.3, 180.4, 165.5 (d, ¹J_{C,F} = 250.9 Hz), 163.5, 156.5, 153.3, 151.0, 150.4, 142.0, 141.6, 140.7, 140.4, 139.6, 138.8, 135.4, 134.6, 134.4, 134.4, 134.4, 132.7 (d, ³J_{C,F} = 9.1 Hz), 132.1, 131.9, 131.0 (d, ⁴J_{C,F} = 2.9 Hz), 130.3, 130.1, 130.0, 129.5, 129.4, 125.5, 124.7, 124.3, 118.7, 117.0, 117.0, 115.5 (d, ²J_{C,F} = 21.9 Hz), 113.0, 111.6, 21.4, 21.4, 21.3, 17.8, 17.7, 17.2, 16.1 ppm. ¹⁹F-NMR (282 MHz, CD₂Cl₂): δ = -72.2 (d, ¹J_{P,F} =

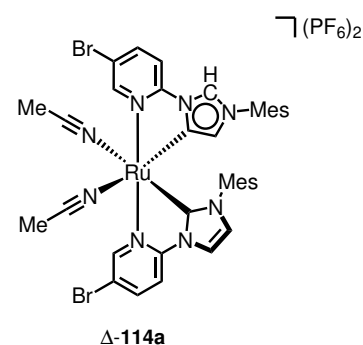
711.7 Hz, PF_6^-), -109.3 (s, F) ppm. **HRMS (ESI)**: m/z calcd. for $\text{C}_{48}\text{H}_{44}\text{Br}_2\text{N}_7\text{O}_2\text{Ru}_1\text{S}_1$ $[\text{M}-\text{PF}_6^-]^+$: 1044.0677, found: 1044.0709. **IR** (film): $\tilde{\nu} = 3142, 3052, 2922, 2856, 1676, 1599, 1514, 1470, 1362, 1306, 1239, 1150, 1100, 1071, 1037, 956, 838, 697, 629, 586, 548, 471, 422$ cm^{-1} . **CD** (CH_3OH): λ ($\Delta\epsilon, \text{M}^{-1} \text{cm}^{-1}$): 340 (+7), 291 (-57), 274 (+11), 246 (-42), 235 (-3), 221 (-35) nm.

Synthesis of Complex Δ -114a

In analogy to Δ -114b, auxiliary complex Δ -(*R*)-128a (52 mg, 43 μmol , 1.0 eq) was treated with TFA (33 μL , 43 μmol , 10.0 eq), resulting in the enantiomerically enriched complex Δ -114a (45 mg, 39 μmol , 91%) as a bright yellow solid.

The absolute configuration was assigned based on the configuration of auxiliary complex Δ -(*R*)-128a.

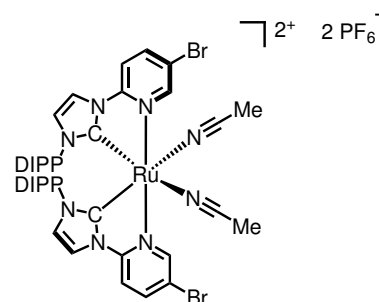
CD (CH_3OH): λ , ($\Delta\epsilon, \text{M}^{-1} \text{cm}^{-1}$): 416 (-7), 326 (+1), 292 (-38), 276 (-2), 252 (-38), 232 (+29), 208 (+10) nm. All other spectroscopical data were in agreement with racemic complex 114a.



Synthesis of Racemic Complex 136b

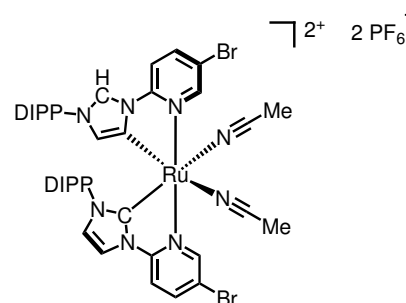
Similar to general procedure C, RuCl_3 (28.2 mg, 136 μmol , 1.00 eq) was reacted with imidazolium salt 135 (134.5 mg, 289 μmol , 2.0 eq) at 180 °C for 23 h. The racemic title compound 136b (66.8 mg, 50 μmol , 40%) was obtained as a yellow crystalline solid.

$^1\text{H-NMR}$ (300 MHz, CD_3CN): $\delta = 8.19$ (d, 2H, $^4J = 2.2$ Hz), 8.09 (d, 2H, $^4J = 2.3$ Hz), 7.95 (dd, 2H, $^3J = 8.8, ^4J = 2.2$ Hz), 7.61 (d, 2H, $^3J = 8.8$ Hz), 7.44 (dd, 2H, $^3J = 7.9, ^4J = 1.4$ Hz), 7.31 (d, 2H, $^3J = 7.8$ Hz), 7.27 (d, 2H, $^4J = 2.2$ Hz), 6.85 (dd, 2H, $^3J = 7.8, ^4J = 1.4$ Hz), 2.48 (hept, 2H, $^3J = 6.7$ Hz, $2 \times \text{CH}(\text{CH}_3)_2$), 1.96 (s, 3H, CH_3), 1.45 (d, 6H, $J = 6.8$ Hz, $2 \times \text{CH}_3$), 1.07 (d, 6H, $^3J = 6.7$ Hz, $2 \times \text{CH}_3$), 0.95 (d, 6H, $^3J = 6.8$ Hz), 0.86 (d, 6H, $^3J = 6.7$ Hz, CH_3) ppm. Note: Two CH signals from the *i*-Pr-group are missing.



Synthesis of *Racemic* Complex **137b**

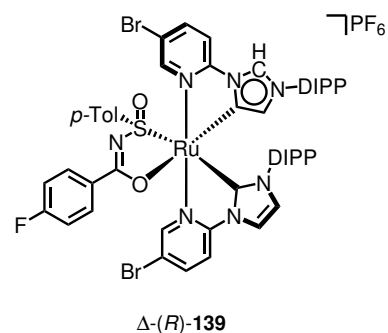
According to general procedure C, RuCl₃ (26.1 mg, 126 μmol, 1.00 eq) was reacted with imidazolium salt **135** (119.2 mg, 256 μmol, 2.0 eq) at 120 °C for 46 h. The *racemic* title compound **137b** (106 mg, 90 μmol, 68%) was obtained as a yellow crystalline solid. Additionally, the *racemic* nNHC complex **136b** (40 mg, 30 μmol, 26%) was obtained during this procedure.



¹H-NMR (300 MHz, CD₃CN): δ = 9.30 (d, 1H, ⁴J = 1.4 Hz, H_{Ar}), 8.91 (d, 1H, ⁴J = 2.2 Hz, H_{Ar}), 8.22 (dd, 1H, ³J = 8.9, ⁴J = 2.2 Hz, H_{Ar}), 8.19 (d, 1H, ⁴J = 2.2 Hz, H_{Ar}), 8.15 (d, 1H, ⁴J = 2.2 Hz, H_{Ar}), 8.08 (dd, 1H, ³J = 5.3, ⁴J = 2.3 Hz, H_{Ar}), 7.95 (dd, 1H, ³J = 8.8, ⁴J = 2.3 Hz, H_{Ar}), 7.81 (d, 1H, ³J = 8.9 Hz, H_{Ar}), 7.62 (d, 1H, ³J = 8.8 Hz, H_{Ar}), 7.56 (t, 1H, ³J = 7.8 Hz, H_{Ar}), 7.52-7.45 (m, 1H, H_{Ar}), 7.38 (d, 2H, ³J = 7.7 Hz, H_{Ar}), 7.35-7.26 (m, 1H, H_{Ar}), 7.24 (d, 1H, ⁴J = 2.3 Hz, H_{Ar}), 6.82 (d, 1H, ³J = 8.0 Hz, H_{Ar}), 6.27 (d, 1H, ⁴J = 1.3 Hz, H_{Ar}), 2.78 (p, 1H, ³J = 6.7 Hz, CHCH₃), 2.35 (p, 1H, ³J = 6.8 Hz, CHCH₃), 2.29-2.20 (m, 1H), 1.83 (q, 1H, ³J = 6.9 Hz, H₃), 1.49 (d, 3H, ³J = 6.9 Hz, CH₃), 1.22 (d, 3H, ³J = 6.8 Hz, CH₃), 1.16 (d, 3H, ³J = 6.8 Hz, CH₃), 1.09 (t, 6H, ³J = 6.9 Hz, CH₃), 1.02 (d, 3H, ³J = 6.8 Hz, CH₃), 0.82 (s, 6H, 2xCH₃) ppm. HRMS (ESI): *m/z* calcd. for C₄₂H₄₇Br₂F₆N₇P₁Ru₁ [M-PF₆⁻]⁺: 1056.0933, found: 1056.0912.

Synthesis of Auxiliary Complex Δ-(*R*)-**139**

An oven dried 50 mL round-bottom flask equipped with nitrogen inlet was charged with *racemic* complex **137b** (60.6 mg, 48.8 μmol, 1.00 eq), sulfinyl benzamide (*S*)-**121d** (13.9 mg, 50.1 μmol, 1.0 eq), K₂CO₃ (14.1 mg, 102 μmol, 2.1 eq) and CH₃CN (5 mL). The reaction mixture was stirred at 40 °C for 2.5 h. After cooling to room temperature, the mixture was filtrated through a pad of celite, rinsed with CH₃CN and the solvents were removed under reduced pressure. Column chromatography (100 mg NH₄PF₆ added as solid on top of column. (CH₂Cl₂/CH₃CN 10:1 → 0:1) provided the title compound Δ-(*R*)-**139** (26.0 mg, 20.0 μmol, 41%, *dr* 4:1) as bright orange to red solid as mixture of diastereomers. Note: The isomer with a 180° rotated orientation of auxiliary **121d** was not isolated, hence both isomers are present which makes the NMR less clear to identify.



The absolute configuration was assigned analogously to complex Δ-(*R*)-**128a**.

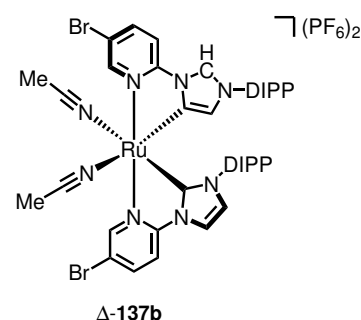
$^1\text{H-NMR}$ (300 MHz, CD_3CN) δ = 10.48 (d, 4J = 2.2 Hz, 1H), 10.44 (d, 4J = 2.2 Hz, 1H), 9.40 (d, 4J = 1.6 Hz, 1H), 9.31 (d, 4J = 2.3 Hz, 1H), 9.07 (d, 4J = 1.3 Hz, 1H), 8.30-7.99 (m, 5H), 7.91-7.03 (m, 22H), 7.00-6.74 (m, 5H), 6.67 (td, 3J = 8.1 Hz, 4J = 1.5 Hz, 4H), 6.56 (d, 4J = 1.3 Hz, 1H), 6.39 (d, 4J = 1.4 Hz, 1H), 2.44 (s, 2H), 2.22 (s, 4H), 2.13 (s, 3H), 1.45-1.28 (m, 10H), 1.21-1.12 (m, 7H), 1.08 (d, 3J = 6.9 Hz, 1H), 0.99 (d, 3J = 6.8 Hz, 3H), 0.90 (t, 3J = 7.2 Hz, 2H), 0.79 (d, 3J = 6.7 Hz, 3H), 0.69 (d, 3J = 6.8 Hz, 4H) ppm.

Synthesis of Complex Δ -137b

In analogy to complex Δ -114b, complex Δ -(*R*)-139 (25.8 mg, 20.0 μmol , 1.0 eq) in CH_3CN (5 mL) was treated with TFA (15.0 μL , 195.0 μmol , 9.7 eq), resulting in the complex Δ -137b (14.0 mg, 14.4 μmol , 57%) as a yellow solid.

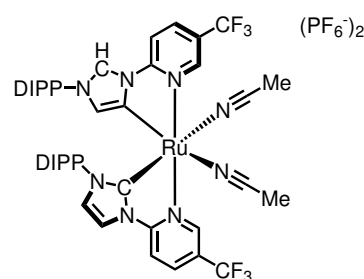
The absolute configuration was assigned based on the configuration of auxiliary complex Δ -(*R*)-139.

The spectroscopical data were in agreement with *racemic* 137b.



Synthesis of *Racemic* Complex 137a

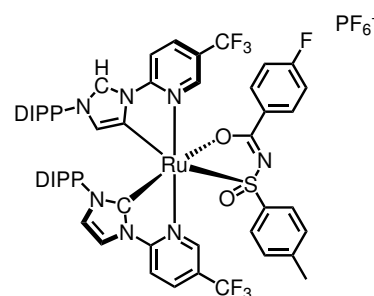
According to general procedure C, RuCl_3 (36.5 mg, 176 μmol , 1.00 eq) was reacted with imidazolium salt 134 (157.8 mg, 347 μmol , 2.0 eq) at 120 °C for 43 h. The flash chromatography was performed with $\text{CH}_2\text{Cl}_2/\text{CH}_3\text{CN}$ (20:1 \rightarrow 10:1) as eluent. The *racemic* title compound 137a (134 mg, 110 μmol , 63%) was obtained as a yellow crystalline solid.



$^1\text{H-NMR}$ (300 MHz, CD_3CN): δ = 9.42 (d, 1H, 4J = 1.3 Hz, H_{Ar}), 9.10-9.07 (m, 1H, H_{Ar}), 8.39-8.33 (m, 2H, H_{Ar}), 8.20-8.11 (m, 2H, H_{Ar}), 8.06 (d, 1H, 3J = 8.8 Hz, H_{Ar}), 7.91 (d, 1H, 3J = 8.7 Hz, H_{Ar}), 7.57 (dd, 1H, 3J = 7.8, 7.8 Hz, H_{Ar}), 7.42-7.33 (m, 4H, H_{Ar}), 7.30-7.23 (m, 2H, H_{Ar}), 6.79 (dd, 1H, 3J = 7.7, 4J = 1.4 Hz, H_{Ar}), 6.27 (d, 1H, 4J = 1.3 Hz, H_{Ar}), 2.81-2.70 (m, 1H, CHCH_3), 2.37 (pent, 1H, 3J = 6.8 Hz, CHCH_3), 2.27-2.16 (m, 1H, CHCH_3), 1.83 (pent, 1H, 3J = 6.8 Hz, CHCH_3), 1.45 (d, 3H, 3J = 7.0 Hz, CHCH_3), 1.23 (d, 3H, 3J = 6.9 Hz, CHCH_3), 1.16 (d, 3H, 3J = 6.8 Hz, CHCH_3), 1.11-0.99 (m, 10H), 0.82 (d, 6H, 3J = 6.8, 2x CHCH_3) ppm.

Synthesis of Auxiliary Complex Δ -(*R*)-138

An oven dried 50 mL round-bottom flask equipped with nitrogen inlet was charged with *racemic* complex **137a** (101 mg, 82.8 μmol , 1.00 eq), sulfinyl benzamide (*S*)-**121d** (22.4 mg, 80.8 μmol , 1.0 eq), K_2CO_3 (22.7 mg, 164.2 μmol , 2.0 eq) and CH_3CN (8 mL). The reaction mixture was stirred at 40 °C for 2 h. After cooling to room temperature, the mixture was filtrated through a pad of celite, rinsed with CH_3CN and the solvents were removed under reduced pressure. Column chromatography (100 mg NH_4PF_6 added as solid on top of column, $\text{CH}_2\text{Cl}_2/\text{CH}_3\text{CN}$ 30:1) provided the title compound Δ -(*R*)-**138** (35.8 mg, 28.2 μmol , 34%) as bright orange to red solid. Note: The isomer with a 180° rotated orientation of auxiliary **121d** was not isolated, hence both isomers are present which makes the NMR less clear to identify.



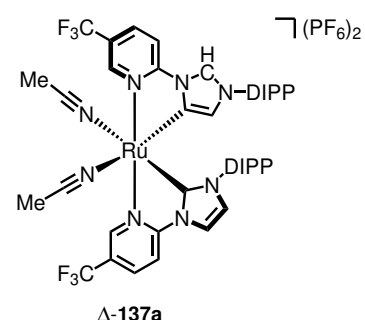
The absolute configuration was assigned analogously to complex Δ -(*R*)-**128a**.

¹H-NMR (300 MHz, CD_3CN): δ = 10.79 (dt, 1H, ⁴*J* = 1.9, 0.9 Hz, H_{Ar}), 9.31 (d, 1H, ⁴*J* = 1.4 Hz, H_{Ar}), 8.30 (dd, 2H, ³*J* = 6.2 Hz, ⁴*J* = 2.2 Hz, H_{Ar}), 8.25-8.17 (m, 2H, H_{Ar}), 8.13-8.06 (m, 2H, H_{Ar}), 7.87 (ddd, 3H, ³*J* = 8.9 Hz, ⁴*J* = 5.0, 2.3 Hz, H_{Ar}), 7.72-7.64 (m, 4H, H_{Ar}), 7.60 (t, 1H, ³*J* = 7.9 Hz, H_{Ar}), 7.49-7.36 (m, 8H, H_{Ar}), 7.32-7.08 (m, 8H, H_{Ar}), 6.86-6.77 (m, 2H, H_{Ar}), 6.67-6.59 (m, 3H, H_{Ar}), 6.37 (d, 1H, ⁴*J* = 1.3 Hz, H_{Ar}), 3.06 (pent, 1H, ³*J* = 6.8 Hz, CHCH_3), 2.61-2.51 (m, 1H, CHCH_3), 1.87-1.76 (m, 1H, CHCH_3), 1.49-1.11 (m, 9H), 1.00 (d, 3H, ³*J* = 6.8 Hz, CH_3), 0.90 (t, 3H, ³*J* = 7.2 Hz, CH_3), 0.78 (d, 3H, ³*J* = 6.7 Hz, CH_3), 0.70 (d, 4H, ³*J* = 6.8 Hz, CH_3) ppm.

Synthesis of Complex Δ -137a

In analogy to complex Δ -**114b**, complex Δ -(*R*)-**138** (35.8 mg, 27.7 μmol , 1.0 eq) in CH_3CN (7 mL) was treated with TFA (20.7 μL , 269.0 μmol , 9.7 eq), resulting in the complex Δ -**137a** (23.6 mg, 19.3 μmol , 91%) as a yellow solid.

The absolute configuration was assigned based on the configuration of auxiliary complex Δ -(*R*)-**138**.

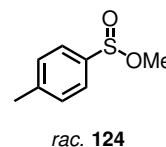


The spectroscopical data were in agreement with *racemic* **137a**.

5.5. Synthesis of Auxiliaries

Synthesis of *Racemic* Menthyl *p*-Tolylsulfinate (**124**)

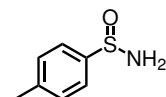
Following a published procedure,^[163] *p*-tolylsulfide **188** (2070 mg, 8.40 mmol, 1.0 eq) was dissolved in MeOH (20 mL). *N*-brom succinimide (NBS, 2374 mg, 13.3 mmol, 1.6 eq) was added in portions over a period of 20 min at room temperature. After full conversion of the starting material was observed via TLC, the reaction mixture was diluted with CH₂Cl₂ (50 mL) and washed with a saturated aqueous solution of NaHSO₃ (15 mL). The aqueous layer was extracted with CH₂Cl₂ (50 mL). The combined organic layer were washed with a saturated aqueous solution of NaHCO₃ (3x10 mL), dried over Na₂SO₄ and the solvents removed under reduces pressure. The *racemic* title compound **124** was obtained as an colorless liquid (2906 mg, 17.07 mmol, 99%) in sufficient purity and used without further purification.



¹H-NMR (300 MHz, CDCl₃): δ = 7.64-7.55 (m, 2H, *H*_{Ar}), 7.38-7.30 (m, 2H, *H*_{Ar}), 3.46 (s, 3H, OCH₃), 2.43 (s, 3H, CH₃) ppm. ¹³C-NMR (75 MHz, CDCl₃): δ = 143.0, 141.2, 129.9, 125.5, 49.5, 29.7, 21.6 ppm. HRMS (ESI): *m/z* calcd. for C₈H₁₁O₂S₁ [M + H]⁺: 171.0474, found: 171.0479.

Synthesis of *Racemic* *p*-Tolylsulfonamide (**125**)

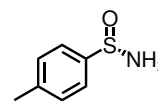
Following a published procedure,^[137] *racemic* menthyl *p*-toluenesulfinate (**124**, 1018 mg, 5.98 mmol, 1.00 eq) was dissolved in THF (15 mL) and cooled to -78 °C. A solution of LiHMDS (1 M in THF, 9.0 mL, 9.00 mmol, 1.35 eq) was added over a period of 1 h. The reaction mixture was allowed to warm up to room temperature within 3 h. After full conversion of the starting material was observed via TLC, a saturated aqueous solution of NH₄Cl (10 mL) was added and stirred for 30 min at room temperature. The mixture was extracted with EtOAc (3x60 mL), dried over Na₂SO₄ and the solvent removed under reduces pressure. The crude product was recrystallized from *n*-hexane/EtOAc (2:1 v/v, 40 mL). The *racemic* title compound **125** (489 mg, 3.15 mmol, 53%) was obtained as a pale yellow crystalline solid.



¹H-NMR (300 MHz, CDCl₃): δ = 7.66-7.56 (m, 2H, *H*_{Ar}), 7.37-7.28 (m, 2H, *H*_{Ar}), 4.30 (s, 2H, NH₂), 2.41 (s, 3H, CH₃) ppm. ¹³C-NMR (75 MHz, CDCl₃): δ = 143.5, 141.5, 129.6 (2C), 125.3(2C), 21.3 (CH₃) ppm. HRMS (ESI): *m/z* calcd. for C₇H₁₀N₁O₁S₁ [M + H]⁺: 156.0478, found: 156.0482. HPLC: Daicel Chiralpak OD-H (250 x 4.6 mm), *n*-Hexane/*i*-PrOH 90:10, 1 mL min⁻¹, 25 °C, 254 nm, *t*_R (*R*) = 14.63 min, *t*_R (*S*) = 17.29 min.

Synthesis of (S)-*p*-Tolylsulfonamide (125)

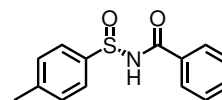
Following a published procedure,^[137] (1*R*,2*S*,5*R*)-(-)-Menthyl (*S*)-*p*-toluenesulfinate (**124**, 1963 mg, 6.69 mmol, 1.00 eq) was dissolved in THF (16 mL) and cooled to $-78\text{ }^{\circ}\text{C}$. A solution of LiHMDS (1 M in THF, 9.0 mL, 9.00 mmol, 1.35 eq) was added over a period of 1 h. The reaction mixture was allowed to warm up to room temperature within 3 h. After full conversion of the starting material was observed via TLC, a saturated aqueous solution of NH_4Cl (10 mL) was added and stirred for 30 min at room temperature. The mixture was extracted with EtOAc (4x50 mL), dried over Na_2SO_4 and the solvent removed under reduced pressure. The crude product was purified via column chromatography ($\text{CH}_2\text{Cl}_2/\text{MeOH}$ 15:1) and the target product **125** was obtained as a colorless, crystalline solid. To improve the enantiopurity, the product was recrystallized from *n*-hexane/EtOAc (2:1 v/v, 40 mL) to give enantiopure **125** (735 mg, 4.74 mmol, 71%, >99% *ee*).



¹**H-NMR** (250 MHz, CDCl_3): δ = 7.62 (d, 2H, 3J = 8.2 Hz, H_{Ar}), 7.31 (d, 2H, 3J = 8.0 Hz, H_{Ar}), 4.3 (s, br, 2H, NH_2), 2.4 (s, 3H, CH_3) ppm. ¹³**C-NMR** (75 MHz, CDCl_3): δ = 143.7, 141.6, 129.7 (2C), 125.5 (2C), 21.5 (CH_3) ppm. **HRMS (ESI)**: m/z calcd. for $\text{C}_7\text{H}_9\text{N}_1\text{O}_1\text{S}_1\text{Na}_1$ [$\text{M} + \text{Na}$]⁺: 178.0297, found: 178.0301. **IR** (film): $\tilde{\nu}$ = 3187, 3091, 2920, 2867, 1589, 1482, 1394, 1085, 1005, 972, 912, 803, 707, 622, 571, 523, 441, 407 cm^{-1} . **M.p.**: $106\text{ }^{\circ}\text{C}$ (EtOAc). **HPLC**: Daicel Chiralpak OD-H (250 x 4.6 mm), *n*-Hexane/*i*-PrOH 90:10, 1 mL min^{-1} , $25\text{ }^{\circ}\text{C}$, 254 nm, t_R (*R*) = 14.63 min, t_R (*S*) = 17.29 min.

Synthesis of (S)-*N*-(*p*-Tolylsulfinyl)benzamide (121a)

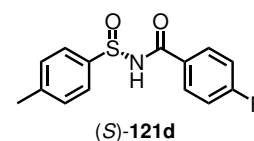
According to a published procedure,^[138] (*S*)-**125** (156.1 mg, 1.00 mmol, 1.0 eq) was dissolved in THF (4 mL) and cooled to $-78\text{ }^{\circ}\text{C}$. At this temperature, *n*-BuLi (1.6 M in *n*-hexane, 1.3 mL, 2.1 mmol, 2.1 eq) was added slowly over a period of 5 min, followed by benzoic anhydride (**126**, 265.9 mg, 1.18 mmol, 1.2 eq) as a solid in one portion. The reaction was allowed to warm up to room temperature over night. Saturated aqueous solution of NH_4Cl (5 mL) was added, the mixture was extracted with EtOAc (3x30 mL), and the combined organic layers were dried with brine and Na_2SO_4 . The solvent was removed under reduced pressure and the crude product was purified by column chromatography ($\text{CH}_2\text{Cl}_2/\text{MeOH}$ 100:1). The title compound **121a** (226.2 mg, 0.87 mmol, 87%, >99% *ee*) was obtained as a colorless solid.



¹**H-NMR** (300 MHz, CDCl_3): δ = 8.23 (s, br, 1H, NH), 7.83 – 7.76 (m, 2H, H_{Ar}), 7.72 – 7.65 (m, 2H, H_{Ar}), 7.61 – 7.53 (m, 1H, H_{Ar}), 7.52 – 7.41 (m, 2H, H_{Ar}), 7.40 – 7.32 (m, 2H, H_{Ar}), 2.45 (s, 3H, CCH_3) ppm. ¹³**C-NMR** (75 MHz, CDCl_3): δ = 167.5, 142.7, 140.8, 133.2, 131.8, 130.2 (2C), 128.9 (2C), 128.1 (2C), 125.0 (2C), 21.6 (CH_3) ppm. **HRMS (ESI)**: m/z calcd. for $\text{C}_{14}\text{H}_{14}\text{N}_1\text{O}_2\text{S}_1$ [$\text{M} + \text{H}^+$]⁺: 260.0740, found: 260.0747. **IR** (film): $\tilde{\nu}$ = 3364, 3220, 3062, 1647, 1602, 1491, 1451, 1385, 1240, 1178, 1144, 1095, 1064, 1022, 930, 881, 804, 754, 714, 688, 640, 618, 525, 499, 456, 423 cm^{-1} . **M.p.**: $111\text{ }^{\circ}\text{C}$ (MeOH). **HPLC**: Chiralpak IB-N5 (250 x 4.6 mm), $\text{H}_2\text{O} + 0.1\%$ TFA/ CH_3CN 65:35, 1.0 mL min^{-1} , $20\text{ }^{\circ}\text{C}$, 254 nm, t_R (minor) = 17.7 min, t_R (major) = 19.9 min.

Synthesis of (S)-4-Fluoro-N-(p-Tolylsulfinyl)benzamide (121d)

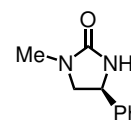
Following the previous described protocol, sulfinamide (S)-**125** (257.1 mg, 1.65 mmol, 1.0 eq) and 4-fluorobenzoyl chloride (**127**, 0.24 mL, 2.03 mmol, 1.2 eq) provided sulfinyl benzamide **121d** (397.5 mg, 1.43 mmol, 86%) as a slight red crystalline solid.



¹H-NMR (500 MHz, CDCl₃): δ = 8.44 (s, 1H, NH), 7.86–7.81 (m, 2H, H_{Ar}), 7.67–7.62 (m, 2H, H_{Ar}), 7.38–7.33 (m, 2H, H_{Ar}), 7.15–7.09 (m, 2H, H_{Ar}), 2.44 (s, 3H, CH₃) ppm. ¹³C-NMR (126 MHz, CDCl₃): δ = 166.3, 165.8 (d, ¹J_{C,F} = 255.1 Hz), 143.0, 140.7, 130.7 (d, ³J_{C,F} = 9.4 Hz, 2C), 130.3 (2C), 128.0 (d, ⁴J_{C,F} = 3.2 Hz), 124.9 (2C), 116.2 (d, ²J_{C,F} = 22.0 Hz, 2C), 21.7 (CH₃) ppm. ¹⁹F-NMR (235 MHz, CDCl₃): δ = -104.7 ppm. HRMS (ESI): *m/z* calcd. For C₁₄H₁₂F₁N₁O₂S₁Na₁ [M + Na]⁺: 300.0465, found: 300.0473. IR (film): $\tilde{\nu}$ = 3151, 3064, 2824, 1674, 1597, 1510, 1487, 1424, 1393, 1305, 1234, 1165, 1084, 1051, 1013, 887, 855, 805, 763, 676, 624, 589, 512, 474, 428 cm⁻¹. M.p.: 62 °C (MeOH). HPLC: Chiralpak IB-N5 (250 x 4.6 mm), 0.6 mL min⁻¹, H₂O+0.1% TFA/CH₃CN 70:30, 20 °C, 254 nm, *t*_R (major) = 62.15 min, *t*_R (minor) = 63.93 min.

5.6. General Procedure for Asymmetric C,H Amination

Following the general procedure D, *N*-benzoyloxyurea (**76**, 55.6 mg, 0.2 mmol, 1.0 eq), catalyst (0.9 mol%) and K₃CO₃ (83.5 mg, 0.60 mmol, 3.1 eq) in freshly distilled CH₂Cl₂ (2 mL) were used, providing the amination product **77** (34.2 mg, 0.194 mmol, 99% yield, 86% *ee*) as a colorless solid.

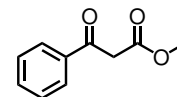


¹H-NMR (300 MHz, CDCl₃): δ = 7.44-7.28 (m, 5H, H_{Ar}), 4.82-4.62 (m, 2H), 3.78 (t, 1H, ³J = 8.8 Hz), 3.22 (dd, 1H, ³J = 8.8, 7.4 Hz), 2.82 (s, 3H, NCH₃) ppm. HPLC: Daicel Chiralpak IA (250 x 4.6 mm), *n*-hexane/*i*-PrOH 90:10, 1 mL min⁻¹, 30 °C, 220 nm, *t*_R (R) = 12.6 min, *t*_R (S) = 14.8 min. All other spectroscopic data were in agreement with the literature.^[118]

5.7. Azirination

Synthesis of Methyl 3-Oxo-3-phenylpropanoate (**145**)

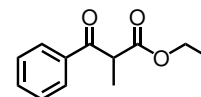
Following a modified procedure,^[140] a flame-dried 25 mL round-bottom flask equipped with nitrogen inlet was charged with NaH (60 wt% in oil, 339 mg, 14.1 mmol, 3.33 eq), THF (4 mL) and dimethyl carbonate (**144**, 0.7 mL, 8.31 mmol, 2.0 eq). Over a period of 5 min, a solution of acetophenone (510 mg, 4.24 mmol, 1.0 eq) in THF (2 mL) was added and stirred for 10 min at room temperature, followed by 13 h at 72 °C. After full conversion was observed via TLC (*n*-pentane/EtOAc 10:1), saturated NH₄Cl solution (5 mL) was added, extracted with CH₂Cl₂ (3x30 mL), dried over NaSO₄ and the solvents were removed under reduced pressure. The crude product was purified by flash chromatography (*n*-pentane/EtOAc 10:1 → 7:1) and the title compound **145a** (727 mg, 4.08 mmol, 96%, Ratio Keto/Enol 80/20) was obtained as a colorless oil.



¹H-NMR (250 MHz, CDCl₃): δ = 12.49 (s, 1H, OH_{Enol}), 8.02-7.83 (m, 2H, H_{Ar}), 7.84-7.72 (m, 1H, H_{Ar}), 7.68-7.53 (m, 1H, H_{Ar}), 7.56-7.36 (m, 3H, H_{Ar}), 5.68 (s, 1H, H_{olef.,Enol}), 4.01 (s, 2H, CH_{2,Keto}), 3.81 (s, 1H, CH₃), 3.76 (s, CH₃) ppm. R_f = 0.22 (*n*-pentane/EtOAc 10:1)

Synthesis of Ethyl 2-Methyl-3-oxo-3-phenylpropanoate (**146**)

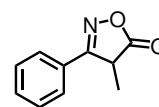
Following a modified literature procedure,^[77] a 100 mL round bottom flask was charged with Ethylbenzoylacetate (**189**, 9070 mg, 47.2 mmol, 1.0 eq), K₂CO₃ (8327 mg, 60.23 mmol, 1.3 eq) methylene iodine (5.0 mL, 80.3 mmol, 1.7 eq) and Acetone (50 mL), equipped with reflux condenser and heated to 56 °C for 4 h. After cooling to room temperature, the mixture was filtered through a pad of celite and the solvents were removed under reduced pressure. The target product **146** (10 g, 47 mmol, 99%) was obtained as an orange oil and used without further purification. Note: Although reaction monitoring via TLC is possible with long plates (> 7 cm), GC monitoring is highly recommended.



¹H-NMR (250 MHz, CDCl₃): δ = 8.03-7.92 (m, 2H, H_{Ar}), 7.64-7.53 (m, 1H, H_{Ar}), 7.53-7.40 (m, 2H, H_{Ar}), 4.37 (q, 1H, ³J = 7.1 Hz, CHCH₃), 4.14 (q, 2H, ³J = 7.1 Hz, CH₂CH₃), 1.49 (d, 3H, ³J = 7.1 Hz, CHCH₃), 1.16 (t, 3H, ³J = 7.1 Hz, CH₂CH₃) ppm. ¹³C-NMR (63 MHz, CDCl₃): δ = 196.0, 171.0, 136.0, 133.6, 128.8, 128.7, 61.5, 48.5, 14.1, 13.9 ppm. HRMS (ESI): *m/z* calcd. for C₁₂H₁₄O₃Na₁ [M+Na]⁺ 229.0835, found: 229.084. R_f = 0.47 (*n*-pentane/EtOAc 5:2). R_f = 0.47 (*n*-pentane/EtOAc 2.5:1) GC/MS: R_t = 5.401 min Temperature profile: Initial temperature 50 °C for 2 min, final temperature 250 °C, rate 30 °C min⁻¹.

Synthesis of 4-Methyl-3-phenylisoxazol-5(4H)-one (147)

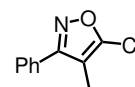
Following a slight modified literature procedure,^[141] a 25 mL N₂-flask was charged with β -ketoester **146** (1003 mg, 4.86 mmol, 1.0 eq), NH₂OH·HCl (689 mg, 9.78 mmol, 2.0 eq), pyridine (1.2 mL, 14.9 mmol, 3.1 eq), EtOH (5 mL) and stirred at 60 °C for 17 h. After cooling to room temperature, the mixture was diluted with water (20 mL), extracted with EtOAc (3x30 mL), the combined organic layers washed with aqueous HCl-solution (20 mL, 1 M) and dried over Na₂SO₄. The solvents were removed under reduced pressure and the crude product was recrystallized from EtOH. The title compound **147** (770 mg, 4.40 mmol, 90%) was obtained as a colorless crystalline solid.



¹H-NMR (250 MHz, CDCl₃): δ = 8.09 (s, 1H, OH_{Enol}), 7.73-7.63 (m, 2H, H_{Ar}), 7.63-7.42 (m, 5H, H_{Ar}), 3.84 (q, 1H, ³J = 7.9 Hz, CHCH₃), 2.04 (s, 1H, CH_{3,Enol}), 1.58 (d, 3H, ³J = 7.9 Hz, CH_{3,Keto}) ppm. ¹³C-NMR (63 MHz, CDCl₃): δ = 178.8, 167.3, 132.1, 131.4, 129.4, 127.5, 127.1, 39.6, 14.7, 7.9 ppm. HRMS (ESI): *m/z* calcd. for C₁₀H₉N₁O₂Na₁ [M+Na]⁺: 198.0525, found: 198.0530.

Synthesis of 5-Chloro-4-methyl-3-phenylisoxazole (148)

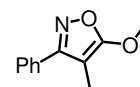
Following a modified literature procedure^[77], a two neck flask equipped with a schlenk extention and reflux condenser was charged with isoxazolone **147** (701 mg, 4.00 mmol, 1.0 eq), POCl₃ (3.6 mL, 39.4 mmol, 10 eq), NEt₃ (0.4 mL, 2.9 mmol, 0.7 eq) and heated to reflux temperature for 21 h. After cooling to room temperature, the mixture was poured onto a mixture of ice and an saturated aqueous solution of NaHCO₃ (ca. 50 mL) and extracted with EtOAc (3x70 mL). The combined organic layers were washed with brine, dried over Na₂SO₄, the solvents removed under reduced pressure and the crude product purified via flash chromatography (*n*-pentane/EtOAc 20:1). The product **148** (709 mg, 3.66 mmol, 92%) was obtained as a yellow oil.



¹H-NMR (300 MHz, CDCl₃): δ = 7.73-7.58 (m, 2H, H_{Ar}), 7.56-7.43 (m, 3H, H_{Ar}), 2.13 (s, 3H, CH₃) ppm. ¹³C-NMR (75 MHz, CDCl₃): δ = 164.0, 152.1, 130.1, 129.2, 129.0, 128.0, 108.6, 8.2 (CH₃) ppm. HRMS (ESI): *m/z* calcd. for C₁₀H₈Cl₁N₁O₁Na₁ [M+Na]⁺: 216.0187, found: 216.0189. IR (film): $\tilde{\nu}$ = 1737, 1613, 1577, 1453, 1384, 1243, 1177, 1097, 1042, 1013, 898, 769, 695, 568, 509 cm⁻¹. R_f = 0.41 (*n*-pentane/EtOAc 20:1).

Synthesis of 5-Methoxy-4-methyl-3-phenylisoxazole (56a)

Following a modified literature procedure,^[77] a 10 mL PTFE sealed pressure tube was charged with NaH (60 wt% in oil, 72 mg, 1.8 mmol, 1.5 eq) and MeOH (0.4 mL). After the gas formation depleted, a solution of isoxazole **148** (239 mg, 1.22 mmol, 1.0 eq) in

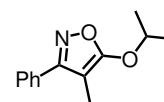


MeOH (1.4 mL) and stirred at 65 °C for 90 h. The mixture was cooled to room temperature, diluted with *n*-pentane (10 mL) and purified via flash chromatography (*n*-pentane/EtOAc 20:1). The title compound **56a** (159 mg, 0.84 mmol, 69%) was obtained as a yellow oil.

¹H-NMR (300 MHz, CDCl₃): δ = 7.68-7.58 (m, 2H, H_{Ar}), 7.49-7.40 (m, 3H, H_{Ar}), 4.12 (s, 3H, OCH₃), 1.96 (s, 3H, CH₃) ppm. ¹³C-NMR (75 MHz, CDCl₃): δ = 169.7, 164.9, 130.5, 129.6, 128.8 (2C), 127.9 (2C), 86.7, 58.0, 6.6 ppm. HRMS (ESI): *m/z* calcd. for C₁₁H₁₂N₁O₂ [M+H]⁺: 190.0863, found: 190.0867. R_f = 0.18 (*n*-pentane/EtOAc 20:1).

Synthesis of 5-Methoxy-4-methyl-3-phenylisoxazole (56b)

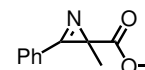
Following a modified literature procedure,^[77] a 10 mL PTFE sealed pressure tube was charged with NaH (60 wt% in oil, 90 mg, 2.25 mmol, 1.5 eq) and *i*-PrOH (2 mL). After the gas formation depleted, **148** (300 mg, 1.52 mmol, 1.0 eq) was added and stirred at 70 °C for 39 h. The mixture was cooled to room temperature, diluted with *n*-pentane (10 mL) and purified via flash chromatography (*n*-pentane/EtOAc 20:1). The title compound **56b** (193 mg, 1.02 mmol, 67%) was obtained as a colorless oil.



¹H-NMR (300 MHz, CDCl₃): δ = 7.71-7.60 (m, 2H, H_{Ar}), 7.52-7.40 (m, 3H, H_{Ar}), 4.93 (hept, 1H, ³J = 6.2 Hz, CH(CH₃)₂), 1.96 (s, 3H, CH₃), 1.43 (d, 6H, J = 6.2 Hz, CH(CH₃)₂) ppm. ¹³C-NMR (75 MHz, CDCl₃): δ = 169.3, 164.5, 130.6, 129.5, 128.8, 127.9, 88.7, 76.0, 22.7, 6.9 ppm.

Synthesis of Methyl 2-Methyl-3-phenyl-2H-azirine-2-carboxylate (190)

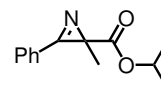
According to general procedure E, isoxazole **56a** (20 mg, 0.1 mmol, 1.0 eq) was used, providing the target product **190** (19 mg, 0.10 mmol, 96%) as a yellow oil.



¹H-NMR (250 MHz, CDCl₃): δ = 7.69-7.59 (m, 2H, H_{Ar}), 7.49-7.41 (m, 3H, H_{Ar}), 4.12 (s, 3H, OCH₃), 1.96 (s, 3H, CH₃) ppm. ¹³C-NMR (75 MHz, CDCl₃): δ = 173.7, 163.7, 133.8, 130.2, 129.5, 122.7, 52.6, 35.6, 17.9 ppm. HRMS (ESI): *m/z* calcd. for C₁₁H₁₁N₁O₂Na₁ [M+Na]⁺: 212.0682, found: 212.0680. HPLC: Chiralpak OD-H (250 x 4.6 mm), 1.0 mL min⁻¹, *n*-Hexane/*i*-PrOH 98:02, 20 °C, 254 nm, *t*_R (minor) = 10.125 min, *t*_R (major) = 11.017 min.

Synthesis of Isopropyl 2-Methyl-3-phenyl-2H-azirine-2-carboxylate (**191**)

According to general procedure E, isoxazole **56b** (20 mg, 0.092 mmol, 1.0 eq) was used, providing the target product **191** (17 mg, 0.08 mmol, 87%) as a yellow oil.

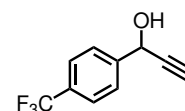


$^1\text{H-NMR}$ (300 MHz, CDCl_3): δ = 7.83 (dt, 2H, 3J = 6.7 Hz, 4J = 1.6 Hz, H_{Ar}), 7.58 (ddd, 3H, 3J = 8.6, 6.1 Hz, 4J = 2.4 Hz, H_{Ar}), 5.01 (hept, 1H, 3J = 6.3 Hz, $\text{CH}(\text{CH}_3)_2$), 1.60 (s, 3H, CH_3), 1.21 (d, 3H, 3J = 6.3 Hz, CHCH_3CH_3), 1.15 (d, 3H, 3J = 6.2 Hz, CHCH_3CH_3) ppm. $^{13}\text{C-NMR}$ (75 MHz, CDCl_3): δ = 172.7, 163.9, 133.6, 130.1, 129.4, 122.9, 69.0, 35.9, 21.9, 21.8, 17.9 ppm. **HPLC**: Chiralpak IC (250 x 4.6 mm), 1.0 mL min^{-1} , *n*-Hexane/*i*-PrOH 90:10, 20 °C, 254 nm, t_R (major) = 8.606 min, t_R (minor) = 9.406 min.

5.8. Propargyl Substrates

Synthesis of Propargyl Alcohol **172**

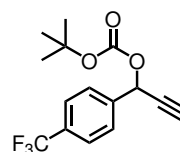
Following a modified literature procedure,^[153] a 100 mL N_2 -flask was charged with TMS-acetylene (**171**, 1.3 mL, 9.132 mmol, 1.03 eq) and THF (30 mL), cooled to -78 °C. *n*-BuLi (1.6 M in *n*-hexane, 5.5 mL, 8.80 mmol, 1.0 eq) was added at this temperature over a period of 5 min. After stirring for 10 min, the reaction mixture was allowed to warm up to 0 °C for 20 min and cooled to -78 °C. A solution of *p*- CF_3 -benzaldehyde (**170**, 1550 mg, 8.90 mmol, 1.00 eq) in THF (10 mL) was added over a period of 10 min. The reaction mixture was stirring at this temperature for 20 min and allowed to warm up to 0 °C for 30 min. At this temperature, MeOH (20 mL) and K_2CO_3 (350 mg, 2.53 mmol, 0.3 eq) were added and stirred for 2 h. After TLC showed full conversion, a saturated aqueous solution of NH_4Cl (10 mL) was added, extracted with EtOAc (3x40 mL), dried over brine and Na_2SO_4 and the solvents were removed under reduced pressure. The crude product was purified by flash chromatography (*n*-pentane/EtOAc 20:1 \rightarrow 5:1). The title compound **172** (1348 mg, 6.74 mmol, 76%) was obtained as a yellow oil.



$^1\text{H-NMR}$ (250 MHz, CDCl_3): δ = 7.72-7.60 (m, 4H, H_{Ar}), 5.53 (dd, 1H, 3J = 6.1 Hz, 4J = 2.2 Hz), 2.71 (d, 1H, 4J = 2.3 Hz), 2.36 (dd, 1H, 3J = 6.1 Hz, 4J = 2.0 Hz) ppm. $^{19}\text{F-NMR}$ (235 MHz, CDCl_3): δ = -62.6 ppm.

Synthesis of Propargyl Carbamate **173**

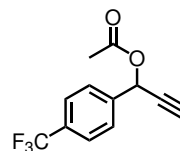
Following a modified literature procedure,^[164] a 25 mL N₂-flask was charged with propargyl alcohol **172** (509 mg, 2.54 mmol, 1.00 eq), **192** (850 mg, 3.89 mmol, 1.53 eq) and CH₂Cl₂ (2.5 mL). The mixture was cooled to 0 °C and **97** (31.1 mg, 254 μmol, 0.10 eq) was added in one portion, which turned the solution bright yellow. After 1 h, the solution turned slowly to a red color. After stirring for 5 h, water (10 mL) was added and extracted with EtOAc (3x30 mL), dried over brine and Na₂SO₄. The solvents were removed under reduced pressure and the crude product was purified via flash chromatography (*n*-pentane/EtOAc 20:1). The title compound **173** (582 mg, 1.94 mmol, 76%) was obtained as a colorless liquid.



¹H-NMR (500 MHz, CDCl₃): δ = 7.69-7.61 (m, 4H, H_{Ar}), 6.28 (d, 1H, ⁴J = 2.3 Hz, CHC), 2.72 (d, 1H, ⁴J = 2.3 Hz, CH), 1.50 (s, 9H, C(CH₃)₃) ppm. ¹³C-NMR (126 MHz, CDCl₃): δ = 152.4, 140.2, 131.4 (q, J = 32.6 Hz), 128.1, 125.8 (q, J = 3.8 Hz), 124.0 (q, ¹J = 272.3 Hz), 83.8, 79.4, 76.8, 67.4, 27.8 ppm. ¹⁹F-NMR (282 MHz, CDCl₃): δ = -62.8 ppm. HRMS (ESI): *m/z* calc. For C₁₅H₁₅F₃O₃Na₁ [M+Na]⁺: 323.0866, found: 323.0865. IR (film): $\tilde{\nu}$ = 3302, 2983, 2938, 2128, 1743, 1621, 1469, 1419, 1370, 1322, 1251, 1157, 1122, 1066, 1011, 954, 841, 770, 670, 608, 520, 466, 402 cm⁻¹.

Synthesis of Acetate **174**

Following a modified literature procedure,^[165] a 10 mL N₂-flask was charged with propargyl alcohol **172** (537 mg, 2.69 mmol, 1.00 eq), DMAP (**97**, 37 mg, 0.303 mmol, 0.11 eq) and CH₂Cl₂ (3.8 mL). The mixture was cooled to 0 °C, NEt₃ (0.5 mL, 3.59 mmol, 1.34 eq) and Ac₂O (0.35 mL, 3.70 mmol, 1.38 eq) were added and stirred at this temperature for 5 h. After full conversion was observed via TLC, a saturated aqueous solution of NH₄Cl-solution (5 mL) was added, extracted with CH₂Cl₂ (3x30 mL), dried over brine and Na₂SO₄. The solvents were removed *in vacuo* and the obtained crude product was purified via flash chromatography (*n*-pentane/EtOAc 15:1 → 10:1). The title compound **174** (476 mg, 1.96 mmol, 73%) was obtained as a colorless oil.

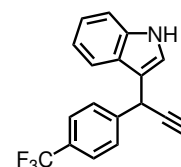


¹H-NMR (500 MHz, CDCl₃): δ = 7.65 (s, 4H, H_{Ar}), 6.49 (d, 1H, ⁴J = 2.3 Hz, CHOAc), 2.69 (d, 1H, ⁴J = 2.3 Hz, CH), 2.13 (s, 3H, CH₃) ppm. ¹³C-NMR (126 MHz, CDCl₃): δ = 169.6, 140.2, 131.2 (q, ³J = 32.6 Hz), 128.0, 125.7 (q, ⁴J = 3.8 Hz), 123.8 (q, J = 272.3 Hz), 79.5, 76.1, 64.5, 20.9 ppm. ¹⁹F-NMR (235 MHz, CDCl₃): δ = -62.8 ppm. HRMS (ESI): *m/z* calc. For C₁₂H₉F₃O₂Na₁ [M⁺Na⁺]⁺: 265.0447, found: 265.0455. IR (film): $\tilde{\nu}$ = 3300, 1742, 1621, 1419, 1372, 1322, 1221, 1165, 1118, 1065, 1015, 958, 914, 831, 764, 673, 647, 601, 553, 463 cm⁻¹.

5.9. Propargylic Substitution

Synthesis of Propargyl Indole 176

A representative procedure for the propargylic substitution is given here and is based on a published procedure.^[166] An oven dried pressure tube was charged with indole (48 mg, 0.410 mmol, 2.23 eq), complex **114b** (2.0 mg, 1.80 μ mol, 1.0 mol%), evacuated and flushed with N₂ and added **173** (55.1 mg, 0.183 mmol, 1.00 eq) in THF (0.5 mL). NEt₃ (5.5 μ L, 39.7 μ mol, 0.22 eq) was added, sealed and placed in a pre-heated oil-bath at 60 °C upon which the solution turned deep red. After 48 h the reaction was stopped as no full conversion was observed within this time. The mixture was purified via flash chromatography two times (*n*-pentane/EtOAc 10:1 and 5:1 the 2nd time of the product containing fractions). The title compound **176** (8.8 mg, 29 μ mol, 16%) was obtained as a brown liquid as well as remaining **173** (6.0 mg, 19 μ mol, 10%).



¹H-NMR (300 MHz, CDCl₃): δ = 8.07 (s, 1H, NH), 7.67-7.54 (m, 4H, H_{Ar}), 7.48 (d, 1H, ³J = 7.9 Hz, H_{Ar}), 7.38 (d, 1H, ³J = 8.2 Hz), 7.24-7.17 (m, 1H, H_{Ar}), 7.16 (d, 1H, ⁴J = 2.5 Hz, H_{Ar}), 7.12-7.03 (m, 1H, H_{Ar}), 5.32 (d, 1H, ⁴J = 2.5 Hz, CHC), 2.48 (d, 1H, ⁴J = 2.6 Hz, CH) ppm. ¹³C-NMR (75 MHz, CDCl₃): δ = 144.9, 136.9, 128.3, 125.7, 125.6, 122.9, 122.7, 120.0, 119.4, 115.5, 111.5, 84.0, 72.1, 34.7 ppm. HRMS (ESI): *m/z* calc. For C₁₈H₁₃F₃N₁ [M+H]⁺: 300.0995, found: 300.1001. HPLC: Chiralpak OD-H (250 x 4.6 mm), 1.0 mL min⁻¹, *n*-Hexane/*i*-PrOH 90:10, 25 °C, 254 nm, *t*_R (minor) = 11.998 min, *t*_R (major) = 20.581 min.

6. References

- [1] P. J. Walsh, M. C. Kozlowski, *Fundamentals of asymmetric catalysis*, University Science Books: Sausalito, California, **2009**.
- [2] P. T. Anastas, M. M. Kirchhoff, T. C. Williamson, *Applied Catalysis A: General* **2001**, *221*, 3–13.
- [3] *Comprehensive asymmetric catalysis*, (Ed.: E. N. Jacobsen), Springer, Berlin, **2004**.
- [4] G. L. Hamilton, E. J. Kang, M. Mba, F. D. Toste, *Science* **2007**, *317*, 496–499.
- [5] B. List, *Chem. Rev.* **2007**, *107*, 5413–5415.
- [6] J. A. Osborn, F. H. Jardine, J. F. Young, G. Wilkinson, *J. Chem. Soc. A* **1966**, 1711–1732.
- [7] T. Katsuki, K. B. Sharpless, *J. Am. Chem. Soc.* **1980**, *102*, 5974–5976.
- [8] E. N. Jacobsen, I. Marko, W. S. Mungall, G. Schroeder, K. B. Sharpless, *J. Am. Chem. Soc.* **1988**, *110*, 1968–1970.
- [9] M. Kitamura, T. Ohkuma, S. Inoue, N. Sayo, H. Kumobayashi, S. Akutagawa, T. Ohta, H. Takaya, R. Noyori, *J. Am. Chem. Soc.* **1988**, *110*, 629–631.
- [10] *The IUPAC Compendium of Chemical Terminology*, (Ed.: V. Gold), International Union of Pure and Applied Chemistry (IUPAC), Research Triangle Park, NC, **2019**.
- [11] R. H. Crabtree, *Coord. Chem. Rev.* **2013**, *257*, 755–766.
- [12] L. Pardatscher, M. J. Bitzer, C. Jandl, J. W. Kück, R. M. Reich, F. E. Kühn, W. Baratta, *Dalton Trans.* **2019**, *48*, 79–89.
- [13] Á. Vivancos, C. Segarra, M. Albrecht, *Chem. Rev.* **2018**, *118*, 9493–9586.
- [14] H.-W. Wanzlick, H.-J. Schönherr, *Angew. Chem. Int. Ed.* **1968**, *7*, 141–142.
- [15] K. Öfele, *J. Organomet. Chem.* **1968**, *12*, P42–P43.
- [16] A. J. Arduengo, R. L. Harlow, M. Kline, *J. Am. Chem. Soc.* **1991**, *113*, 361–363.
- [17] D. Bourissou, O. Guerret, F. P. Gabbaï, G. Bertrand, *Chem. Rev.* **2000**, *100*, 39–92.
- [18] F. Glorius, *N-Heterocyclic Carbenes in Transition Metal Catalysis*, Springer Berlin / Heidelberg, Berlin, Heidelberg, **2007**.
- [19] S. Díez-González, N. Marion, S. P. Nolan, *Chem. Rev.* **2009**, *109*, 3612–3676.
- [20] H. Jacobsen, A. Correa, A. Poater, C. Costabile, L. Cavallo, *Coord. Chem. Rev.* **2009**, *253*, 687–703.
- [21] R. H. Crabtree, *J. Organomet. Chem.* **2005**, *690*, 5451–5457.
- [22] C. A. Tolman, *Chem. Rev.* **1977**, *77*, 313–348.
- [23] B. J. Dunne, R. B. Morris, A. G. Orpen, *J. Chem. Soc. Dalton Trans.* **1991**, 653.
- [24] A. T. Termaten, M. Schakel, A. W. Ehlers, M. Lutz, A. L. Spek, K. Lammertsma, *Chem. Eur. J.* **2003**, *9*, 3577–3582.
- [25] X. Hu, I. Castro-Rodriguez, K. Meyer, *J. Am. Chem. Soc.* **2004**, *126*, 13464–13473.

6. References

- [26] X. Hu, I. Castro-Rodriguez, K. Olsen, K. Meyer, *Organometallics* **2004**, *23*, 755–764.
- [27] A. R. Chianese, A. Kovacevic, B. M. Zeglis, J. W. Faller, R. H. Crabtree, *Organometallics* **2004**, *23*, 2461–2468.
- [28] M.-T. Lee, C.-H. Hu, *Organometallics* **2004**, *23*, 976–983.
- [29] M. S. Sanford, J. A. Love, R. H. Grubbs, *J. Am. Chem. Soc.* **2001**, *123*, 6543–6554.
- [30] J. A. Love, M. S. Sanford, M. W. Day, R. H. Grubbs, *J. Am. Chem. Soc.* **2003**, *125*, 10103–10109.
- [31] P. L. Arnold, S. Pearson, *Coord. Chem. Rev.* **2007**, *251*, 596–609.
- [32] M. N. Hopkinson, C. Richter, M. Schedler, F. Glorius, *Nature (London U. K.)* **2014**, *510*, 485–496.
- [33] N. M. Scott, S. P. Nolan, *Eur. J. Inorg. Chem.* **2005**, *2005*, 1815–1828.
- [34] S. Gründemann, A. Kovacevic, M. Albrecht, J. W. Faller, R. H. Crabtree, *J. Am. Chem. Soc.* **2002**, *124*, 10473–10481.
- [35] X. Hu, I. Castro-Rodriguez, K. Meyer, *J. Am. Chem. Soc.* **2003**, *125*, 12237–12245.
- [36] H. Lebel, M. K. Janes, A. B. Charette, S. P. Nolan, *J. Am. Chem. Soc.* **2004**, *126*, 5046–5047.
- [37] B. Cetinkaya, P. Dixneuf, M. F. Lappert, *J. Chem. Soc. Dalton Trans.* **1974**, 1827.
- [38] M. F. Lappert, P. L. Pye, G. M. McLaughlin, *J. Chem. Soc. Dalton Trans.* **1977**, 1272–1282.
- [39] A. J. Arduengo, M. Tamm, S. J. McLain, J. C. Calabrese, F. Davidson, W. J. Marshall, *J. Am. Chem. Soc.* **1994**, *116*, 7927–7928.
- [40] D. S. McGuinness, K. J. Cavell, B. F. Yates, B. W. Skelton, A. H. White, *J. Am. Chem. Soc.* **2001**, *123*, 8317–8328.
- [41] T. M. Trnka, J. P. Morgan, M. S. Sanford, T. E. Wilhelm, M. Scholl, T.-L. Choi, S. Ding, M. W. Day, R. H. Grubbs, *J. Am. Chem. Soc.* **2003**, *125*, 2546–2558.
- [42] I. J. B. LIN, C. S. VASAM, *Comments Inorg. Chem.* **2004**, *25*, 75–129.
- [43] M. Muehlhofer, T. Strassner, E. Herdtweck, W. A. Herrmann, *J. Organomet. Chem.* **2002**, *660*, 121–126.
- [44] H. Türkmen, T. Pape, F. E. Hahn, B. Çetinkaya, *Eur. J. Inorg. Chem.* **2008**, *2008*, 5418–5423.
- [45] S. Csihony, D. A. Culkin, A. C. Sentman, A. P. Dove, R. M. Waymouth, J. L. Hedrick, *J. Am. Chem. Soc.* **2005**, *127*, 9079–9084.
- [46] S. Gründemann, A. Kovacevic, M. Albrecht, J. W. Faller, R. H. Crabtree, *Chem. Commun.* **2001**, 2274–2275.
- [47] A. Kovacevic, K. R. Meadows, M. Counts, D. J. Arthur, *Inorg. Chim. Acta* **2011**, *373*, 259–261.
- [48] A. Kovacevic, S. Gründemann, J. R. Miecznikowski, E. Clot, O. Eisenstein, R. H. Crabtree, *Chem. Commun.* **2002**, *100*, 2580–2581.
- [49] Robert H. Crabtree, *Pure Appl. Chem.* **2003**, 435–443.
- [50] K. J. Cavell, D. S. McGuinness, *Coord. Chem. Rev.* **2004**, *248*, 671–681.
- [51] F. McLachlan, C. J. Mathews, P. J. Smith, T. Welton, *Organometallics* **2003**, *22*, 5350–5357.
- [52] X. Hu, I. Castro-Rodriguez, K. Meyer, *Organometallics* **2003**, *22*, 3016–3018.

- [53] A. A. Danopoulos, N. Tsoureas, J. A. Wright, M. E. Light, *Organometallics* **2004**, *23*, 166–168.
- [54] D. Bacciu, K. J. Cavell, I. A. Fallis, L.-L. Ooi, *Angew. Chem. Int. Ed.* **2005**, *44*, 5282–5284.
- [55] S. Saha, T. Ghatak, B. Saha, H. Doucet, J. K. Bera, *Organometallics* **2012**, *31*, 5500–5505.
- [56] J. B. Sweeney, *Chem. Soc. Rev.* **2002**, *31*, 247–258.
- [57] *Aziridines and epoxides in organic synthesis*, (Ed.: A. K. Yudin), WILEY-VCH, Weinheim, **2006**.
- [58] C. J. Thibodeaux, W.-c. Chang, H.-w. Liu, *Chem. Rev.* **2012**, *112*, 1681–1709.
- [59] A. Padwa in *Comprehensive Heterocyclic Chemistry III*, Elsevier, **2008**, pp. 1–104.
- [60] J. Xuan, X.-D. Xia, T.-T. Zeng, Z.-J. Feng, J.-R. Chen, L.-Q. Lu, W.-J. Xiao, *Angew. Chem. Int. Ed.* **2014**, *53*, 5653–5656.
- [61] T. Li, X. Xin, C. Wang, D. Wang, F. Wu, X. Li, B. Wan, *Org. Lett.* **2014**, *16*, 4806–4809.
- [62] N. S. Y. Loy, S. Kim, C.-M. Park, *Org. Lett.* **2015**, *17*, 395–397.
- [63] T. Li, F. Xu, X. Li, C. Wang, B. Wan, *Angew. Chem. Int. Ed.* **2016**, *128*, 2911–2915.
- [64] T. W. MILLER, E. W. TRISTRAM, F. J. WOLF, *J. Antibiot.* **1971**, *24*, 48–50.
- [65] C. E. Salomon, D. H. Williams, D. J. Faulkner, *J. Nat. Prod.* **1995**, *58*, 1463–1466.
- [66] T. F. Molinski, C. M. Ireland, *J. Org. Chem.* **1988**, *53*, 2103–2105.
- [67] I. Piskunova, A. Eremeev, A. Mishnev, I. Vosekalna, *Tetrahedron* **1993**, *49*, 4671–4676.
- [68] M.-N. Zhao, W. Zhang, X.-C. Wang, Y. Zhang, D.-S. Yang, Z.-H. Guan, *Org. Biomol. Chem.* **2018**, *16*, 4333–4337.
- [69] K. Banert, *Tetrahedron Lett.* **1985**, *26*, 5261–5264.
- [70] R. A. Abramovitch, M. Konieczny, W. Pennington, S. Kanamathareddy, M. Vedachalam, *J. Chem. Soc. Chem. Commun.* **1990**, 269.
- [71] T. Patonay, J. Jekő, É. Juhász-Tóth, *Eur. J. Org. Chem.* **2008**, *2008*, 1441–1448.
- [72] U. J. Vogelbacher, M. Ledermann, T. Schach, G. Michels, U. Hees, M. Regitz, *Angew. Chem. Int. Ed.* **1988**, *100*, 304–306.
- [73] K. Okamoto, T. Shimbayashi, M. Yoshida, A. Nanya, K. Ohe, *Angew. Chem. Int. Ed.* **2016**, *55*, 7199–7202.
- [74] S. Rieckhoff, M. Titze, W. Frey, R. Peters, *Org. Lett.* **2017**, *19*, 4436–4439.
- [75] A. V. Agafonova, I. A. Smetanin, N. V. Rostovskii, A. F. Khlebnikov, M. S. Novikov, *Chem. Heterocycl. Comp.* **2017**, *53*, 1068–1071.
- [76] N. Rostovskii, A. Agafonova, I. Smetanin, M. Novikov, A. Khlebnikov, J. Ruvinskaya, G. Starova, *Synthesis* **2017**, *28*, 4478–4488.
- [77] K. Okamoto, A. Nanya, A. Eguchi, K. Ohe, *Angew. Chem. Int. Ed.* **2018**, *57*, 1039–1043.
- [78] K. I. Mikhailov, E. E. Galenko, A. V. Galenko, M. S. Novikov, A. Y. Ivanov, G. L. Starova, A. F. Khlebnikov, *J. Org. Chem.* **2018**, *83*, 3177–3187.
- [79] P. A. Sakharov, M. S. Novikov, A. F. Khlebnikov, *J. Org. Chem.* **2018**, *83*, 8304–8314.

6. References

- [80] P. A. Sakharov, A. N. Koronatov, A. F. Khlebnikov, M. S. Novikov, A. G. Glukharev, E. V. Rogacheva, L. A. Kraeva, V. V. Sharoyko, T. B. Tennikova, N. V. Rostovskii, *RSC Adv.* **2019**, *9*, 37901–37905.
- [81] L. Gentilucci, Y. Grijzen, L. Thijs, B. Zwanenburg, *Tetrahedron Lett.* **1995**, *36*, 4665–4668.
- [82] F. A. Davis, G. V. Reddy, H. Liu, *J. Am. Chem. Soc.* **1995**, *117*, 3651–3652.
- [83] F. A. Davis, C.-H. Liang, H. Liu, *J. Org. Chem.* **1997**, *62*, 3796–3797.
- [84] F. A. Davis, H. Liu, C.-H. Liang, G. V. Reddy, Y. Zhang, T. Fang, D. D. Titus, *J. Org. Chem.* **1999**, *64*, 8929–8935.
- [85] F. A. Davis, J. Deng, *Org. Lett.* **2007**, *9*, 1707–1710.
- [86] X. Li, Y. Du, Z. Liang, X. Li, Y. Pan, K. Zhao, *Org. Lett.* **2009**, *11*, 2643–2646.
- [87] X. Duan, X. Kong, X. Zhao, K. Yang, H. Zhou, D. Zhou, Y. Zhang, J. Liu, J. Ma, N. Liu, Z. Wang, *Tetrahedron Lett.* **2016**, *57*, 1446–1450.
- [88] X. Duan, K. Yang, J. Liu, X. Kong, J. Liang, D. Zhou, H. Zhou, Y. Zhang, N. Liu, S. Feng, G. Gu, J. Lu, N. Song, D. Zhang, J. Ma, *Adv. Synth. Catal.* **2016**, *358*, 3161–3166.
- [89] J. Sun, X. Zhen, H. Ge, G. Zhang, X. An, Y. Du, *Beilstein J. Org. Chem.* **2018**, *14*, 1452–1458.
- [90] M. Wang, J. Hou, W. Yu, J. Chang, *J. Org. Chem.* **2018**, *83*, 14954–14961.
- [91] C. Li, J. Yuan, Q. Zhang, C. Bhujanga Rao, R. Zhang, Y. Zhao, B. Deng, D. Dong, *J. Org. Chem.* **2018**, *83*, 14999–15008.
- [92] Y. Zhang, X. Zhao, C. Zhuang, S. Wang, D. Zhang-Negrerie, Y. Du, *Adv. Synth. Catal.* **2018**, *360*, 2107–2112.
- [93] E. Babaoglu, G. Hilt, *Chem. Eur. J.* **2020**, *26*, 8879–8884.
- [94] N. Ramkumar, L. G. Voskressensky, U. K. Sharma, E. V. van der Eycken, *Chem. Heterocycl. Comp.* **2019**, *55*, 795–801.
- [95] F. Wang, N. Zhu, P. Chen, J. Ye, G. Liu, *Angew. Chem. Int. Ed.* **2015**, *54*, 9356–9360.
- [96] Y.-T. He, Q. Wang, J. Zhao, X.-Y. Liu, P.-F. Xu, Y.-M. Liang, *Chem. Commun.* **2015**, *51*, 13209–13212.
- [97] Y.-T. He, Q. Wang, J. Zhao, X.-Z. Wang, Y.-F. Qiu, Y.-C. Yang, J.-Y. Hu, X.-Y. Liu, Y.-M. Liang, *Adv. Synth. Catal.* **2015**, *357*, 3069–3075.
- [98] Q. Meng, F. Chen, W. Yu, B. Han, *Org. Lett.* **2017**, *19*, 5186–5189.
- [99] F. Palacios, A. M. O. de Retana, E. M. de Marigorta, J. M. de los Santos, *Eur. J. Org. Chem.* **2001**, 2401–2414.
- [100] M. M. H. Verstappen, G. J. A. Ariaans, B. Zwanenburg, *J. Am. Chem. Soc.* **1996**, *118*, 8491–8492.
- [101] S. Sakamoto, T. Inokuma, Y. Takemoto, *Org. Lett.* **2011**, *13*, 6374–6377.
- [102] H. Hu, Y. Liu, L. Lin, Y. Zhang, X. Liu, X. Feng, *Angew. Chem. Int. Ed.* **2016**, *128*, 10252–10255.
- [103] M. Chavarot, S. Ménage, O. Hamelin, F. Charnay, J. Pécaut, M. Fontecave, *Inorg. Chem.* **2003**, *42*, 4810–4816.
- [104] L. Zhang, E. Meggers, *Chem. - Asian J.* **2017**, *12*, 2335–2342.

- [105] S.-Y. Yao, X.-Y. Chen, Y.-L. Ou, B.-H. Ye, *Inorg. Chem.* **2017**, *56*, 878–885.
- [106] L. Zhang, E. Meggers, *Acc. Chem. Res.* **2017**, *50*, 320–330.
- [107] M. Carmona, R. Rodríguez, V. Passarelli, F. J. Lahoz, P. García-Orduña, D. Carmona, *J. Am. Chem. Soc.* **2018**, *140*, 912–915.
- [108] S.-W. Li, Q. Wan, Q. Kang, *Org. Lett.* **2018**, *20*, 1312–1315.
- [109] M. Carmona, R. Rodríguez, V. Passarelli, D. Carmona, *Organometallics* **2019**, *38*, 988–995.
- [110] L.-P. Li, H.-L. Peng, L.-Q. Wei, B.-H. Ye, *Inorg. Chem.* **2019**, *58*, 785–793.
- [111] L.-P. Li, H.-L. Peng, B.-H. Ye, *Inorg. Chem.* **2019**, *58*, 12245–12253.
- [112] L. Hu, S. Lin, S. Li, Q. Kang, Y. Du, *ChemCatChem* **2020**, *12*, 118–121.
- [113] Q. Wan, L. Chen, S. Li, Q. Kang, Y. Yuan, Y. Du, *Org. Lett.* **2020**, *22*, 9539–9544.
- [114] Y. Zheng, Y. Tan, K. Harms, M. Marsch, R. Riedel, L. Zhang, E. Meggers, *J. Am. Chem. Soc.* **2017**, *139*, 4322–4325.
- [115] S. Chen, Y. Zheng, T. Cui, E. Meggers, K. N. Houk, *J. Am. Chem. Soc.* **2018**, *140*, 5146–5152.
- [116] T. Cui, J. Qin, K. Harms, E. Meggers, *Eur. J. Inorg. Chem.* **2019**, *2019*, 195–198.
- [117] Z. Zhou, S. Chen, J. Qin, X. Nie, X. Zheng, K. Harms, R. Riedel, K. N. Houk, E. Meggers, *Angew. Chem. Int. Ed.* **2019**, *58*, 1088–1093.
- [118] Z. Zhou, Y. Tan, T. Yamahira, S. Ivlev, X. Xie, R. Riedel, M. Hemming, M. Kimura, E. Meggers, *Chem* **2020**, *6*, 2024–2034.
- [119] Z. Zhou, S. Chen, Y. Hong, E. Winterling, Y. Tan, M. Hemming, K. Harms, K. N. Houk, E. Meggers, *J. Am. Chem. Soc.* **2019**, *141*, 19048–19057.
- [120] S. Y. Hong, Y. Park, Y. Hwang, Y. B. Kim, M.-H. Baik, S. Chang, *Science* **2018**, *359*, 1016–1021.
- [121] J. Qin, Z. Zhou, T. Cui, M. Hemming, E. Meggers, *Chem. Sci.* **2019**, *10*, 3202–3207.
- [122] S. Gründemann, M. Albrecht, A. Kovacevic, J. W. Faller, R. H. Crabtree, *J. Chem. Soc. Dalton Trans.* **2002**, 2163–2167.
- [123] C. Janiak, *J. Chem. Soc. Dalton Trans.* **2000**, 3885–3896.
- [124] K. Harms, E. Winterling, E. Meggers, CCDC 2069775: Experimental Crystal Structure Determination, **2021**.
- [125] D. Cuperly, P. Gros, Y. Fort, *J. Org. Chem.* **2002**, *67*, 238–241.
- [126] E. Winterling, K. Harms, E. Meggers, CCDC 2106464: Experimental Crystal Structure Determination, **2021**.
- [127] E. Winterling, K. Harms, E. Meggers, CCDC 2106463: Experimental Crystal Structure Determination, **2021**.
- [128] K. S. Bejoymohandas, A. Kumar, S. Varughese, E. Varathan, V. Subramanian, M. L. P. Reddy, *J. Mater. Chem. C* **2015**, *3*, 7405–7420.
- [129] T. Mietke, T. Cruchter, E. Winterling, M. Tripp, K. Harms, E. Meggers, *Chem. Eur. J.* **2017**, *23*, 12363–12371.

- [130] D. S. Surry, S. L. Buchwald, *Chem. Sci.* **2011**, *2*, 27–50.
- [131] C. L. McMullin, B. Rühle, M. Besora, A. G. Orpen, J. N. Harvey, N. Fey, *J. Mol. Catal. A Chem* **2010**, *324*, 48–55.
- [132] B. T. Ingoglia, S. L. Buchwald, *Org. Lett.* **2017**, *19*, 2853–2856.
- [133] L. Bernet, R. Lalrempuia, W. Ghattas, H. Mueller-Bunz, L. Vigara, A. Llobet, M. Albrecht, *Chem. Commun.* **2011**, *47*, 8058–8060.
- [134] E. Winterling, S. I. Ivlev, E. Meggers, CCDC 2088021: Experimental Crystal Structure Determination, **2021**.
- [135] Y. Grell, N. Demirel, K. Harms, E. Meggers, *Organometallics* **2019**, *38*, 3852–3859.
- [136] M. Helms, Auxiliärvermittelte Synthese enantiomerenreiner, cyclometallierter Iridium(III)- und Rhodium(III)-Komplexe, **2016**.
- [137] F. A. Davis, Y. Zhang, Y. Andemichael, T. Fang, D. L. Fanelli, H. Zhang, *J. Org. Chem.* **1999**, *64*, 1403–1406.
- [138] M. Steurer, C. Bolm, *J. Org. Chem.* **2010**, *75*, 3301–3310.
- [139] H. D. Flack, *Acta Crystallogr A Found Crystallogr* **1983**, *39*, 876–881.
- [140] A. Granados, A. D. Olmo, F. Peccati, T. Billard, M. Sodupe, A. Vallribera, *J. Org. Chem.* **2018**, *83*, 303–313.
- [141] T. Hellmuth, W. Frey, R. Peters, *Angew. Chem. Int. Ed.* **2015**, *54*, 2788–2791.
- [142] C. Wang, L.-A. Chen, H. Huo, X. Shen, K. Harms, L. Gong, E. Meggers, *Chem. Sci.* **2015**, *6*, 1094–1100.
- [143] S. Horiuchi, H. Tanaka, E. Sakuda, Y. Arikawa, K. Umakoshi, *Chem. Eur. J.* **2016**, *22*, 17533–17537.
- [144] L. Li, F. Han, X. Nie, Y. Hong, S. Ivlev, E. Meggers, *Angew. Chem. Int. Ed.* **2020**, 12392–12395.
- [145] X. Nie, Z. Yan, S. Ivlev, E. Meggers, *J. Org. Chem.* **2020**, *86*, 750–761.
- [146] Y. Tan, F. Han, M. Hemming, J. Wang, K. Harms, X. Xie, E. Meggers, *Org. Lett.* **2020**, DOI 10.1021/acs.orglett.0c02452.
- [147] Y. Nishibayashi, I. Wakiji, M. Hidai, *J. Am. Chem. Soc.* **2000**, *122*, 11019–11020.
- [148] Y. Nishibayashi, H. Imajima, G. Onodera, M. Hidai, S. Uemura, *Organometallics* **2004**, *23*, 26–30.
- [149] G. Hattori, H. Matsuzawa, Y. Miyake, Y. Nishibayashi, *Angew. Chem. Int. Ed.* **2008**, *47*, 3781–3783.
- [150] R. J. Detz, M. M. E. Delville, H. Hiemstra, J. H. van Maarseveen, *Angew. Chem. Int. Ed.* **2008**, *47*, 3777–3780.
- [151] G. Hattori, K. Sakata, H. Matsuzawa, Y. Tanabe, Y. Miyake, Y. Nishibayashi, *J. Am. Chem. Soc.* **2010**, *132*, 10592–10608.
- [152] R. J. Detz, Z. Abiri, R. Le Griel, H. Hiemstra, J. H. van Maarseveen, *Chem. Eur. J.* **2011**, *17*, 5921–5930.
- [153] S. Kawanishi, S. Oki, D. Kundu, S. Akai, *Org. Lett.* **2019**, *21*, 2978–2982.
- [154] X. Huang, T. R. Quinn, K. Harms, R. D. Webster, L. Zhang, O. Wiest, E. Meggers, *J. Am. Chem. Soc.* **2017**, *139*, 9120–9123.

- [155] J. A. Woods, R. Lalrempuia, A. Petronilho, N. D. McDaniel, H. Müller-Bunz, M. Albrecht, S. Bernhard, *Energy Environ. Sci.* **2014**, *7*, 2316–2328.
- [156] Á. Vivancos, M. Beller, M. Albrecht, *ACS Catal.* **2018**, *8*, 17–21.
- [157] S. C. Sau, P. K. Hota, S. K. Mandal, M. Soleilhavoup, G. Bertrand, *Chem. Soc. Rev.* **2020**, *49*, 1233–1252.
- [158] J. Liu, J. Chen, J. Zhao, Y. Zhao, L. Li, H. Zhang, *Synthesis* **2003**, 2661–2666.
- [159] S. Suravajjala, J. R. Polam, L. C. Porter, *J. Organomet. Chem.* **1993**, *461*, 201–205.
- [160] G. R. Fulmer, A. J. M. Miller, N. H. Sherden, H. E. Gottlieb, A. Nudelman, B. M. Stoltz, J. E. Bercaw, K. I. Goldberg, *Organometallics* **2010**, *29*, 2176–2179.
- [161] Y. Hong, L. Jarrige, K. Harms, E. Meggers, *J. Am. Chem. Soc.* **2019**, *141*, 4569–4572.
- [162] A. F. Stange, S. Tokura, M. Kira, *J. Organomet. Chem.* **2000**, *612*, 117–124.
- [163] J. L. García Ruano, J. Alemán, C. Fajardo, A. Parra, *Org. Lett.* **2005**, *7*, 5493–5496.
- [164] K. Tsuchida, M. Yuki, K. Nakajima, Y. Nishibayashi, *Chem. Lett.* **2018**, *47*, 671–673.
- [165] X.-C. Hang, W.-P. Gu, Q.-Y. Chen, J.-C. Xiao, *Tetrahedron* **2009**, *65*, 6320–6324.
- [166] K. Tsuchida, Y. Senda, K. Nakajima, Y. Nishibayashi, *Angew. Chem. Int. Ed.* **2016**, *55*, 9728–9732.
- [167] X-Area Pilatus3_SV, Darmstadt, Germany, **2016**.
- [168] X-Area LANA, Darmstadt, Germany, **2016**.
- [169] XT V2014/1, Madison, Wisconsin, USA, **2014**.
- [170] X-Area Recipe, Darmstadt, Germany, **2015**.
- [171] X-Area Integrate, Darmstadt, Germany, **2016**.
- [172] G. M. Sheldrick, *Acta Crystallogr. Sect. A: Found. Adv.* **2015**, *71*, 3–8.
- [173] G. M. Sheldrick, *Acta Crystallogr. Sect. C: Struct. Chem.* **2015**, *71*, 3–8.
- [174] K. Brandenburg, Diamond - Crystal and Molecular Structure Visualization, Bonn, Germany, **2014**.
- [175] C. B. Hübschle, G. M. Sheldrick, B. Dittrich, *J. Appl. Crystallogr.* **2011**, *44*, 1281–1284.
- [176] X-Area, Darmstadt, Germany, **2018**.
- [177] LANA - Laue Analyzer, Darmstadt, Germany, **2019**.
- [178] X-RED32, Darmstadt, Germany, **2018**.
- [179] APEX3, Madison, Wisconsin, USA, **2018**.
- [180] SADABS, Madison, Wisconsin, USA, **2016**.
- [181] L. Krause, R. Herbst-Irmer, G. M. Sheldrick, D. Stalke, *J. Appl. Crystallogr.* **2015**, *48*, 3–10.
- [182] D. Kratzert, I. Krossing, *J. Appl. Crystallogr.* **2018**, *51*, 928–934.

A. Appendix

A.1. List of Synthesized Compounds

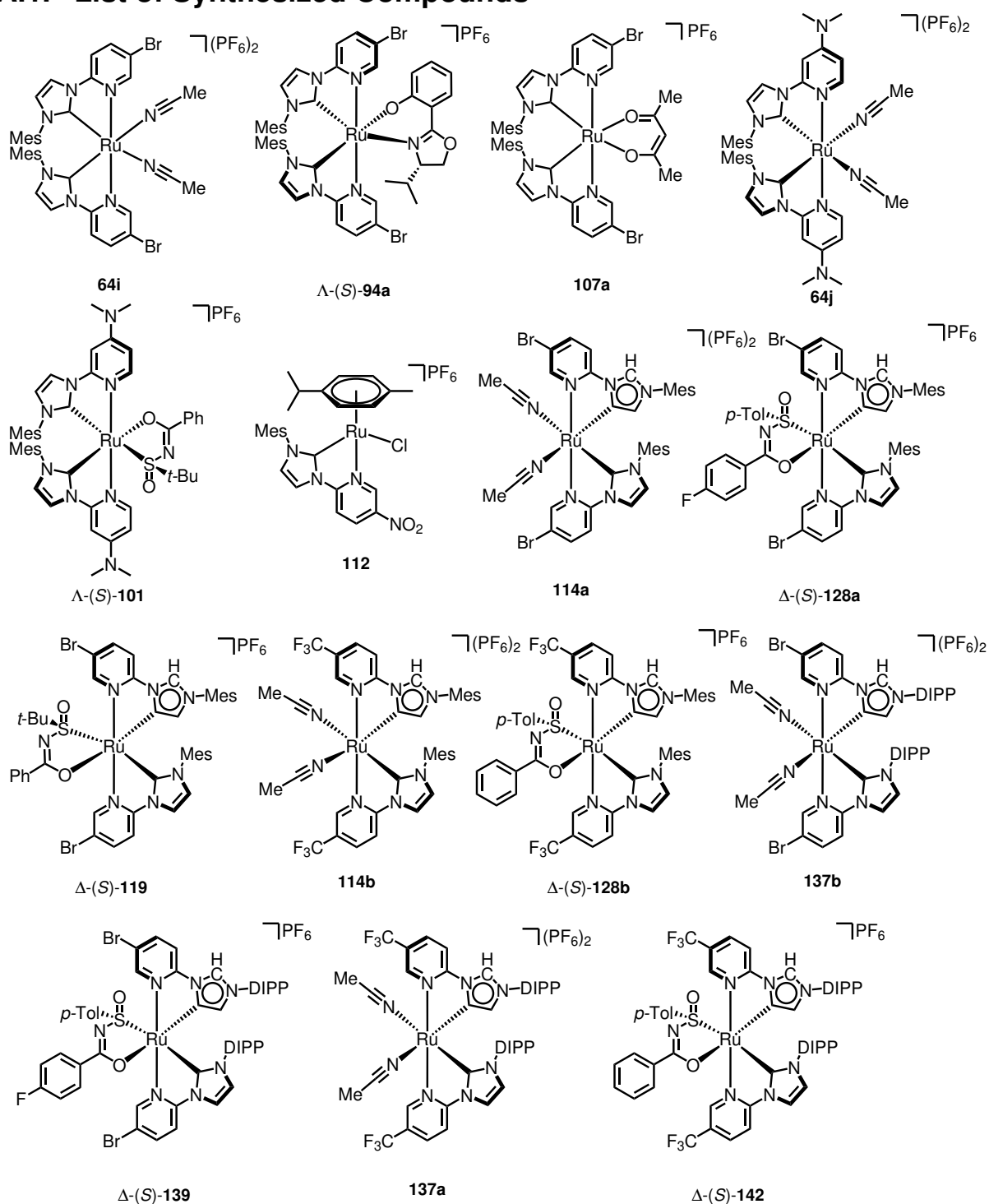


Figure 35: List of synthesized ruthenium complexes.

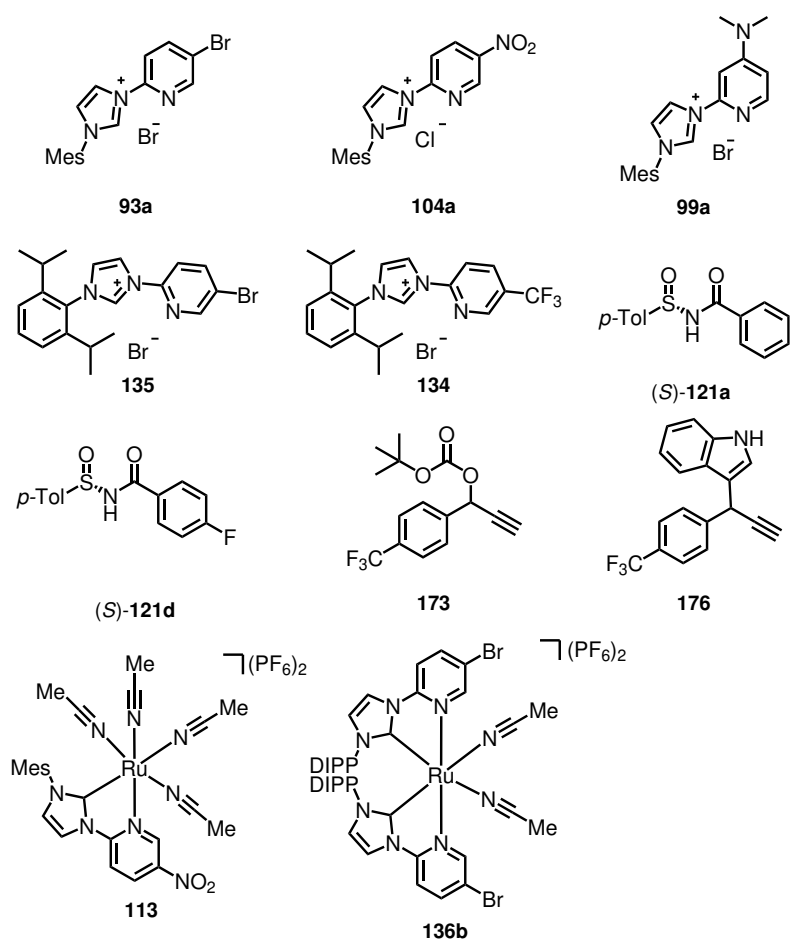


Figure 36: List of synthesized ruthenium complexes, imidazolium salts, auxiliaries and propargylic substrates.

A.2. NMR Yield Calculation

Assignment of key signals as reported in Table 7.

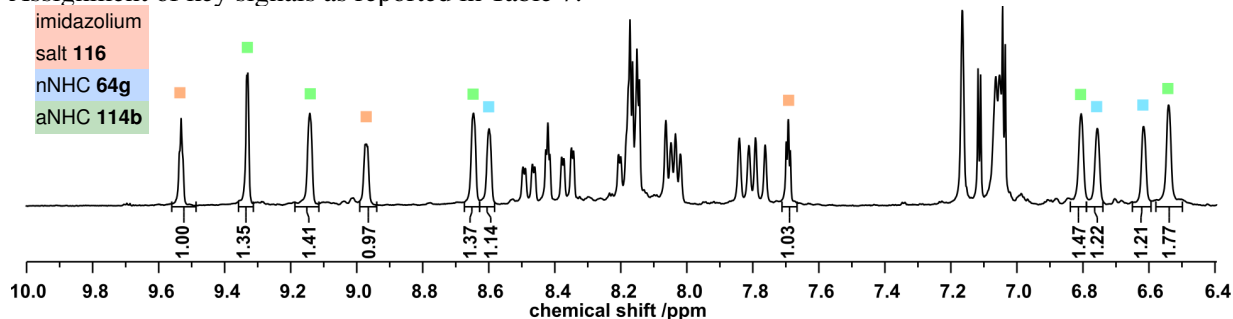


Figure 37: ^1H -NMR of a crude mixture of unreacted imidazolium salt **116**, nNHC **64g** and aNHC **114b**. Key signals are assigned to corresponding compound. For a more detailed assignment, see Figure 38.

NMR yield calculations shown in Table 7 in chapter 3.1.3 are based on imidazolium salt equivalents using the formula 1. The given parameters are Int_i as integral from the NMR of substance i , H_i as a scaling factor ($H = 1$ for imidazolium salt **116** and aNHC **114b**, $H = 2$ for nNHC **64g** due to its C_2 -symmetry).

$$NMR\ Yield_i = \frac{Int_i/H_i}{\sum(Int_n/H_n)} \quad (1)$$

An exemplary calculation for Table 7 entry 2, the arithmetic mean of integrals as shown in Figure 37 for individual compounds was used:

$$\begin{aligned} NMR\ Yield_{aNHC} &= \frac{Int_{aNHC}/H_{aNHC}}{(Int_{aNHC}/H_{aNHC}) + (Int_{nNHC}/H_{nNHC}) + (Int_{imidazolium\ salt}/H_{imidazolium\ salt})} \\ &= \frac{1.47/1}{(1.53/1) + (1.19/2) + (1/1)} \\ &= 0.480 \hat{=} 48.0\% \end{aligned}$$

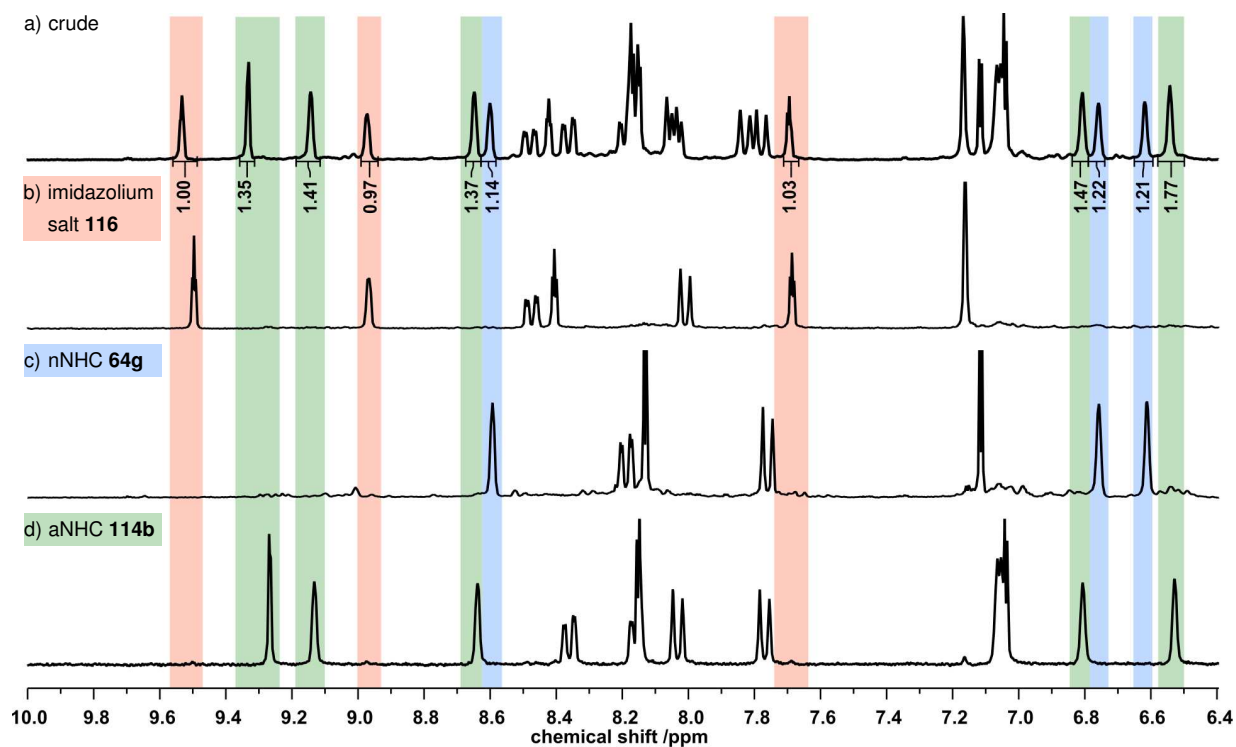


Figure 38: a) NMR spectrum of crude reaction mixture used for NMR yield calculation of Table 7, entry 2. NMR spectra of each individual species are given and clear assignment of key signals are indicated by individual color.

NMR spectrum of the compound obtained during the synthesis of complex **64j** as reported in chapter 3.1.2.

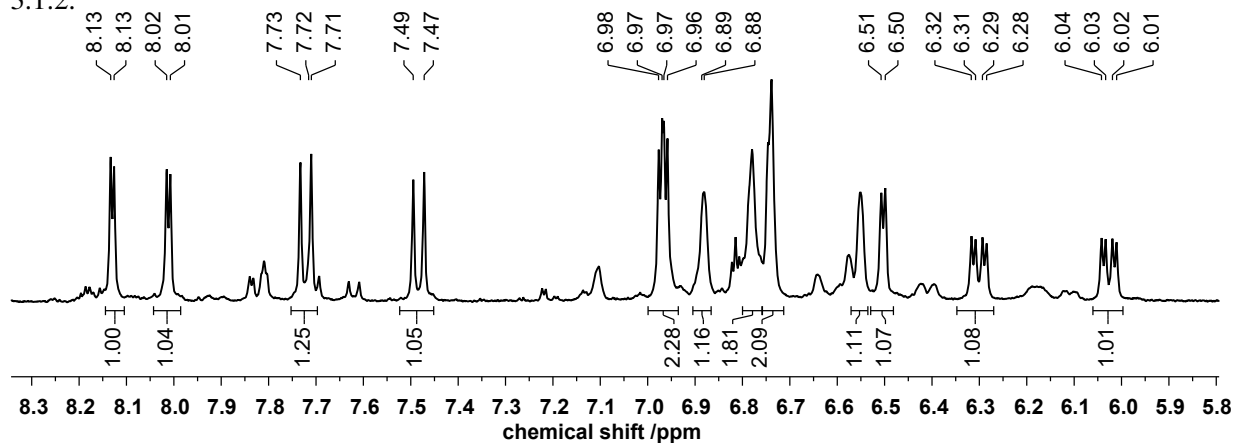


Figure 39: ¹H-NMR spectrum of the unknown compound and the impurities recorded in CD₂Cl₂.

A.3. Late Stage Transition Metal Catalyzed Cross Coupling

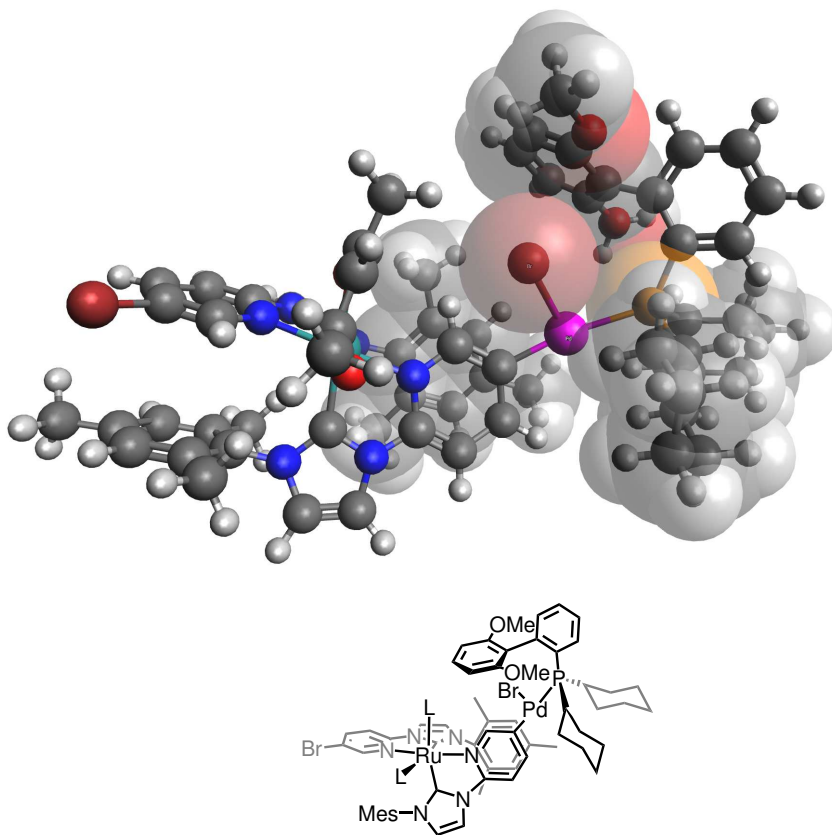


Figure 40: *Top:* Three dimensional representation of putative intermediate after oxidative addition of palladium into the C–Br bond and coordinated SPhos ligand with added Van der Waals spheres close to the palladium. *Bottom:* ChemDraw representation with the back orientated ligand in grey.

A.4. 2H-Azirine Extended Screening Table

Detailed reaction conditions from chapter 3.2.1 for the ring contraction reaction.

Table 16: Screening Table for Azirination

Entry	cat	cat. loading /mol%	R	T /°C	t /h	solvent	Comment	yield /%	ee /%
1	Λ - 64b	2.5	Me	40	3	DCE		96	8
2	Λ - 149	2.5	Me	40	3	DCE		85	8
3	Λ - 64e	2.5	Me	40	3	DCE		92	41
4	Λ - 64o	2.0	Me	40	3	DCE		94	32
5	Λ - 64i	2.2	Me	40	3	DCE		76	45
6	none	-	Me	40	3	DCE		0	n.d.
7	Λ - 64o	1.0	Me	40	3	DCE		86	36
8	Λ - 64i	1.0	Me	40	3	DCE		87	43
9	Λ - 64i	0.2	Me	40	3	DCE		77	46
10	Λ - 64i	1	<i>i</i> -Pr	40	3	DCE		87	31
11	Λ - 64i	0.5	<i>i</i> -Pr	40	3	DCE		93	32
12	Λ - 64i	1	Me	0	22	DCE		30	2
13	Λ - 64i	0.5	Me	25	4	MeOH		86	61
14	Λ - 64i	0.5	Me	25	4	Acetone		64	16
15	Λ - 64i	0.5	Me	25	4	1,2-DCB		18	41
16	Λ - 64i	0.5	Me	25	4	EtOAc		74	25
17	Λ - 64i	0.5	Me	25	4	MeNO ₂		82	63
18	Λ - 64i	0.5	Me	25	4	HFIP		88	25
19	Λ - 64i	0.5	Me	25	2.5	<i>i</i> -PrOH		87	45
20	Λ - 64i	0.5	Me	25	2.5	DMF		20	35
21	Λ - 64i	0.5	Me	25	2.5	ethandiole		34	54
22	Λ - 64i	0.5	Me	60*	2.5	CH ₃ CN		12	33
23	Λ - 64i	0.5	Me	25	6.5	<i>t</i> -AmOH		46	68
24	Λ - 64i	1	Me	25	3	MeOH	PPh ₃	95	32

Table 16: (continued)

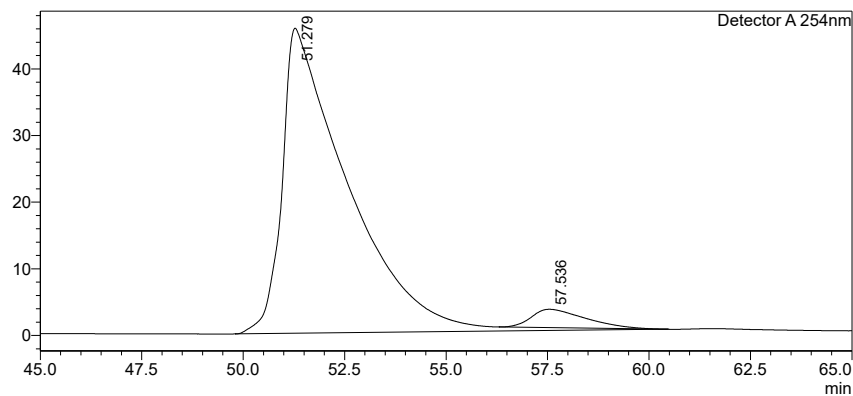
Entry	cat	cat. loading /mol%	R	<i>T</i> /°C	<i>t</i> /h	solvent	Comment	yield /%	<i>ee</i> /%
25	Λ - 64i	0.5	Me	25	3	DCE	PPh ₃	95	30
26	Λ - 64i	1	Me	60*	3	MeOH	PMe ₃	53	30
27	Λ - 64i	1	Me	25	21	DCE	Capsule	48	29
28	Λ - 64i	1	Me	25	5	MeOH	5% H ₂ O	61	48
29	Λ - 64i	1	Me	25	4	MeOH	3.5% imidazole	11	36
30	Λ - 64i	1	Me	25	4	MeOH	3,5% pyrazole	13	25
31	Λ - 64i	1	Me	25	4	MeOH	3.5% 3,5Me ₂ Pyridin- <i>N</i> -Oxide	70	52
32	Λ - 64i	1	Me	25	6	MeOH		90	67
33	Λ - 64i	1	Me	25	2.5	MeOH	+10% product added (45% <i>ee</i>)	90	51
34	Λ - 64i	1	Me	25	6	MeOH	dark	65	67
35	Λ - 64i	0.5	Me	25	6	MeOH	dark	81	61
36	Λ - 64i	0.5	Me	25	6	MeOH	dark	66	53
37	Λ - 64i	1	Me	25	5	MeOH	dark	65	67
38	Λ - 64i	1	Me	25	5	MeOH	dark	69	59
39	Λ - 64i	1	Me	25	5	MeOH	blue LED	n.d.	0
40	Λ - 64i	-	Me	25	5	MeOH	blue LED	n.d.	-

A.5. HPLC Spectra

HPLC spectrum of enantioenriched complex Δ -**114a** obtained as the decomposition product during the column chromatography of auxiliary complex **128a**.

<Chromatogram>

mAU



<Peak Table>

Detector A 254nm

Peak#	Ret. Time	Area	Area%	Name
1	51.279	5195852	95.287	
2	57.536	257011	4.713	
Total		5452863	100.000	

Figure 41: HPLC spectrum of remaining **114a** during column chromatography with of 90.6% *ee*.

Ruthenium Complexes

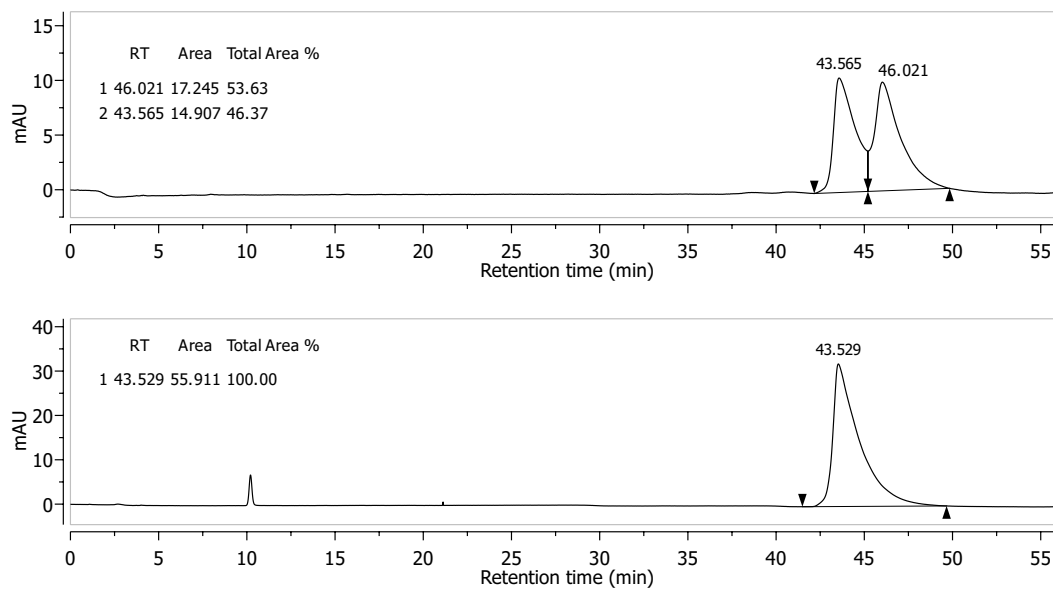


Figure 42: HPLC spectrum of *racemic* (top) complex **64i** and Δ -**64i** (bottom).

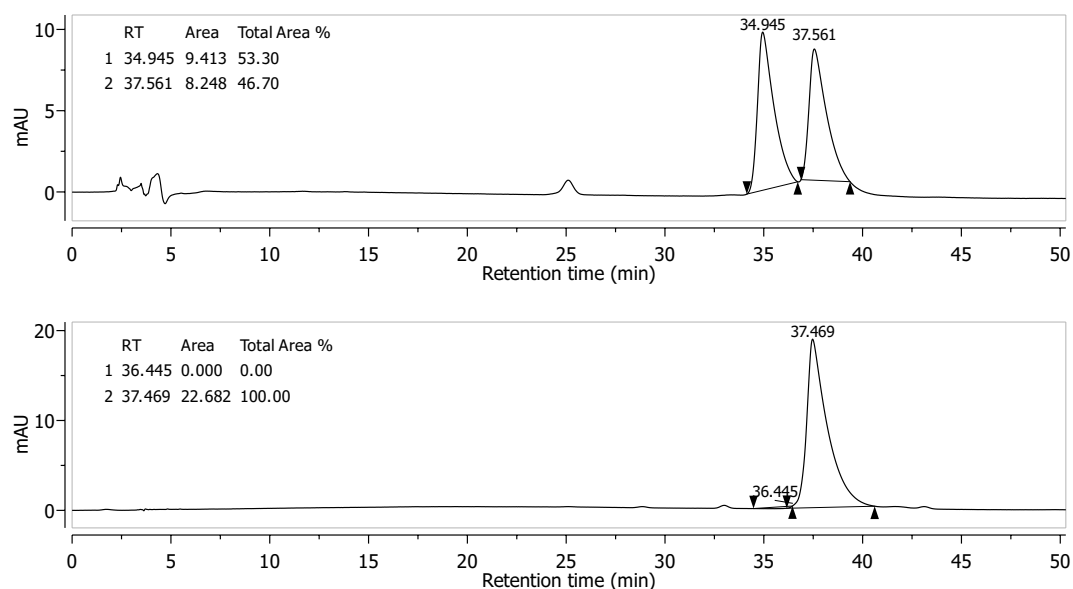


Figure 43: HPLC spectrum of *racemic* (top) complex **114a** and Δ -**114a** (bottom). Chiralpak IB-N5 (250 x 4.6 mm), 1.0 mL min⁻¹, H₂O+0.1% TFA/CH₃CN 70:30 for 15 min, gradient to 63:37 in 55 min, 25 °C, 254 nm.

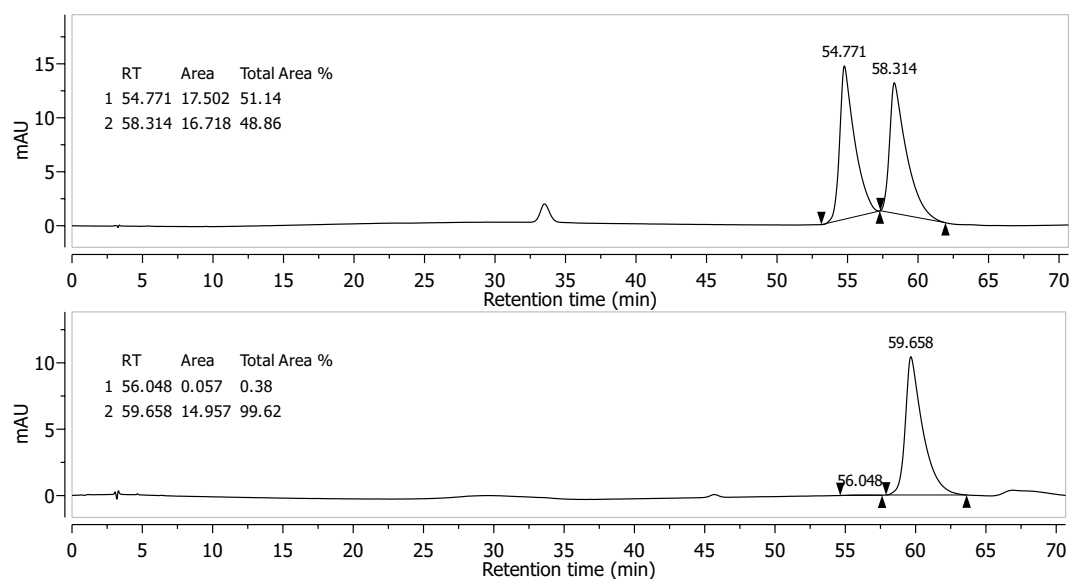


Figure 44: HPLC spectrum of *racemic* (top) complex **114b** and Δ -**114b** (bottom). Chiralpak IB-N5 (250 x 4.6 mm), 1.0 mL min⁻¹, H₂O+0.1% TFA/CH₃CN 70:30 for 15 min, gradient to 63:37 in 55 min, 25 °C, 254 nm.

Auxiliaries

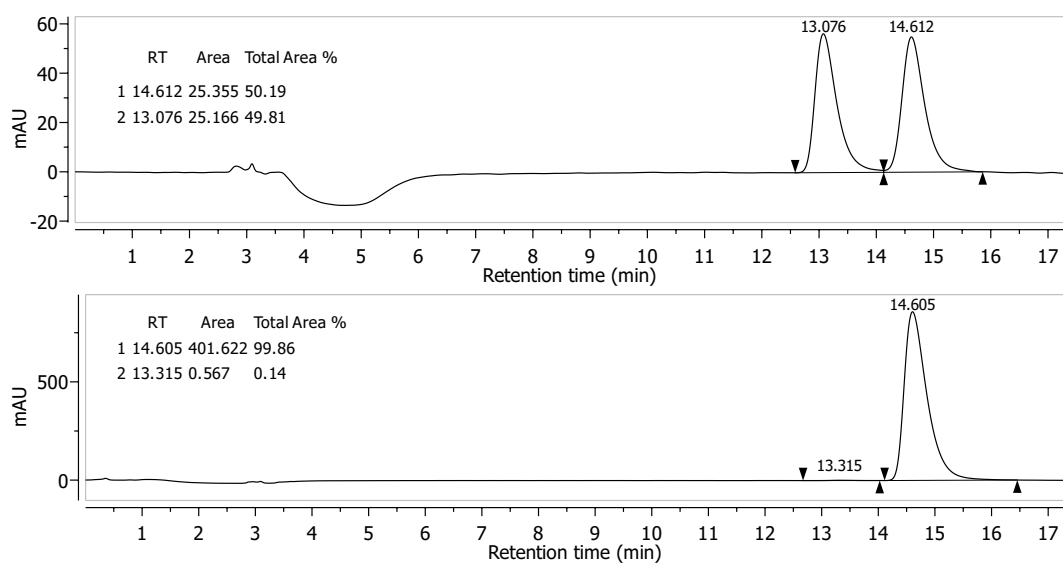
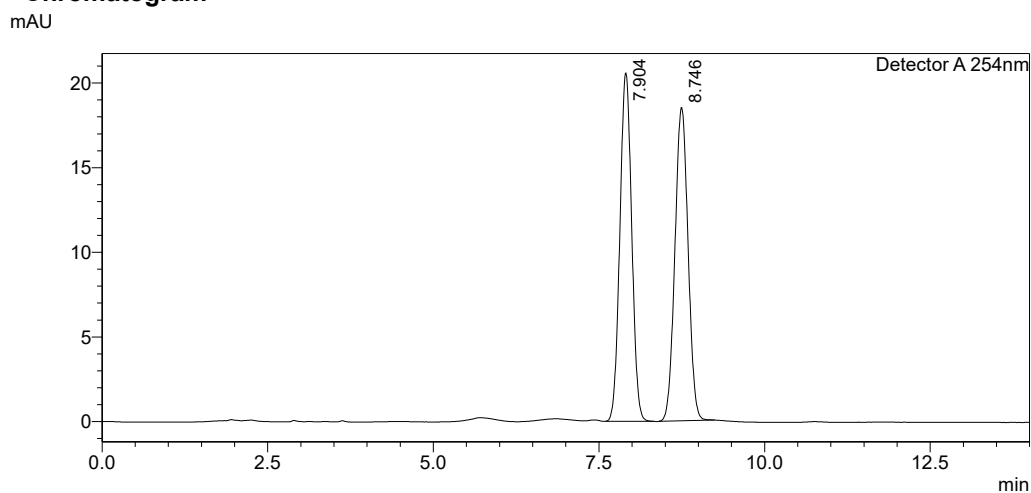


Figure 45: HPLC spectrum of *racemic* (top) sulfinamide **125** and (*S*)-**125** (bottom).

<Chromatogram>



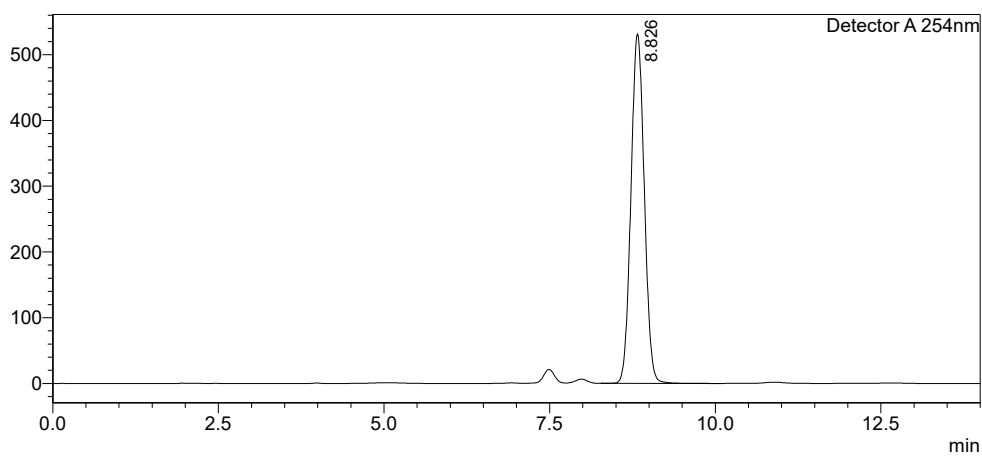
<Peak Table>

Detector A 254nm			
Peak#	Ret. Time	Area	Area%
1	7.904	255354	49.986
2	8.746	255499	50.014
Total		510853	100.000

Figure 46: HPLC spectrum of auxiliary *racemic* **121a**.

<Chromatogram>

mAU

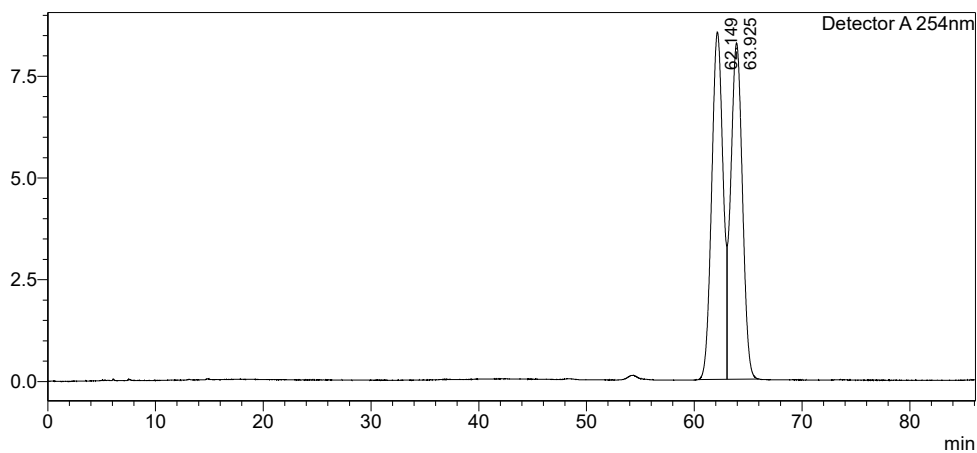
**<Peak Table>**

Detector A 254nm

Peak#	Ret. Time	Area	Area%
1	8.826	7438027	100.000
Total		7438027	100.000

Figure 47: HPLC spectrum of auxiliary (*S*)-121a.**<Chromatogram>**

mAU

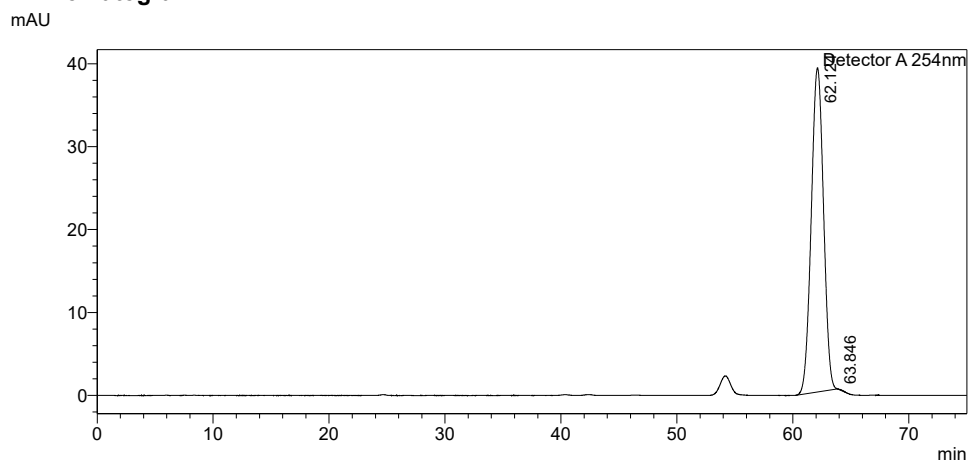
**<Peak Table>**

Detector A 254nm

Peak#	Ret. Time	Area	Height	Conc.	Unit	Mark	Name
1	62.149	626914	8533	0.000			
2	63.925	621909	8258	0.000		V	
Total		1248823	16791				

Figure 48: HPLC spectrum of auxiliary *racemic* 121d.

<Chromatogram>

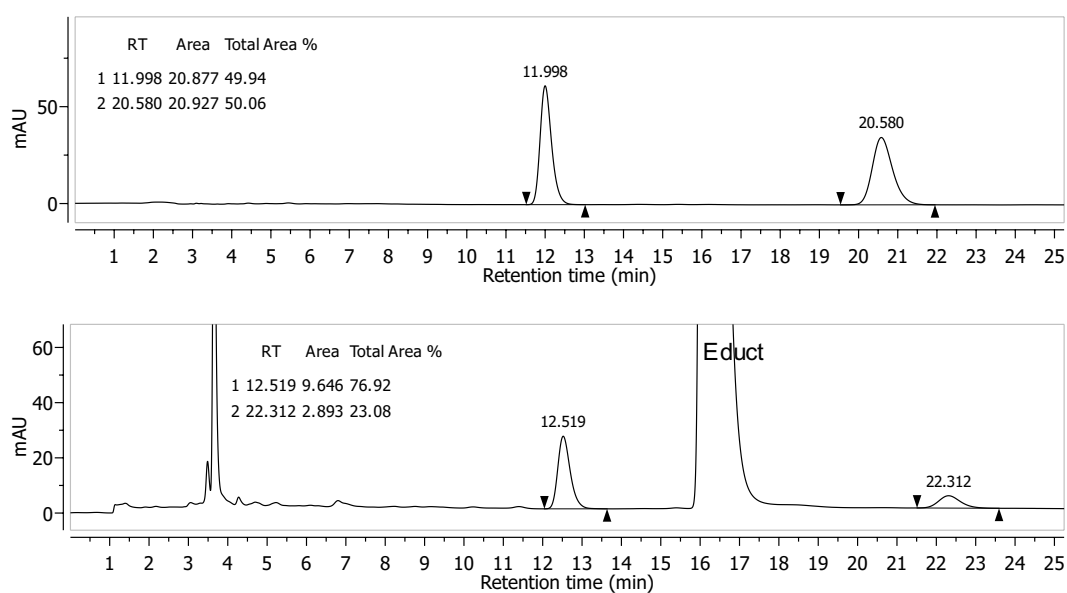


<Peak Table>

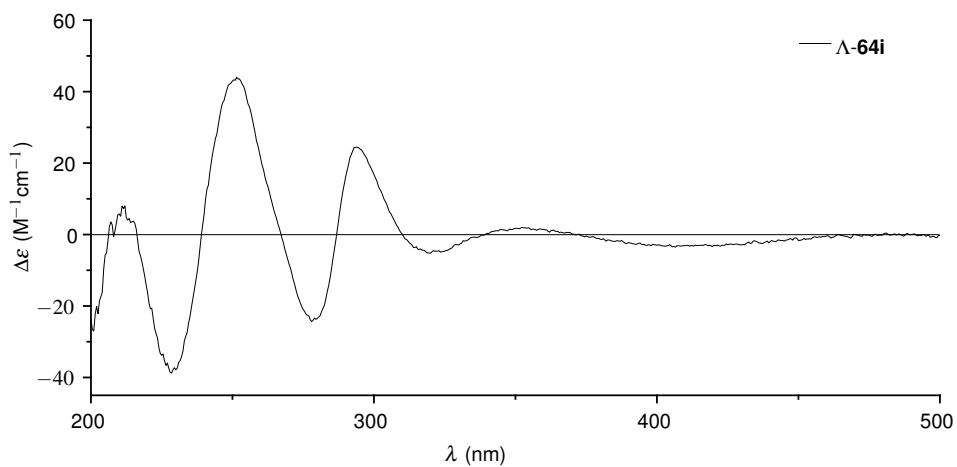
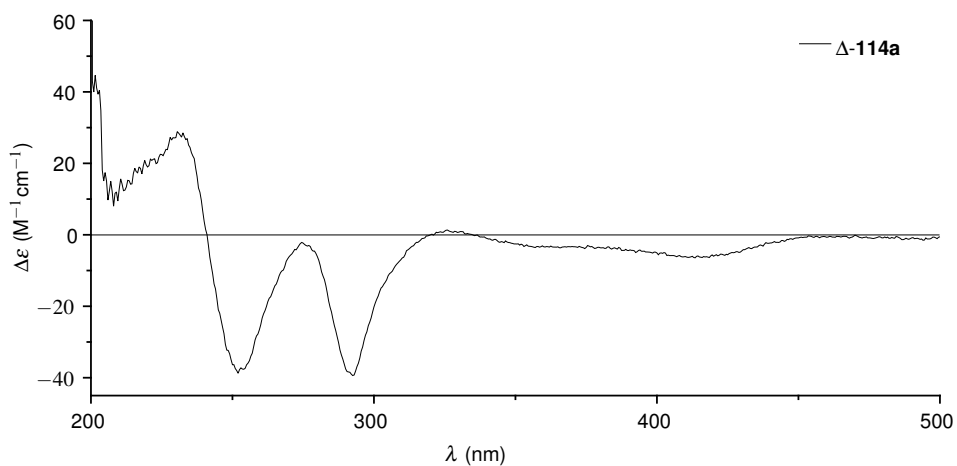
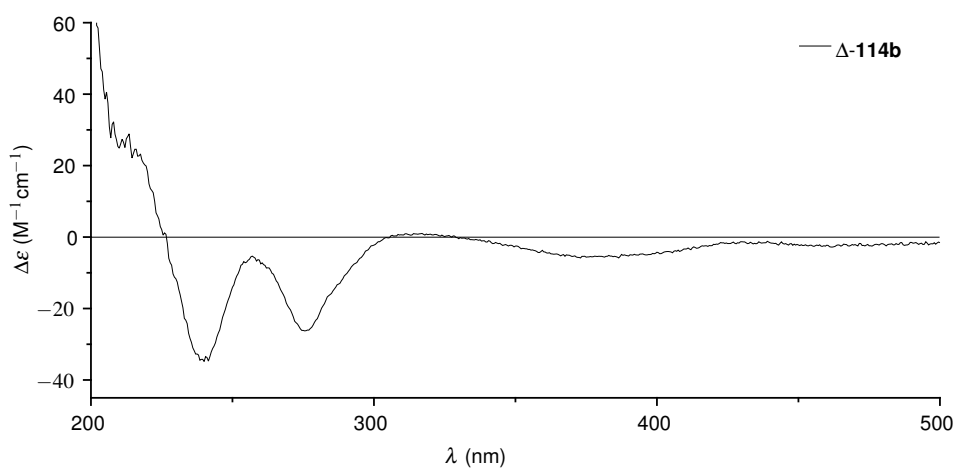
Detector A 254nm			
Peak#	Ret. Time	Area	Area%
1	62.124	2867380	99.931
2	63.846	1991	0.069
Total		2869371	100.000

Figure 49: HPLC spectrum of auxiliary (S)-121d.

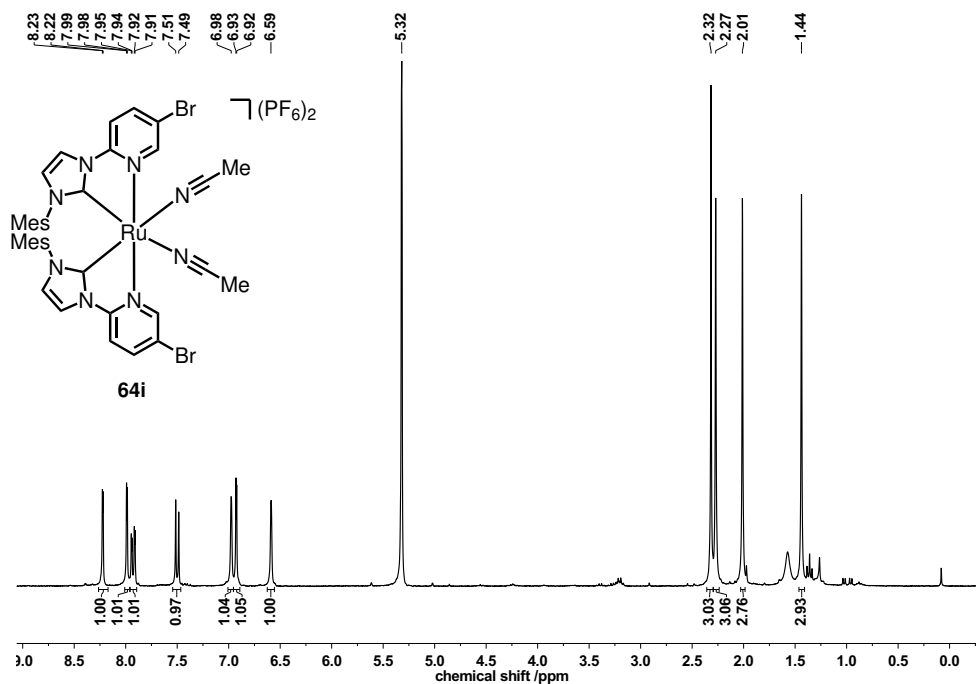
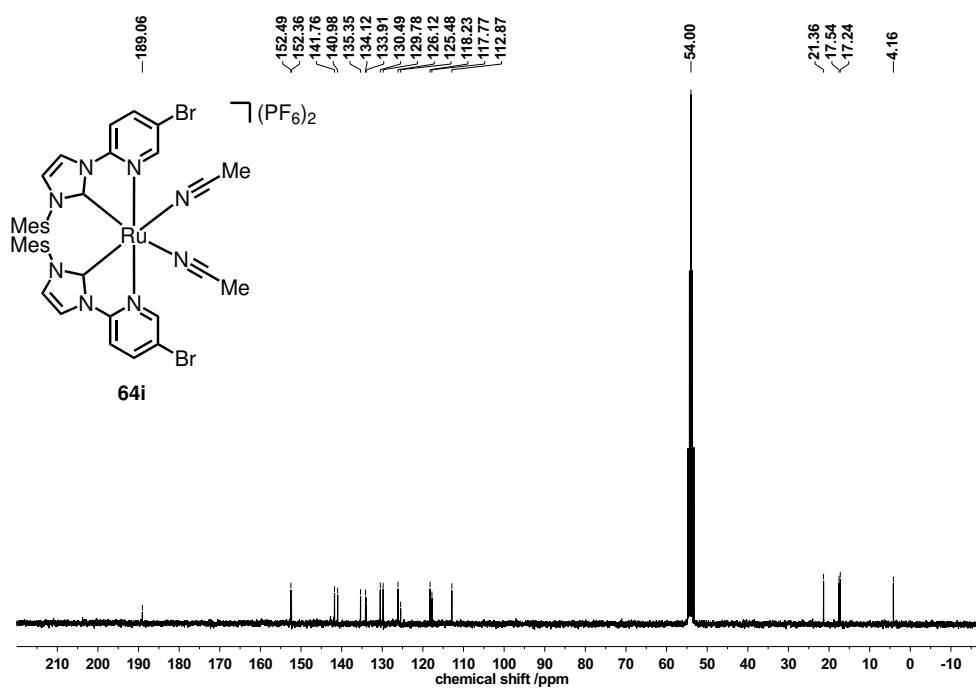
Catalysis Products

Figure 50: HPLC spectrum of *racemic* (top) compound **176** and a crude measurement of enantioenriched **176** (bottom).

A.6. CD-Spectra

Figure 51: CD-spectrum of complex Δ -64i (MeOH, 0.2 mM).Figure 52: CD-spectrum of complex Δ -114a (MeOH, 0.2 mM).Figure 53: CD-spectrum of complex Δ -114b (MeOH, 0.2 mM).

A.7. Representative NMR Spectra

Figure 54: $^1\text{H-NMR}$ spectrum (300 MHz, 300 K) of complex **64i** in CD_2Cl_2 .Figure 55: $^{13}\text{C-NMR}$ spectrum (75 MHz, 300 K) of complex **64i** in CD_2Cl_2 .

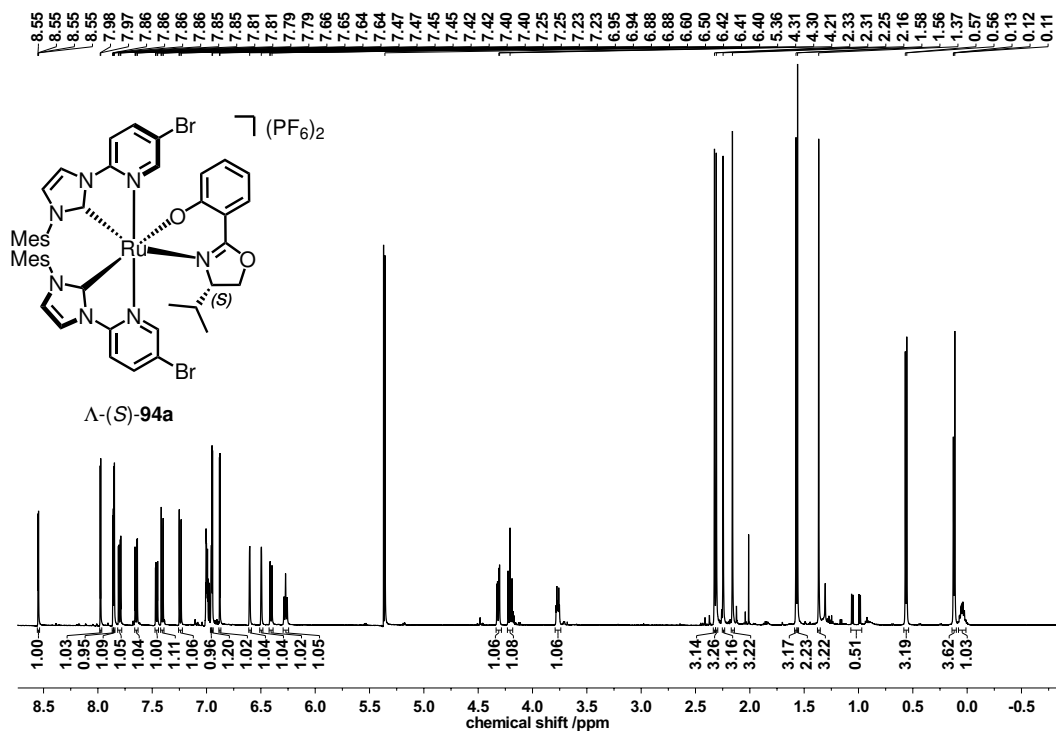


Figure 56: ^1H -NMR spectrum (500 MHz, 300 K) of complex Λ -(S)-94a in CD_2Cl_2 .

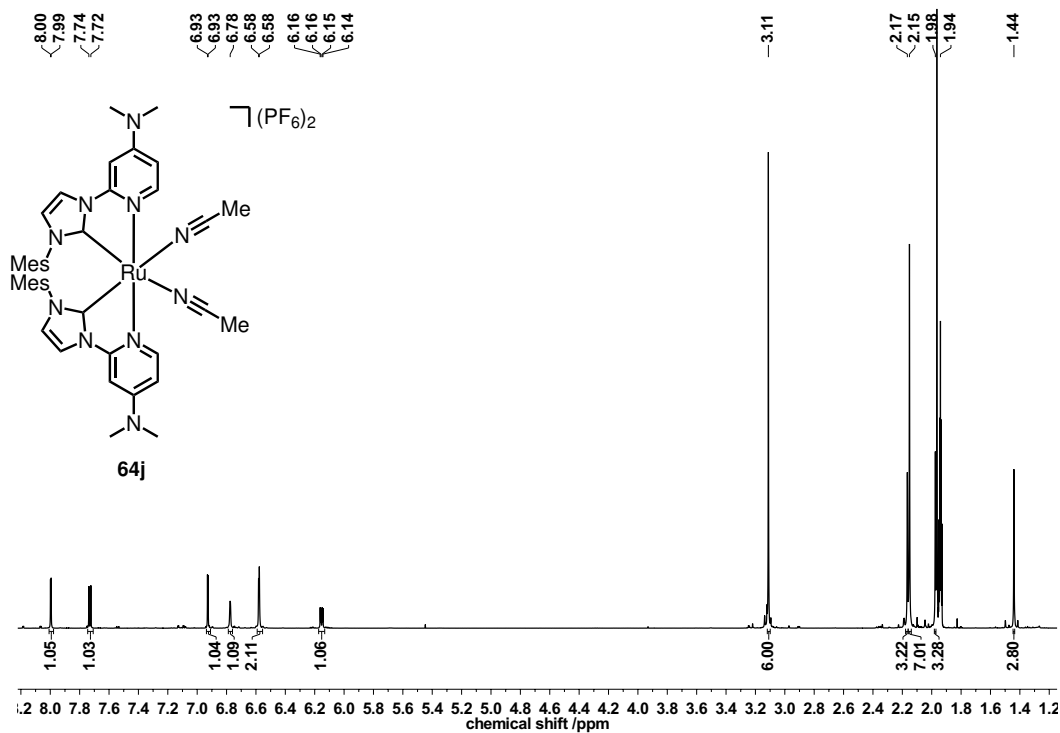


Figure 57: ^1H -NMR spectrum (500 MHz, 300 K) of complex 64j in CD_3CN .

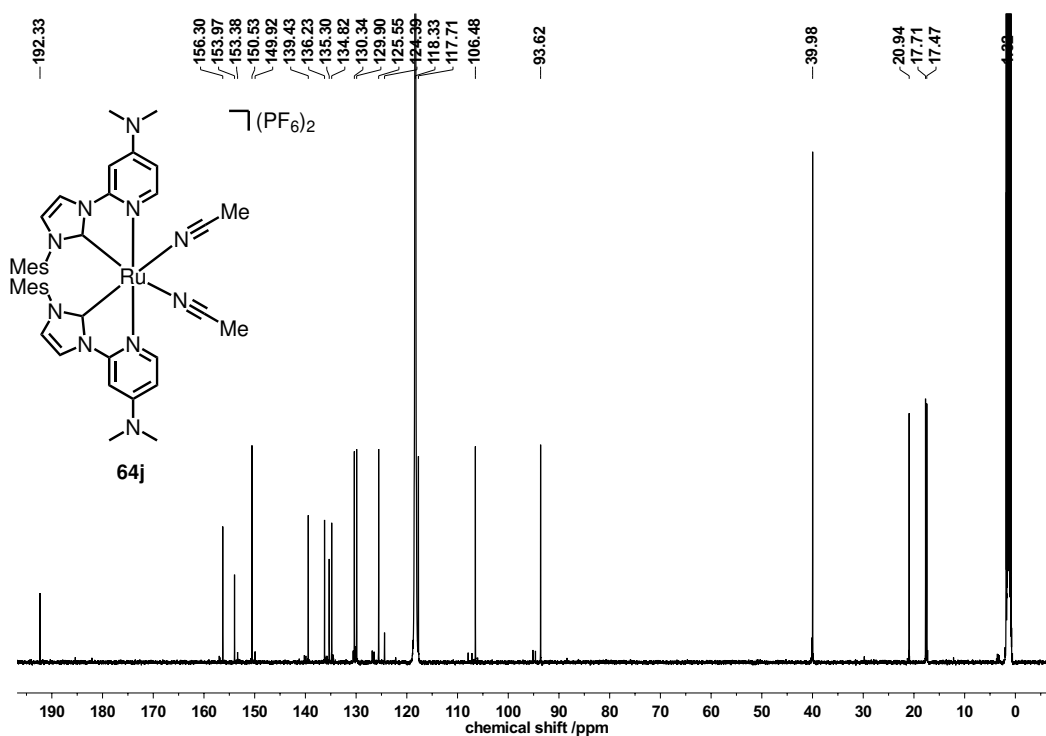


Figure 58: ^{13}C -NMR spectrum (126 MHz, 300 K) of complex **64j** in CD_3CN .

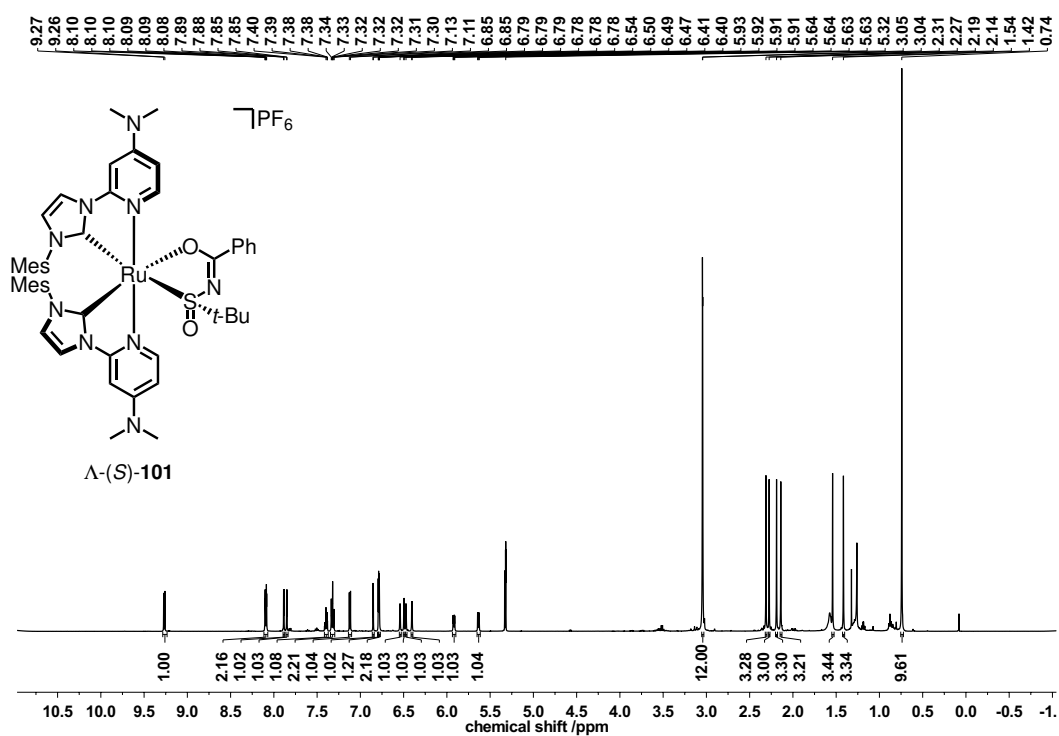


Figure 59: ^1H -NMR spectrum (500 MHz, 300 K) of complex Λ -(*S*)-**101** in CD_2Cl_2 .

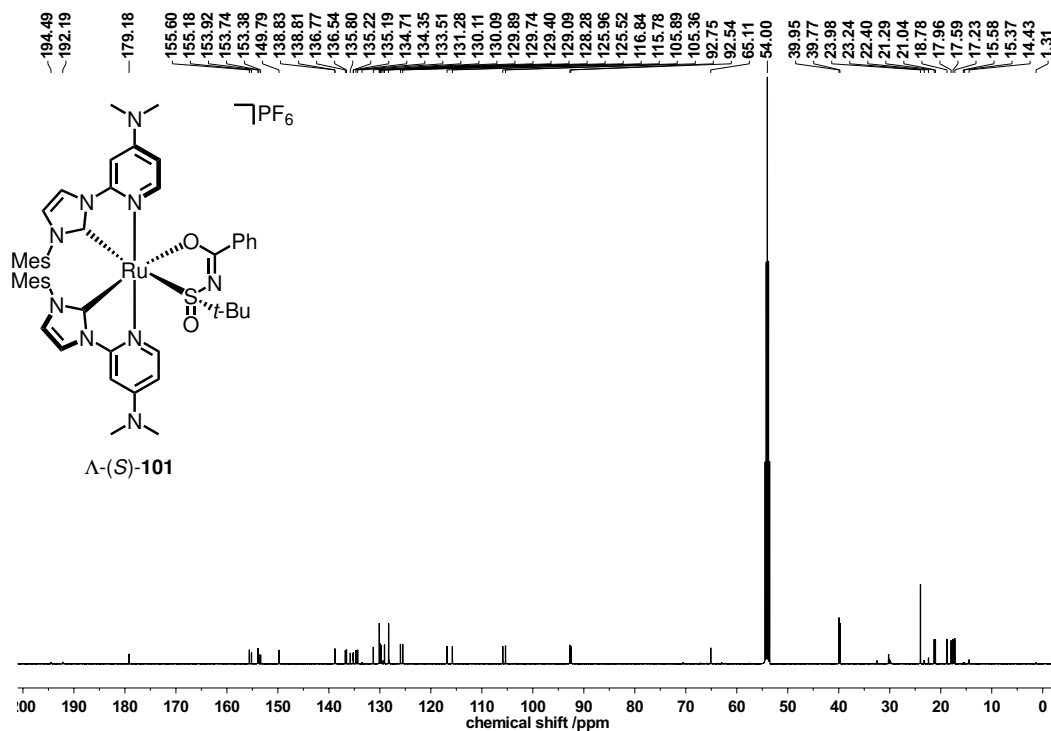


Figure 60: ^{13}C -NMR spectrum (126 MHz, 300 K) of complex Λ -(S)-101 in CD_2Cl_2 .

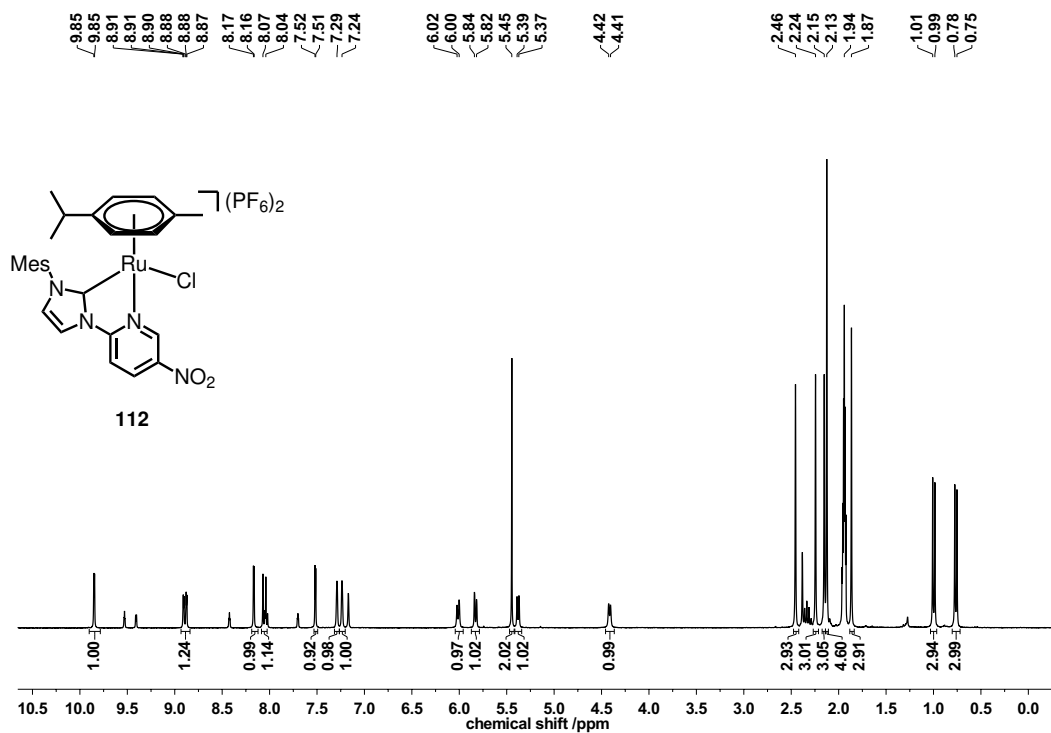


Figure 61: ^1H -NMR spectrum (300 MHz, 300 K) of complex 112 in CD_2Cl_2 .

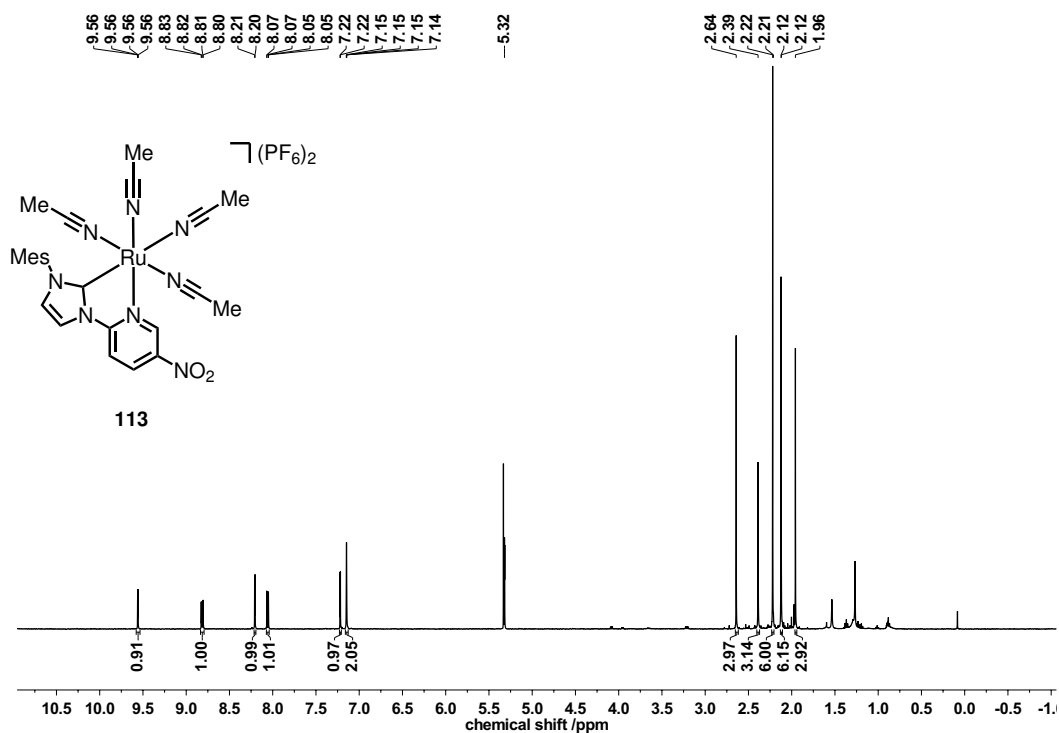


Figure 62: $^1\text{H-NMR}$ spectrum (500 MHz, 300 K) of complex **113** in CD_2Cl_2 .

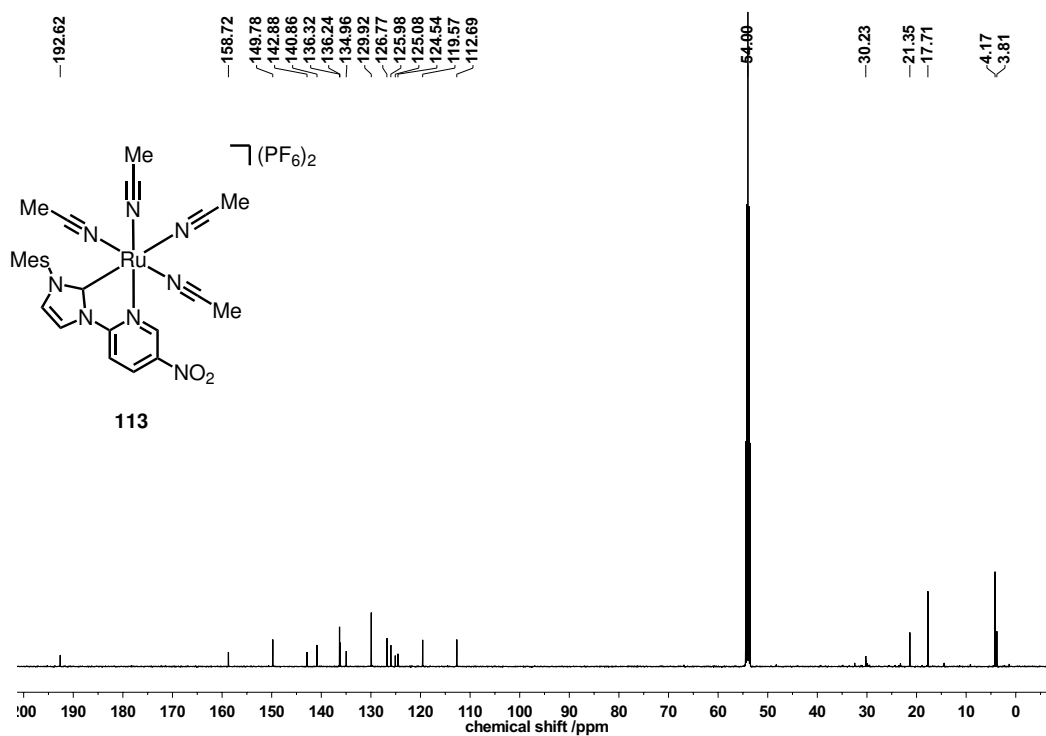


Figure 63: $^{13}\text{C-NMR}$ spectrum (126 MHz, 300 K) of complex **113** in CD_2Cl_2 .

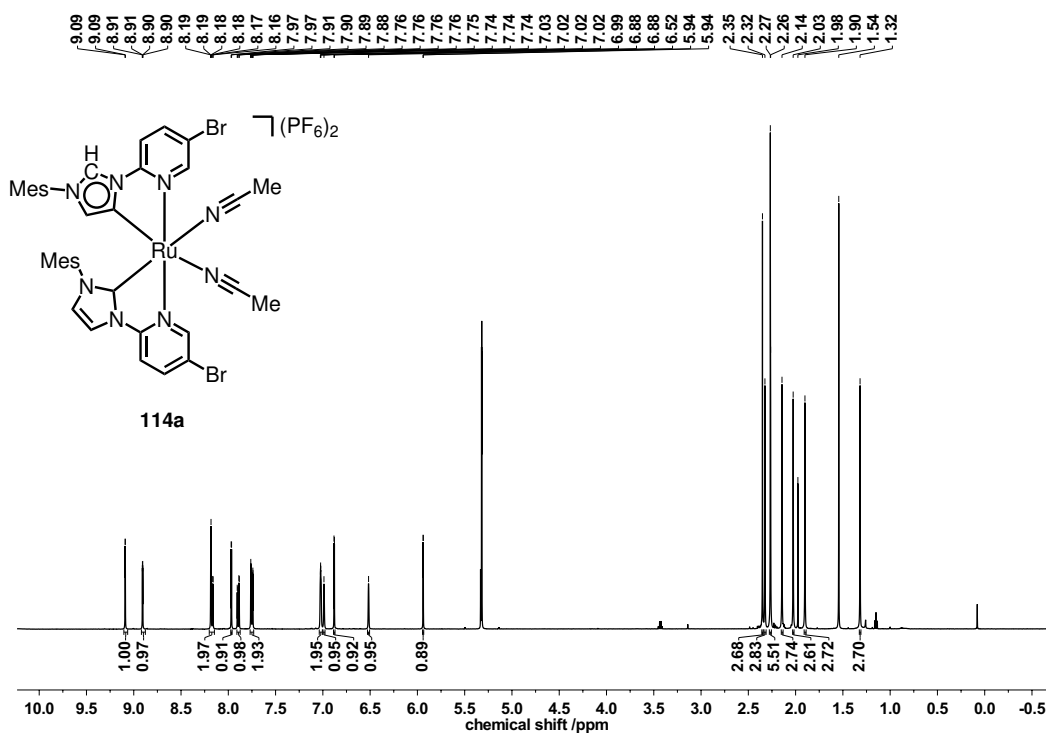


Figure 66: $^1\text{H-NMR}$ spectrum (500 MHz, 300 K) of complex **114a** in CD_2Cl_2 .

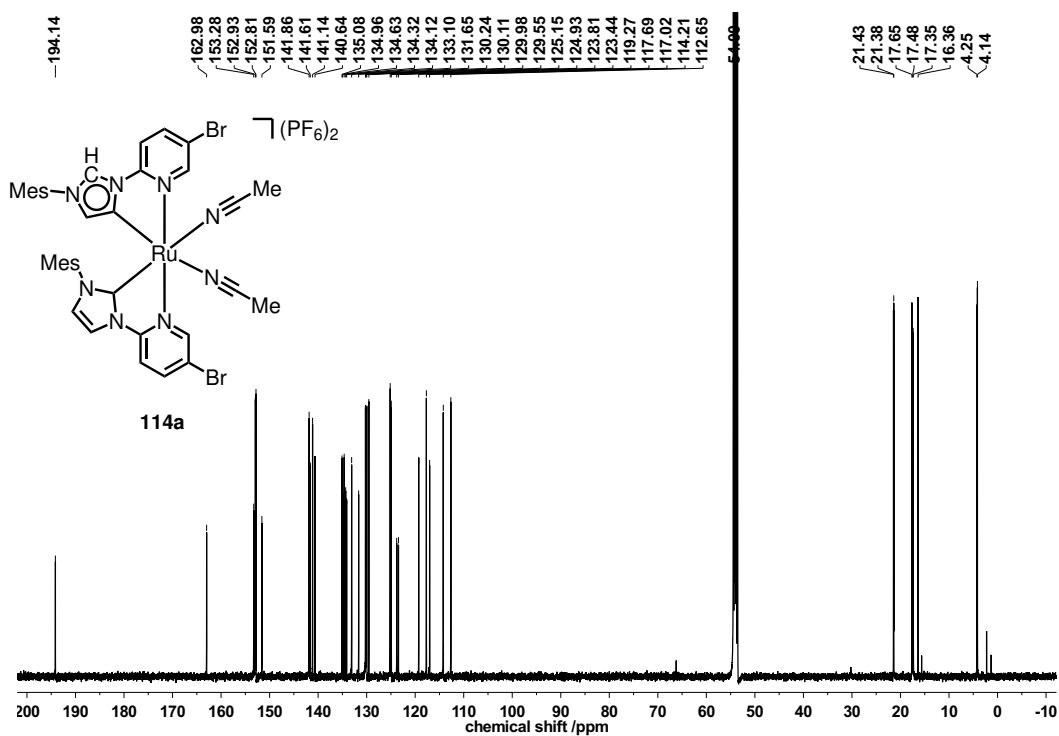


Figure 67: $^{13}\text{C-NMR}$ spectrum (126 MHz, 300 K) of complex **114a** in CD_2Cl_2 .

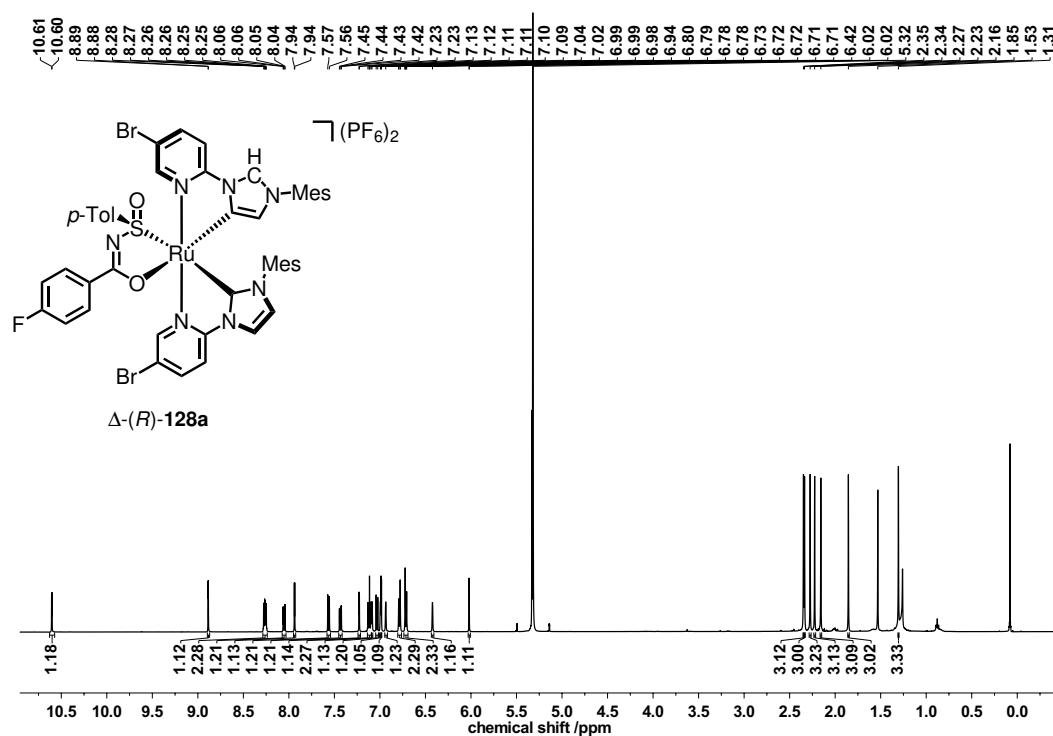


Figure 68: $^1\text{H-NMR}$ spectrum (500 MHz, 300 K) of complex $\Delta\text{-(R)-128a}$ in CD_2Cl_2 .

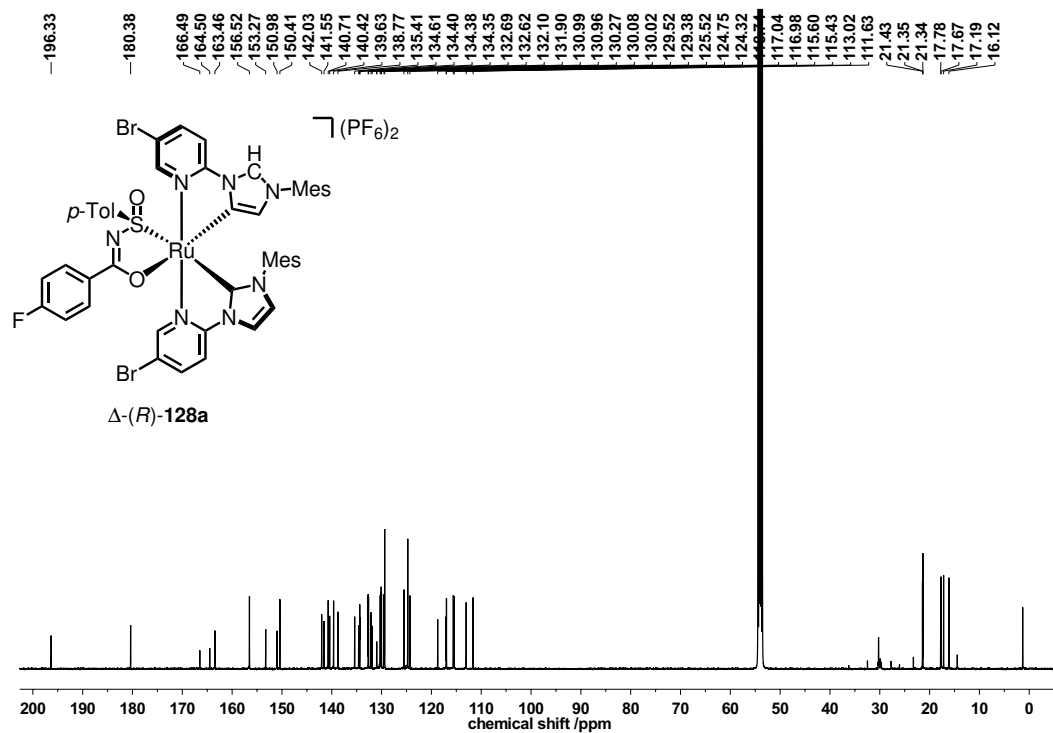


Figure 69: $^{13}\text{C-NMR}$ spectrum (126 MHz, 300 K) of complex $\Delta\text{-(R)-128a}$ in CD_2Cl_2 .

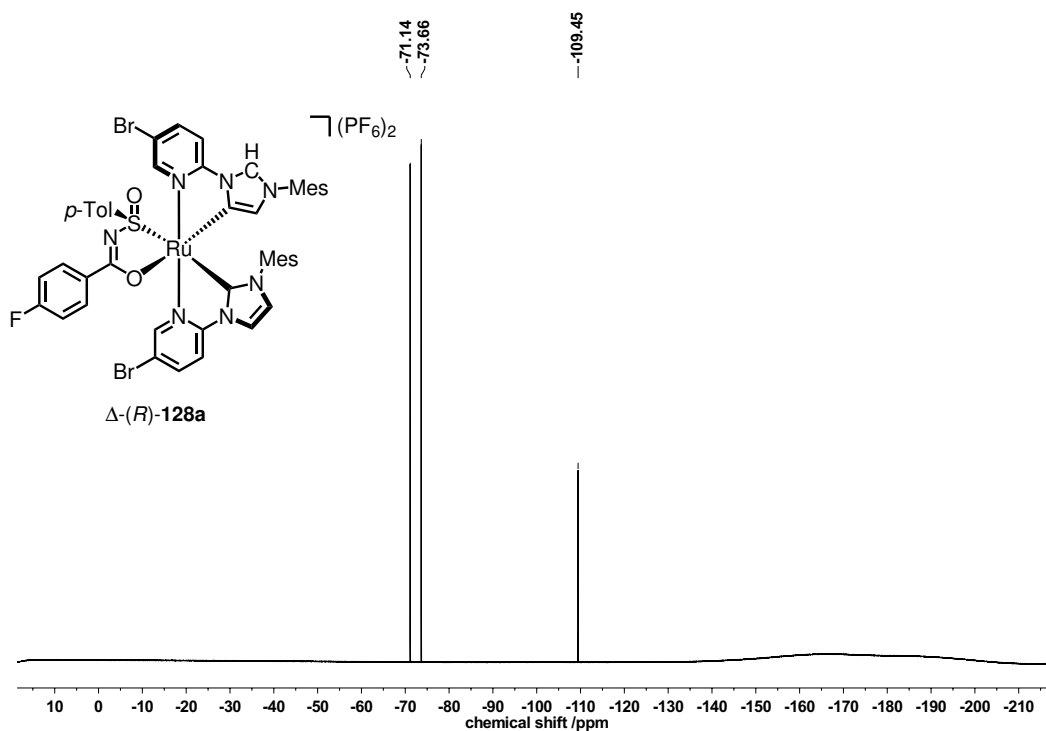


Figure 70: ^{19}F -NMR spectrum (282 MHz, 300 K) of complex Δ -(R)-128a in CD_2Cl_2 .

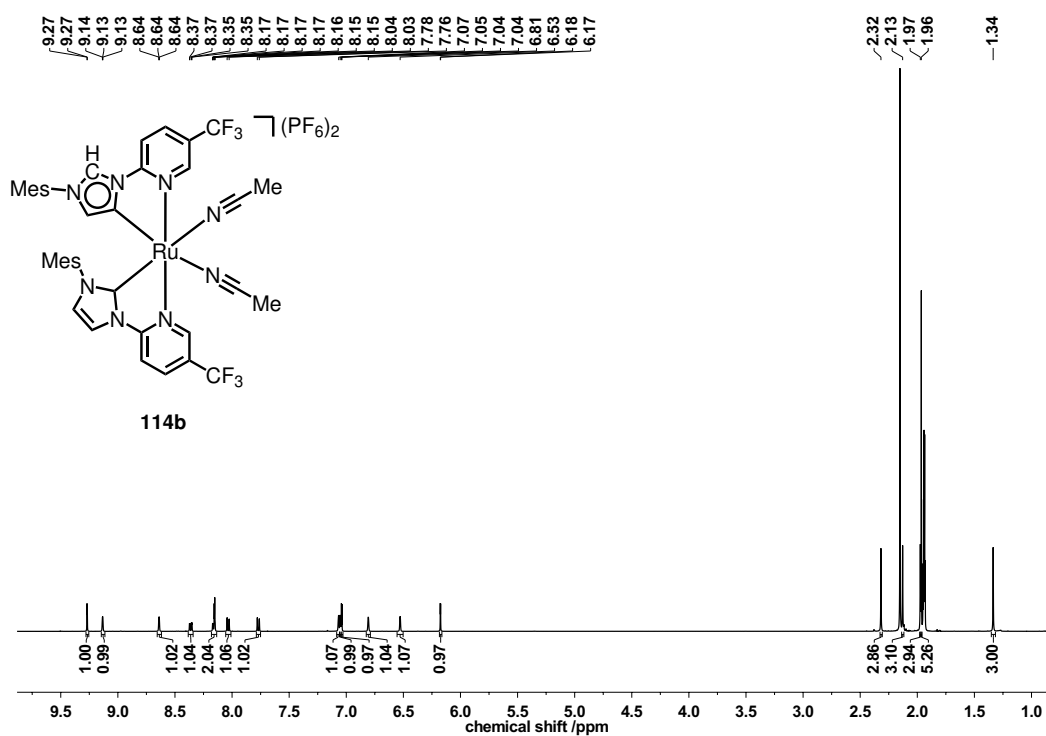


Figure 71: 1H -NMR spectrum (500 MHz, 300 K) of complex 114b in CD_3CN .

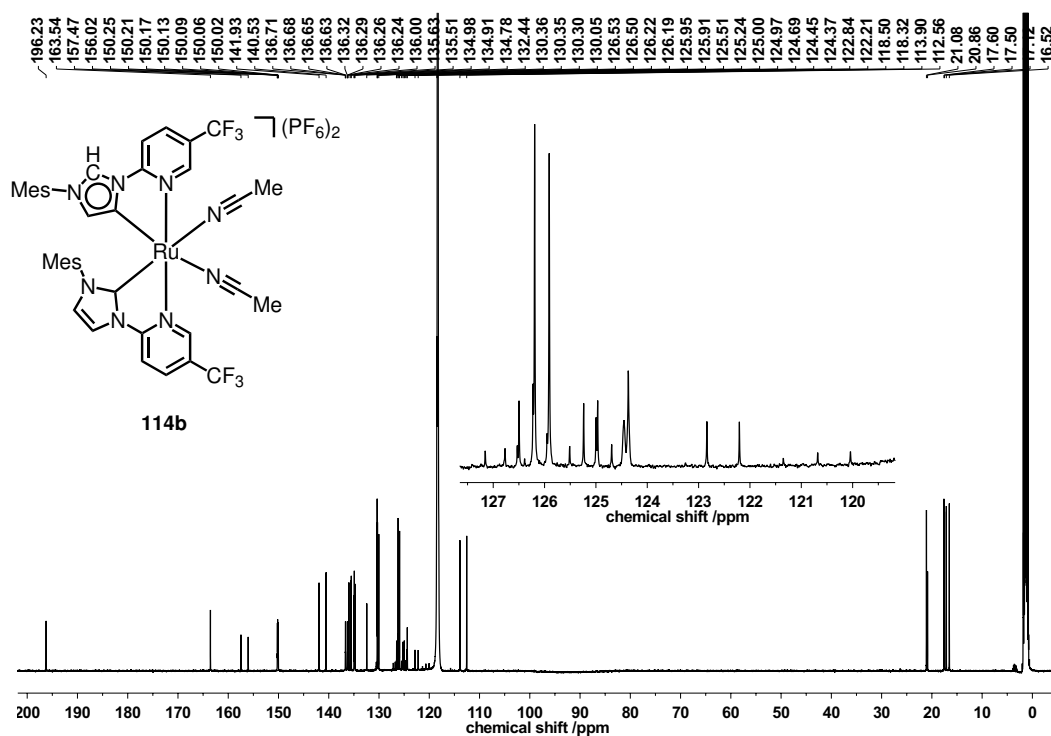


Figure 72: ^{13}C -NMR spectrum (126 MHz, 300 K) of complex **114b** in CD_3CN .

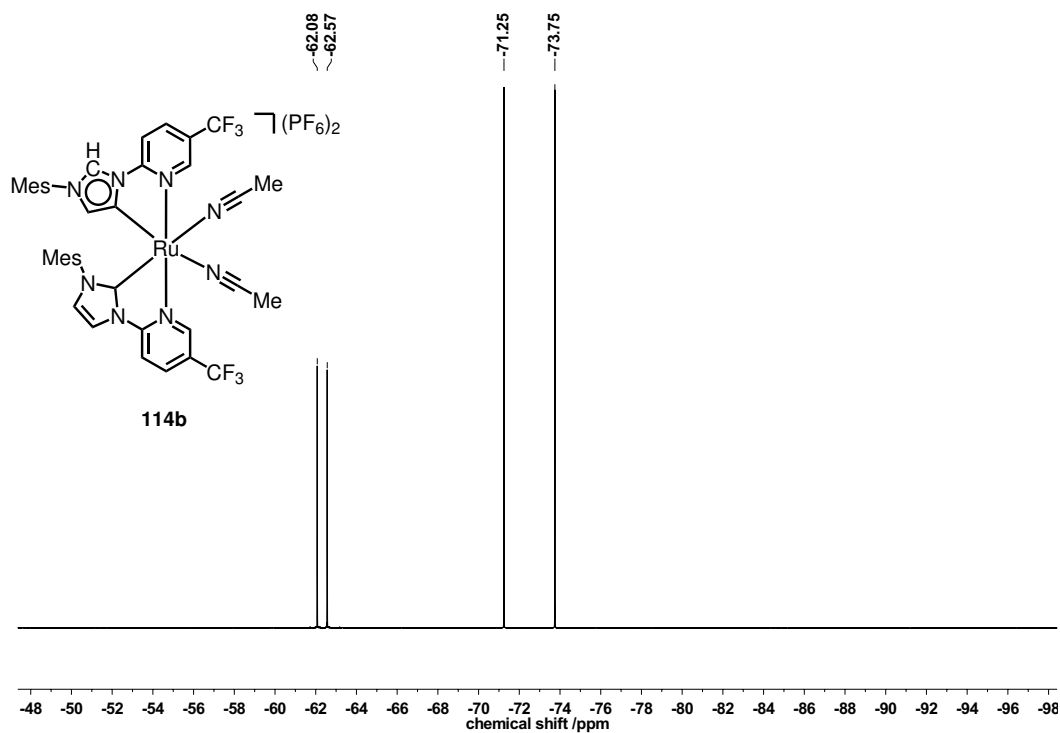


Figure 73: ^{19}F -NMR spectrum (282 MHz, 300 K) of complex **114b** in CD_3CN .

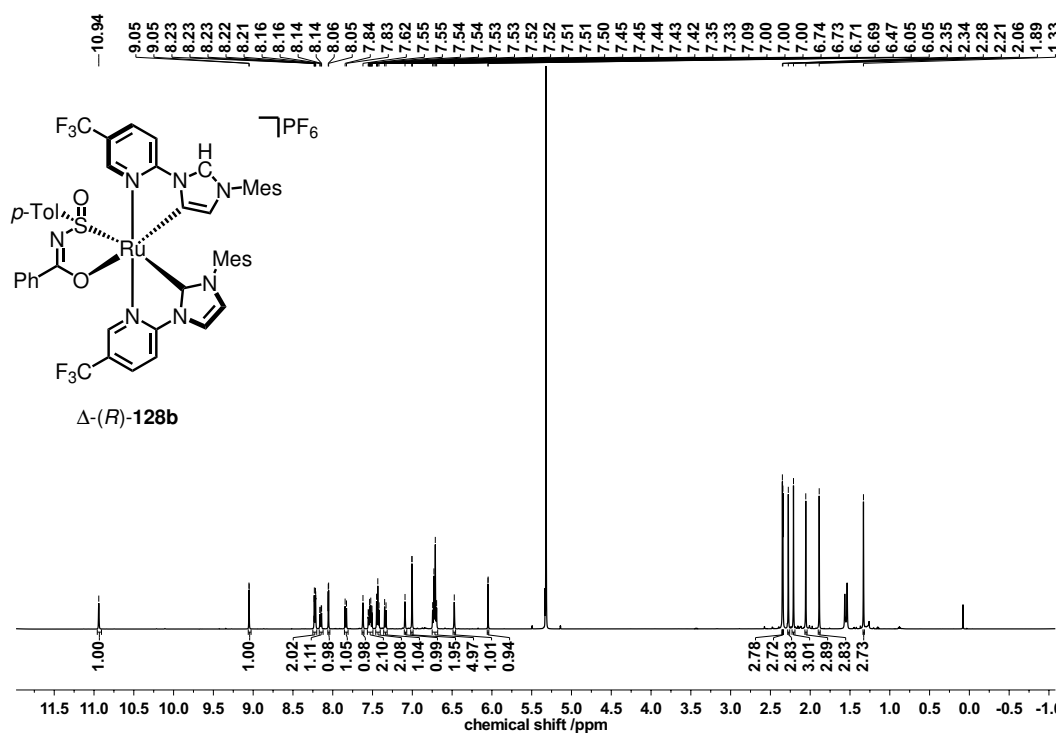


Figure 74: $^1\text{H-NMR}$ spectrum (500 MHz, 300 K) of complex $\Delta\text{-(R)-128b}$ in CD_2Cl_2 .

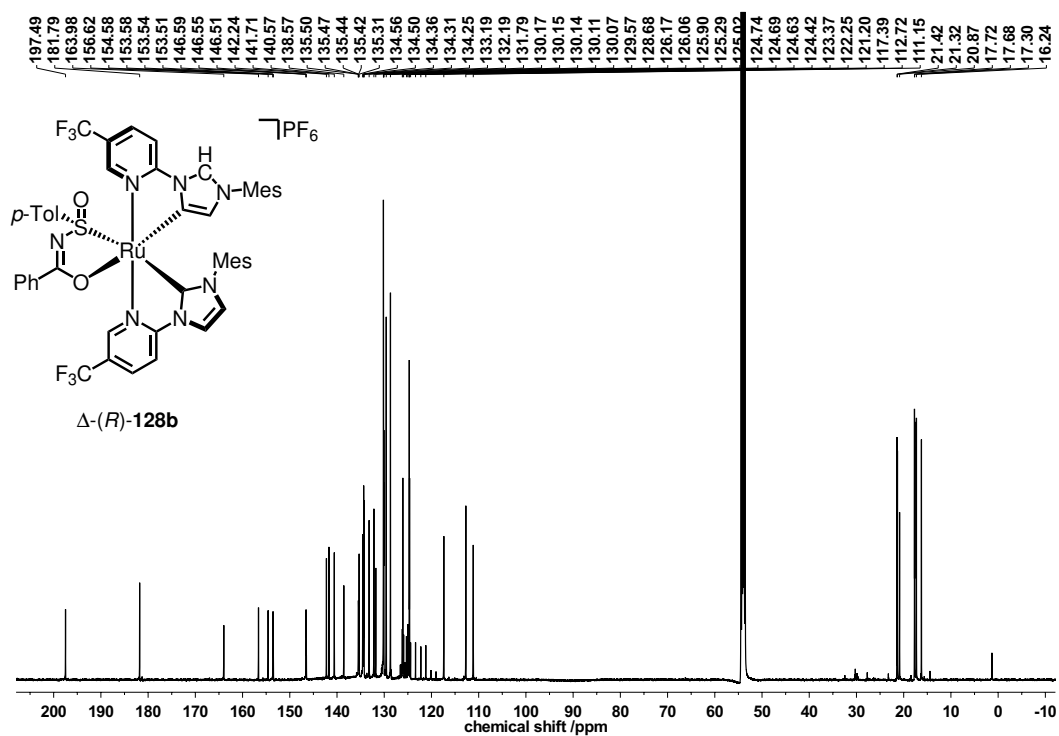


Figure 75: $^{13}\text{C-NMR}$ spectrum (126 MHz, 300 K) of complex $\Delta\text{-(R)-128b}$ in CD_2Cl_2 .

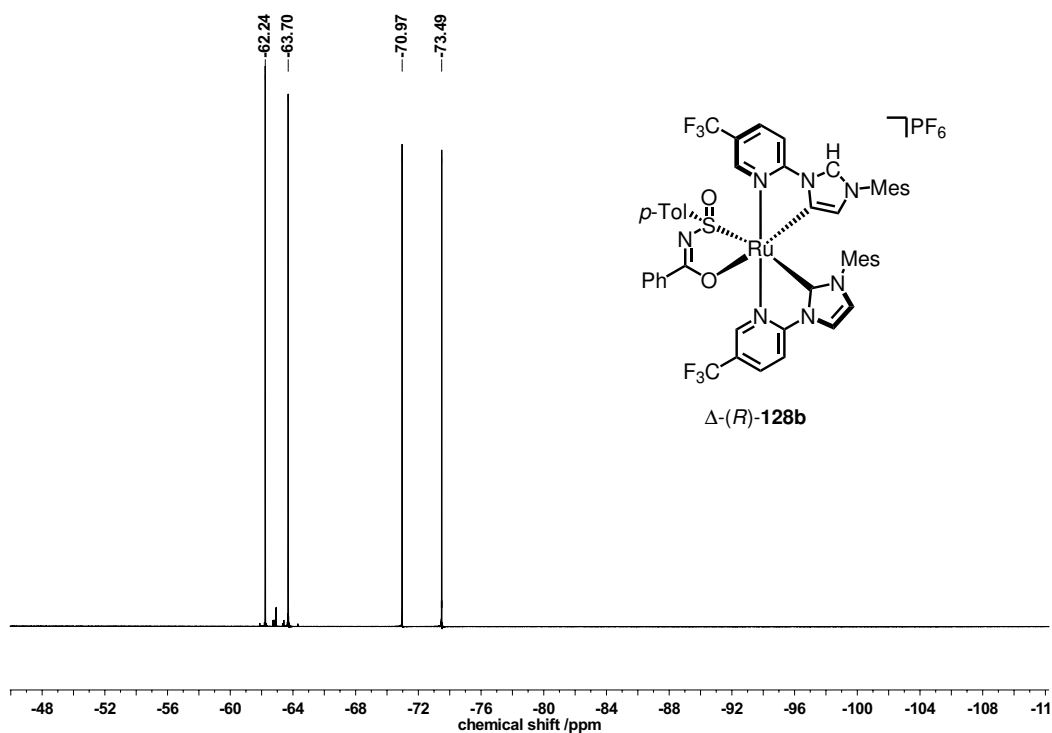


Figure 76: ¹⁹F-NMR spectrum (282 MHz, 300 K) of complex Δ -(R)-128b in CD₂Cl₂.

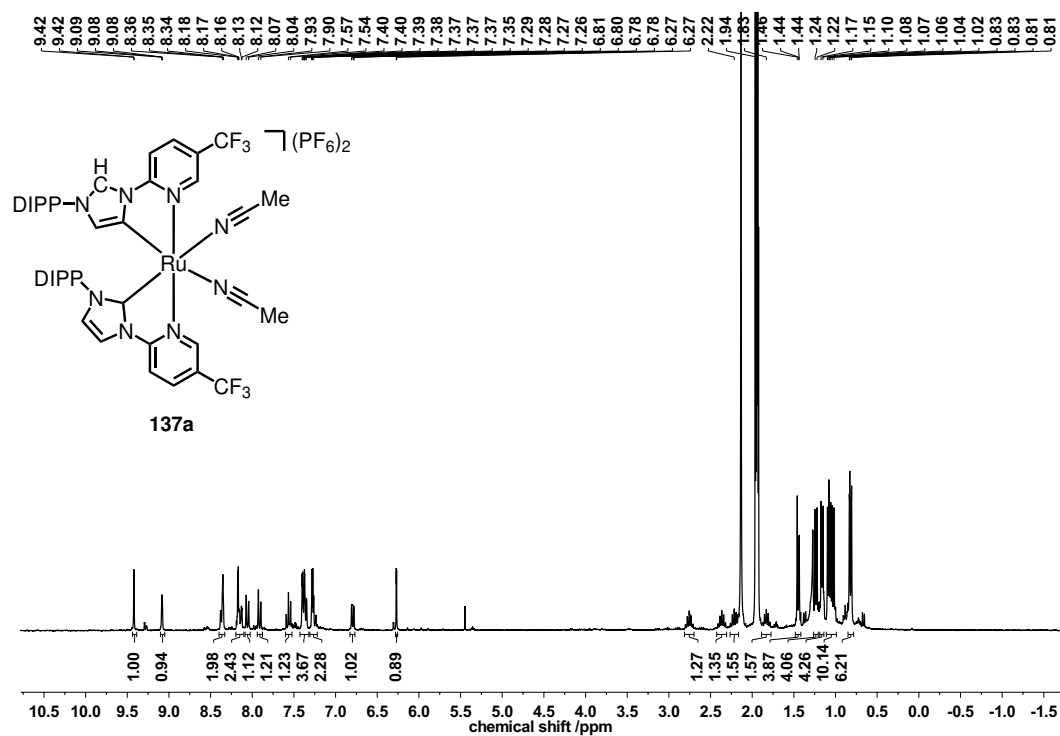


Figure 77: ¹H-NMR spectrum (300 MHz, 300 K) of complex 137a in CD₃CN.

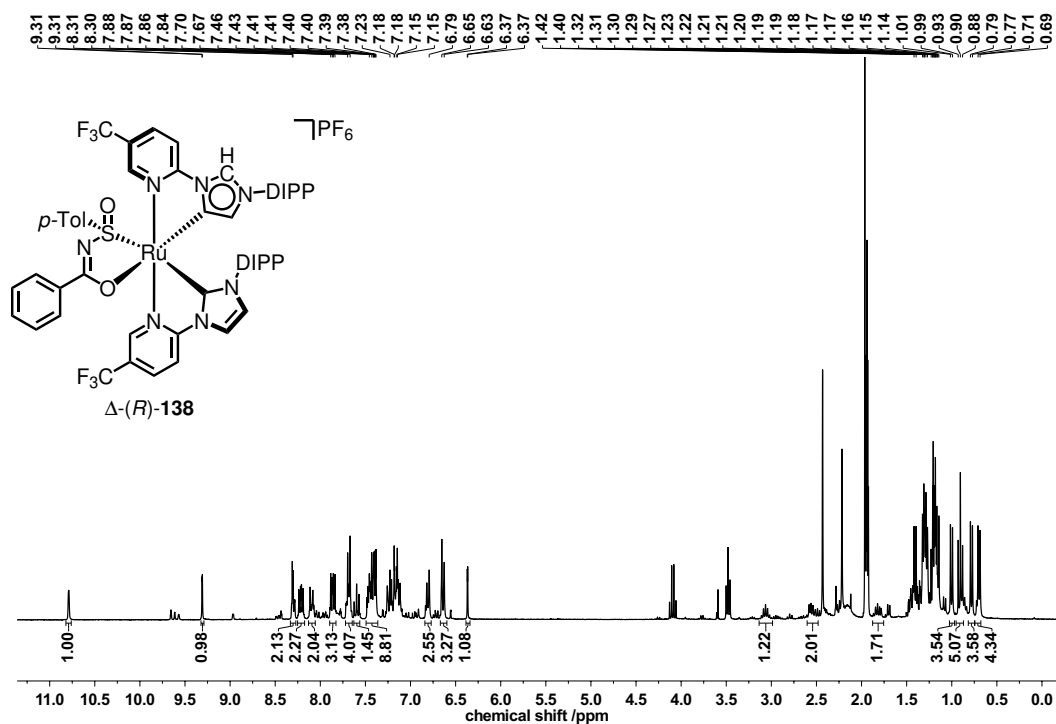


Figure 78: $^1\text{H-NMR}$ spectrum (300 MHz, 300 K) of complex $\Delta\text{-(R)-138}$ in CD_3CN as a mixture of diastereomers.

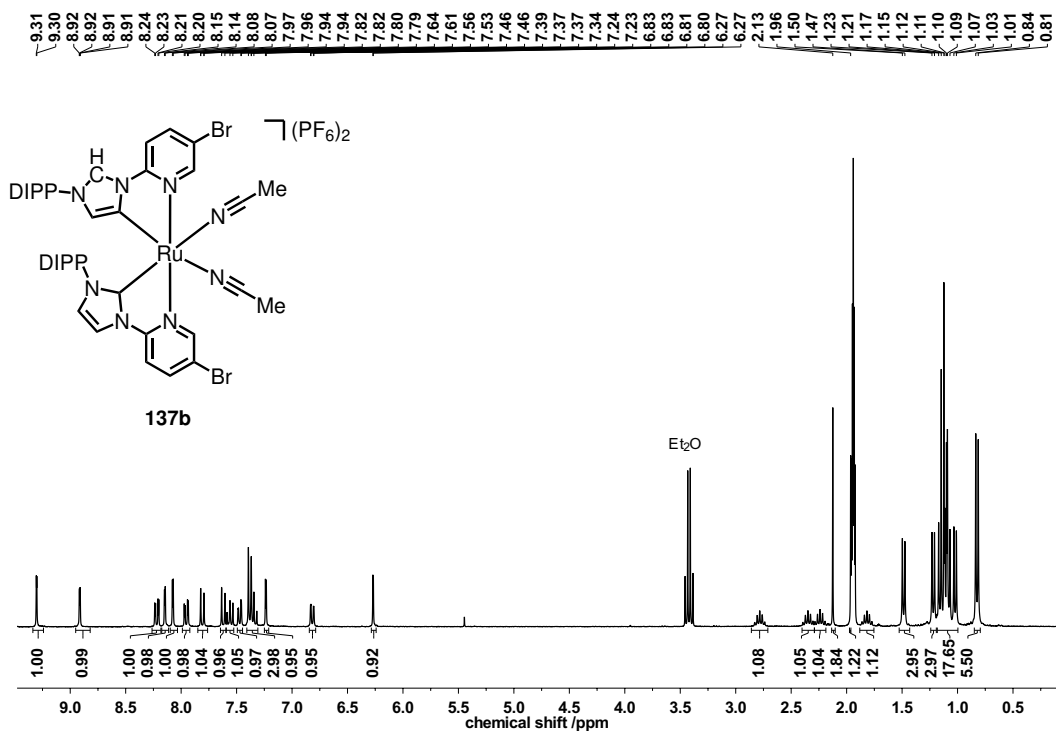


Figure 79: $^1\text{H-NMR}$ spectrum (300 MHz, 300 K) of complex **137b** in CD_3CN .

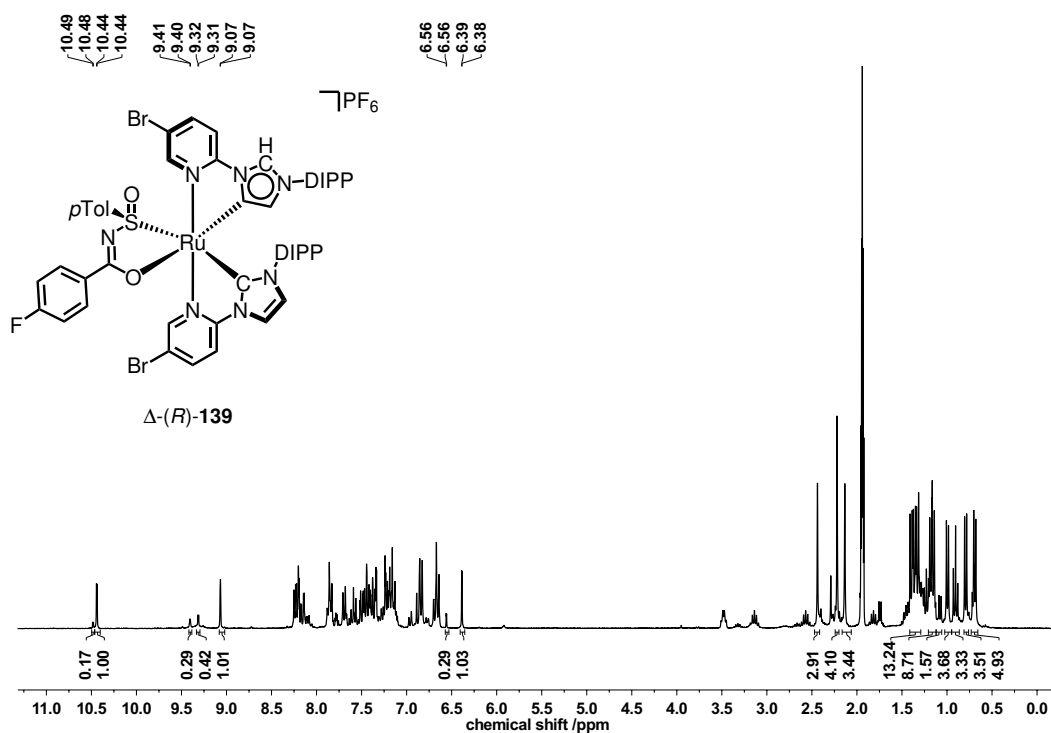


Figure 80: ¹H-NMR spectrum (300 MHz, 300 K) of complex Δ -(R)-139 in CD₃CN as a mixture of diastereomers.

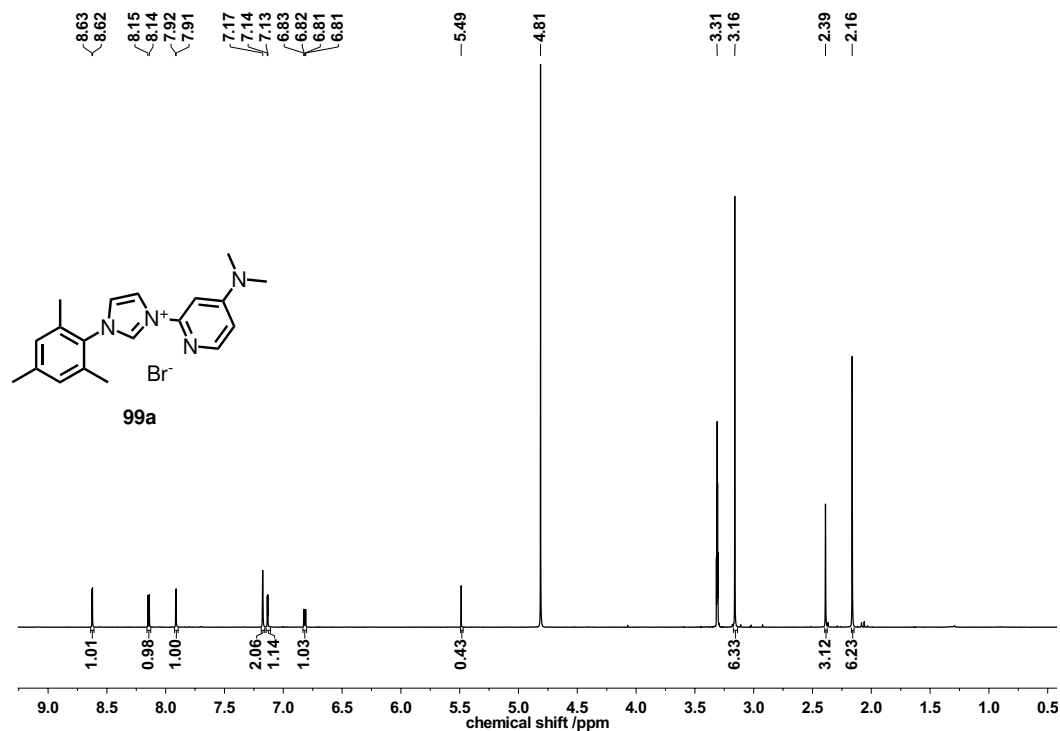


Figure 81: ¹H-NMR spectrum (500 MHz, 300 K) of imidazolium salt 99a in MeOH-d₄.

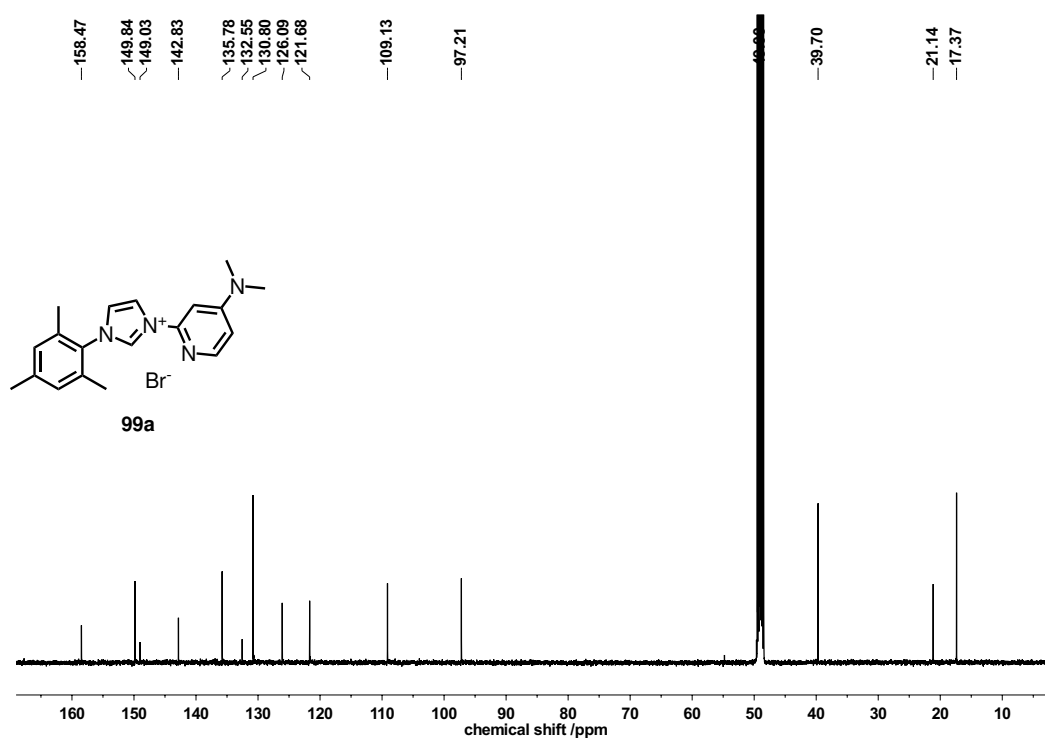


Figure 82: ^{13}C -NMR spectrum (126 MHz, 300 K) of imidazolium salt **99a** in MeOH- d_4 .

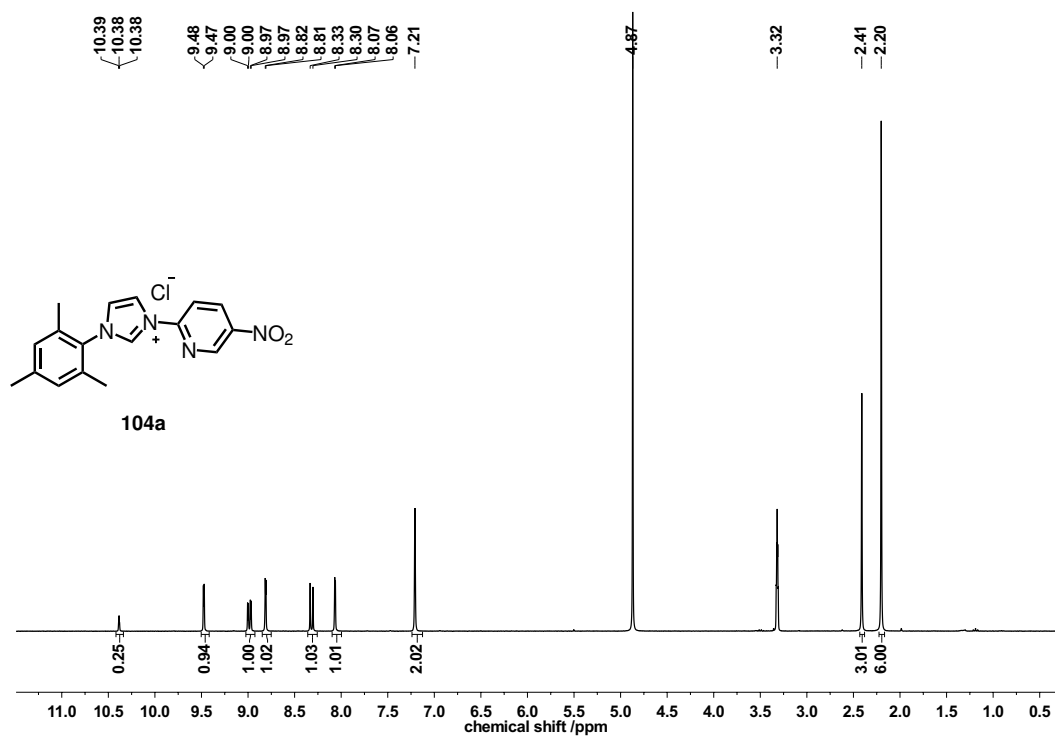


Figure 83: ^1H -NMR spectrum (300 MHz, 300 K) of imidazolium salt **104a** in MeOH- d_4 .

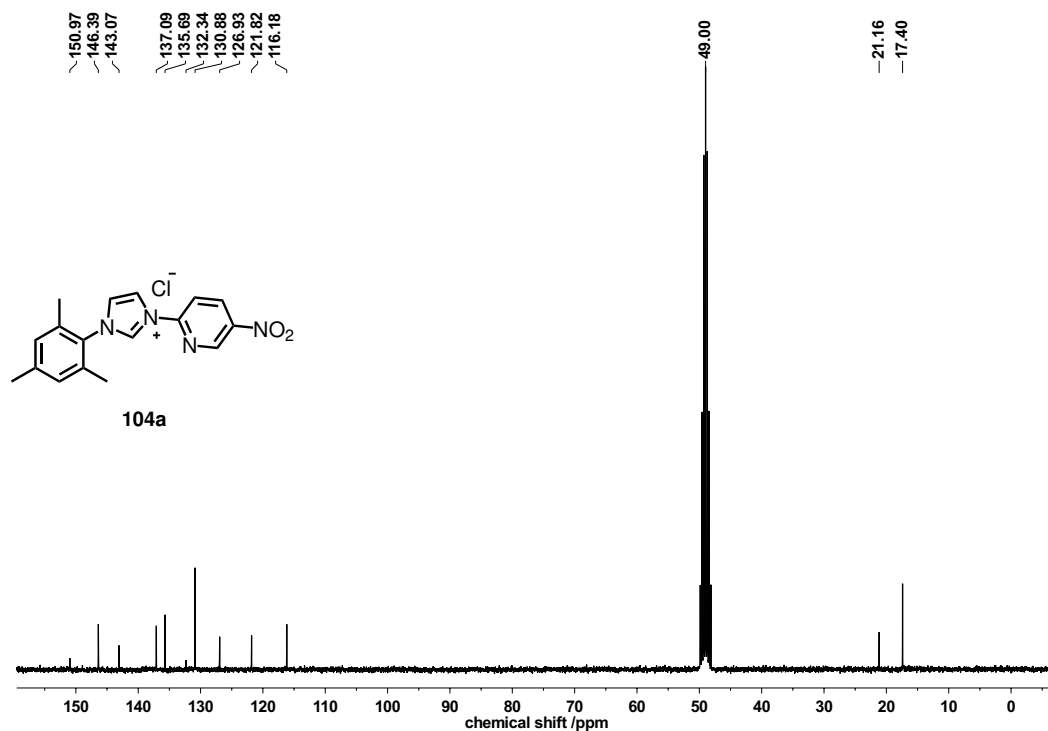


Figure 84: ¹³C-NMR spectrum (75 MHz, 300 K) of imidazolium salt **104a** in MeOH-d₄.

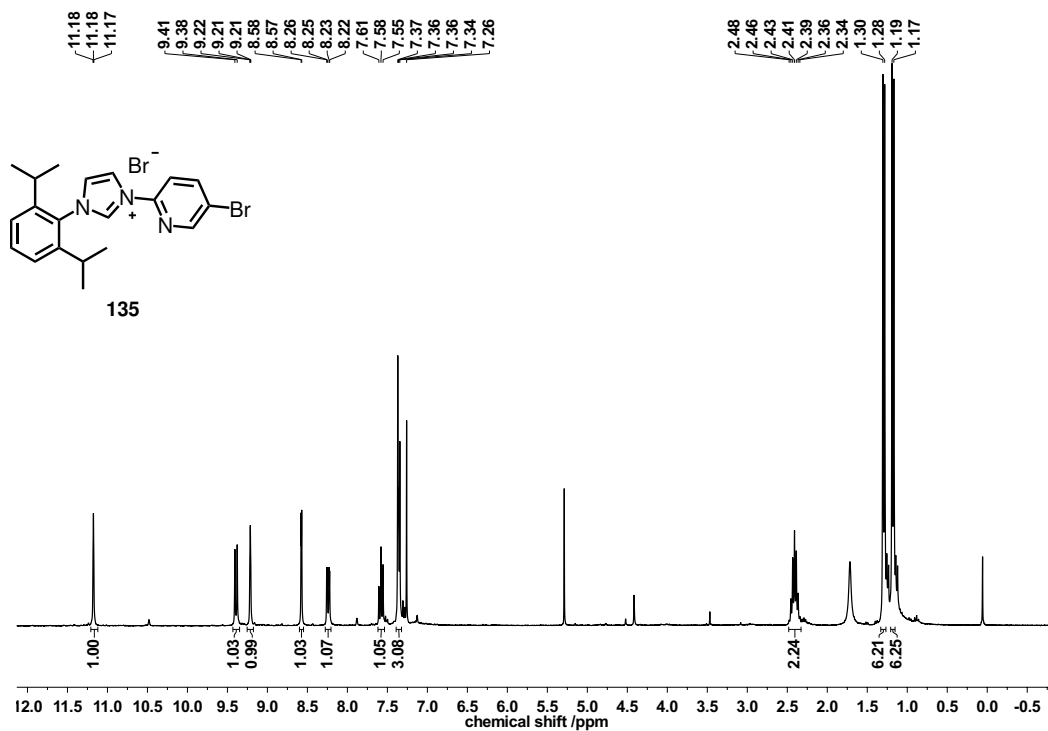


Figure 85: ¹H-NMR spectrum (300 MHz, 300 K) of imidazolium salt **135** in CDCl₃.

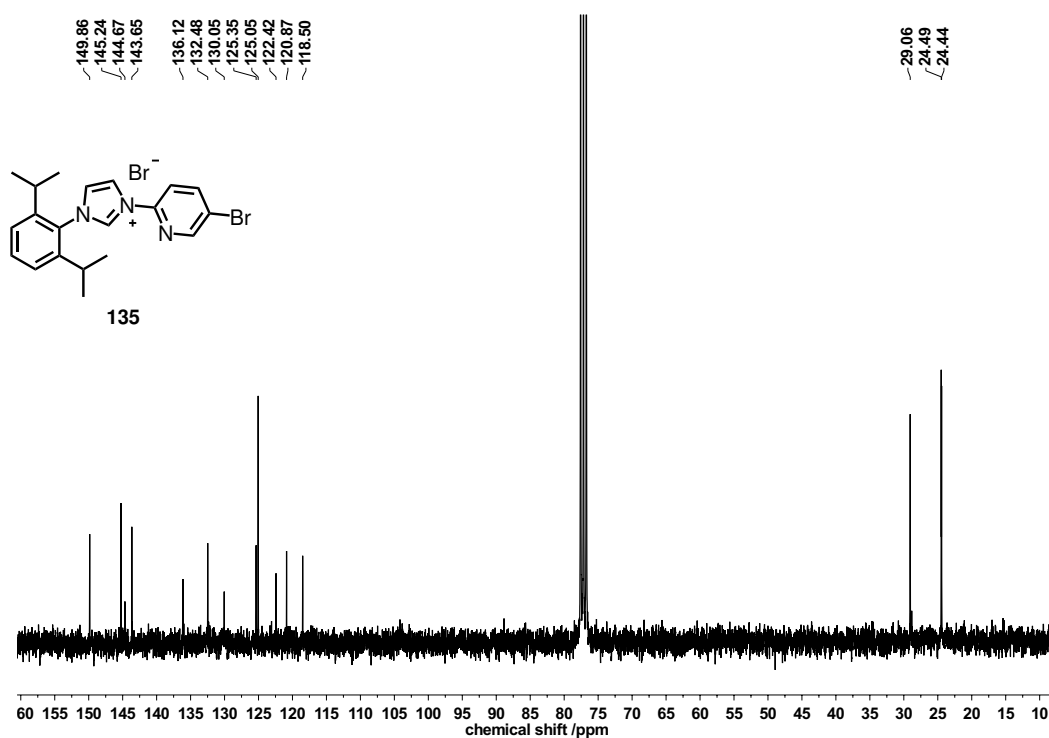


Figure 86: ^{13}C -NMR spectrum (75 MHz, 300 K) of imidazolium salt **135** in CDCl_3 .

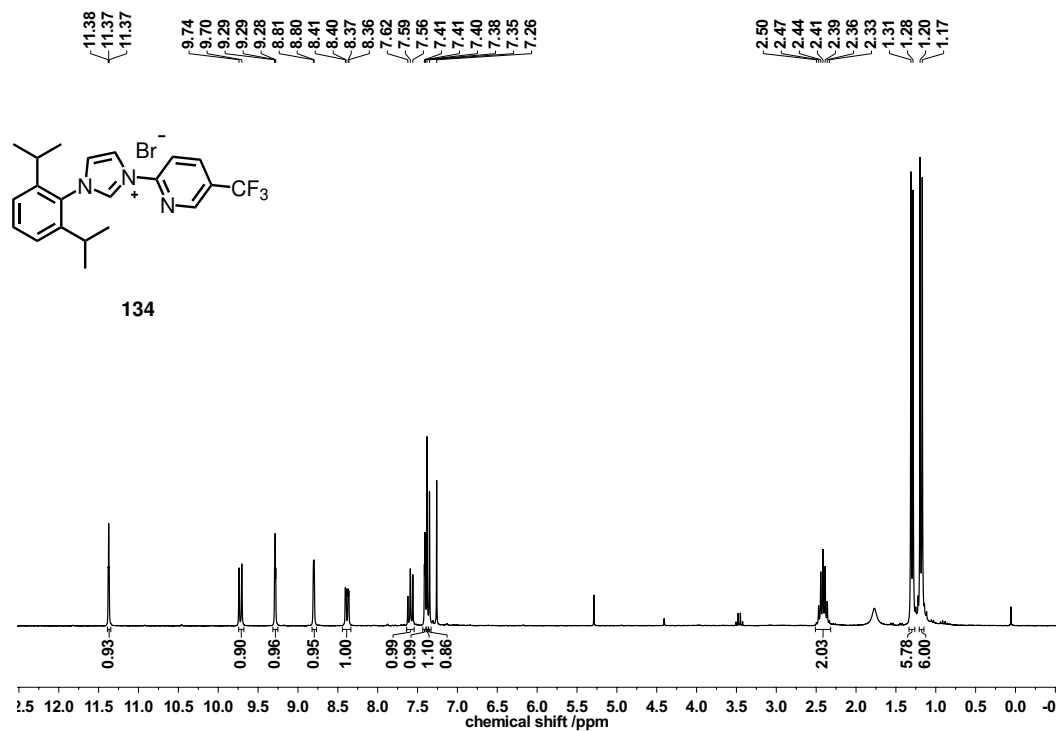


Figure 87: ^1H -NMR spectrum (250 MHz, 300 K) of imidazolium salt **134** in CDCl_3 .

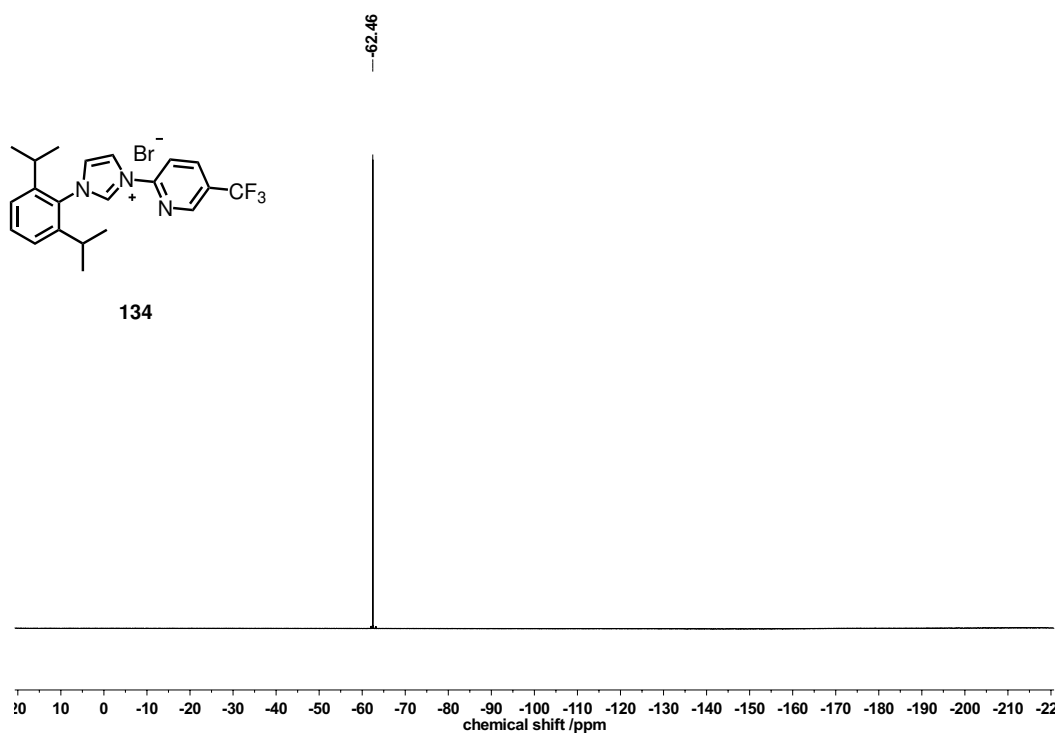


Figure 88: ^{19}F -NMR spectrum (235 MHz, 300 K) of imidazolium salt **134** in CDCl_3 .

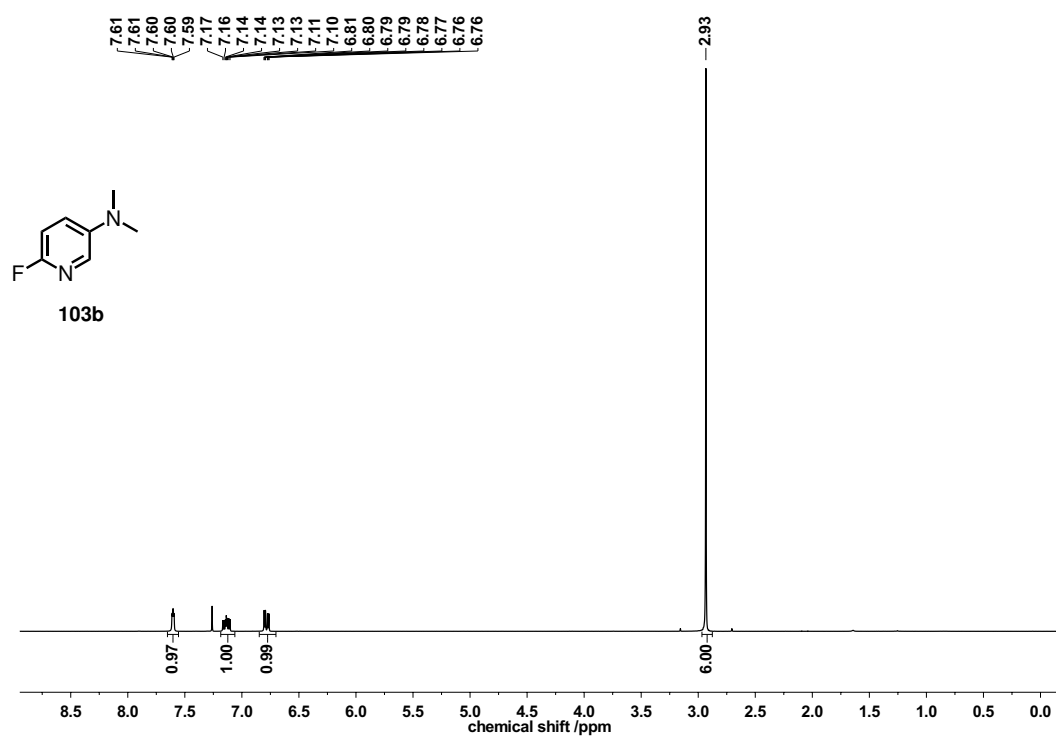


Figure 89: ^1H -NMR spectrum (300 MHz, 300 K) of pyridine **103b** in CDCl_3 .

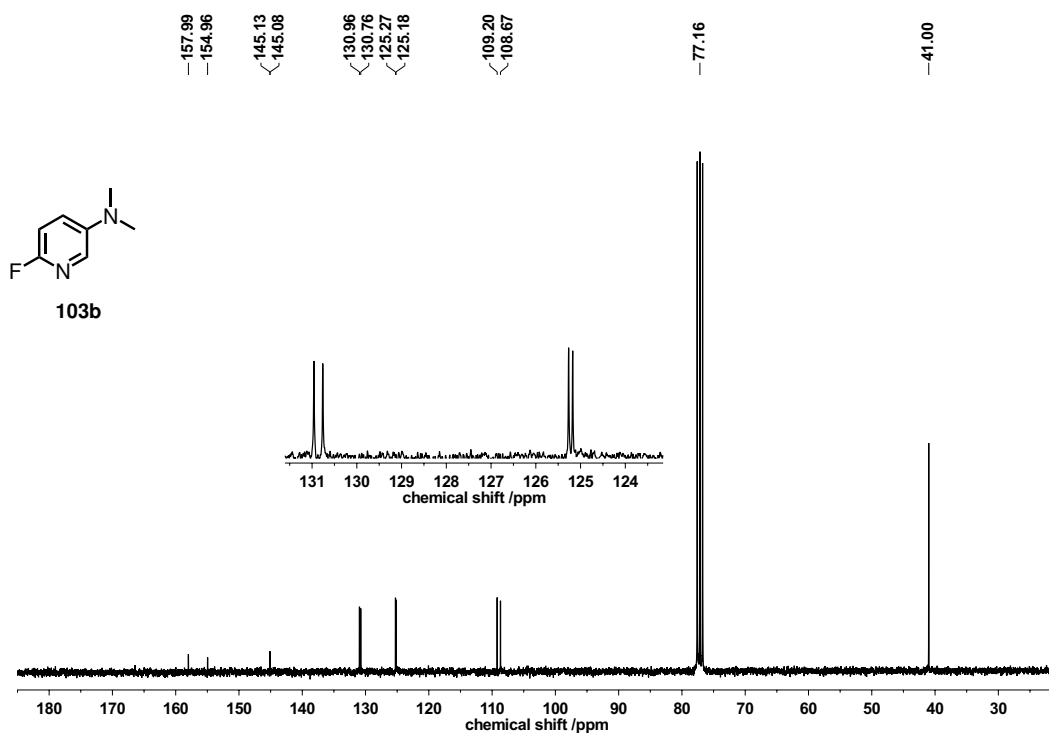


Figure 90: ¹³C-NMR spectrum (75 MHz, 300 K) of pyridine **103b** in CDCl₃.

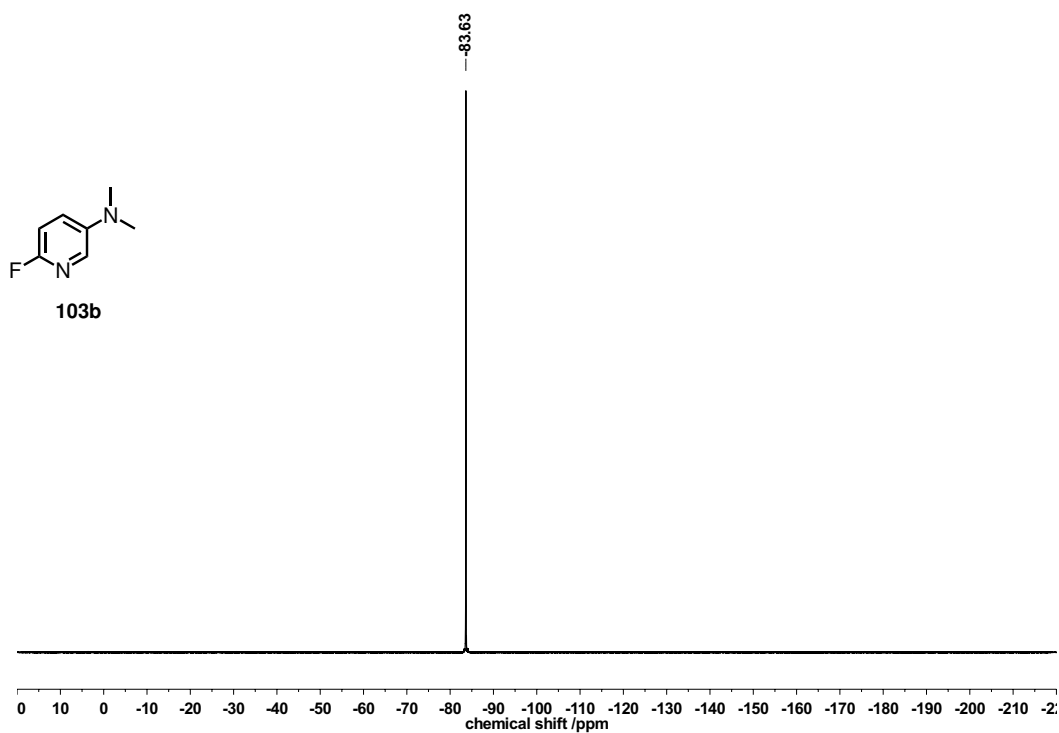


Figure 91: ¹⁹F-NMR spectrum (235 MHz, 300 K) of pyridine **103b** in CDCl₃.

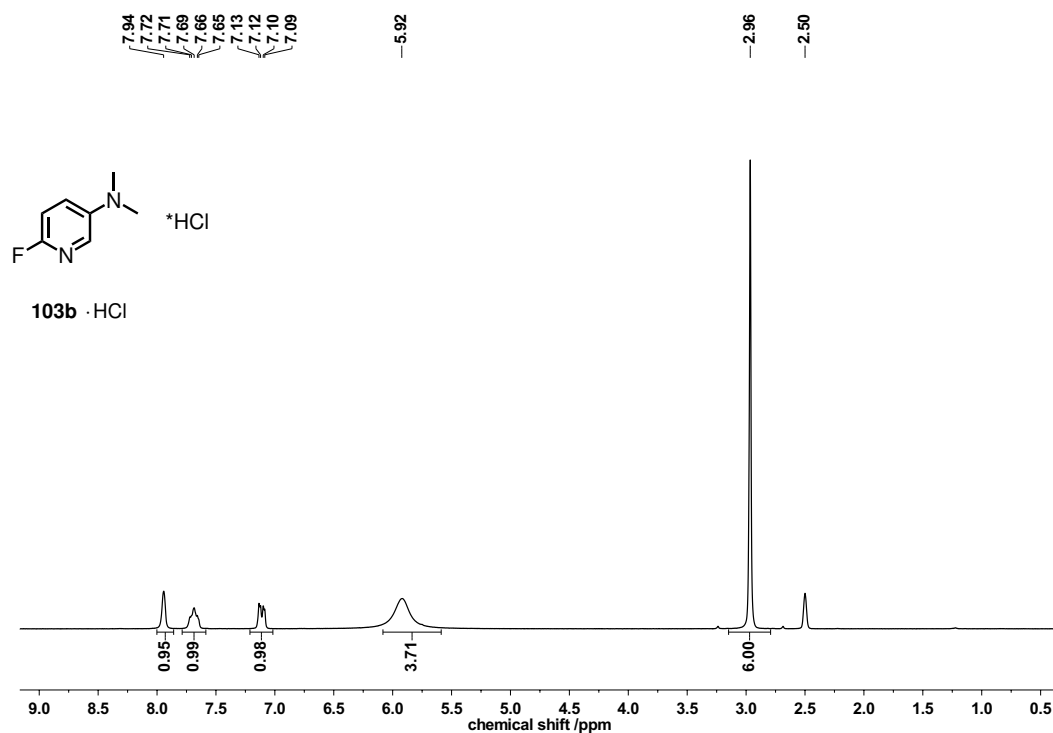


Figure 92: ¹H-NMR spectrum (300 MHz, 300 K) of pyridinium salt **103b · HCl** in CDCl₃.

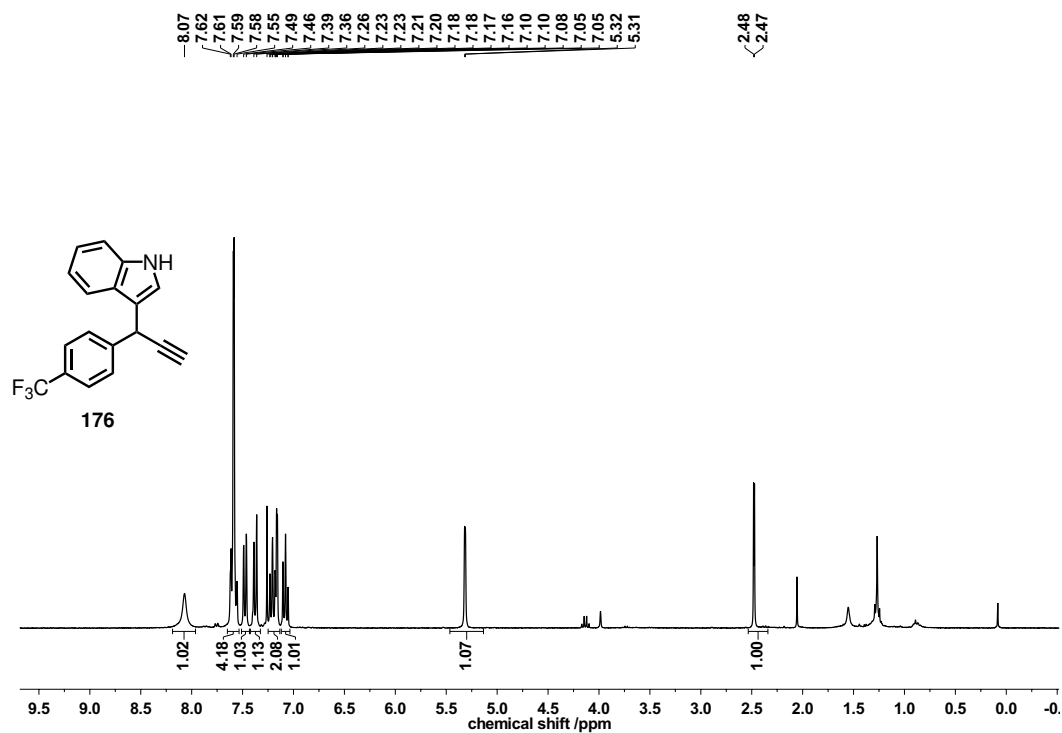


Figure 93: ¹H-NMR spectrum (300 MHz, 300 K) of compound **176** in CDCl₃.

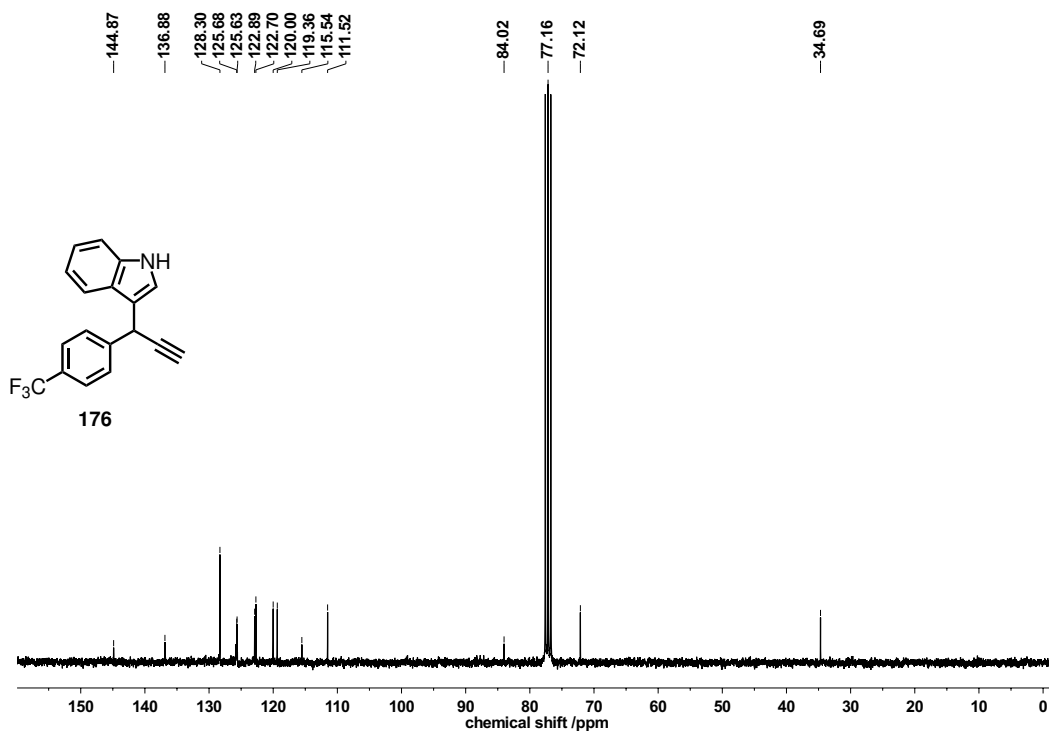


Figure 94: ¹³C-NMR spectrum (75 MHz, 300 K) of compound **176** in CDCl₃.

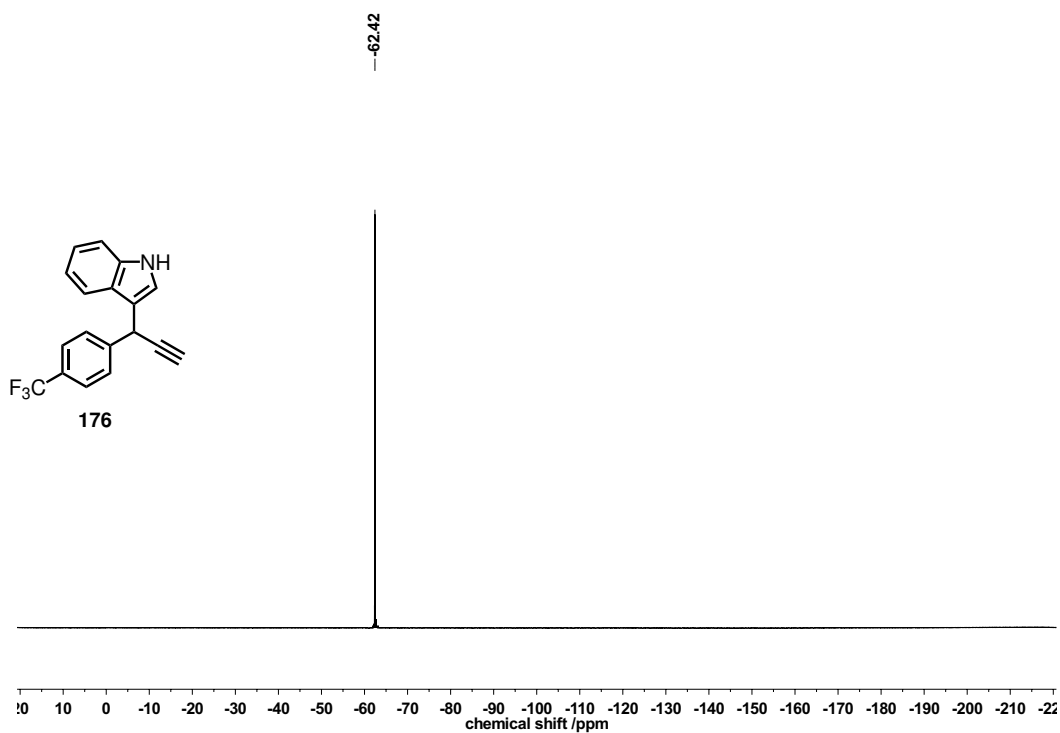


Figure 95: ¹⁹F-NMR spectrum (235 MHz, 300 K) of compound **176** in CDCl₃.

B. Crystallographic Appendix

Complex 64i

Single crystals suitable for analysis were obtained by slow diffusion of Et₂O into a solution of **64i** in CH₃CN over night. Data was collected^[167] with an STOE STADIVARI diffractometer equipped with CuK α radiation, a graded multilayer mirror monochromator ($\lambda = 1.54186 \text{ \AA}$) and a DECTRIS PILATUS 300K detector using an oil-coated shock-cooled crystal at 100(2) K. Absorption effects were corrected semi-empirical using multiscanned reflexions (STOE LANA, absorption correction by scaling of reflection intensities.).^[168] Cell constants were refined using 38803 of observed reflections of the data collection. The structure was solved by direct methods by using the program XT V2014/1 (Bruker AXS Inc., 2014)^[169] and refined by full matrix least squares procedures on F² using SHELXL-2018/1 (Sheldrick, 2018). The non-hydrogen atoms have been refined anisotropically, carbon bonded hydrogen atoms were included at calculated positions and refined using the ‘riding model’ with isotropic temperature factors at 1.2 times (for CH₃ groups 1.5 times) that of the preceding carbon atom. CH₃ Groups were allowed to rotate about the bond to their next atom to fit the electron density. [PF₆⁻] anions happened to be disordered and were refined using restraints. The Crystal structure^[124], data, and details of **64i** are presented in Table 17 and Figure 96.

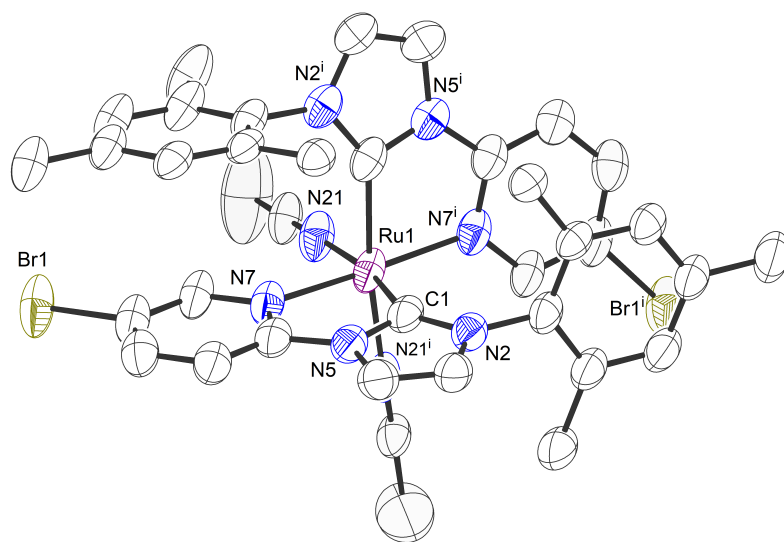


Figure 96: Crystal structure of racemic **64i**. The [PF₆⁻] anions and the hydrogen atoms are omitted for clarity. Displacement ellipsoids are shown at 50% probability level at 100 K.

Table 17: Crystal data and structure refinement for **64i**.

Crystal data		
Identification code	EW128	
Habitus, colour	nugget, colourless	
Crystal size	0.50×0.19×0.17 mm ³	
Crystal system	Monoclinic	
Space group	C2/c	Z = 4
Unit cell dimensions	a = 11.3296(5) Å	α = 90°
	b = 29.0787(14) Å	β = 103.036(3)°
	c = 13.5300(6) Å	γ = 90°
Volume	4342.6(3) Å ³	
Cell determination	38803 peaks with Theta 4.3° to 76.4°	
Empirical formula	C ₃₈ H ₃₈ Br ₂ F ₁₂ N ₈ P ₂ Ru	
Moiety formula	C ₃₈ H ₃₈ Br ₂ N ₈ Ru, 2 (F ₆ P)	
Formula weight	1157.59	
Density (calculated)	1.771 Mg m ⁻³	
Absorption coefficient	6.601 mm ⁻¹	
F(000)	2296	
Data collection:		
Diffractometer type	STOE STADIVARI	
Wavelength	1.541 86 Å	
Temperature	100(2) K	
Theta range for data collection	4.284 to 75.731°	
Index ranges	-14 ≥ h ≥ 13	
	-31 ≥ k ≥ 36	
	-14 ≥ l ≥ 16	
Data collection software	X-Area Pilatus3 SV 1.31.127.0 (STOE, 2016) ^[167]	
Cell refinement software	X-Area Recipe 1.33.0.0 (STOE, 2015) ^[170]	
Data reduction software	X-Area Integrate 1.71.0.0 (STOE, 2016) ^[171]	
	X-Area LANA 1.68.2.0 (STOE, 2016) ^[168]	
Solution and refinement:		
Reflections collected	20593	
Independent reflections	4453 [R(int) = 0.0622]	
Completeness to theta = 67.686°	99.6	
Observed reflections	4137[I > 2σ(I)]	
Reflections used for refinement	4453	
Extinction coefficient	X = 0.00049(8)	

Absorption correction	Semi-empirical from equivalents ^[168]
Max. and min. transmission	0.4484 and 0.0610
Largest diff. peak and hole	0.689 and $-1.308 \text{ e } \text{\AA}^{-3}$
Solution	intrinsic phases ^[172]
Refinement	Full-matrix least-squares on F^2 ^[173]
Treatment of hydrogen atoms	Calculated positions, constr. ref.
Programs used	XT V2014/1 (Bruker AXS Inc., 2014) ^[172] SHELXL-2018/1 (Sheldrick, 2018) ^[173] DIAMOND (Crystal Impact) ^[174] ShelXle (Hübschle, Sheldrick, Dittrich, 2011) ^[175]
Data / restraints / parameters	4453 / 118 / 337
Goodness-of-fit on F^2	1.087
R index (all data)	$wR^2 = 0.2019$
R index conventional [$I > 2\sigma(I)$]	$R1 = 0.0707$
CCDC No.	2069775

Complex 64j

Single crystals suitable for analysis were obtained by slow diffusion of Et_2O into a solution of **64j** in CH_3CN over night. Data was collected^[167] with an STOE STADIVARI diffractometer equipped with with $\text{CuK}\alpha$ radiation, a graded multilayer mirror monochromator ($\lambda = 1.54178 \text{ \AA}$) and a DECTRIS PILATUS 300K detector using an oil-coated shock-cooled crystal at 100(2) K. Absorption effects were corrected semi-empirical using multiscanned reflexions (STOE LANA, absorption correction by scaling of reflection intensities).^[168] Cell constants were refined using 74742 of observed reflections of the data collection. The structure was solved by direct methods by using the program XT V2014/1 (Bruker AXS Inc., 2014)^[169] and refined by full matrix least squares procedures on F^2 using SHELXL-2018/3 (Sheldrick, 2018). The non-hydrogen atoms have been refined anisotropically, carbon bonded hydrogen atoms were included at calculated positions and refined using the ‘riding model’ with isotropic temperature factors at 1.2 times (for CH_3 groups 1.5 times) that of the preceding carbon atom. CH_3 groups were allowed to rotate about the bond to their next atom to fit the electron density. Disorder of solvent (Et_2O , CH_3CN) was refined using restraints for both the thermal parameters and geometry. The Crystal structure, data, and details of **64j** are presented in Table 18 and Figure 97.

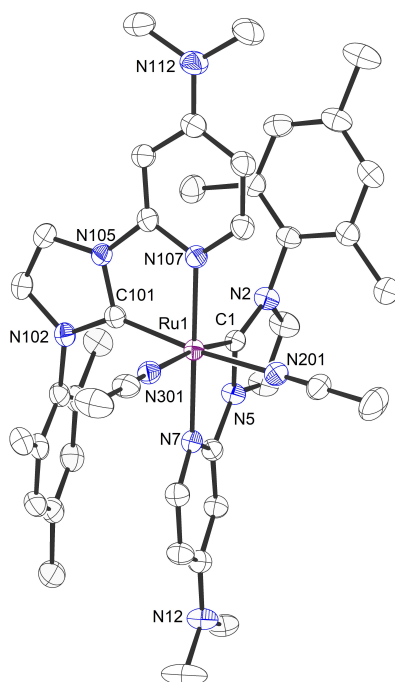


Figure 97: Crystal structure of racemic **64j**. The $[\text{PF}_6]^-$ anions and the hydrogen atoms are omitted for clarity. Displacement ellipsoids are shown at 50% probability level at 100 K.

Table 18: Crystal data and structure refinement for **64j**.

Crystal data

Identification code	EW167a	
Habitus, colour	needle, pale yellow	
Crystal size	0.35×0.09×0.05 mm ³	
Crystal system	Monoclinic	
Space group	P21/c	Z = 4
Unit cell dimensions	a = 12.4927(2) Å	α = 90°
	b = 29.4279(5) Å	β = 101.085(2)°
	c = 14.6484(3) Å	γ = 90°
Volume	5284.78(17) Å ³	
Cell determination	74742 peaks with Theta 3.0 to 76.2°	
Empirical formula	C ₄₇ H _{58.10} F ₁₂ N _{12.20} O _{0.15} P ₂ Ru	
Moiety formula	C ₄₂ H ₅₀ N ₁₀ Ru, 2 (F ₆ P), 0.15 (C ₄ H ₁₀ O), 2.2 (C ₂ H ₃ N)	
Formula weight	1187.36	
Density (calculated)	1.492 Mg m ⁻³	
Absorption coefficient	3.758 mm ⁻¹	
F(000)	2435	

Data collection:

Diffractometer type	STOE STADIVARI
Wavelength	1.541 78 Å
Temperature	100(2) K
Theta range for data collection	3.003 to 75.715°
Index ranges	$-15 \geq h \geq 15$ $-21 \geq k \geq 36$ $-17 \geq l \geq 18$
Data collection software	X-Area Pilatus3 SV 1.31.127.0 (STOE, 2016) ^[167]
Cell refinement software	X-Area Recipe 1.33.0.0 (STOE, 2015) ^[170]
Data reduction software	X-Area Integrate 1.71.0.0 (STOE, 2016) ^[171] X-Area LANA 1.68.2.0 (STOE, 2016) ^[168]

Solution and refinement:

Reflections collected	69365
Independent reflections	10905 [R(int) = 0.0394]
Completeness to theta = 67.679°	99.9%
Observed reflections	9015[I > 2σ(I)]
Reflections used for refinement	10905
Absorption correction	Semi-empirical from equivalents ^[168]
Max. and min. transmission	0.1812 and 0.0415
Largest diff. peak and hole	0.612 and -0.371 e Å ⁻³
Solution	intrinsic phases ^[172]
Refinement	Full-matrix least-squares on F ² ^[173]
Treatment of hydrogen atoms	Calculated positions, constr. ref.
Programs used	XT V2014/1 (Bruker AXS Inc., 2014) ^[169] SHELXL-2018/3 (Sheldrick, 2018) ^[173] DIAMOND (Crystal Impact) ^[174] ShelXle (Hübschle, Sheldrick, Dittrich, 2011) ^[175]
Data / restraints / parameters	10905 / 373 / 810
Goodness-of-fit on F ²	1.014
R index (all data)	wR ² = 0.0884
R index conventional [I > 2σ(I)]	R1 = 0.0334
CCDC No.	2106464

Complex 64g

Single crystals suitable for analysis were obtained by slow diffusion of Et₂O into a solution of **64g** in CH₃CN over night. A suitable crystal of **64g** was selected under inert oil and mounted using a MiTe-

Gen loop. Intensity data of the crystal were recorded with a STADIVARI diffractometer (Stoe & Cie). The diffractometer was operated with Cu-K α radiation (1.541 86 Å, microfocus source) and equipped with a Dectris PILATUS 300K detector. Evaluation, integration and reduction of the diffraction data was carried out using the X-Area software suite.^[176] Multi-scan and numerical absorption corrections were applied with the LANA and X-RED32 modules of the X-Area software suite.^[177,178] The structure was solved using dual-space methods (SHELXT-2014/5) and refined against F^2 (SHELXL-2018/3 using ShelXle interface).^[172,173,175] All non-hydrogen atoms were refined with anisotropic displacement parameters. The hydrogen atoms were refined using the “riding model” approach with isotropic displacement parameters 1.2 times (1.5 times for the methyl groups) of that of the preceding carbon atom. CCDC 2063290 contains the supplementary crystallographic data. The Crystal structure, data, and details of **64g** are presented in Table 19 and Figure 98.

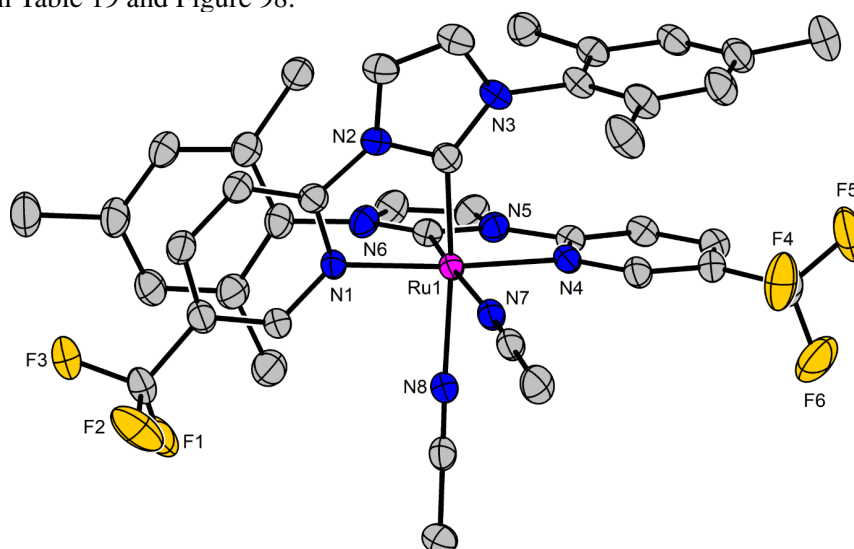


Figure 98: Crystal structure of racemic **64g**. The $[\text{PF}_6]^-$ anions and the hydrogen atoms are omitted for clarity. Displacement ellipsoids are shown at 50% probability level at 100 K.

Table 19: Crystal data and structure refinement for **64g**.

Crystal data

Identification code	EW567
Empirical formula	$\text{C}_{40}\text{H}_{38}\text{F}_{18}\text{N}_8\text{P}_2\text{Ru}$
Molar mass	$1135.79 \text{ g mol}^{-1}$
Space group (No.)	P21/n (14)
a	$11.30600(10) \text{ \AA}$
b	$30.2742(3) \text{ \AA}$
c	$13.6068(2) \text{ \AA}$
β	$103.5930(10)^\circ$
V	$4526.88(9) \text{ \AA}^{-3}$
Z	4

$\rho_{calc.}$	1.667 g cm ⁻³
μ	4.527 mm ⁻¹
Color	yellow
Crystal habitus	plate
Crystal size	0.473×0.327×0.054 mm ³
T	100 K
λ	1.54186 (Cu-K α)
Θ range	2.919 to 74.507°
Range of Miller indices	$-14 \geq h \geq 12$ $-37 \geq k \geq 27$ $-16 \geq l \geq 16$
Absorption correction	multi-scan and numerical
T_{min}, T_{max}	0.1175, 0.4377
R_{int}, R_{σ}	0.0332, 0.0171
Completeness of the data set	0.999
No. of measured reflections	54245
No. of independent reflections	9229
No. of parameters	633
No. of restraints	0
S (all data)	1.068
R(F) ($I \geq 2\sigma(I)$, all data)	0.0455, 0.0475
wR(F ²) ($I \geq 2\sigma(I)$, all data)	0.1286, 0.1304
Extinction coefficient	not refined
$\Delta\rho_{max}, \Delta\rho_{min}$	1.657 and $-1.025 \text{ e } \text{\AA}^{-3}$
CCDC No.	2063290

Complex 114a

Single crystals suitable for analysis were obtained by slow diffusion of Et₂O into a solution of **114a** in CH₂Cl₂ over night. A suitable crystal was selected under inert oil and mounted using a MiTeGen loop. Intensity data of the crystal were recorded with a D8 Quest diffractometer (Bruker AXS). The instrument was operated with Mo-K α radiation (0.710 73 Å, microfocus source) and equipped with a PHOTON 100 detector. Evaluation, integration and reduction of the diffraction data was carried out using the Bruker APEX 3 software suite.^[179] Multi-scan and numerical absorption corrections were applied using the SADABS program.^[180,181] The structure was solved using dual-space methods (SHELXT-2014/5) and refined against F² (SHELXL-2018/3 using ShelXle interface).^[172,173,175] All non-hydrogen atoms were refined with anisotropic displacement parameters. The hydrogen atoms were refined using the “riding model” approach with isotropic displacement parameters 1.2 times (1.5 times for terminal methyl groups) of that

of the preceding carbon atom. One DCM molecule exhibit disorder between approximately two positions and was refined accordingly using the DSR plugin implemented in ShelXle.^[182] CCDC 2088021 contains the supplementary crystallographic data. The Crystal structure, data, and details of **114a** are presented in Table 20 and Figure 99.

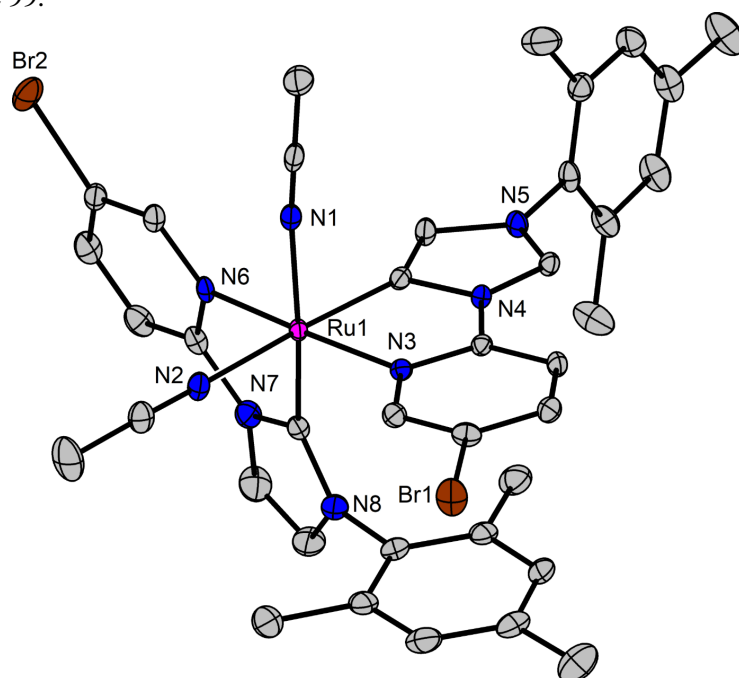


Figure 99: Crystal structure of racemic **114a**. The $[\text{PF}_6^-]$ anions, solvent molecules and the hydrogen atoms are omitted for clarity. Displacement ellipsoids are shown at 50% probability level at 100 K.

Table 20: Crystal data and structure refinement for **114a**.

Crystal data

Identification code	EW658
Empirical formula	$\text{C}_{40}\text{H}_{42}\text{Br}_2\text{Cl}_4\text{F}_{12}\text{N}_8\text{P}_2\text{Ru}$
Molar mass	$1327.44 \text{ g mol}^{-1}$
Space group (No.)	$P1^- (2)$
a	$12.6142(8) \text{ \AA}$
b	$14.2975(9) \text{ \AA}$
c	$14.9453(9) \text{ \AA}$
α	$73.791(2)^\circ$
β	$86.164(2)^\circ$
γ	$80.547(2)^\circ$
V	$2552.5(3) \text{ \AA}^{-3}$
Z	2
$\rho_{\text{calc.}}$	1.727 g cm^{-3}
μ	2.228 mm^{-1}

Color	yellow
Crystal habitus	block
Crystal size	0.396×0.241×0.128 mm ³
T	100 K
λ	0.71073 (Mo-K α)
Θ range	2.143 to 29.682°
Range of Miller indices	$-17 \geq h \geq 17$ $-19 \geq k \geq 19$ $-20 \geq l \geq 20$
Absorption correction	multi-scan and numerical
T_{min}, T_{max}	0.5691, 0.8481
R_{int}, R_{σ}	0.0502, 0.0498
Completeness of the data set	0.999
No. of measured reflections	69272
No. of independent reflections	14400
No. of parameters	659
No. of restraints	47
S (all data)	1.028
R(F) ($I \geq 2\sigma(I)$, all data)	0.0403, 0.0653
wR(F ²) ($I \geq 2\sigma(I)$, all data)	0.0737, 0.0810
Extinction coefficient	0.00038(11)
$\Delta\rho_{max}, \Delta\rho_{min}$	0.708 and $-0.812 \text{ e } \text{\AA}^{-3}$
CCDC No.	2088021

Complex 114b

Single crystals suitable for analysis were obtained by slow diffusion of Et₂O into a solution of **114b** in CH₃CN over night. A suitable crystal of **114b** was selected under inert oil and mounted using a MiTeGen loop. Intensity data of the crystal were recorded with a D8 Quest diffractometer (Bruker AXS). The instrument was operated with Mo-K α radiation (0.710 73 Å, microfocus source) and equipped with a PHOTON 100 detector. Evaluation, integration and reduction of the diffraction data was carried out using the Bruker APEX 3 software suite.^[179] Multi-scan and numerical absorption corrections were applied using the SADABS program.^[180,181] The structure was solved using dual-space methods (SHELXT-2014/5) and refined against F² (SHELXL-2018/3 using ShelXle interface).^[172,173,175] All non-hydrogen atoms were refined with anisotropic displacement parameters. The hydrogen atoms were refined using the “riding model” approach with isotropic displacement parameters 1.2 times (1.5 times for terminal methyl groups) of that of the preceding carbon atom. CCDC 2063289 contains the supplementary crystallographic data for this paper. The Crystal structure, data, and details of **114b** are presented in Table 21 and Figure 100.

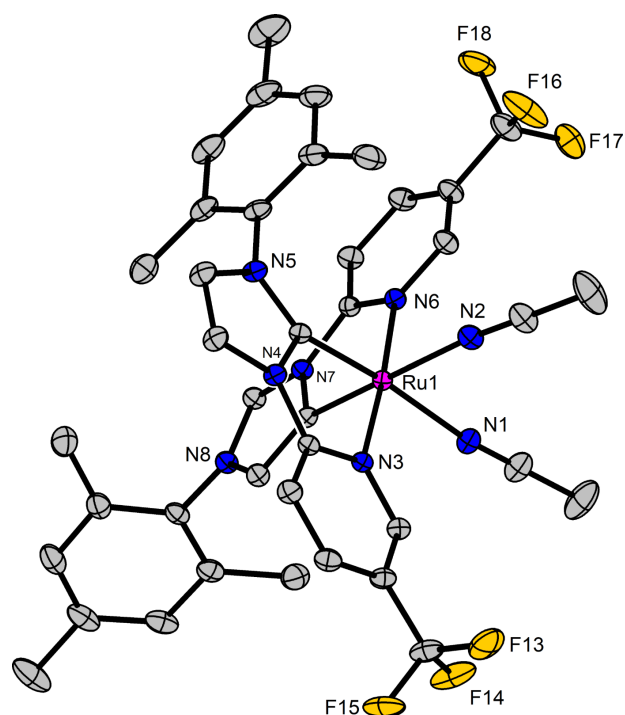


Figure 100: Crystal structure of racemic **114b**. The $[\text{PF}_6^-]$ anions, solvent molecules and the hydrogen atoms are omitted for clarity. Displacement ellipsoids are shown at 50% probability level at 100 K.

Table 21: Crystal data and structure refinement for **114b**.

Crystal data

Identification code	EW431
Empirical formula	$\text{C}_{46}\text{H}_{47}\text{F}_{18}\text{N}_{11}\text{P}_2\text{Ru}$
Molar mass	$1258.95 \text{ g mol}^{-1}$
Space group (No.)	$P1^- (2)$
a	$12.0596(7) \text{ \AA}$
b	$12.4611(7) \text{ \AA}$
c	$20.3246(11) \text{ \AA}$
α	$93.416(2)^\circ$
β	$103.585(2)^\circ$
γ	$110.922(2)^\circ$
V	$2738.3(3) \text{ \AA}^3$
Z	2
ρ_{calc}	1.527 g cm^{-3}
μ	0.450 mm^{-1}
Color	yellow
Crystal habitus	block

Crystal size	0.429×0.120×0.078 mm ³
T	100 K
λ	0.71073 (Mo-K α)
Θ range	2.031 to 30.584°
Range of Miller indices	$-17 \geq h \geq 17$ $-17 \geq k \geq 17$ $-29 \geq l \geq 28$
Absorption correction	multi-scan
T_{min}, T_{max}	0.8581, 1.0000
R_{int}, R_{σ}	0.0302, 0.0176
Completeness of the data set	0.999
No. of measured reflections	156560
No. of independent reflections	16789
No. of parameters	715
No. of restraints	0
S (all data)	1.055
R(F) ($I \geq 2\sigma(I)$, all data)	0.0316, 0.0367
wR(F ²) ($I \geq 2\sigma(I)$, all data)	0.0772, 0.0800
Extinction coefficient	0.0055(3)
$\Delta\rho_{max}, \Delta\rho_{min}$	1.341 and -0.951 e Å ⁻³
CCDC No.	2063289

Complex Δ -(S)-128a

Single crystals suitable for analysis were obtained by slow diffusion of Et₂O into a solution of **128a** in CH₂Cl₂ over night. A suitable crystal was selected under inert oil and mounted using a MiTeGen loop. Intensity data of the crystal were recorded with a D8 Quest diffractometer (Bruker AXS). The instrument was operated with Mo-K α radiation (0.71073 Å, microfocus source) and equipped with a PHOTON 100 detector. Evaluation, integration and reduction of the diffraction data was carried out using the Bruker APEX 3 software suite.^[179] Since the crystal was found to be non-merohedrally twinned, the multi-scan absorption correction was applied using the TWINABS program.^[180,181] The structure was solved using dual-space methods (SHELXT-2014/5) and refined against F² (SHELXL-2018/3 using ShelXle interface).^[172,173,175] All non-hydrogen atoms were refined with anisotropic displacement parameters. The hydrogen atoms were refined using the “riding model” approach with isotropic displacement parameters 1.2 times (1.5 times for terminal methyl groups) of that of the preceding carbon atom. One CH₂Cl₂ solvent molecule exhibit rotational disorder and was refined accordingly using the DSR plugin implemented in SHELXLE.^[182] Both [PF₆]⁻ anions show signs of rotational disorder. An attempt to

refine it either manually or using the DSR plugin did not improve the model. The Crystal structure, data, and details of **128a** are presented in Table 22 and Figure 101.

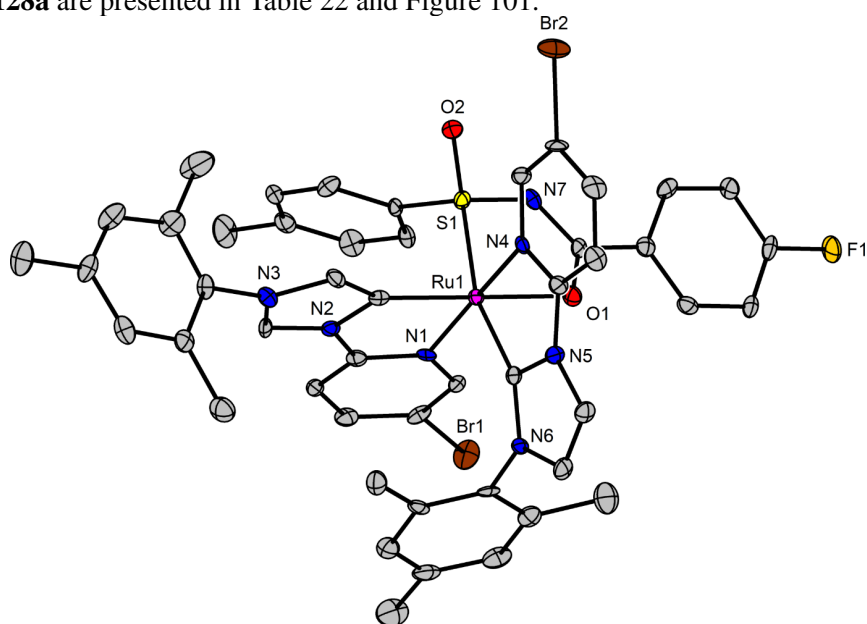


Figure 101: Crystal structure of Δ -(*S*)-**128a**. The $[\text{PF}_6^-]$ anions, solvent molecules and the hydrogen atoms are omitted for clarity. Displacement ellipsoids are shown at 50% probability level at 100 K.

Table 22: Crystal data and structure refinement for Δ -(*S*)-**128a**.

Crystal data

Identification code	EW634
Empirical formula	$\text{C}_{50}\text{H}_{47}\text{Br}_2\text{Cl}_4\text{F}_7\text{N}_7\text{O}_2\text{PRuS}$
Molar mass	$1376.66 \text{ g mol}^{-1}$
Space group (No.)	$P2_1(4)$
a	$11.6856(8) \text{ \AA}$
b	$23.3446(17) \text{ \AA}$
c	$20.4624(14) \text{ \AA}$
β	$93.671(2)^\circ$
V	$5570.6(7) \text{ \AA}^{-3}$
Z	4
$\rho_{\text{calc.}}$	1.641 g cm^{-3}
μ	2.044 mm^{-1}
Color	orange
Crystal habitus	block
Crystal size	$0.222 \times 0.198 \times 0.106 \text{ mm}^3$
T	100 K
λ	$0.71073 \text{ (Mo-K}\alpha)$

☉ range	1.955 to 28.384°
Range of Miller indices	$-15 \geq h \geq 15$ $-31 \geq k \geq 31$ $-27 \geq l \geq 27$
Absorption correction	multi-scan
T_{min}, T_{max}	0.5107, 0.5633
R_{int}, R_{σ}	0.0761, 0.0914
Completeness of the data set	0.999
No. of measured reflections	168342
No. of independent reflections	27949
No. of parameters	1395
No. of restraints	66
S (all data)	1.091
R(F) ($I \geq 2\sigma(I)$, all data)	0.0587, 0.0878
wR(F ²) ($I \geq 2\sigma(I)$, all data)	0.0735, 0.0799
Extinction coefficient	0.00031(5)
Flack parameter x	-0.003(3)
Volume fraction of the 2 nd twin component	0.0601(6)
$\Delta\rho_{max}, \Delta\rho_{min}$	1.180 and $-0.633 \text{ e } \text{\AA}^{-3}$
CCDC No.	2063291

Complex 137b

Single crystals suitable for analysis were obtained by slow diffusion of Et₂O into a solution of **137b** in CH₃CN over night. A suitable crystal of **137b** was selected under inert oil and mounted using a MiTe-Gen loop. Intensity data of the crystal were recorded with a D8 Quest diffractometer (Bruker AXS). The instrument was operated with Mo-K α radiation (0.710 73 Å, microfocus source) and equipped with a PHOTON 100 detector. Evaluation, integration and reduction of the diffraction data was carried out using the Bruker APEX 3 software suite.^[179] Multi-scan and numerical absorption corrections were applied using the SADABS program.^[180,181] The structure was solved using dual-space methods (SHELXT-2014/5) and refined against F² (SHELXL-2018/3 using ShelXle interface).^[172,173,175] All non-hydrogen atoms were refined with anisotropic displacement parameters. The hydrogen atoms were refined using the “riding model” approach with isotropic displacement parameters 1.2 times (1.5 times for terminal methyl groups) of that of the preceding carbon atom. The two [PF₆⁻] anions exhibit complicated disorder, which could be sufficiently modelled using three disordered species in each case with the help of the DSR plugin [7] and the SUMP command in SHELXL. Both CH₃CN and Et₂O solvent molecules are clearly present in the crystal structure, although they were accompanied with areas of negative density on the difference Fourier map. To prevent this, they had to be refined underoccupied. CCDC 2088020 contains the supple-

mentary crystallographic data. The Crystal structure, data, and details of **137b** are presented in Table 23 and Figure 102.

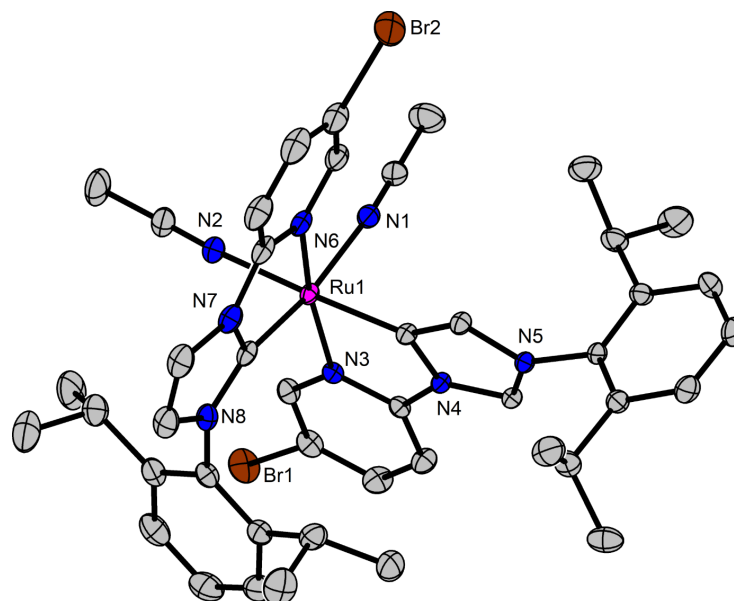


Figure 102: Crystal structure of racemic **137b**. The $[\text{PF}_6^-]$ anions, solvent molecules and the hydrogen atoms are omitted for clarity. Displacement ellipsoids are shown at 50% probability level at 100 K.

Table 23: Crystal data and structure refinement for **137b**

Crystal data

Identification code	EW517
Empirical formula	$\text{C}_{49.33}\text{H}_{61.52}\text{Br}_2\text{F}_{12}\text{N}_{8.90}\text{O}_{0.88}\text{P}_2\text{Ru}$
Molar mass	$1344.14 \text{ g mol}^{-1}$
Space group (No.)	$C2/c(15)$
a	$44.590(2) \text{ \AA}$
b	$13.7841(7) \text{ \AA}$
c	$19.7462(10) \text{ \AA}$
β	$110.634(2)^\circ$
V	$11358.2(10) \text{ \AA}^{-3}$
Z	8
ρ calc.	1.572 g cm^{-3}
μ	1.823 mm^{-1}
Color	yellow
Crystal habitus	block
Crystal size	$0.686 \times 0.473 \times 0.296 \text{ mm}^3$
T	100 K
λ	$0.71073 \text{ (Mo-K}\alpha)$

Θ range	1.952 to 29.682°
Range of Miller indices	$-62 \geq h \geq 62$ $-19 \geq k \geq 19$ $-27 \geq l \geq 27$
Absorption correction	multi-scan
T_{min}, T_{max}	0.4522, 1.0000
R_{int}, R_{σ}	0.0310, 0.0177
Completeness of the data set	0.999
No. of measured reflections	163619
No. of independent reflections	16062
No. of parameters	968
No. of restraints	2810
S (all data)	0.988
R(F) ($I \geq 2\sigma(I)$, all data)	0.0316, 0.0405
wR(F ²) ($I \geq 2\sigma(I)$, all data)	0.0742, 0.0791
Extinction coefficient	0.000151(16)
$\Delta\rho_{max}, \Delta\rho_{min}$	2.549 and $-2.410 \text{ e } \text{\AA}^{-3}$
CCDC No.	2088020

C. List of Abbreviations

$\tilde{\nu}$	Wavenumber	eq	Equivalents
δ	Chemical shift	er	enantiomeric ratio
μ	Micro	ESI	Electron-spray-ionisation
ρ	Density	EtOH	Ethanol
$^{\circ}\text{C}$	Degree Celsius	EtOAc	Ethyl acetate
m/z	Mass per ionization	EWG	Electron Withdrawing Group
t_R	Retention time	h	Hour
<i>Ar</i>	Aromatic (NMR)	HAT	Hydrogen Atom Transfer
M	Molarity	HFIP	Hexafluoro- <i>iso</i> -propanole
acac	Acetylacetone	HPLC	High-performance liquid chromatography
aNHC	abnormal <i>N</i> -heterocyclic carbene	HRMS	High resolution mass spectroscopy
CaH₂	Calcium hydride	<i>i</i>-AmOH	Isoamyl alcohol
calcd.	Calculated	IR	Infrared
cat.	Catalyst	<i>i</i>-Pr	<i>iso</i> -Propyl
CD	Circular Dichroism	IUPAC	International Union of Pure and Applied Chemistry
CH₃CN	Acetonitrile	K	Kelvin
Cp	Cyclopentadienyl	KIEs	Kinetic Isotope Effects
CV	Cyclic Voltammetry	LG	Leaving Group
d	Doublette (NMR)	LiHMDS	Lithium bis(trimethylsilyl)amide
1,2-DCB	1,2-Dichlorobenzene	m	Multiplette (NMR)
DCE	1,2-Dichloroethane	m	mass
dd	Dublette from Dublette (NMR)	M	Molare mass
DFT	Density functional theory	M.p.	Melting point
CDCl₃	Deuterated Chloroform	Meoc	Methoxycarbonyl
CD₂Cl₂	Deuterated Dichloroethane	MeOH	Methanol
Et₂O	Diethyl ether	Mes	Mesityl (2,4,6-trimethylphenyl)
DIPP	2,6-Diisopropylphenyl	mg	Milligram
DMSO	Dimethylsulfoxide	MHz	Megahertz
DMAE	<i>N,N</i> -Dimethylaminoethanol	min	Minute
DMF	<i>N,N</i> -Dimethylformamide	mmol	Millimole
DMSO-<i>d</i>₆	Deuterated Dimethylsulfoxide	<i>n</i>-BuLi	<i>n</i> -Butyl-Lithium
<i>dr</i>	Diastereomeric ratio	<i>n</i>-Hex	<i>n</i> -Hexane
EDG	Electron Donating Group	Na	Sodium
EI	Electron Ionization		
<i>ee</i>	Enantiomeric excess		

NaCl	Sodium Chloride	sol.	Solution
NEt₃	triethylamine	SPhos	Dicyclohexyl(2',6'-dimethoxy[1,1'-biphenyl]-2-yl)phosphane
NH₄Cl	Ammonium chloride	TFA	Trifluoroacetic acid
NH₄PF₆	Ammonium hexafluorophosphate	THF	Tetrahydrofuran
NHC	N-Heterocyclic carbene	TLC	Thin layer chromatography
N₂	Nitrogen	TOF	Turnover frequency
nNHC	normal <i>N</i> -heterocyclic carbene	TON	Turnover number
NMR	Nuclear magnetic resonance	Et₃N	Triethylamine
<i>p</i>-tol	<i>para</i> -Tolyl	TfOH	Trifluoromethanesulfonic acid
ppm	Parts per million	Trisphat	Tris[tetrachlorobenzene-1,2-bis(olato)]-phosphate(V)
R_f	Retention factor	UV-Vis	Ultra violet and visible spectra
<i>rac.</i>	Racemic	V	Volume
rNHC	Remote <i>N</i> -heterocyclic carbene	H₂O	Water
RuPhos	2-Dicyclohexylphosphino-2',6'-diisopropoxybiphenyl		
sat.	Saturated		

D. Statement

An den Vorsitzenden des Prüfungsausschusses in Chemie
Fachbereich Chemie der Philipps-Universität Marburg
Hans-Meerwein-Straße
D-35032 Marburg

Erklärung

gemäß §10, Abs. 1 der Promotionsordnung der Mathematisch-Naturwissenschaftlichen Fachbereiche
und des Medizinischen Fachbereichs für seine mathematisch-naturwissenschaftlichen Fächer der
Philipps-Universität Marburg vom 15.07.2009

Ich erkläre, dass eine Promotion noch an keiner anderen Hochschule als der Philipps-Universität
Marburg, Fachbereich Chemie, versucht wurde und versichere, dass ich meine vorgelegte Dissertation
mit dem Titel

*Einfluss elektronischer Faktoren auf die katalytische
Aktivität von chiral-at-metal Ruthenium Komplexen*

selbst und ohne fremde Hilfe verfasst, nicht andere als die in ihr angegebenen Quellen oder Hilfsmittel
benutzt, alle vollständig oder sinngemäß übernommenen Zitate als solche gekennzeichnet sowie die
Dissertation in der vorliegenden oder ähnlichen Form noch bei keiner anderen in- oder ausländischen
Hochschule anlässlich eines Promotionsgesuches oder zu anderen Prüfungszwecken eingereicht habe.

Marburg, den

(Erik Winterling)

E. Curriculum Vitae

Persönliche Daten

Aus Datenschutzgründen in dieser Version entfernt.